

Horst Ecker

Suppression of Self-excited Vibrations in Mechanical Systems by Parametric Stiffness Excitation

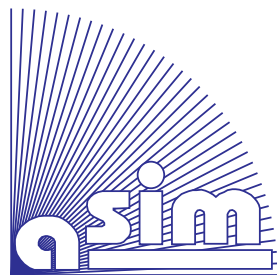


ISBN Ebook 978-3-903347-11-3

ISBN Print 978-3-901608-61-2



DOI: 10.11128/fbs.11



Fortschrittsberichte Simulation

FBS Band 11

Herausgegeben von ASIM
Arbeitsgemeinschaft **Simulation**, Fachausschuß 4.5 der GI

Horst Ecker

Suppression of Self-excited Vibrations in Mechanical Systems by Parametric Stiffness Excitation

ARGESIM / ASIM – Verlag, Wien, 2005
ISBN Print 978-3-901608-61-2

Ebook Reprint 2020
ISBN Ebook 978-3-903347-11-3
DOI: 10.11128/fbs.11

ASIM Fortschrittsberichte Simulation / ARGESIM Reports

Herausgegeben von ASIM, Arbeitsgemeinschaft Simulation, Fachausschuß 4.5 der GI und der ARGESIM

Betreuer der Reihe:

Prof. Dr.-Ing. Th. Pawletta (ASIM)
Hochschule Wismar
Phillip-Müller-Str., 23952 Wismar, Germany
Tel: +49-3841-753-406
Email: pawel@mb.hs-wismar.de

Dr.-Ing. habil. D.P.F. Schwarz (ASIM)
Fraunhofer-Institut für Integrierte Schaltungen
Zeunerstr. 38, 01069 Dresden, Germany
Tel: +49-351- 4640 - 730
Email: schwarz@eas.iis.fhg.de

Prof. Dr. F. Breitenecker (ARGESIM / ASIM)
Abt. Simulationstechnik, Technische Universität Wien
Wiedner Hauptstraße 8 - 10, A - 1040 Wien
Tel: +43-1-58801-10115
Email: Felix.Breitenecker@tuwien.ac.at

FBS Band 11

Titel: Suppression of Self-excited Vibrations in Mechanical Systems by Parametric Stiffness Excitation

Autor: Horst Ecker
Horst.Ecker@tuwien.ac.at

Begutachter des Bandes:

Prof. Dr. F. Breitenecker, Prof. Dr. H. Springer; TU Wien

ARGESIM / ASIM – Verlag, Wien, 2005

ISBN Print 978-3-901608-61-2

Ebook Reprint 2020 (Scan)

ISBN Ebook 978-3-903347-11-3

DOI: 10.11128/fbs.11

Das Werk ist urheberrechtlich geschützt. Die dadurch begründeten Rechte, insbesondere die der Übersetzung, des Nachdrucks, der Entnahme von Abbildungen, der Funksendung, der Wiedergabe auf photomechanischem oder ähnlichem Weg und der Speicherung in Datenverarbeitungsanlagen bleiben, auch bei nur auszugsweiser Verwertung, vorbehalten.

© by ARGESIM/ ASIM, Wien, 2005

Die Wiedergabe von Gebrauchsnamen, Handelsnamen, Warenbezeichnungen usw. in diesem Werk berechtigt auch ohne besondere Kennzeichnung nicht zur Annahme, daß solche Namen im Sinne der Warenzeichen- und Markenschutz - Gesetzgebung als frei zu betrachten wären und daher von jedermann benutzt werden dürften.

Preface

This monograph was submitted as a Habilitation Thesis at the Vienna University of Technology in Vienna, Austria. Some parts are based on several papers published previously, other parts present new and original material. For most parts of the already published content, a significant revision has been carried out to adjust it to follow the main thread of this monograph.

The material documented in this publication represents findings and results obtained within several years of work in the field of parametrically excited systems. Since the research effort is continued and even intensified, thanks to research funding granted by the Austrian Science Foundation (FWF)¹, this monograph can be seen as an intermediate step of documentation and reflects the current state of the ongoing research project on parametric vibration cancelling.

Although there is just my name mentioned as being the author of this monograph, I will use the plural form "we", known as the *pluralis auctoris*, throughout the main part of the text. This style should not only include the reader in what the author has to tell, but "we" may also be understood in the true sense of a number of persons, namely those with whom I have worked together and who have all contributed to this publication in some way. Let me therefore mention and thank them briefly.

This monograph would have never been written if Prof. Dr. Aleš Tondl had not made me curious about the interaction of self-excitation and parametric excitation. I still remember clearly the occasion when we both started our discussions on this topic, it was during a lunch break at the SIRM conference in February 1998 in Darmstadt. This was the

¹FWF - Fonds zur Förderung der Wissenschaften, Project P-16248, started on April 1, 2003

beginning of a very inspiring and productive cooperation which continues until today. I am very grateful that I had and still have the opportunity to work together with Prof. Tondl, an internationally respected scientist in the fields of nonlinear dynamics and one of the founders of modern rotor dynamics.

Equally important for the research progress achieved during the last years was the scientific environment provided by the Institute of Machine Dynamics and Measurement under the leadership of Prof. Dr. Helmut Springer. He always acted both ways as a scientific mentor and a true friend and I owe him a lot for his kind help and support during all these years.

Numerical simulation plays a major role in the numerical studies that have been carried out. Adequate software tools can make life a lot easier and considerably help to save time and effort. For the simulation part of this work the simulation language and environment ACSL was exclusively used, post-processing and graphical representation of data was done with MATLAB. Having access to these powerful software packages was of great help and contributed significantly to the progress made during the last years. Therefore I would like to thank the responsible persons at the Computing Center of TU-Vienna for providing campus software. Special thanks have to go to Prof. Felix Breitenecker for his continuous effort to promote and support all kinds of simulation software at TU-Vienna and to the European distributor of ACSL, Mrs. Ingrid Bausch-Gall, for her generous support of academic institutions.

Some of the results presented have been acquired together with outstanding diploma students like Andreas Matthias and Thomas Pumhössel. Kanjuro Makihara was a visiting Ph.D. student from Tokyo University for one year who enjoyed Austria and parametric vibration suppression at the same time. We had very fruitful discussions and he came up with some smart ideas which we will pursue in the future. Fadi Dohnal recently started his Ph.D. studies on this topic and has already proven to be a very valuable member of our small group. He fell in love with some analytical methods and helped to make the respective part of this monograph more clear and informative.

During the last years friends and colleagues like Markus Nagl, Norbert Steinschaden and Martin Hirschmanner have been always ready to give advice and help when computer problems did plague me or they simply cheered me up when needed. Last but not least our helpful secretaries Christine Paolini, Karin Matschir and Renate Mühlberger have a

good share on the wealth of related articles and books which have been collected in the past. Also their help in typing some parts of this monograph is highly appreciated. With respect to the layout of the cover and some graphics inside, the support of Manfred Schneeberger and Markus Nemetz is acknowledged.

Final words of thanks and appreciation have to go to my dear wife Elisabeth, who sacrificed countless days and weeks of joint activities and of leisure time. Instead, she was left alone in managing our daily life for quite some time. As if this would not have been enough she was also a very critical editor with respect to my usage of the English language. For example she reduced the occurrence of my favorite word "however" from a three-digit number to as few as 57... Also she did proof-read every single page of this document, and if the reader still finds some typos I have probably introduced them afterwards or forgotten to correct them. Thank you so much, darling!

Book-projects seem to have an intrinsic mechanism of damping, which slows them down, if not a sufficient amount of energy is provided at all times. Publishing this thesis as a volume in the series of ARGESIM Reports did take a lot longer than expected. Undecided layout questions, additional proof reading, some improvements here and there, and of course other, more urgent tasks on the author's as well as on the publisher's side, delayed printing until the end of year 2005.

Meanwhile, work on parametrically excited systems was continued at TU-Vienna and led to a number of publications, which are not cited in the references. For an overview of recent contributions and an in-depth discussion of latest research results the reader is referred to Fadi Dohnal's dissertation on "Damping of mechanical vibrations by parametric excitation", finished also by this time at TU-Vienna, Institute of Mechanics and Mechatronics.

Finally, I would like to thank ASIM, and in particular Prof. Felix Breitenecker, very much for the opportunity to publish this monograph as an ARGESIM Report.

Horst Ecker

Vienna, December 2005

Contents

1	Introduction	1
1.1	Self-excitation in mechanical systems	2
1.1.1	The effect of negative damping	3
1.1.2	Flow-induced self-excitation	5
1.1.3	Friction-induced self-excitation	8
1.1.4	Destabilizing forces in rotor systems	10
1.2	Parametric excitation in mechanical systems	13
1.2.1	Review on parametric excitation research	14
1.2.2	Parametric resonance	15
1.2.3	Stabilization by parametric excitation	19
1.3	Parametric Vibration Cancelling	21
1.4	Realization of parametric excitation	24
2	Analysis of systems with periodic coefficients	29
2.1	Analytical methods	31
2.1.1	Method of Successive Approximation	31
2.1.2	Averaging Method	39
2.1.3	Tondl-Floquet method	45
2.1.4	Summary on analytical methods	51
2.2	Numerical methods	53
2.2.1	Numerical simulation	53
2.2.2	Floquet method	56
2.2.3	Continuation method	58
3	Investigation of 2-dof systems	61
3.1	Generic 2-dof system	61
3.1.1	Self-excitation mechanism	63

3.1.2	Rescaling frequency and time	64
3.1.3	Normal form representation	65
3.2	Basic simulation results	67
3.3	Numerical stability investigation	80
3.4	Comparison of analytical and numerical results	88
3.5	Anti-resonance at $\Omega_2 - \Omega_1$	93
3.6	Anti-resonance at $\Omega_1 + \Omega_2$	94
4	Equivalent damping of parametric excitation	101
4.1	System without coupling damper	102
4.2	System with non-zero coupling damper	109
4.3	Computational aspects	116
5	Parametric absorber for vibration suppression	119
5.1	Main system with parametric absorber	120
5.2	Cancelling flow-induced vibrations	122
5.2.1	Effect of gravity forces	122
5.2.2	Modelling of flow-generated forces	125
5.2.3	Results of a numerical study	127
5.2.4	Remarks and conclusion	140
5.3	Suppression of friction-induced vibrations	141
5.3.1	Analytical representation of dry friction	142
5.3.2	Single-mass model with friction	144
5.3.3	System with Parametric Absorber	147
5.3.4	Results for system with conventional absorber	149
5.3.5	Results for system with parametric absorber	153
5.4	Concluding remarks	159
6	Vibration cancelling in a rotor system	161
6.1	Rotor model with parametric stiffness excitation	163
6.1.1	Self-excitation mechanisms	165
6.1.2	Equations of motion	166
6.1.3	Eigenvalue analysis	169
6.2	Method of investigation	171
6.3	Study of a balanced rotor	173
6.3.1	Self-excitation due to internal damping	173
6.3.2	Self-excitation due to destabilizing gap forces	183
6.4	Study of a rotor with mass unbalance	194
6.4.1	Self-excitation due to internal damping	195

Contents

6.5 Concluding remarks	204
7 Synopsis and outlook	207
Bibliography	211
Authors Index	221
Index	225

Chapter 1

Introduction

In general a mechanical system will perform vibrations if an excitation is applied. Frequently these vibrations are unwanted and require attention if the vibration amplitudes exceed a certain level. Depending on the nature of the excitation, different strategies and methods of vibration reduction are in use. The main focus of this monograph is the cancellation, or at least the reduction, of self-induced vibrations in mechanical systems by means of parametric excitation.

Let us first summarize in a brief review the different excitation types as mentioned later in this text. Probably the most common type of excitation in a mechanical system is the *external excitation*, also known as *forced excitation*. Unbalance excitation in rotating machinery is frequently mentioned as an example as well as the excitation of a structure which is attached to a vibrating foundation (base). In the latter example the primary source of excitation is the oscillating displacement of the foundation, but in fact this is an excitation due to the internal forces of the connecting elements.

A mechanical system under the influence of an external excitation will perform forced vibrations. Vibration amplitudes are determined by the dynamical properties of the system and the amplitude of excitation. In the case of a linear system, vibration amplitudes are proportional to excitation amplitudes and damping properties of the system. Vibration reduction for the whole system is mainly achieved by choosing these parameters appropriately. Vibration reduction, especially at certain locations of the system, can be achieved by attaching a vibration absorber,

which is basically a tuned single-dof (degree of freedom) system added to the original system. See [80] for a rather complete and up-to-date survey on such systems.

Although mentioned in first place, external excitation will only play a minor role in this monograph. We will almost exclusively deal with mechanical systems where two other types of excitation mechanisms are present and play a dominant role: Self-Excitation (SE) and Parametric Excitation (PE). As in most practical cases, self-excitation will be the source of unwelcomed vibrations. We will discuss mechanisms that lead to self-excitation and give examples in the next section. Later in this chapter we will concentrate on the parametric excitation and its role as a mean to suppress self-excited vibrations.

1.1 Self-excitation in mechanical systems

Self-induced vibrations, sometimes also called self-sustained vibrations, are caused by a *self-excitation* (SE) mechanism. This mechanism converts a non-oscillatory excitation to an oscillatory excitation within the system. Famous examples taken from the area of civil engineering are wind-induced vibrations of large structures, i.e. bridges or power lines, where kinetic energy from the (constant) airflow is transferred into the vibrational motion of the structure. If the energy source which feeds the self-excitation mechanism has a large capacity, excessive and violent vibrations can occur and vibration amplitudes may exceed design limits. In such a situation a total failure of the structure will happen. Fortunately this is rarely the case, but has nevertheless occurred in the past. The collapse of the Tacoma Narrows Bridge in November 1940 is one of the best known examples.

Avoiding unwanted self-excited vibrations is mandatory whenever there is a danger that such vibrations might occur. Measures have to be taken against them already at the design stage. Frequently (aerodynamic) parameters have to be kept within certain limits in order to prevent self-induced vibrations. However, if the structure can change its shape during operation (e.g. formation of an ice-coating around power lines), it can be difficult to find effective counter-measures.

Self-excited vibrations are also frequently encountered in mechanical engineering. Besides flow-structure interaction there are also other mechanisms to generate self-excited vibrations like

1.1. Self-excitation in mechanical systems

- chatter vibrations of machine-tool systems,
- shimmy of wheels,
- airplane wing flutter,
- stick-slip oscillations,
- whirling and whipping in rotating machinery.

In the following sections different mechanisms are briefly explained and some examples are given. The main purpose of this introductory part is to give reasons for the ongoing research and to outline possible areas of application for the vibration cancellation method presented and discussed later.

1.1.1 The effect of negative damping

To explain this mechanism of self-excitation by giving an example of a simple system we consider a mechanical oscillator in which an external force acts on the system. The equation of motion of this single degree of freedom system is

$$m\ddot{x} + c\dot{x} + kx = F \quad (1.1)$$

where m is the mass, c is the viscous damping coefficient and k is the stiffness coefficient. The symbol F denotes the external force and we assume that this force is proportional to the velocity \dot{x} and hence defined as

$$F = b\dot{x} \quad (1.2)$$

with b a suitable constant coefficient. As we will see in the following sections, the assumption on the nature of F is based on observations of real self-excited systems, where this type of external force is encountered frequently.

Combining Eqs. (1.1) and (1.2) leads to the elementary homogeneous differential equation of second order with constant coefficients

$$\ddot{x} + \frac{(c-b)}{m}\dot{x} + \frac{k}{m}x = 0. \quad (1.3)$$

By applying the usual Ansatz $x = e^{\lambda t}$ we obtain the characteristic (algebraic) equation

$$\lambda^2 + \lambda \frac{(c-b)}{m} + \frac{k}{m} = 0. \quad (1.4)$$

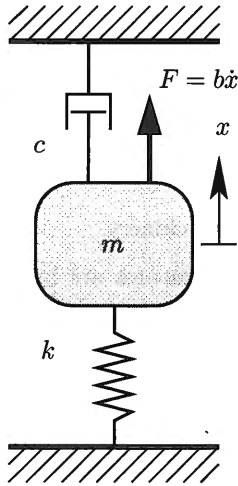


Figure 1.1: Single mass system with negative damping $(c - b) < 0$ as a mechanism for self-excitation.

The roots of this equation are the eigenvalues λ_1 and λ_2 of the system

$$\lambda_{1,2} = -\frac{c-b}{2m} \pm \frac{1}{2m} \sqrt{(c-b)^2 - 4mk}. \quad (1.5)$$

In this context we are primarily interested in the weakly damped case, where $((c-b)^2 - 4mk) < 0$ holds and the eigenvalues are a pair of conjugate complex numbers $p_{1,2} = \alpha \pm i\beta$. For this case the solution of Eq. (1.3) is

$$x = e^{\alpha t} (C_1 \cos \beta t + C_2 \sin \beta t), \quad (1.6)$$

a harmonic function with an amplitude that is dominated by the time behavior of the factor $e^{\alpha t}$.

Since $\alpha = -(c-b)/2m$, the coefficients c and b determine whether the real part α of the eigenvalues is negative or positive. If $c > b$ holds, the resulting (total) damping coefficient for the system is positive and α is negative, hence the system is stable. Initial vibration amplitudes due to a disturbance will decrease with time and finally vanish.

However, if $c < b$ the opposite is true and the system exhibits negative damping. Due to the positive real part of the eigenvalues the exponential function will be increasing with time and, accordingly, the amplitude of vibration will drastically increase. The system is said to be unstable.

1.1. Self-excitation in mechanical systems

In this case, the damping force does positive work on the system. This work is converted into additional kinetic energy, and the effect of the damping force is to increase the displacement instead of reducing it.

This brief review of well known facts has been included because the essentials of self-excitation can be seen clearly and unobstructedly from this simple single degree of freedom system.

1.1.2 Flow-induced self-excitation

Flow-induced vibrations have become increasingly important in the past because designers are using materials to their limit, causing machines and structures to become lighter but also more flexible. The headline "flow-induced vibrations" subsumes a number of distinctly different fluid-dynamic mechanisms, which can be classified by the nature of the flow and the interacting structure. In [5] R.D.Blevins gives a comprehensive overview and introduces two main categories, namely flow-induced vibrations due to steady flow and due to unsteady flow. Since we just want to point out basic mechanisms that lead to self-excitation, we will only consider aerodynamic instability due to a steady flow. An extensive discussion would be beyond the scope of this chapter and the reader is therefore referred to the reference given.

An aerodynamical instability which is known since the beginning of the last century is the so-called *galloping instability*. Galloping can occur in lightweight, flexible structures that are exposed to a flow. The classic example of galloping is the vibration of ice-coated power lines. The low structural damping of the cables combined with a climate and geographical topology in some areas which favor steady moderate wind velocities can result in large amplitudes of oscillation, see e.g. P. Hagedorn and M. Kraus [32].

A single degree of freedom system as shown in Fig. 1.2(a) is sufficient to explain the basic principle of this self-excitation mechanism. Mass m is supported by a spring-damper combination k and c and is exposed to a steady flow V_{flow} coming from a direction perpendicular to the vertical motion x of the mass. If the mass moves vertically with velocity \dot{x} then the angle of the flow relative to the mass α (angle of attack) is defined by

$$\tan \alpha = -\frac{\dot{x}}{V_{flow}}, \quad (1.7)$$

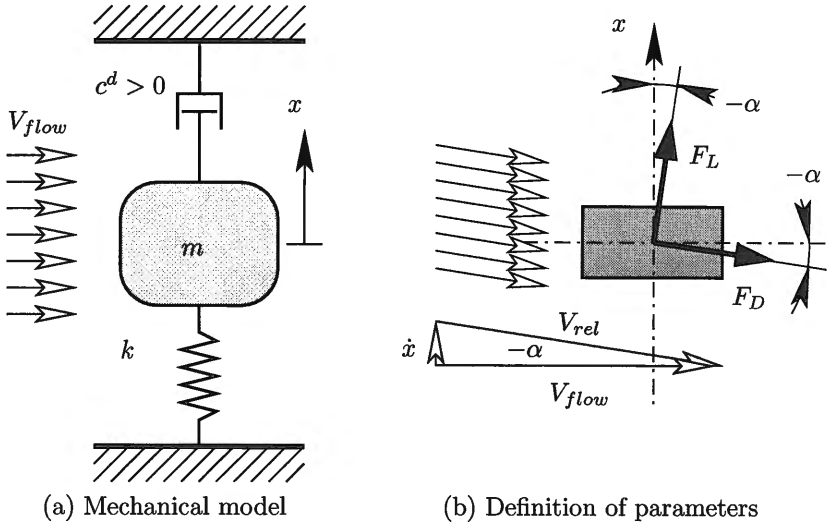


Figure 1.2: Single-dof system exposed to a steady cross-flow generating movement-induced vibrations

see Fig. 1.2(b). The flow velocity relative to the mass is simply

$$V_{rel}^2 = \dot{x}^2 + V_{flow}^2. \quad (1.8)$$

This relative flow V_{rel} generates a drag force F_D in the direction of the flow and a lift force F_L perpendicular to that. It is assumed that both forces can be computed according to

$$F_D = \frac{\rho}{2} V_{rel}^2 A C_D(\alpha), \quad (1.9)$$

$$F_L = \frac{\rho}{2} V_{rel}^2 A C_L(\alpha). \quad (1.10)$$

In Eqs. (1.9) and (1.10) ρ is the fluid density, A is the cross-section area and $C_D(\alpha)$ and $C_L(\alpha)$ are drag and lift coefficients, respectively. The resulting aerodynamic force F_A acting on the mass is

$$F_A = \frac{\rho}{2} V_{flow}^2 A C_x, \quad (1.11)$$

1.1. Self-excitation in mechanical systems

with the resulting vertical aerodynamic force coefficient

$$C_x(\alpha) = \frac{V_{rel}^2}{V_{flow}^2} (C_L \cos \alpha + C_D \sin \alpha). \quad (1.12)$$

The nonlinear equation of motion for mass m is given as

$$m\ddot{x} + c^d \dot{x} + kx = F_A = \frac{\rho}{2} V_{flow}^2 A C_x(\alpha). \quad (1.13)$$

Since the angle of attack depends only on \dot{x} and V_{flow} (see Eq. 1.7), one can approximate $C_x(\alpha)$ by a polynomial expression of arbitrary order

$$C_x(\alpha) = C_x(\dot{x}, V_{flow}) = a_1 \frac{\dot{x}}{V_{flow}} + a_2 \frac{\dot{x}^2}{V_{flow}^2} + \dots \quad (1.14)$$

by numerical curve-fitting of measurement data. For a stability investigation of the trivial solution a first order approximation is sufficient. The coefficient a_1 of the linear term may be obtained from an expansion of C_x about $\alpha = 0$

$$C_x = C_x(\alpha = 0) + \frac{\partial C_x(\alpha = 0)}{\partial \alpha} \alpha + 0(\alpha^2). \quad (1.15)$$

For small angles of attack Eq. (1.13) may be linearized and we obtain $\alpha = -\dot{x}/V_{flow}$ and from Eq. (1.12)

$$\frac{\partial C_x}{\partial \alpha} = \left(\frac{\partial C_D}{\partial \alpha} - C_L \right) \sin \alpha + \left(\frac{\partial C_L}{\partial \alpha} + C_D \right) \cos \alpha. \quad (1.16)$$

After inserting and cleaning up, the linearized equation of motion reads

$$m\ddot{x} + c^d \dot{x} + kx = -\frac{\rho}{2} V_{flow}^2 A \left(\frac{\partial C_L}{\partial \alpha} + C_D \right) \frac{\dot{x}}{V_{flow}}. \quad (1.17)$$

and in short notation

$$m\ddot{x} + c\dot{x} + kx = 0, \quad (1.18)$$

with

$$c = c^d + c^{ad}, \quad c^{ad} = \frac{\rho}{2} V_{flow}^2 A \left(\frac{\partial C_L}{\partial \alpha} + C_D \right). \quad (1.19)$$

We recognize a similar result as in the previous Section 1.1.1. If $c > 0$, the single dof-system is stable. In the case of a negative contribution

from aerodynamic damping $c^{ad} < 0$, it is necessary that $c^d > |c^{ad}|$ holds to ensure the stability of the trivial solution. Negative values for c^{ad} can occur for certain shapes of the mass, e.g. for a cube-shaped body.

This analysis shows that the flow-induced self-excitation of the galloping type can be treated like a linear system with negative damping, if linearization for small angles of attack is possible.

A similar analysis can be carried out for the torsional stability of a mass with a rotational degree of freedom in an airflow. Such a system can be used to model self-excitation due to stall flutter of turbine blades and other structures that may exhibit torsional vibrations. See Blevins [5] for more details.

1.1.3 Friction-induced self-excitation

Friction is another very common mechanism in mechanical systems to induce self-excited vibrations [31]. The generation of friction forces is a complex process which depends on several parameters. A key parameter in systems with dry friction is the relative velocity between sliding surfaces. The characteristics of dry friction as observed in mechanical systems and especially the dependency of friction on the sliding speed have been subject of numerous investigations, see for example [40] and [27]. It is typical and also essential for the dynamic system that in many cases the friction decreases with increasing velocity. Such a speed-range with a negative slope of the friction function usually occurs at low velocities and may start at or in the vicinity of zero velocity. Figure 1.3 shows schematically the characteristic diagram of the dimensionless friction force $F_{fric}/F_{normal} = \mu(v_{rel})$ as a function of the relative velocity v_{rel} between two contacting surfaces. Note the velocity range $0 \leq v < v_{min}$ for which the function exhibits a negative slope. Of course the same principal behavior occurs if the relative velocity changes direction, as can be seen in the third quadrant of the diagram.

Now, to demonstrate how friction can cause self-excitation, we will study again a one-mass system under the action of a friction force. Figure 1.4 shows a single mass m on a moving belt running at constant speed v_{belt} . The force acting on the mass due to friction between the mass and the belt is given by

$$F_{fric} = mg \mu(v_{belt} - \dot{x}), \quad (1.20)$$

with friction coefficient $\mu(v_{rel})$ and a load factor $g > 0$. The mass is connected to the inertial reference frame via a linear and constant

1.1. Self-excitation in mechanical systems

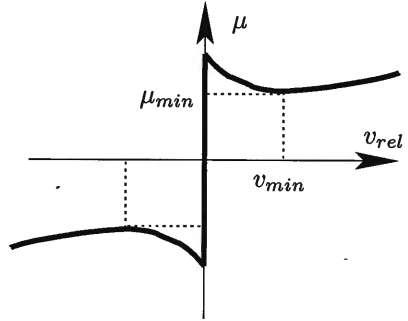


Figure 1.3: Typical shape of the friction coefficient μ as a function of the relative velocity v_{rel} between two contacting surfaces.

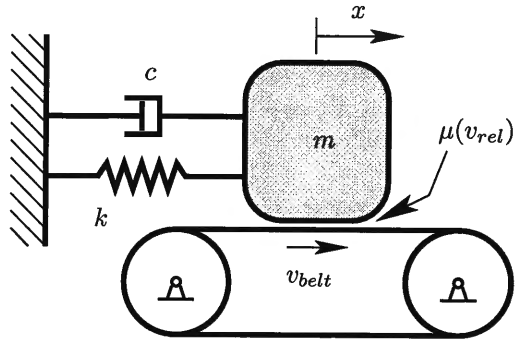


Figure 1.4: Single mass system on a moving belt.

spring k and a viscous damper c . This simple system is governed by the equation of motion

$$m\ddot{x} + c\dot{x} + kx = F_{fric} = mg \mu(v_{belt} - \dot{x}). \quad (1.21)$$

For this brief analysis we can linearize the function $\mu(v_{rel})$ for small positive velocities and obtain

$$\begin{aligned} \mu_{lin} &= \frac{\partial \mu(v_{rel} = 0^+)}{\partial v_{rel}} v_{rel} + \mu(v_{rel} = 0^+), \\ &= \mu' v_{rel} + \mu_0, \quad (0 \leq v_{rel} \ll v_{min}). \end{aligned} \quad (1.22)$$

Inserting the linearized friction function into Eq. (1.21) leads to

$$m\ddot{x} + (c + mg \mu')\dot{x} + kx = mg (\mu' v_{belt} + \mu_0). \quad (1.23)$$

The constant force on the right hand side results in a steady deflection x_{st} of the mass due to the friction force. The stability of this trivial solution depends on the sign of the generalized damping parameter $c_{gen} = (c + mg\mu')$. For a negative slope $\mu' < 0$ holds, but if c is large enough $c_{gen} > 0$ is still possible. Otherwise $c_{gen} < 0$ and the mass cannot rest at a steady deflection x_{st} because self-excited vibrations will occur due to negative damping.

This very simple analysis does not give useful results for large amplitudes. The linearized model can only be used to study the stability of the trivial (stationary) solution. It is not capable of predicting large amplitudes, which are bounded for this example, when assuming a friction function as shown in Fig. 1.3. What we can see from this analysis is that the self-excitation mechanism of dry friction is also based on negative damping which is introduced to the system.

The investigation of systems with a negative damping element, as carried out later in this monograph, will therefore lead to results and findings that are applicable to quite a number of different models and seemingly different self-excitation mechanisms.

1.1.4 Destabilizing forces in rotor systems

In the previous examples we finally ended up with negative damping as the basic reason for self-excited oscillations. However, this is not the only mechanism to generate this kind of vibrations. In rotor dynamics self-sustained vibrations are very common and can result also from other mechanisms than negative damping. Well known phenomena in rotating machinery which are attributed to self-excitation are for example:

- Hysteretic whirl due to internal damping
- Forward whirl due to gyroscopic moments
- Fluid bearing whip (oil whip)
- Labyrinth seal instability
- Tip-clearance excitation (steam whirl)
- Instability of hollow rotor partly filled with fluid

The most important categories of instability in rotating machinery are generally called *whirling* and *whipping*. The unifying generality is the

1.1. Self-excitation in mechanical systems

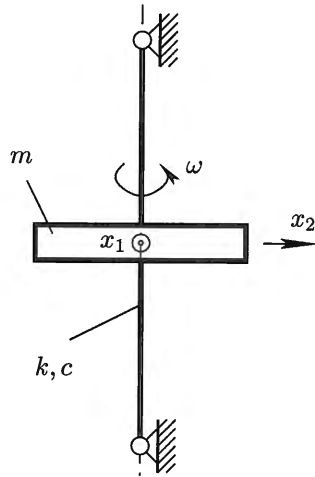


Figure 1.5: Model of a simple Jeffcott/Laval-rotor with elastic shaft.

generation of a tangential force, normal to an arbitrary radial deflection (or velocity) of a rotating shaft, whose magnitude is proportional to (or varies monotonically with) that deflection (velocity). At some "onset" rotational speed (critical speed), this tangential force will exceed the stabilizing external damping forces, which are generally present, and induce a whirling motion of increasing amplitudes. These amplitudes are only bounded by nonlinearities which ultimately limit the deflections. See Yamamoto and Ishida [101] and Harris [33] for a detailed discussion of these phenomena.

Here we will have a brief look at the most simple rotor system to illustrate the principle self-excitation mechanisms present in rotating machinery.

A generic equation of motion in matrix notation for a rotor model as shown in Fig. 1.5 is given by

$$\mathbf{M}\ddot{\mathbf{x}} + (\mathbf{C} + \mathbf{G})\dot{\mathbf{x}} + (\mathbf{K} + \mathbf{N})\mathbf{x} = \mathbf{0} \quad (1.24)$$

with a mass matrix \mathbf{M} , a damping matrix \mathbf{C} , a gyroscopic matrix \mathbf{G} , a stiffness matrix \mathbf{K} , a matrix of non-conservative forces \mathbf{N} and a vector \mathbf{x} containing the deflections of the mass. Since the stability of a linear system is only determined by the homogeneous set of equations, external (unbalance) excitation is not considered here.

The rotor system of Fig. 1.5 consists of a flexible, massless shaft with bending stiffness k and internal damping parameter c . The shaft is supported by two rigid bearings at both ends. A rigid mass m is attached to the shaft in the midspan position. The two degrees of freedom of this system are the deflections x_1, x_2 of the mass. The shaft rotates at a constant angular speed ω . This system can be described in terms of the system matrices of Eq. (1.24) as follows

$$\begin{aligned} \mathbf{M} &= \begin{bmatrix} m & 0 \\ 0 & m \end{bmatrix}, \quad \mathbf{C} = \begin{bmatrix} c & 0 \\ 0 & c \end{bmatrix}, \quad \mathbf{G} = \begin{bmatrix} 0 & 0 \\ 0 & 0 \end{bmatrix}, \\ \mathbf{K} &= \begin{bmatrix} k & 0 \\ 0 & k \end{bmatrix}, \quad \mathbf{N} = \begin{bmatrix} 0 & \omega c \\ -\omega c & 0 \end{bmatrix}, \quad \mathbf{x} = \begin{bmatrix} x_1 \\ x_2 \end{bmatrix}. \end{aligned} \quad (1.25)$$

Note that internal damping of the shaft not only manifests itself in a conventional damping matrix \mathbf{C} but also generates the skew-symmetric matrix \mathbf{N} with coefficients depending upon the rotational speed ω of the rotor. The forces $\mathbf{f}_{\text{non}} = \mathbf{N}\mathbf{x}$ are proportional to the deflection \mathbf{x} of the rotor and are often called *non-conservative forces* as opposed to the conservative forces $\mathbf{f}_{\text{con}} = \mathbf{K}\mathbf{x}$. It is also important to realize that these non-conservative forces \mathbf{f}_{non} always act in a perpendicular direction to the rotor deflection, as can be seen from the individual components $f_{\text{non}-x_1} = \omega c x_2$ and $f_{\text{non}-x_2} = -\omega c x_1$. In fact, this is the essence of this kind of self-excitation mechanism in rotating systems.

To investigate the stability of the system for a given rotational speed, we expand the system described by Eqs. (1.24) and (1.25) to a first order system

$$\dot{\mathbf{y}} = \mathbf{A}\mathbf{y} \quad (1.26)$$

with

$$\mathbf{y} = [x_1, x_2, \dot{x}_1, \dot{x}_2]^T, \quad \mathbf{A} = \begin{bmatrix} \mathbf{0} & \mathbf{I} \\ -\mathbf{M}^{-1}(\mathbf{K} + \mathbf{N}) & -\mathbf{M}^{-1}\mathbf{C} \end{bmatrix}, \quad (1.27)$$

and calculate the eigenvalues of \mathbf{A} . We obtain two pairs of conjugate complex eigenvalues

$$\lambda_{1,2} = \frac{-c + \sqrt{c^2 - 4mk \pm i4mc\omega}}{2m}, \quad (1.28)$$

$$\lambda_{3,4} = \frac{-c - \sqrt{c^2 - 4mk \pm i4mc\omega}}{2m}. \quad (1.29)$$

1.2. Parametric excitation in mechanical systems

The critical rotor speed ω_{crit} for the onset of self-excited vibrations can be determined from $\max(\Re(\lambda_{1,2}(\omega_{crit})), \Re(\lambda_{3,4}(\omega_{crit}))) = 0$, and for the externally undamped system we obtain the natural (bending) frequency of the rotor as the critical speed

$$\omega_{crit} = \sqrt{\frac{k}{m}}, \quad (1.30)$$

as one can see from substituting Eq. (1.30) into Eq. (1.28)

$$\frac{-c + \sqrt{c^2 - 4mk \pm i4m\omega_{crit}}}{2m} = \frac{-c + \sqrt{(c \pm i2\sqrt{mk})^2}}{2m} = \pm i\sqrt{\frac{k}{m}}. \quad (1.31)$$

Of course, in a real rotor system there is always some external damping present, and this additional damping would shift away the critical speed ω_{crit} from the natural frequency towards higher speeds.

This example points out a basic principle of self-excitation frequently encountered in rotor dynamics. A very simple model has been employed to demonstrate the essence of the mechanism. As shown, non-conservative forces can be generated due to internal damping of the shaft. However, such forces can also appear due to fluid forces within gaps between rotor and housing as encountered in labyrinth seals. For a comprehensive survey and an in-depth discussion of rotor instability the reader is referred to the rich literature in rotor dynamics, e.g. recent books as those by T. Yamamoto and Y. Ishida [101], by R. Gasch, R. Nordmann and W. Pfützner [26] and by D. Childs [13], or the classic book by A. Tondl [82].

1.2 Parametric excitation in mechanical systems

Many mechanical systems as well as electrical systems lead to differential equations with periodic, time-varying coefficients when a mathematical model is established. The expressions in the system equations with time-dependent coefficient(s) are frequently referred to as *Parametric Excitation*(PE).

The *playground swing* is frequently mentioned as a vivid explanation for parametric excitation [46]. When children (and sometimes adults)

enjoy the swing, they "pump" them up by moving up- and downwards to accelerate the swinging motion. Thereby they apply a parametric excitation to the swing (i.e. pendulum) by varying the effective length at twice the natural frequency of the pendulum. However, detailed investigations by W. Case [11], [12] on how a swing is operated effectively show that forced excitation plays the major role. But nevertheless, a pendulum can be excited by changing its length periodically, and therefore the practical explanation given is still of value.

1.2.1 Review on parametric excitation research

We will start this section with a very brief (and of course limited) review of the research on parametric excitation as conducted in the past for readers interested in the historical background. First scientific studies on parametrically excited systems date back to 1831 when M. Faraday studied a liquid in an open container subjected to a vertical vibration of a certain frequency and amplitude. As long as the amplitude of this effective gravity modulation remains below a critical threshold, the fluid surface is flat. For larger values an instability sets in and standing wave patterns appear on the surface, known as the so-called "Faraday instability". The critical amplitude can be predicted from the hydrodynamic equations of motion and their boundary conditions. As one might suppose, there is a close mechanical analogy to the parametrically driven pendulum, see T.B.Benjamin and F.Ursell [3].

The inducement of vibrations in a stretched string by varying its tension periodically was demonstrated by F. Melde more than a century ago, in 1860. Only a few years later, E. Mathieu studied natural modes of vibration of lakes with elliptical boundaries. The famous equation named after him has its roots in these investigations.

In 1883 J.W. Strutt, also known as the famous Lord Rayleigh, was the first to present theoretical studies that gave explanations for Faraday's instability and other related problems. At the same time G. Floquet developed a theory, commonly called Floquet-theory, that has become probably the most important mathematical method to treat differential equations with periodic coefficients. Much progress was achieved in that decade. In 1886 G.W. Hill published his stability theory of parametric systems. His findings solved a practical problem and gave satisfactory explanation for unsolved problems in celestial mechanics (motion of the earth's moon). Also, his name was given to the general class of peri-

1.2. Parametric excitation in mechanical systems

odic differential equations. Hill's work inspired Rayleigh, who, in 1887, generalized Hill's derivations and established a theory for second order systems including losses or damping.

In the middle of the last century E. Mettler [51], [52] and V.V.Bolotin [6], [7] contributed significantly to the understanding of parametrically excited vibrations. Their works mark the beginning of an increasing interest in this kind of vibrations. Other classical resources are the famous books by J.J. Stoker [79], H. Kauderer [41] and W. Magnus and S. Winkler [45]. About a decade later, G. Schmidt [71] and A. Nayfeh and D.T. Mook [59] summarized the state-of-art in PE research.

Since then, numerous contributions were published, as one can see from the references given by A. Richards in [69] and M. Cartmell [10] which cover the next decade. Even a short review of the achievements during the last 15 years would fill a dozen pages. To illustrate this statement let us just point out that even the most simple equation with parametric excitation, the well-known Mathieu equation, is still being investigated and new results were found recently, see e.g. Kidachi and Onogi [42] and R.H. Rand [68]. However, an overview with respect to mathematical methods suitable for PE-systems will be given in Chapter 2.

1.2.2 Parametric resonance

One of the main characteristics of a system with parametric excitation (PE) is the fact that a vibration response may occur when the PE-frequency is an integer-multiple or fractional-multiple of the system's natural frequency (or frequencies). The motion that is observed for such a response grows exponentially with time and, hence, the system is said to be unstable. In such a case the amplitudes would, theoretically, be unlimited. However, in a real system nonlinear effects also play an important role and will bound the amplitudes, if the system is still functional at this vibration level. With respect to this behavior, parameter excitation and self-excitation resemble each other. Energy provided by an energy source to periodically change a system parameter is absorbed by the system and increases the overall energy level. The example of the playground swing, as mentioned before, illustrates this mechanism. Work done by the person on the swing by moving the body up and down is converted into kinetic energy of the swinging motion. As long as the energy input is maintained, the transfer will continue.

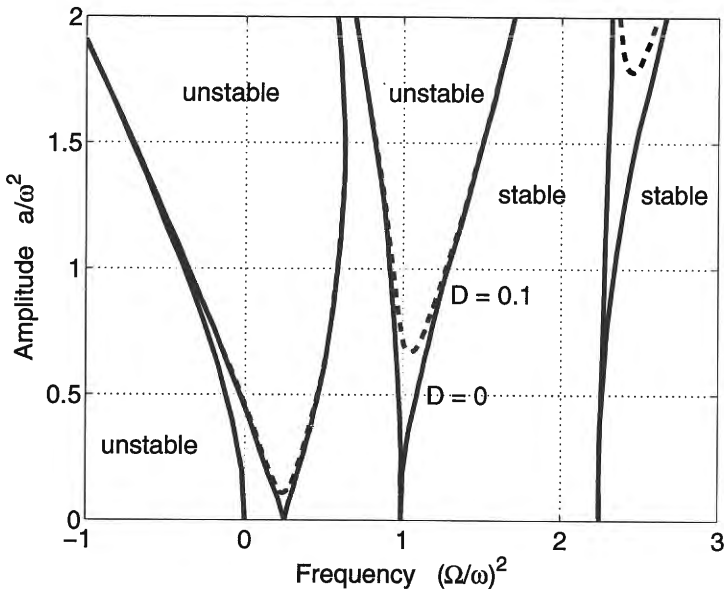


Figure 1.6: Stability chart for a single degree of freedom system as defined by Eq.(1.32)

Damping is also an important factor in PE-excited systems, although it cannot limit vibration amplitudes as in externally excited systems. A sufficiently high level of damping in a system can inhibit the system from becoming unstable at a certain PE-frequency and PE-amplitude. However, the frequency range where instability may occur sometimes also becomes larger with increasing damping.

Let us first consider a single degree of freedom system with additional harmonic stiffness variation as the parametric excitation

$$\ddot{x} + D\dot{x} + (\Omega^2 + a \cos \omega t) x = 0. \quad (1.32)$$

Of course one recognizes the damped version of the Mathieu equation. Figure 1.6 shows the well-known stability chart for such a system. Stable and unstable system behavior is plotted as a function of the normalized and squared values of the PE-frequency and -amplitude. For the case

1.2. Parametric excitation in mechanical systems

when damping is zero $D = 0$ and $\omega \geq 0$, the areas of instability have the shape of tongues that meet the horizontal axis at certain frequencies for the parametric excitation. An infinitesimally small excitation amplitude a can destabilize the system if the parametric resonance condition

$$\frac{2\Omega}{n} = \omega \quad (n = 1, 2, 3, \dots) \quad (1.33)$$

is fulfilled. The integer n is frequently named the *order of resonance*, with $n = 1$ being the first order or main parametric resonance. It occurs when the PE-frequency ω is twice the natural frequency Ω of the undamped system without PE. We recall that "pumping" a swing is done at this very frequency. One can also see that with an increasing level of the PE-amplitude the instability not only occurs at a distinct frequency but within a frequency range. This makes it easier to intentionally operate at a parametric resonance (swing pumping), but on the other hand it might be difficult or even impossible to avoid a PE-resonance in other cases. For higher orders of the parametric resonance and sufficiently high levels of excitation, the resonance condition predicted and calculated by Eq. (1.33) may even lie outside the range actual of instability.

If damping is present ($D > 0$), an excitation amplitude a exceeding a critical value of $a_{crit} \sim D^{1/n}$ is necessary for destabilization. This shows that higher-order parametric resonances ($n > 2$) are in general of little or no importance.

Although the Mathieu equation is a linear differential equation, there is no solution in terms of standard functions. We will discuss methods to investigate such systems and how to obtain charts like Fig. 1.6 in the next chapter.

Let us now consider multi-degree of freedom systems with parametric excitation. For simplicity we consider just the undamped system, expressed in a normalized notation

$$\ddot{\mathbf{x}} + \mathbf{\Omega}^2 \mathbf{x} + \cos(\omega t) \mathbf{P} \mathbf{x} = 0 \quad (1.34)$$

with k generalized coordinates $\mathbf{x} = [x_1, x_2, \dots, x_k]^T$ and

$$\mathbf{\Omega}^2 = \text{diag}(\Omega_1^2, \Omega_2^2, \dots, \Omega_k^2), \quad \mathbf{P} = \begin{bmatrix} p_{11} & \cdots & p_{1k} \\ \vdots & \ddots & \vdots \\ p_{k1} & \cdots & p_{kk} \end{bmatrix} \quad (1.35)$$

as the Ω_k natural frequencies of the system. Matrix \mathbf{P} denotes the amplitudes of the parametric excitation at frequency ω .

With the existence of k natural frequencies the parametric resonance conditions become more complicated. First of all Eq. (1.33) is still valid, if we extend it to all frequencies Ω_k present in the system. We obtain the condition

$$\frac{2\Omega_j}{n} = \omega, \quad (n = 1, 2, 3, \dots), (j = 1 \dots k), \quad (1.36)$$

for the *principal parametric resonances* of the n -th order of the system. In addition to that, resonances may also appear at frequencies corresponding to the sum or the difference of the natural frequencies [30]. These frequencies are nowadays called *parametric combination resonances*, older sources [100] refer to them as vibrations of "summed and differential type".

The condition for dual combination resonance of order n is

$$\frac{|\Omega_i \pm \Omega_j|}{n} = \omega \quad (n = 1, 2, 3, \dots), (i, j = 1 \dots k). \quad (1.37)$$

It is worth noting that also triple combination resonances (consisting of a combination of three frequencies) are possible and have been reported by M. Cartmell [10]. What has been said for the parametric resonances of the Mathieu equation with respect to PE-amplitudes and damping is also valid to a large extent for the principal resonances and the combination resonances of multi-degree of freedom systems. References [71], [100] and [84] discuss various aspects of both types of parametric resonances in detail, show measurement results and also refer to further literature.

In technical systems parametric resonances can be either a good and desirable feature or a bad, sometimes even dangerous characteristic. Parametric excitation can be employed to feed energy into a system. There are a number of applications ranging from physics (particle accelerators) to electrical engineering (parametric amplification), see [10] for an overview and some references. At a parametric resonance the system may exhibit high vibration levels, which is useful in mechanical engineering for some applications as well. For example, A. Olvera et al. [62] improve the performance of oscillating water column (OWC) systems by taking advantage of a parametric resonance.

On the other hand, parametric excitation can be a nuisance when it causes acoustic problems or excessive wear. But it can also be the reason for a severe malfunction of a machine or structure. For example, a longitudinal excitation in power transmission chains or belts can

1.2. Parametric excitation in mechanical systems

cause severe transversal vibrations. A beam or column under oscillating axial loading is also a parametrically excited system. In such a case the static critical load for a failure (buckling) of the structure is significantly reduced and can lead to dangerous situations. A.Tondl reports in [72] about excessive lateral vibrations in an elevator due to the periodically changing stiffness of guidance rails.

1.2.3 Stabilization by parametric excitation

In the previous section basically the effect of destabilizing a system and generating large oscillations (for better or for worse) by parametric excitation was discussed. But in contrast, parametric excitation also offers the possibility to stabilize an otherwise unstable system. The famous example to prove that this is also possible, is the stabilization of an inverted pendulum. A pendulum with vertical base excitation can be described by the Mathieu equation, as given by Eq. (1.32), if we consider $x = \phi$ as the angular deflection of the pendulum. Instead of a detailed discussion of the inverted pendulum we just refer to Fig. 1.6 to point out briefly the basic idea. In this figure a small area of stability emanates from $0 \leq (\Omega/\omega)^2 \leq 0.25$ and reaches into the region of negative PE-frequencies. This area covers combinations of the PE-frequency and PE-amplitude at which the inverted pendulum can be stabilized in its upside down position. To visualize how the inverted pendulum works, without designing an actual experiment, F.J.Elmer has set up a very nice virtual lab on his webpage [24]. Note that for an appropriate set of parameters the inverted position of the pendulum is stable but nevertheless a slow oscillatory motion occurs. This principle is e.g. used in an application in experimental physics when a single ion is caught in a quadrupole mass spectrometer and the equilibrium point of the static electrical field is stabilized by superimposing a rapid oscillation to that field.

The stabilization of the inverted pendulum and all similar applications are related to some extent to the main idea of the research presented in the following chapters: *employing parametric excitation to cancel or reduce self-excited vibrations*. But before giving a short description of this concept let us review those very few publications (from authors other than H. Ecker and/or A. Tondl) that follow a similar concept.

In his thesis P.H. Nguyen [60] explores possibilities for vibration control of non-autonomous dynamic systems using a technique where a sec-

ondary disturbance is supplied to the system with the goal of reducing vibrations. The fundamental concept is to generate a secondary harmonic excitation which appears as time-varying coefficients in the governing equations of motion, i.e. as a parametric excitation. In his work he studies a single-dof system with the parametric excitation appearing as the stiffness coefficient, the damping coefficient, and both coefficients of the governing equation of motion. Cases under consideration are vibration control of the pendulum using a sliding pivot, vibration control of single-dof systems using a modulated stiffness or damping constant, and control of flexural vibration of a simply supported beam using a sliding mass or support. In the case of the beam, the standard/modified Ritz series method is employed in the formulation of the equations of motion. The responses are obtained through numerical integration of the equations of motion. In a special case, an analytical method is applied to validate the numerical work. Nguyen concludes that parametric excitation generated by the dynamics of the systems can reduce the forced response amplitude, as in the cases of the pendulum and the simply supported beam. In contrast, parametric excitation induced by modulating the system parameters does not seem to be effective for vibration control of a SDOF-system with modulated stiffness/damping constants.

H. Okubo et al. [61] investigate the high-speed operation of industrial machines equipped with belt driving systems. The belt is subject to a speed limitation barrier due to the occurrence of bending mode vibration resonances caused by machinery error, for example pulley eccentricity. To fight these resonances of the linear system, the parametric excitation method providing a belt tension fluctuation is proposed through the concept of open-loop vibration control theory. This analysis considers two types of fluctuation excitation featured by the frequency synchronized with one or two times the pulley revolution. In that paper, the mathematical model is analyzed by using the equation of motion of the forced vibration including the parametric excitation.

In their paper [50] R.McDonald and N. Sri Namachchivaya study the stabilization of a gyroscopic system using parametric stabilization near a combination resonance. A gyroscopic system operates near its primary instability, i.e. the bifurcation parameter is such that the system possesses a double zero eigenvalue. The stability of the system is studied for the linear Hamiltonian system, the damped linear system, the forced linear Hamiltonian system, and finally the damped and forced linear system. The addition of the periodic excitation near the critical

1.3. Parametric Vibration Cancelling

combination resonance provides the system with an extended stability region when the excitation frequency is slightly above the combination resonance. This extended stability region is also shown to persist when nonlinearity is added to the system. The results of this work are then discussed for a rotating shaft with periodically perturbed rotation rate.

Non of the previously mentioned papers [60], [61] and [50] are clearly devoted to the task of cancelling self-excited vibrations by means of parametric excitation in a general manner. However, a research group of mathematicians at the University of Utrecht is active in this field and works on similar ideas as A. Tondl and the author. Recently two dissertations [25], [1] have been finished under the supervision of F. Verhulst.

In [25] S. Fatimah investigates the same self-excited two-mass system with a main mass and an absorber mass as the author and A. Tondl in [18]. She employs the averaging method and numerical bifurcation techniques to study the system. A first order approximation is used to analyze the conditions for full vibration suppression. Interesting new results are obtained for the case of a small absorber mass by deriving a second-order approximation. A better qualitative agreement with numerical results is obtained for this approximation compared to previous results. For parameter sets where quenching cannot be achieved, Hopf bifurcations and Neimark-Sacker bifurcations are identified. Also a brief study on self-excited three-mass systems with parametric excitation is included in [25].

Abadi studies the interaction between self-excited and parametric interaction in [1] and uses simplified models of a massless rod or slender structure with concentrated masses which again lead to two- and three-mass systems. For the three-mass system a symmetric and a non-symmetric case are investigated with a 1:2:3 resonance of the quasi-normal system. Concerning the suppression of self-excited vibrations, the importance of the Hopf bifurcation of the non-trivial solution is pointed out.

1.3 Parametric Vibration Cancelling

From the previous introduction it (certainly) has become evident that self-excited vibrations can be an important problem in mechanical systems. For many years, researchers have dealt with different methods to either avoid or to cancel such vibrations. Among others, A. Tondl

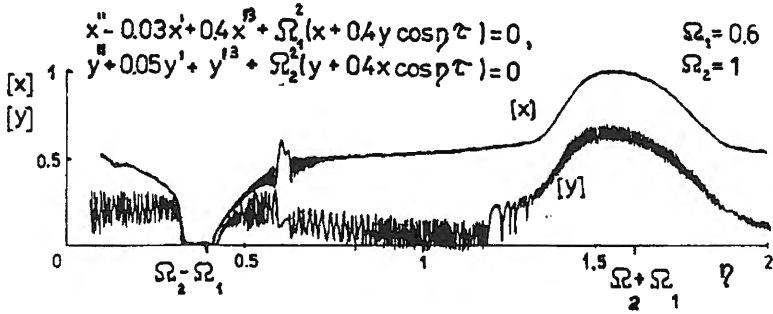


Figure 1.7: Simulation result (obtained with an analog computer) of a self-excited system exhibiting vibration quenching near the parametric combination resonance frequency $\eta_0 = \Omega_2 - \Omega_1$ (from [85] and [87]).

worked in this field in the 70's and investigated the interaction between self-excited vibrations and forced vibrations in [83] and also with respect to parametric excitation in [84]. At that time he encountered the phenomenon that in systems with self-excitation, parametric excitation is capable of completely suppressing self-excited vibrations within certain intervals of its frequency. About ten years later, simulation results for a two-mass system obtained with an analog computer were published in [85], clearly showing vibration suppression at a parametric combination resonance frequency, see Fig. 1.7.

Again, these remarkable observations almost fell into oblivion, but in the late 90's the idea was picked up again by Tondl and analytical conditions for full vibration quenching were formulated in [87]. Let us briefly repeat and summarize the main results of this paper, since it marks the starting point for the increasing interest in this phenomenon.

In [87] a generic linear system of differential equations in normal form with parametric excitation

$$x_s'' + \Omega_s^2 x_s + \varepsilon \sum_{j=1}^n [\Theta_{sj} x_j' - Q_{sj} x_j \cos(\eta \tau)] = 0, \quad (s = 1, 2, \dots, n) \quad (1.38)$$

is considered. Coefficients Θ_{sj} and Q_{sj} are constant and parameter ε is assumed to be small $\varepsilon \ll 1$. In general, instability intervals for the

1.3. Parametric Vibration Cancelling

trivial solution $x_s = x'_s = 0$ may occur in a parametrically excited system near the combination resonance frequencies $\eta_0 = |\Omega_s \mp \Omega_j|$, ($s \neq j$). By applying a method for the determination of quasiharmonic vibrations [81] Tondl obtains a stability condition for the case that all Θ_{jj} are positive. Stability of the trivial solution in the vicinity of a combination resonance frequency η_0 is possible for parametric excitation frequencies

$$\eta = \eta_0 \pm \varepsilon\alpha \quad (1.39)$$

if α satisfies the condition

$$\alpha^2 + \frac{(\Theta_{ss} + \Theta_{jj})^2}{4\Theta_{ss}\Theta_{jj}\eta_0^2} \left(\mp \frac{Q_{sj}Q_{js}}{4\Omega_s\Omega_j} + \Theta_{ss}\Theta_{jj} \right) > 0. \quad (1.40)$$

The minus sign in Eq. (1.40) corresponds to the sum $\Omega_s + \Omega_j = \eta_0$ and the plus sign to the difference $\Omega_s - \Omega_j = \eta_0$ of the natural frequencies of the system. The parametric instability interval

$$\eta_0 - \varepsilon\alpha_{lim} < \eta < \eta_0 + \varepsilon\alpha_{lim} \quad (1.41)$$

is obtained from Eq. (1.40) by changing the inequality to an equation that is solved for the limit value α_{lim} at the (in)stability boundary.

In the case that one of the damping coefficients Θ_{ss} is negative, the trivial solution of the system $x_s = x'_s = 0$ can become unstable, and self-excited vibrations may occur for the system without parametric excitation. However, with $Q_{sj} \neq 0$ the stability analysis [81] can be carried out again for the negative damping coefficient. In order to keep track of signs and use positive values in the following relationships, the substitutions $\Theta_{ss} = -\delta_s < 0$, $\Theta_{jj} = \delta_j > 0$ are used and lead to the following form of the two conditions for stability:

$$\delta_j - \delta_s > 0, \quad (1.42)$$

and

$$\alpha^2 > \frac{(\delta_j - \delta_s)^2}{4\delta_s\delta_j\eta_0^2} \left(\mp \frac{Q_{sj}Q_{js}}{4\Omega_s\Omega_j} - \delta_s\delta_j \right). \quad (1.43)$$

The inequality has changed now from Eq. (1.40) to Eq. (1.43), converting the former interval of *instability* in the neighborhood of η_0 into an interval of *stability*, due to the action of the parametric excitation

$$\eta_0 - \varepsilon\alpha_{lim} < \eta < \eta_0 + \varepsilon\alpha_{lim}. \quad (1.44)$$

The limit value α_{lim} at the stability boundary is calculated by using relationship (1.43) and changing the relational operator from $<$ to $=$. Now the plus sign in Eq. (1.43) corresponds to the sum $\eta_0 = \Omega_s + \Omega_j$ and the minus sign to the difference $\eta_0 = \Omega_s - \Omega_j$. Of course it is necessary that $Q_{sj}Q_{js} < 0$ holds to achieve an interval of stability at $\eta_0 = \Omega_s + \Omega_j$.

In summing up Tondl's findings, we emphasize that self-excited vibrations can be cancelled in principle at a PE-frequency of $\eta \simeq |\Omega_s \mp \Omega_j|$ when the combination parametric resonance occurs at $\eta_0 = |\Omega_s \pm \Omega_j|$. Whether vibration suppression (full cancellation or attenuation of vibration) is achieved or not depends on two conditions which have to be satisfied. In addition to that, the limitations of the approximative analytical method used in this analysis, have to be taken into consideration. In the following Chapter 2 we will discuss analytical results as well as numerical methods to calculate the intervals for vibration cancellation in details.

1.4 Realization of parametric excitation

As the last topic within this introductory chapter we will present some ideas on how parametric excitation can be realized in a mechanical system.

Figure 1.8 shows a number of different possibilities to achieve a continuously and periodically changing stiffness in mechanical systems. On top of the figure two examples of a direct stiffness modulation are shown. In Fig. 1.8(a) a cantilever beam is depicted with a sliding support within the free span of the beam. By moving this support periodically, a time-dependent bending stiffness of the beam is obtained. Figure 1.8(b) shows two linear springs connected to each other on one end. This point of connection represents the center of a circular guideway that guides both other ends of the springs. These spring anchor points are moved periodically along the guideway, which leads to a varying effective stiffness in the vertical direction.

A different approach is used in the next two examples. Figure 1.8(c) shows a beam (or column) which is loaded axially by a periodically changing force. This leads to a periodically changing effective bending stiffness of the beam. A quite similar system is shown in the next Figure (d), where a string is put under tension by a constant force. An

1.4. Realization of parametric excitation

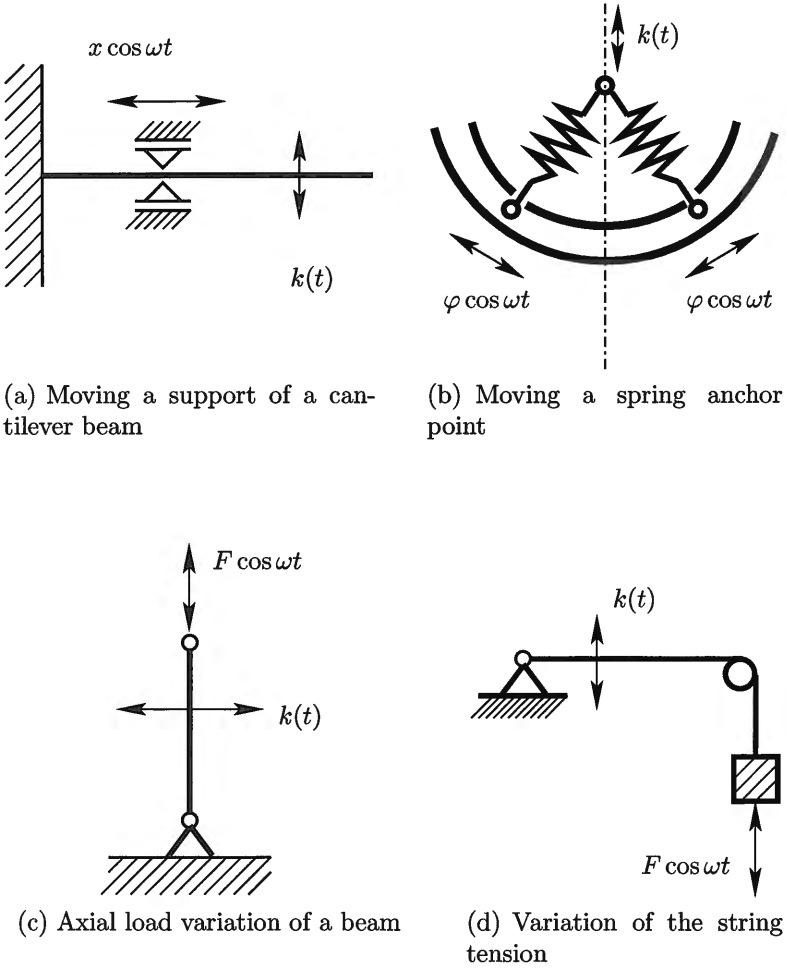


Figure 1.8: Some examples for the realization of continuous parametric stiffness excitation

additional time-varying force is superimposed to the constant tension resulting in a periodically varying string tension. As a consequence, the lateral stiffness of the string also changes with time and may be utilized in a more complex system.

Further design examples are shown in Fig.1.9. Figure (a) on top depicts the well-known pendulum with base excitation as an example for another different mechanism that can be employed. Note that no real spring or mechanical stiffness is present in this system. Accelerating the anchor point of the pendulum harmonically in the vertical direction can be seen as a "quasi-modulation" of the gravity field. Consequently, the restoring moment of the gravity force changes periodically, which has the same effect on the pendulum as if a stiffness is changed. The second figure on top shows an air cushion spring with a pressure supply pump that maintains a periodically changing air pressure within the cushion. It is obvious that this system has a time-varying vertical stiffness.

In some situations it might be easier to achieve a discontinuous variation of a stiffness parameter. Of course a true discontinuous behavior in a mechanical system is rarely seen, if at all. So what is addressed here is a change of stiffness which occurs much (a magnitude) faster than the stiffness variation in the previous examples. In Figs.1.9(c) and (d) two different designs are outlined, just to show that this is also an option for a parametric stiffness variation.

Figure 1.9(c) shows a torsional system with a secondary shaft that can be engaged or disengaged by a clutch. Although a clutch also needs some time to become effective, this system will allow for comparatively fast changes of a torsional stiffness in the system. The second example 1.9(d) presents again a cantilever beam, but this time the fixity of the beam is brought about by two very fast moving stops that clamp the beam vertically and also release at the same speed. Thereby the bending stiffness of the beam can be switched from one value to another.

The design examples shown shall give the interested reader some ideas on how a periodically changing stiffness can be achieved in a mechanical system. Of course there exist more design possibilities even if the design is restricted (almost) exclusively to mechanical components. For mechatronic systems, which may incorporate also electrical components, a much large number of different solutions are conceivable.

1.4. Realization of parametric excitation

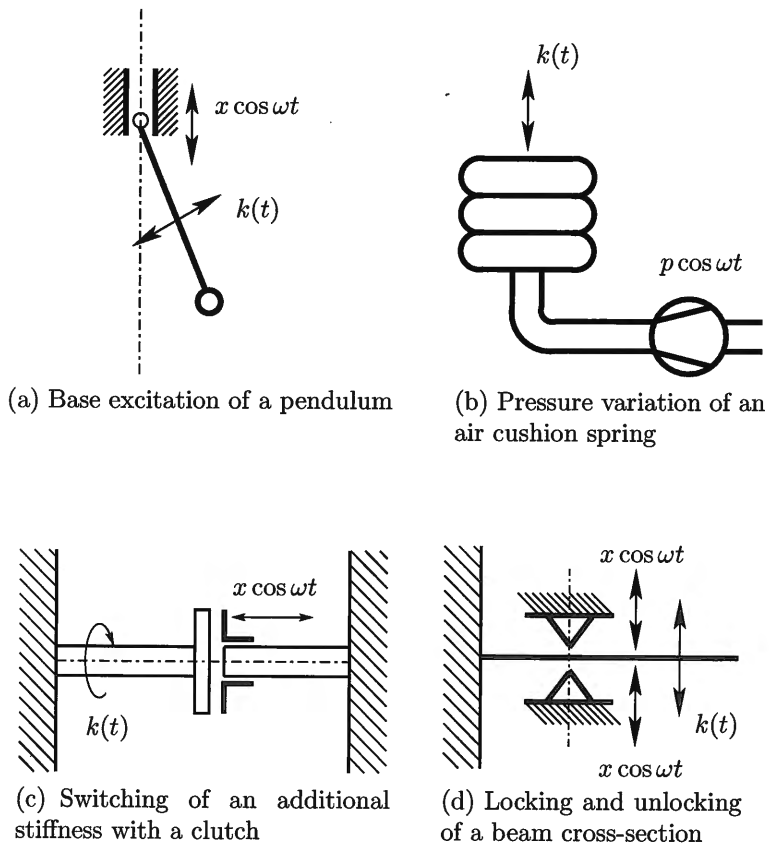


Figure 1.9: Examples of continuous and discontinuous parametric stiffness excitation

Chapter 2

Analysis of systems with periodic coefficients

As discussed in Section 1.2.1, there has been an interest in systems with time-varying coefficients for a long time. Consequently, also mathematical methods to study such systems have been developed already by the pioneers in this field (E. Mathieu, J.W. Strutt alias Lord Rayleigh, G. Floquet, G.W. Hill, A.M. Lyapunov). A. Nayfeh and D.T. Mook [59] give a comprehensive review on early works and also devote a large chapter to basic methods for PE-systems. Other classical resources for mathematical methods are the books of V.A. Yakubovich and V.M. Starzhinskii [99] and G. Schmidt [71] which almost exclusively deal with PE. Other more recent books and textbooks which discuss mathematical methods for PE-systems are [69], [10], [103], [67] and [96].

Different methods have been developed to investigate systems described by differential equations with periodic coefficients and to study their stability behavior. Hill's infinite determinant method [99], the Averaging Method [58], [96], the perturbation technique [59] and the application of Floquet theory [103] are widely used classical methods. Each method has its own specific advantages and disadvantages, areas of suitability and limitations. Discussions and comparisons can be found e.g. in [53], [10], [76], [77], [98] and others. Criteria for the selection of an appropriate method depend on whether the system is linear (or can be linearized), the existence of a small parameter to apply perturbation methods, the size (dimension) of the system and other factors.

In the past, the analysis of time-periodic dynamical systems has made significant progress due to research in this scientific field conducted at various places around the world. S.C. Sinha and his group have published a number of papers during the last several years, e.g. [76], [63], [77], [9], proposing and applying a general technique for the computation of the Floquet-Lyapunov transformation. They show how stability and bifurcation boundaries of time-periodic linear and nonlinear systems can be analyzed.

P. Montagnier and co-authors worked on the numerical integration of linear time-periodic systems [54]. They investigate a spectral method to compute the state-transition matrix of a linear system. By using Chebyshev polynomials to calculate an approximation of the state-transition matrix of the original problem, they avoid the usual way of direct numerical integration of the system, which can be advantageous in certain cases.

In [75] A.P. Seyranian and P. Pedersen introduce sensitivity analysis to general linear periodic systems. A general theory is presented, based on the classical Floquet method for evaluating stability and perturbation technique in the parameter space. Starting from first and higher-order derivatives of the Floquet matrix with respect to problem parameters, the behavior of simple and multiple multipliers of the system is studied under a variation of parameters.

A different approach to the stability analysis of periodic systems is discussed by R.S. Guttalu and H. Flashner in [29] and previous papers cited therein. Their method is based on a point mapping representation of the system's dynamic, introduced by C.S. Hsu [37], [38] and [39]. Guttalu and Flashner present an algorithm to obtain analytical expressions for the point mapping and its dependence on system parameters. The algorithm derives the coefficients of a multinomial expansion of the point mapping up to an arbitrary order in terms of the state variables and of the parameters. Analytical stability and bifurcation conditions are then formulated and expressed as functional relations between the parameters. It is shown that, unlike the perturbation analysis, the proposed method provides very accurate solutions even for large values of parameters and its accuracy is comparable with results obtained from direct numerical integration.

A recently developed approach to investigate the stability of finite-dimensional linear continuous-time periodic (FDLCP) systems is presented in [102] by J. Zhou and T. Hagiwara. Asymptotic stability of

2.1. Analytical methods

FDLCP-systems is studied by harmonic analysis. It is first shown that stability can be examined by the so-called harmonic Lyapunov equation. From this generalized Lyapunov equation, another necessary and sufficient stability criterion is developed. This reduces the stability test to the examination of an approximate FDLCP model whose transition matrix can be determined explicitly.

This overview shall help an interested reader to get started with this class of dynamical systems. It also shows that there are many different methods available or under development to treat parametrically excited systems. A reason for this variety of approaches are the intrinsic difficulties associated with such systems which have interested and challenged scientists for many years. Although quite a number of references were cited in the survey above, this is still an incomplete summary, and numerous further works do exist that could not be mentioned for various reasons.

The following content of this chapter basically consists of two sections. The first section will deal with analytical methods and the second one with numerical methods. The detailed discussions will be restricted to methods that have been applied and found to be useful by the author in the course of studying parametrically excited mechanical systems.

2.1 Analytical methods

In this section three different analytical methods will be presented. We will start with the Method of Successive Approximation which makes use of a method to solve integral-differential equations. Very general results will be obtained for a set of two differential equations. Next, the Method of Averaging is briefly discussed and also applied to a system as used later in the sections containing detailed investigations and numerical examples. Last but not least, a method created and used intensively by A. Tondl to investigate systems with parametric excitation will be presented and an overview on his method will be given. Finally, conclusions will be drawn in a summary on analytical methods.

2.1.1 Method of Successive Approximation

The Integral Equation Method in combination with the Method of Successive Approximation was comprehensively presented and extensively

used by G. Schmidt in [71] and [72] to treat parametrically excited systems. For the sake of completeness the basic concept is summarized in a few lines.

A system of second order differential equations is considered

$$y_i'' + \lambda_i y_i = \Phi_i, \quad (i = 1, 2, \dots, N), \quad (2.1)$$

with primes indicating derivatives with respect to a dimensionless time τ . On the right-hand side time-dependent nonlinear functions

$$\Phi_i = \Phi_i(\tau) = \Phi_i(y_i, y_i', \varepsilon_p; \tau) \quad (2.2)$$

appear, which may also depend on constant parameters ε_p , ($p = 1, 2, \dots, P$). One can prove [71] that every periodic solution of the differential equations (2.1) is also a solution of the integro-differential equations

$$y_i(\tau) = \int_0^{2\pi} G_i(\tau, \sigma) \Phi_i(\sigma) d\sigma + \delta_{\lambda_i}^{n_i^2} (r_i \cos n_i \tau - s_i \sin n_i \tau), \quad (2.3)$$

where the Kronecker symbol

$$\delta_\mu^\nu = \begin{cases} 1 & \text{for } \mu = \nu, \\ 0 & \text{otherwise} \end{cases} \quad (2.4)$$

is used and

$$G_i(\tau, \sigma) = \frac{1}{\pi} \left[\frac{1}{2\lambda_i} + \sum_{\nu=1}^{\infty} \frac{\cos \nu(\tau - \sigma)}{\vartheta \lambda_i - \nu^2} \right] \quad (2.5)$$

are corresponding generalized Green's functions. Symbol ϑ is defined as

$$\vartheta = \vartheta_\mu^\nu = 1 - \delta_\mu^\nu, \quad (2.6)$$

and is introduced to prevent the denominator from vanishing. The bifurcation parameters r_i, s_i appearing in the resonance case

$$\lambda_i = n_i^2 \quad (2.7)$$

are determined from the bifurcation (periodicity) equations

$$r_i = \frac{1}{\pi} \int_0^{2\pi} y_i(\tau) \cos n_i \tau d\tau, \quad s_i = \frac{1}{\pi} \int_0^{2\pi} y_i(\tau) \sin n_i \tau d\tau, \quad (2.8)$$

2.1. Analytical methods

which are equivalent to

$$\int_0^{2\pi} \Phi_i(\tau) \cos n_i \tau d\tau = \int_0^{2\pi} \Phi_i(\tau) \sin n_i \tau d\tau = 0. \quad (2.9)$$

The basic step of the Integral Equation Method is that instead of solving Eqs. (2.1) one evaluates Eqs. (2.3). The solution of Eqs. (2.3) and (2.8), resp. Eqs. (2.9) can be found by the Method of Successive Approximation based upon the following equations for the approximative solutions

$$y_{ik}(\tau) = \int_0^{2\pi} G_i(\tau, \sigma) \Phi_{i,k-1}(\sigma) d\sigma + \delta_{\lambda_i}^{n_i^2} (\tau_i \cos n_i \tau - s_i \sin n_i \tau) \quad (2.10)$$

where

$$\Phi_{i0}[\tau] = \Phi_i(0, 0, \varepsilon_p; \tau), \quad (2.11)$$

$$\Phi_{ik}[\tau] = \Phi_i(y_{jk}, y'_{jk}, \varepsilon_p; \tau), \quad (k = 1, 2, 3, \dots).$$

The convergence of the method can be proved for parameters ε_p which do not have to be small, but may not exceed certain upper limits, see [71].

The Method of Successive Approximation is based on the Integral Equation Method and is a method to solve analytically the boundary value problem with periodic boundary conditions

$$\begin{aligned} y_i'' + \lambda_i y_i &= \Phi_i(y_i, y'_i, \varepsilon_p; \tau) & (i = 1, 2, \dots, N) \\ y_i(0) &= y_i(2\pi) \\ y'_i(0) &= y'_i(2\pi) \end{aligned} \quad (2.12)$$

by a stepwise (successive) approximation of the solution. For the analysis of parametrically excited systems this method has proven to be very useful. In [23] N. Eicher uses the method to investigate parametric resonances of systems of differential equations and we will apply his results in the following.

In this monograph mainly two mass systems are considered. One reason is that this size of problem can still be handled analytically. We will start from a general, homogeneous system of two linear differential equations of second order as it is used for mechanical systems with two

degrees of freedom. The normal form representation of such a system is expanded by a general, coupled, harmonic parametric excitation:

$$\begin{aligned} u_1'' + \Theta_{11}u_1' + \Theta_{12}u_2' + \lambda_1 u_1 - (Q_{11}^c \cos m\tau + Q_{11}^s \sin m\tau)u_1 & \quad (2.13) \\ - (Q_{12}^c \cos m\tau + Q_{12}^s \sin m\tau)u_2 & = 0, \end{aligned}$$

$$\begin{aligned} u_2'' + \Theta_{21}u_1' + \Theta_{22}u_2' + \lambda_2 u_2 - (Q_{21}^c \cos m\tau + Q_{21}^s \sin m\tau)u_1 & \quad (2.14) \\ - (Q_{22}^c \cos m\tau + Q_{22}^s \sin m\tau)u_2 & = 0. \end{aligned}$$

The arbitrary frequencies $\lambda_{1,2}$ are represented by predetermined frequencies $\Lambda_{1,2}$ with special properties (see below) and a frequency variation $\alpha_{1,2}$

$$\lambda_i = \Lambda_i(1 - \alpha_i), \quad (i = 1, 2). \quad (2.15)$$

Now Eqs. (2.13) and (2.14) can be rearranged and written as a matrix equation

$$\mathbf{u}'' + \Lambda \mathbf{u} = -\Theta \mathbf{u}' + \alpha \Lambda \mathbf{u} + (Q^c \cos m\tau + Q^s \sin m\tau) \mathbf{u} = \Phi(\mathbf{u}, \mathbf{u}', \alpha; \tau) \quad (2.16)$$

with

$$\begin{aligned} \mathbf{u} &= \begin{bmatrix} u_1 \\ u_2 \end{bmatrix}, & \Lambda &= \begin{bmatrix} \Lambda_1 & 0 \\ 0 & \Lambda_2 \end{bmatrix}, \\ \Theta &= \begin{bmatrix} \Theta_{11} & \Theta_{12} \\ \Theta_{21} & \Theta_{22} \end{bmatrix}, & \alpha &= \begin{bmatrix} \alpha_1 & 0 \\ 0 & \alpha_2 \end{bmatrix}, & (2.17) \\ Q^c &= \begin{bmatrix} Q_{11}^c & Q_{12}^c \\ Q_{21}^c & Q_{22}^c \end{bmatrix}, & Q^s &= \begin{bmatrix} Q_{11}^s & Q_{12}^s \\ Q_{21}^s & Q_{22}^s \end{bmatrix}. \end{aligned}$$

To apply the Method of Successive Approximation in accordance with its mathematical background [71], N. Eicher restricts in [23] the predetermined frequencies

$$\begin{aligned} \Lambda_1 &= n_1^2, \\ \Lambda_2 &= n_2^2, & n_{1,2} &\in \mathbb{N}, & (2.18) \\ n_2 &> n_1 \end{aligned}$$

to integer values. This assumption does not impose the same restriction on frequencies $\lambda_{1,2}$ because of the real-valued frequency variation parameters $\alpha_{1,2}$, see Eq. (2.15). However, Eqs. (2.18) do have consequences which will become evident soon.

2.1. Analytical methods

It is known from [87] that parametric vibration cancelling will only occur at parametric combination resonance frequencies of the second kind. Since in general resonance frequencies of the first order are most pronounced, we restrict the analysis to second kind, order-one frequencies and define the parameter of the parametric excitation frequency m in Eq. (2.16) by the resonance condition

$$m = m^{(\pm)} = n_2 \pm n_1. \quad (2.19)$$

Note that this definition includes both types of second kind frequencies, the *difference type* $m^{(-)} = n_2 - n_1$ and the *summation type* $m^{(+)} = n_1 + n_2$. We will carry out further analysis for both types and symbol " (\pm) " will be used wherever we have to distinguish between both of them.

In Eqs. (2.15) the frequency variations α_i were introduced. With the approximations

$$\sqrt{\lambda_i} = \sqrt{\Lambda_i(1 - \alpha_i)} \doteq n_i \left(1 - \frac{\alpha_i}{2}\right) \quad (i = 1, 2) \quad (2.20)$$

$$\sqrt{\lambda} \doteq m \left(1 - \frac{\alpha}{2}\right) \quad (2.21)$$

and similar to Eq. (2.19)

$$\sqrt{\lambda} \doteq \sqrt{\lambda_2} \pm \sqrt{\lambda_1} \quad (2.22)$$

we obtain

$$\alpha m = \alpha_2 n_2 \pm \alpha_1 n_1. \quad (2.23)$$

With definition Eq. (2.19) the limitation on n_i in Eqs. (2.18) is transferred to the PE-frequency m and allows only integer values $m \in \mathbb{N}$. Of course, this would restrict the application of results quite severely. We will leave this problem aside for the moment, continue with the analysis and come back on this matter later.

Application of Successive Approximation to system Eq. (2.16) leads for the resonance case of Eqs. (2.18) to the zero order approximation

$$\begin{aligned} u_i^{(0)} &= 0, & (i = 1, 2) \\ \text{hence } \Phi_i^{(0)} &= 0. \end{aligned} \quad (2.24)$$

Based on the zero order approximation, the first order approximation is built according to Eq. (2.3). With Eq. (2.24) the integral term vanishes and as first order approximation the solution of the homogeneous

differential equations

$$u_i^{(1)} = r_i \cos n_i \tau + s_i \sin n_i \tau \quad (i = 1, 2) \quad (2.25)$$

is obtained with yet undetermined coefficients r_i , s_i . Substituting solution (2.25) into the right-hand side of system Eq.(2.16) leads to the definition equation

$$\mathbf{S} [r_1, s_1, r_2, s_2]^T = \mathbf{0} \quad (2.26)$$

with a partitioned matrix for a more clear presentation

$$\mathbf{S} = \begin{bmatrix} \mathbf{S}_{11} & \mathbf{S}_{12} \\ \mathbf{S}_{21} & \mathbf{S}_{22} \end{bmatrix}, \quad (2.27)$$

$$\mathbf{S}_{11} = \begin{bmatrix} \alpha_1 n_1^2 + \delta_m^{2n_1} \frac{Q_{11}^c}{2} & \delta_m^{2n_1} \frac{Q_{11}^s}{2} - \Theta_{11} n_1 \\ \delta_m^{2n_1} \frac{Q_{11}^s}{2} + \Theta_{11} n_1 & \alpha_1 n_1^2 - \delta_m^{2n_1} \frac{Q_{11}^c}{2} \end{bmatrix}, \quad (2.28)$$

$$\mathbf{S}_{12} = \begin{bmatrix} \delta_m^{(n_2(\pm)n_1)} \frac{Q_{12}^c}{2} & (\pm) \delta_m^{(n_2(\pm)n_1)} \frac{Q_{12}^s}{2} - \delta_{n_1}^{n_2} \Theta_{12} n_2 \\ \delta_m^{(n_2(\pm)n_1)} \frac{Q_{12}^s}{2} + \delta_{n_1}^{n_2} \Theta_{12} n_2 & (\pm) \delta_m^{(n_2(\pm)n_1)} \frac{Q_{12}^c}{2} \end{bmatrix}, \quad (2.29)$$

$$\mathbf{S}_{21} = \begin{bmatrix} \delta_m^{(n_2(\pm)n_1)} \frac{Q_{21}^c}{2} & \delta_m^{(n_2(\pm)n_1)} \frac{Q_{21}^s}{2} - \delta_{n_1}^{n_2} \Theta_{21} n_1 \\ (\pm) \delta_m^{(n_2(\pm)n_1)} \frac{Q_{21}^s}{2} + \delta_{n_1}^{n_2} \Theta_{21} n_1 & (\pm) \delta_m^{(n_2(\pm)n_1)} \frac{Q_{21}^c}{2} \end{bmatrix}, \quad (2.30)$$

$$\mathbf{S}_{22} = \begin{bmatrix} \alpha_2 n_2^2 + \delta_m^{2n_2} \frac{Q_{22}^c}{2} & \delta_m^{2n_2} \frac{Q_{22}^s}{2} - \Theta_{22} n_2 \\ \delta_m^{2n_2} \frac{Q_{22}^s}{2} + \Theta_{22} n_2 & \alpha_2 n_2^2 - \delta_m^{2n_2} \frac{Q_{22}^c}{2} \end{bmatrix}. \quad (2.31)$$

To exclude the simultaneous occurrence of combination resonances of the first kind and first order ($m = 2n_{1,2}$) together with the second kind resonance we may remove the responsible coefficients by setting

$$Q_{11,22}^{c,s} = 0, \quad \Theta_{12} = 0, \quad \Theta_{21} = 0. \quad (2.32)$$

2.1. Analytical methods

To obtain non-zero coefficients $r_i \neq 0$, $s_i \neq 0$ it is required that

$$\det(\mathbf{S}) = 0. \quad (2.33)$$

Evaluating Eq. (2.33) leads to expressions for $\alpha_i n_i$ which can be inserted in Eq. (2.23) and lead, after lengthy but straightforward calculation, to the solution for the stability boundary as defined in Eq. (2.21):

$$\begin{aligned} \sqrt{\lambda} = & m(\pm) \left(\frac{Q_{12}^s Q_{21}^c}{4} - \frac{Q_{12}^c Q_{21}^s}{4} \right) \frac{\Theta_{11} - \Theta_{22}}{4\Theta_{11}\Theta_{22}n_1n_2} \quad (2.34) \\ & \pm \frac{(\Theta_{11} + \Theta_{22})}{2} \left[\left(\frac{Q_{12}^s Q_{21}^c}{4} - \frac{Q_{12}^c Q_{21}^s}{4} \right)^2 \left(\frac{1}{2\Theta_{11}\Theta_{22}n_1n_2} \right)^2 \right. \\ & \left. (\pm) \left(\frac{Q_{12}^c Q_{21}^c}{4} + \frac{Q_{12}^s Q_{21}^s}{4} \right) \left(\frac{1}{\Theta_{11}\Theta_{22}n_1n_2} \right) - 1 \right]^{1/2}. \end{aligned}$$

Now let us come back to Eq. (2.18) and the restriction $n_{1,2} \in \mathbb{N}$ as imposed in the original work [23]. This rather stringent condition originates from the application of the Fredholm-theorems which are used by the Method of Integral Equations. Although no proof is given here to justify the next step from a pure mathematical point of view, we will relax this condition for practical applications. This is motivated by a comparison of the results obtained from the Method of Successive Approximation for any $n_{1,2} \in \mathbb{R}$ with other methods which shows that the results are identical. This will be shown also in the following sections.

We now summarize the final results of the Method of Successive Approximation and change the notation as a consequence of the transition to a general parametric excitation frequency η . A homogeneous system of two linear differential equations of second order with a general, coupled, harmonic parametric excitation

$$\mathbf{u}'' + \Theta \mathbf{u}' + \Omega^2 \mathbf{u} + (\mathbf{Q}^c \cos \eta\tau + \mathbf{Q}^s \sin \eta\tau) \mathbf{u} = 0, \quad (2.35)$$

with $\mathbf{u} = [u_1, u_2]^T$ and

$$\begin{aligned} \Theta &= \begin{bmatrix} \Theta_{11} & \Theta_{12} \\ \Theta_{21} & \Theta_{22} \end{bmatrix}, \quad \Omega^2 = \begin{bmatrix} \Omega_1^2 & 0 \\ 0 & \Omega_2^2 \end{bmatrix}, \\ \mathbf{Q}^c &= \begin{bmatrix} Q_{11}^c & Q_{12}^c \\ Q_{21}^c & Q_{22}^c \end{bmatrix}, \quad \mathbf{Q}^s = \begin{bmatrix} Q_{11}^s & Q_{12}^s \\ Q_{21}^s & Q_{22}^s \end{bmatrix}, \end{aligned} \quad (2.36)$$

is considered. This system is similar to the system of Eqs. (2.13), (2.14). Note that the sign of Q_{ij} can be changed without loss of generality since it only introduces a phase shift π to the parametric excitation with respect to an arbitrarily chosen starting time.

The stability limits for parametric combination resonance frequencies $\eta_{2(\pm)1/1}^{cr}$ of the second kind and first order are defined as

$$\eta_{lo}^{lim} \leq \eta_{2(\pm)1/1}^{cr} \leq \eta_{hi}^{lim} \quad (2.37)$$

with

$$\eta_{hi}^{lim} = \eta_{2(\pm)1/1}^{cr} (\pm) T_1 + T_2 \sqrt{T_3(\pm)T_4 - 1}, \quad (2.38)$$

$$\eta_{lo}^{lim} = \eta_{2(\pm)1/1}^{cr} (\pm) T_1 - T_2 \sqrt{T_3(\pm)T_4 - 1}. \quad (2.39)$$

Symbols T_i are introduced for a shorter notation of expressions in Eq. (2.34)

$$T_1 = \left(\frac{Q_{12}^s Q_{21}^c}{4} - \frac{Q_{12}^c Q_{21}^s}{4} \right) \frac{\Theta_{11} - \Theta_{22}}{4\Theta_{11}\Theta_{22}\Omega_1\Omega_2}, \quad (2.40)$$

$$T_2 = \frac{(\Theta_{11} + \Theta_{22})}{2}, \quad (2.41)$$

$$T_3 = \left(\frac{Q_{12}^s Q_{21}^c}{4} - \frac{Q_{12}^c Q_{21}^s}{4} \right)^2 \left(\frac{1}{2\Theta_{11}\Theta_{22}\Omega_1\Omega_2} \right)^2, \quad (2.42)$$

$$T_4 = \left(\frac{Q_{12}^c Q_{21}^c}{4} + \frac{Q_{12}^s Q_{21}^s}{4} \right) \left(\frac{1}{\Theta_{11}\Theta_{22}\Omega_1\Omega_2} \right). \quad (2.43)$$

Note that, with Eq. (2.37) and also (2.38), (2.39), one has to substitute for symbol $(\pm) \rightarrow +$ for the summation type $m^{(+)}$ combination resonance and $(\pm) \rightarrow -$ if the difference type $m^{(-)}$ is to be considered.

This result holds for a quite general system with multi-location, single-frequency parametric excitation. Since the parametric excitation is represented by sine- and cosine-functions with independent coefficients, a phase angle between different sources of the parametric excitation may be considered.

The stability limits calculated by Eqs. (2.37) define a frequency interval in terms of the parametric excitation. In general this is an *interval of instability* caused by the parametric combination resonance of either the summation type or the difference type. However, in the case of parametric vibration quenching the situation reverses and the interval becomes a frequency interval of *stability*. The equations for the stability limits do not tell which conditions prevail on which side of the boundary. This has to be found out by other means.

2.1. Analytical methods

2.1.2 Averaging Method

The Averaging Method has been already used in the 19th century. After being favored by Van der Pol in the 20's of the last century, the first proof of the method's asymptotic behavior was given. Later Krylov, Bogoliubov and Mitropolski made the method popular and it is still associated with their names [58]. A survey of the theory of averaging was compiled by J.A.Sanders and F.Verhulst and can be found in [70].

The Method of Averaging is quite powerful and has the advantage that it is not restricted to periodic solutions. However, it requires that a sufficiently small parameter can be identified in the system. For brevity of the notation we will explain the basic idea of the method for a single generic second order differential equation and apply it later to a 2dof-system. We consider

$$y'' + \Omega^2 y = \varepsilon \Phi(y, y') \quad (2.44)$$

where ε denotes a sufficiently small quantity and $\Phi(y, y')$ is a general nonlinear function. If $\varepsilon = 0$ holds, the solution of Eq. (2.44) is known to be

$$y = r_0 \cos \Omega t + s_0 \sin \Omega t = a_0 \cos(\Omega t + \psi_0) \quad (2.45)$$

where r_0, s_0 and a_0, ψ_0 are constants, respectively. To investigate the solution when parameter $\varepsilon \neq 0$, we assume that the solution can still be written in the form of Eq. (2.45), provided that r_0, s_0, a_0, ψ_0 are considered to be functions of time t rather than constants. So we introduce the solution of Eq. (2.44) as

$$y(t) = a(t) \cos(\Omega t + \psi(t)). \quad (2.46)$$

Since Eqs. (2.44) and (2.46) are two equations in the three unknowns y , a and ψ , we may add an additional condition. It is straightforward to introduce the derivative of Eq. (2.45)

$$y'(t) = -a_0 \Omega \sin(\Omega t + \psi_0) = -a \Omega \sin(\Omega t + \psi). \quad (2.47)$$

To derive equations for $a(t)$ and $\psi(t)$ we differentiate Eq. (2.46) with respect to t and obtain

$$y'(t) = -a \Omega \sin(\Omega t + \psi) + a' \cos(\Omega t + \psi) - a \psi' \sin(\Omega t + \psi). \quad (2.48)$$

Since $y'(t)$ has to be the same in Eqs. (2.47) and (2.48), we find by comparing that

$$a' \cos(\Omega t + \psi) - a \psi' \sin(\Omega t + \psi) = 0. \quad (2.49)$$

must hold. By differentiating Eq. (2.47) we get

$$y'' = -a\Omega^2 \cos(\Omega t + \psi) - a'\Omega \sin(\Omega t + \psi) - a\psi'\Omega \cos(\Omega t + \psi) \quad (2.50)$$

and this enables us to substitute for y' and y'' in Eq. (2.44)

$$a'\Omega \sin(\phi) + a\psi'\Omega \cos(\phi) = -\varepsilon\Phi(a, \phi) \quad (2.51)$$

with $\phi = (\Omega t + \psi)$. From Eqs. (2.49) and (2.51) we can express

$$a' = -\frac{\varepsilon}{\Omega} \sin \phi \Phi(a, \phi), \quad (2.52)$$

$$\psi' = -\frac{\varepsilon}{a\Omega} \cos \phi \Phi(a, \phi). \quad (2.53)$$

Note that the set of equations (2.46), (2.54) and (2.55) are still equivalent to the original problem of Eq. (2.44) since no approximation has been made so far. For small ε also a' and ψ' will be small quantities and hence a , ψ will vary much slower with time compared to $\phi = (\Omega t + \psi)$. If a , ψ will not change much within a period of oscillation of Ωt , we may average Eqs. (2.52), (2.53) over one period $2\pi/\Omega$ and consider a , ψ , a' , ψ' to be constant while performing the averaging. So we finally obtain the equations that describe the (slow) variation of a , ψ ,

$$a' = -\frac{\varepsilon}{2\pi\Omega} \int_0^{2\pi} \sin \phi \Phi(a, \phi) d\phi, \quad (2.54)$$

$$\psi' = -\frac{\varepsilon}{2\pi a\Omega} \int_0^{2\pi} \cos \phi \Phi(a, \phi) d\phi. \quad (2.55)$$

By carrying out the integration in Eqs. (2.54), (2.55) we obtain a set of two autonomous first order differential equations that have to be solved for a and ψ , respectively, which are the sought for time-dependent coefficients in Eq. (2.46).

As mentioned earlier, the method of averaging is also applicable in cases when the function $\Phi(a, \phi)$ is not periodic but is a finite sum of periodic functions with periods which are incommensurate, as for example

$$\Phi = y(\cos \omega_1 t + \cos \omega_2 t) \quad \omega_1 \neq \omega_2 \in \mathbb{R}. \quad (2.56)$$

This is the situation for the parametrically excited system, when the excitation frequency is chosen such that it matches a combination resonance frequency. In [70] Sanders and Verhulst formulate and proof a

2.1. Analytical methods

theorem that covers that case, see also [96]. However, the drawback is that the validity is only guaranteed up to a point in time proportional to $1/\varepsilon$. This means that good results can only be expected for $\varepsilon \ll 1$ and that the method becomes increasingly poor when this condition is violated.

We now apply the Method of Averaging to the same general system of two linear differential equations which has been investigated previously by the Method of Successive Approximation, see Eq. (2.35). To shorten the analysis a bit we drop the parametric excitation by the sine-function and set $\mathbf{Q}^s = \mathbf{0}$. Since it will finally turn out that both methods give in principle identical results, there is no need to analyze the full system again. The analysis for the full system using the Method of Averaging, with all steps meticulously documented, was carried out by F. Dohnal in [14]. Starting from

$$\mathbf{u}'' + \bar{\Theta}\mathbf{u}' + \Omega^2\mathbf{u} + \cos \eta\tau \bar{\mathbf{Q}}^c\mathbf{u} = \mathbf{0} \quad (2.57)$$

we extract a small parameter ε from $\bar{\Theta}$ and $\bar{\mathbf{Q}}^c$ and obtain the system to be analyzed as

$$\mathbf{u}'' + \Omega^2\mathbf{u} = -\varepsilon (\Theta\mathbf{u}' + \cos \eta\tau \mathbf{Q}^c\mathbf{u}), \quad (2.58)$$

$$\mathbf{u} = \begin{bmatrix} u_1 \\ u_2 \end{bmatrix}, \quad \Theta = \begin{bmatrix} \Theta_{11} & \Theta_{12} \\ \Theta_{21} & \Theta_{22} \end{bmatrix}, \quad (2.59)$$

$$\Omega^2 = \begin{bmatrix} \Omega_1^2 & 0 \\ 0 & \Omega_2^2 \end{bmatrix}, \quad \mathbf{Q}^c = \begin{bmatrix} Q_{11}^c & Q_{12}^c \\ Q_{21}^c & Q_{22}^c \end{bmatrix}.$$

We introduce a normalized time $\bar{\tau}$ and carry out the transformation

$$\bar{\tau} = \eta\tau, \quad (\cdot)' = \frac{d}{d\tau} = \eta \frac{d}{d\bar{\tau}} = \eta(\cdot)'\bar{\tau}, \quad u_i(\tau) = v_i(\bar{\tau}) \quad (2.60)$$

for Eq. (2.58).

$$\mathbf{v}'' + \frac{1}{\eta^2}\Omega^2\mathbf{v} = -\frac{\varepsilon}{\eta^2} (\eta\Theta\mathbf{v}' + \cos \bar{\tau}\mathbf{Q}^c\mathbf{v}). \quad (2.61)$$

In the next step the parametric excitation frequency is pinned down to a preselected value η_0 . To enable the investigation of frequencies in the vicinity of η_0 , a frequency variation σ is introduced and the deviation from the main frequency is related to the small parameter ε

$$\eta = \eta_0 + \varepsilon\sigma. \quad (2.62)$$

For a substitution in Eq. (2.61) a first order expansion of Eq. (2.62) is needed

$$\frac{1}{\eta^2} = \frac{1}{(\eta_0 + \varepsilon\sigma)^2} = \frac{1}{\eta_0^2} \left(1 - \varepsilon \frac{2\sigma}{\eta_0} \right) + \mathcal{O}(\varepsilon^2). \quad (2.63)$$

Substituting Eq. (2.62), (2.63) in Eq. (2.61) gives

$$\mathbf{v}'' + \frac{1}{\eta_0^2} \mathbf{\Omega}^2 \mathbf{v} = -\frac{\varepsilon}{\eta_0^2} \left(\eta_0 \mathbf{\Theta} \mathbf{v}' + \cos \bar{\tau} \mathbf{Q}^c \mathbf{v} - \frac{2\sigma}{\eta_0} \mathbf{\Omega}^2 \mathbf{v} \right). \quad (2.64)$$

Similar to Eq. (2.46) in the introduction to the method above, we assume now the solution for $\mathbf{v}(\bar{\tau})$ to be of the form

$$v_i = x_i(\bar{\tau}) \cos \frac{\Omega_i}{\eta_0} \bar{\tau} + y_i(\bar{\tau}) \sin \frac{\Omega_i}{\eta_0} \bar{\tau}, \quad (i = 1, 2). \quad (2.65)$$

To carry on with matrix notation it is more convenient to use the sum of the harmonic functions rather than the previously used form with a phase angle. For an easy notation we introduce the following matrices

$$\begin{aligned} {}^k \mathbf{C} &= \begin{bmatrix} \left(\frac{\Omega_1}{\eta_0}\right)^k \cos\left(\frac{\Omega_1}{\eta_0} \bar{\tau}\right) & 0 \\ 0 & \left(\frac{\Omega_2}{\eta_0}\right)^k \cos\left(\frac{\Omega_2}{\eta_0} \bar{\tau}\right) \end{bmatrix} \\ {}^k \mathbf{S} &= \begin{bmatrix} \left(\frac{\Omega_1}{\eta_0}\right)^k \sin\left(\frac{\Omega_1}{\eta_0} \bar{\tau}\right) & 0 \\ 0 & \left(\frac{\Omega_2}{\eta_0}\right)^k \sin\left(\frac{\Omega_2}{\eta_0} \bar{\tau}\right) \end{bmatrix}. \end{aligned} \quad (2.66)$$

Using these symbols Eqs. (2.65) read

$$\mathbf{v} = {}^0 \mathbf{C} \mathbf{x} + {}^0 \mathbf{S} \mathbf{y}, \quad (2.67)$$

and we may also introduce

$$\mathbf{v}' = -{}^1 \mathbf{S} \mathbf{x} + {}^1 \mathbf{C} \mathbf{y}. \quad (2.68)$$

Of course, Eq. (2.68) is only valid if

$${}^0 \mathbf{C} \mathbf{x}' + {}^0 \mathbf{S} \mathbf{y}' = \mathbf{0} \quad (2.69)$$

holds. Differentiating Eq. (2.68) leads to

$$\mathbf{v}'' = -{}^2 \mathbf{C} \mathbf{x} - {}^1 \mathbf{S} \mathbf{x}' - {}^2 \mathbf{S} \mathbf{y} + {}^1 \mathbf{C} \mathbf{y}' \quad (2.70)$$

2.1. Analytical methods

and completes the set of substitutions necessary for the transformation of Eq. (2.64). Taking into account the following identities

$${}^2\mathbf{C}\mathbf{x} = \frac{\Omega^2}{\eta_0^2} {}^0\mathbf{C}\mathbf{x}, \quad {}^2\mathbf{S}\mathbf{y} = \frac{1}{\eta_0^2} \Omega^2 {}^0\mathbf{S}\mathbf{y}, \quad (2.71)$$

we obtain from Eq. (2.64) after substituting Eqs. (2.67), (2.68) and (2.70)

$$\begin{aligned} -{}^1\mathbf{S}\mathbf{x}' + {}^1\mathbf{C}\mathbf{y}' &= \frac{\varepsilon}{\eta_0^2} \left[\frac{2\sigma}{\eta_0} \Omega^2 ({}^0\mathbf{C}\mathbf{x} + {}^0\mathbf{S}\mathbf{y}) \right] \\ &+ \frac{\varepsilon}{\eta_0^2} \left[\eta_0 \Theta ({}^1\mathbf{S}\mathbf{x} - {}^1\mathbf{C}\mathbf{y}) - \cos \bar{\tau} \mathbf{Q}^c ({}^0\mathbf{C}\mathbf{x} + {}^0\mathbf{S}\mathbf{y}) \right]. \end{aligned} \quad (2.72)$$

Together with Eq. (2.69) this equation defines a set of four first order differential equations for the unknowns $\mathbf{x} = [x_1, x_2]^T$, $\mathbf{y} = [y_1, y_2]^T$,

$$\begin{bmatrix} \mathbf{x}' \\ \mathbf{y}' \end{bmatrix} = \begin{bmatrix} x_1' \\ x_2' \\ y_1' \\ y_2' \end{bmatrix} = \frac{\varepsilon}{\eta_0^2} \begin{bmatrix} \Psi_1 \\ \Psi_2 \\ \Psi_3 \\ \Psi_4 \end{bmatrix}, \quad (2.73)$$

with linear functions $\Psi_i(x_1, x_2, y_1, y_2, \bar{\tau})$ that are obtained from solving the linear algebraic system defined by Eq. (2.69), (2.72) for x_i' , y_i' .

Now we are at the point to investigate the system for special values of η_0 and of course we are especially interested in the behavior at the parametric combination resonance frequencies $\eta_0^{cr} = \Omega_2 - \Omega_1$ in the arguments of the harmonic functions $\cos(\frac{\Omega_i}{\eta_0} \bar{\tau})$, $\sin(\frac{\Omega_i}{\eta_0} \bar{\tau})$ of ${}^k\mathbf{C}$ and ${}^k\mathbf{S}$, respectively. The following step in the Method of Averaging is straightforward but laborious, because it requires averaging all periodic expressions over one period. Computer algebra programs like MAPLE or MATHEMATICA are quite useful in this process, see [14]. It would need by far too much space to print all these expressions and therefore just the final result is given.

After some lengthy calculations we obtain the quite compact result

$$\begin{bmatrix} \mathbf{x}' \\ \mathbf{y}' \end{bmatrix} = \frac{\varepsilon}{\eta_0^2} \left[\mathbf{A}_{\Omega_2 - \Omega_1} \right] \begin{bmatrix} \mathbf{x} \\ \mathbf{y} \end{bmatrix} \quad (2.74)$$

with the coefficient matrix

$$\mathbf{A}_{\Omega_2 - \Omega_1} = \frac{\varepsilon}{\eta_0^2} \begin{bmatrix} -\frac{1}{2}\eta_0\Theta_{11} & 0 & -\Omega_1\sigma & \frac{\eta_0 Q_{12}^c}{4\Omega_1} \\ 0 & -\frac{1}{2}\eta_0\Theta_{22} & \frac{\eta_0 Q_{21}^c}{4\Omega_2} & -\Omega_2\sigma \\ \Omega_1\sigma & -\frac{\eta_0 Q_{12}^c}{4\Omega_1} & -\frac{1}{2}\eta_0\Theta_{11} & 0 \\ -\frac{\eta_0 Q_{21}^c}{4\Omega_2} & \Omega_2\sigma & 0 & -\frac{1}{2}\eta_0\Theta_{22} \end{bmatrix} \quad (2.75)$$

valid for the parametric combination resonance $\eta_{2-1/1}^{cr} = \Omega_2 - \Omega_1$. The characteristic equation is obtained from $\det(\mathbf{A} - \lambda \mathbf{I}) = 0$ and reads

$$a_4\lambda^4 + a_3\lambda^3 + a_2\lambda^2 + a_1\lambda + a_0 = 0, \quad (2.76)$$

with coefficients a_i which we abstain from listing here to prevent this section from becoming overloaded.

To examine the stability of the trivial solution $[x_1, x_2, y_1, y_2]^T = \mathbf{0}$, the Routh-Hurwitz criterion can be applied to the polynomial Eq. (2.76). Four conditions are obtained from which two non-trivial conditions follow

$$a_3 > 0, \quad (2.77)$$

$$\alpha_0\sigma^4 + \alpha_1\sigma^2 + \alpha_2 > 0, \quad (2.78)$$

with $\alpha_i(a_0, a_1, a_2, a_3)$ being expressions built from the coefficients a_i of the characteristic polynomial. After substitution, Eq. (2.77) leads to a simple first condition for stability, which is independent of the frequency variation σ

$$\Theta_{11} + \Theta_{22} > 0. \quad (2.79)$$

The condition (2.78) can be converted from an equation by changing $>$ to $=$. By solving for the frequency variation σ one obtains the stability boundaries

$$\sigma_{lo,hi} = \mp \frac{(\Theta_{11} + \Theta_{22})}{2} \sqrt{-\frac{Q_{12}^c Q_{21}^c}{4\Omega_1 \Omega_2 \Theta_{11} \Theta_{22}} - 1}. \quad (2.80)$$

The interval of stability is now defined by

$$\eta_0 + \varepsilon\sigma_{lo} < \eta < \eta_0 + \varepsilon\sigma_{hi}. \quad (2.81)$$

2.1. Analytical methods

A comparison with the previous result from the Method of Successive Approximation is easy to carry out. One has to take the result Eqs. (2.37) and cancel all expressions in the abbreviation terms $T_{1,3,4}$ which contain the coefficients Q_{jk}^s of the sine-functions. By doing so one ends up with exactly the same formula as in Eq. (2.80). Apparently the only difference is that the Method of Averaging relates the result to the parameter ε . To obtain complete agreement with the Method of Successive Approximation, this parameter must be assumed to be 1. However, according to the cited references the latter method is restricted to integer-valued excitation frequencies, although it did give good results for arbitrary values. Since both methods are first order approximations of the real solution they lead to the same results. The restrictions imposed are different as the methods are, but at the end the order of the approximation determines the result.

Note that both methods presented use a quite different approach and did not make use of the Floquet-theorem, which is frequently employed when analyzing systems with periodic coefficients. Therefore we will now discuss a third method which is based on that theorem.

2.1.3 Tondl-Floquet method

The following method was introduced by A. Tondl in [81]. In his book [82] the method was formulated in a more general way to make it also suitable for systems of differential equations where the complex notation is preferred, as for example in rotor systems. As this method has been used almost exclusively by A. Tondl, it has not been given a name so far. Therefore it seems to be appropriate to introduce a descriptive expression and it is quite obvious to call it the "Tondl-Floquet"-method. Floquet's name is included to point out that there is an important step in the method that makes use of Floquet's theorem.

The Tondl-Floquet-method was applied in the joint publications of the author with A. Tondl, see [88], [18], [92] and [20]. As these are mostly conference publications, the description of the method was significantly shortened and reference was given to previous publications. However, the book [82] is out of print and a more recent reference to the method [89] may also be difficult to locate. Therefore, mainly the background of the method is repeated here, also to supplement the references previously mentioned.

A system governed by the following set of linear differential equations

with periodic coefficients is considered

$$z_s'' + \Omega_s^2 z_s + \varepsilon \sum_{k=1}^n [\Theta_{sk}(\tau) z_k' + Q_{sk}(\tau) z_k] = 0, \quad (s = 1, 2, \dots, n). \quad (2.82)$$

Such a system may be obtained from an actual model of a mechanical system after linearization and transformation to a normal system. The natural frequencies of that part of the system with time-invariant coefficients are denoted Ω_s . It is further assumed that a small parameter $\varepsilon \ll 1$ can be identified and extracted from the time-varying part of the system. Functions $\Theta_{sk}(\tau)$, $Q_{sk}(\tau)$ are general complex periodic functions with period $2\pi/\eta$. Accordingly, z_s is also a complex vector $z_s = x_s + iy_s$, with the imaginary unit $i = \sqrt{-1}$. After a time transformation $\tau = T/\eta$ in Eqs. (2.82) and by reusing the superscript ($'$) for derivatives with respect to the new time T one obtains

$$z_s'' - \lambda_s^2 z_s + \varepsilon \sum_{k=1}^n \left[\frac{\Theta_{sk}}{\eta} z_k' + \frac{Q_{sk}}{\eta^2} z_k \right] = 0, \quad (s = 1, 2, \dots, n), \quad (2.83)$$

where $\lambda_s = i \frac{\Omega_s}{\eta}$ and Θ_{sk} , Q_{sk} are now periodic with period 2π . By introducing new variables ξ and χ defined as

$$z_s' + \lambda_s z_s = \xi_s, \quad z_s' - \lambda_s z_s = \chi_s, \quad (2.84)$$

the second order system of Eqs. (2.83) can be transformed into a first order system

$$\xi_s' = \lambda_s \xi_s - \frac{\varepsilon}{2} \sum_{k=1}^n \left[\frac{\Theta_{sk}}{\eta} (\xi_k + \chi_k) + \frac{1}{\lambda_k} \frac{Q_{sk}}{\eta^2} (\xi_k - \chi_k) \right], \quad (2.85)$$

$$\chi_s' = -\lambda_s \chi_s - \frac{\varepsilon}{2} \sum_{k=1}^n \left[\frac{\Theta_{sk}}{\eta} (\xi_k + \chi_k) + \frac{1}{\lambda_k} \frac{Q_{sk}}{\eta^2} (\xi_k - \chi_k) \right]. \quad (2.86)$$

For this system the Floquet theorem can be applied

$$\xi_s = u_s(T) \exp(\mu T), \quad \chi_s = v_s(T) \exp(\mu T), \quad (2.87)$$

where u_s, v_s are periodic functions of T with period 2π . The characteristic exponent μ can be expanded and written in the form

$$\mu = \lambda + i\varepsilon\gamma(\varepsilon), \quad (2.88)$$

2.1. Analytical methods

where λ is one of the roots λ_s of the characteristic equation of the time-invariant part of system (2.82). Substitution of Eq. (2.87) in Eqs. (2.85), (2.86) we get

$$u'_s = (\lambda_s - \lambda) u_s - \varepsilon \left\{ i\gamma u_s + \frac{1}{2} \sum_{k=1}^n \left[\frac{\Theta_{sk}}{\eta} (u_k + v_k) + \frac{1}{\lambda_k} \frac{Q_{sk}}{\eta^2} (u_k - v_k) \right] \right\}, \quad (2.89)$$

$$v'_s = -(\lambda_s + \lambda) v_s - \varepsilon \left\{ i\gamma v_s + \frac{1}{2} \sum_{k=1}^n \left[\frac{\Theta_{sk}}{\eta} (u_k + v_k) + \frac{1}{\lambda_k} \frac{Q_{sk}}{\eta^2} (u_k - v_k) \right] \right\},$$

$(s = 1, 2, \dots, n).$

We are interested in the stability boundaries of the parametric combination resonance frequencies of the second kind

$$\eta_{r(\pm)j/N}^{cr} = \frac{\Omega_r(\pm)\Omega_j}{N}, \quad (\Omega_r > \Omega_j), \quad (N \in \mathbb{N}, N \neq 0). \quad (2.90)$$

The stability interval is defined by the boundary values as

$$\eta_{lo}^{lim} \leq \eta_{r(\pm)j/N}^{cr} \leq \eta_{hi}^{lim} \quad (2.91)$$

with $\eta_{lo/hi}^{lim}$ being the values on the stability threshold for the the trivial solution. The boundary values may also be expressed as

$$\eta_{lo/hi}^{lim} = \frac{\Omega_r(\pm)\Omega_j}{N} \pm \varepsilon\beta(\varepsilon), \quad (2.92)$$

or

$$\lambda_{r-lo/hi}^{lim}(\pm)\lambda_{j-lo/hi}^{lim} = iN \pm \varepsilon i\alpha(\varepsilon), \quad (2.93)$$

where $\lambda_{j-lo/hi}^{lim}$, $\lambda_{r-lo/hi}^{lim}$ are the roots of the characteristic equation corresponding to the value $\eta_{lo/hi}^{lim}$ and α and β are a real function of ε .

Without loss of generality we can choose the upper stability boundary to carry on with the analysis and switch to a more convenient notation

$$\eta_{r(\pm)j/N}^{cr} = \eta_0, \quad \eta_{hi}^{lim} = \eta_*, \quad \lambda_{k-hi}^{lim} = \lambda_k^*. \quad (2.94)$$

Using Eq. (2.93) with the brief notation of (2.94) and seeking the stability interval in the neighborhood of $\eta_0 = \frac{\Omega_r - \Omega_j}{N}$, the following equations are obtained from Eq. (2.89):

$$\begin{aligned} u'_j &= -\varepsilon \left\{ i\gamma u_j + \frac{1}{2} \sum_{k=1}^n \left[\frac{\Theta_{jk}}{\eta_*} (u_k + v_k) + \frac{1}{\lambda_k^*} \frac{Q_{jk}}{\eta_*^2} (u_k + v_k) \right] \right\}, \\ u'_r &= iN u_r - \varepsilon \{ i\alpha u_r \} \\ &\quad -\varepsilon \left\{ i\gamma u_r + \frac{1}{2} \sum_{k=1}^n \left[\frac{\Theta_{rk}}{\eta_*} (u_k + v_k) + \frac{1}{\lambda_k^*} \frac{Q_{rk}}{\eta_*^2} (u_k + v_k) \right] \right\}, \end{aligned} \quad (2.95)$$

$$\begin{aligned} u'_s &= (\lambda_s^* - \lambda_j^*) u_s \\ &\quad -\varepsilon \left\{ i\gamma u_s + \frac{1}{2} \sum_{k=1}^n \left[\frac{\Theta_{sk}}{\eta_*} (u_k + v_k) + \frac{1}{\lambda_k^*} \frac{Q_{sk}}{\eta_*^2} (u_k - v_k) \right] \right\}, \\ v'_s &= -(\lambda_s^* + \lambda_j^*) v_s \\ &\quad -\varepsilon \left\{ i\gamma v_s + \frac{1}{2} \sum_{k=1}^n \left[\frac{\Theta_{sk}}{\eta_*} (u_k + v_k) + \frac{1}{\lambda_k^*} \frac{Q_{sk}}{\eta_*^2} (u_k - v_k) \right] \right\}, \end{aligned} \quad (2.96)$$

with indices defined as $(s = 1, 2, \dots, n)$, $(s \neq j, s \neq r)$. It is further assumed that the relations

$$\begin{aligned} \lambda_s^* - \lambda_j^* &\neq Mi, & (s \neq j), \\ \lambda_s^* + \lambda_j^* &\neq Mi, & (s \neq r), (M \in \mathbb{N}) \end{aligned} \quad (2.97)$$

hold. Seeking the solution as a power expansion

$$\begin{aligned} u_s &= u_{s0} + \varepsilon u_{s1} + O(\varepsilon^2), \\ v_s &= v_{s0} + \varepsilon v_{s1} + O(\varepsilon^2), \end{aligned} \quad (2.98)$$

and for initial conditions

$$\begin{aligned} u_{j0} &= A, & u_{r0} &= B, \\ v_{s0} &= 0, & (s \neq j, r); & v_{s0} &= 0, \end{aligned} \quad (2.99)$$

we obtain the zero order approximation

$$\begin{aligned} u_{j0} &= A, & u_{r0} &= B \exp(iNT), \\ v_{s0} &= 0, & u_{s0} &= 0, & (s \neq j, r). \end{aligned} \quad (2.100)$$

2.1. Analytical methods

The first order approximation reads

$$\begin{aligned}
 u'_{j1} &= -i\gamma_0 A - \\
 &\quad \frac{1}{2} \left[\left(\frac{\Theta_{jj}}{\eta_0} + \frac{1}{\lambda_j} \frac{Q_{jj}}{\eta_0^2} \right) A + \left(\frac{\Theta_{jr}}{\eta_0} + \frac{1}{\lambda_r} \frac{Q_{jr}}{\eta_0^2} \right) B \exp(iNT) \right], \\
 u'_{r1} &= iN u_{r1} - i(\gamma_0 - \alpha_0) B \exp(iNT) - \\
 &\quad - \frac{1}{2} \left[\left(\frac{\Theta_{rj}}{\eta_0} + \frac{1}{\lambda_j} \frac{Q_{rj}}{\eta_0^2} \right) A + \left(\frac{\Theta_{rr}}{\eta_0} + \frac{1}{\lambda_r} \frac{Q_{rr}}{\eta_0^2} \right) B \exp(iNT) \right], \tag{2.101}
 \end{aligned}$$

$$\begin{aligned}
 u'_{s1} &= (\lambda_s - \lambda_j) u_{s1} - \\
 &\quad \frac{1}{2} \left[\left(\frac{\Theta_{sj}}{\eta_0} + \frac{1}{\lambda_j} \frac{Q_{sj}}{\eta_0^2} \right) A + \left(\frac{\Theta_{sr}}{\eta_0} + \frac{1}{\lambda_r} \frac{Q_{sr}}{\eta_0^2} \right) B \exp(iNT) \right], \\
 v'_{s1} &= -(\lambda_s + \lambda_j) v_{s1} - \\
 &\quad \frac{1}{2} \left[\left(\frac{\Theta_{sj}}{\eta_0} + \frac{1}{\lambda_j} \frac{Q_{sj}}{\eta_0^2} \right) A + \left(\frac{\Theta_{sr}}{\eta_0} + \frac{1}{\lambda_r} \frac{Q_{sr}}{\eta_0^2} \right) B \exp(iNT) \right]. \tag{2.102}
 \end{aligned}$$

From the periodicity condition the following equations are obtained

$$\begin{aligned}
 -i\gamma_0 A - \frac{1}{4\pi} \int_0^{2\pi} \left[\left(\frac{\Theta_{jj}}{\eta_0} + \frac{1}{\lambda_j} \frac{Q_{jj}}{\eta_0^2} \right) A + \right. \\
 \left. \left(\frac{\Theta_{jr}}{\eta_0} + \frac{1}{\lambda_r} \frac{Q_{jr}}{\eta_0^2} \right) B \exp(iNT) \right] dT = 0, \\
 -i(\gamma_0 - \alpha_0) B - \frac{1}{4\pi} \int_0^{2\pi} \left[\left(\frac{\Theta_{rj}}{\eta_0} + \frac{1}{\lambda_j} \frac{Q_{rj}}{\eta_0^2} \right) A \exp(iNT) + \right. \\
 \left. \left(\frac{\Theta_{rr}}{\eta_0} + \frac{1}{\lambda_r} \frac{Q_{rr}}{\eta_0^2} \right) B \right] dT = 0. \tag{2.103}
 \end{aligned}$$

which represent a homogeneous, linear system of algebraic equations in the arbitrary initial conditions A and B of Eqs. (2.99). For non-trivial values of A, B the determinante of the coefficient matrix must vanish and this leads to the following equation which must be satisfied

$$\gamma_0^2 - [\alpha_0 + i(I_{jj} + I_{rr})] \gamma_0 + i\alpha_0 I_{jj} - I_{jj} I_{rr} + I_{jr} I_{rj} = 0, \tag{2.104}$$

with

$$I_{jj} = \frac{1}{4\pi} \int_0^{2\pi} \left(\frac{\Theta_{jj}}{\eta_0} + \frac{1}{\lambda_j} \frac{Q_{jj}}{\eta_0^2} \right) dT, \quad (2.105)$$

$$I_{rr} = \frac{1}{4\pi} \int_0^{2\pi} \left(\frac{\Theta_{rr}}{\eta_0} + \frac{1}{\lambda_r} \frac{Q_{rr}}{\eta_0^2} \right) dT, \quad (2.106)$$

$$I_{jr} = \frac{1}{4\pi} \int_0^{2\pi} \left(\frac{\Theta_{jr}}{\eta_0} + \frac{1}{\lambda_r} \frac{Q_{jr}}{\eta_0^2} \right) \exp(iNT) dT, \quad (2.107)$$

$$I_{rj} = \frac{1}{4\pi} \int_0^{2\pi} \left(\frac{\Theta_{rj}}{\eta_0} + \frac{1}{\lambda_j} \frac{Q_{rj}}{\eta_0^2} \right) \exp(iNT) dT. \quad (2.108)$$

From this analysis a quadratic equation for the coefficient γ_0 , as introduced in Eq. (2.87) with the characteristic exponent μ , is obtained. For stability the imaginary parts of both roots γ_0 must be positive values. This can be determined by using the Routh-Hurwitz criterion for the characteristic equations with complex coefficients, see [82] and [101].

From the application of this criterion the following two conditions are obtained

$$I_{jj} + I_{rr} > 0, \quad (2.109)$$

$$\alpha_0^2 I_{jj} I_{rr} - (I_{jj} + I_{rr})^2 (I_{jr} I_{rj} - I_{jj} I_{rr}) > 0. \quad (2.110)$$

This is the most general form of a result obtained by the Tondl-Floquet method for system Eqs. (2.82). Note that it comprises time-varying coefficients $Q_{sk}(T)$ as well as $\Theta_{sk}(T)$ for z_k and z'_k , respectively. As mentioned in the introduction to this section, applications of the method are found in [88], [18], [92], [20] and in some more references by A. Tondl as being the sole author, see the bibliography.

To give a concrete example of an elaborated result obtained from this method we refer to Section 1.3. There, a still quite generic system Eqs. (1.38) is presented, but, in contrast to system Eqs. (2.82), it uses constant coefficients $\Theta_{sk}(T)$ and a harmonic parametric excitation that is represented just by cosine-functions $Q_{sj} x_j \cos \eta T$. The result of the

2.1. Analytical methods

Tondl-Floquet method for this system are the two stability conditions Eq. (1.42), (1.43). Comparing them with conditions (2.109), (2.110), one easily recognizes the same structure of the result, despite some differently chosen signs and symbols. Furthermore, this example may be compared with the results previously obtained in Sections 2.1.1 and 2.1.2. After rearranging the expressions one can recognize identical results. Therefore we may refrain from including further applications or examples of the Tondl-Floquet method.

2.1.4 Summary on analytical methods

As shown in Sections 2.1.1 to 2.1.3, we obtain identical results for a general system of two differential equations with time-varying coefficients from three substantially different analytical methods¹. Of course, these are not the only methods known and the introduction to this chapter did already mention some more.

The list below refers to other well-known methods which could also be applied and used for the purpose of investigating vibration suppression by parametric excitation:

- Harmonic Balance (see [59], [10])
- Method of Multiple Scales (see [58], [59], [10])
- Poincaré-Linsted method (see [96])
- Method by E.Mettler (see [71])

The references given point to works which give quite detailed explanations of the respective method. Moreover, some of them also compare methods and show results for the same problem obtained by different methods. From these examples it becomes evident that the Harmonic Balance Method, the Method of Averaging and the Method of Multiple Scales lead to the same results when applied to problems as discussed here. From the findings presented in this chapter we conclude that we may also add the Method of Successive Approximation and the Tondl-Floquet Method to the previous ones. All methods applied in this comparison have been used to find a first order approximation. Most methods would also allow to increase the order of approximation. Therefore

¹Valuable support by F.Dohnal with regard to this comparative study is gratefully acknowledged.

it is well founded to assume that all methods mentioned will give in principle identical results when the order of approximation is the same.

Choosing one of the methods for an analytical analysis is therefore a matter of deciding which method is the most convenient to apply. In previous decades this was mainly the question of how much labor and hassle it would be doing all the analysis manually by pencil and (many sheets of) paper. Nowadays an analytical analysis can be performed by using advanced computer algebra software and this puts the question in a different light. There exist quite a number of such programs for symbolic computations and computer algebra, with MAPLE [57] and MATHEMATICA [97] as the most widely known representatives. General purpose algebra software has a wealth of functions and features but methods for an automated stability analysis based on one of the methods discussed earlier is not implemented. Besides the advantage of an interactive usage of such algebra programs they are programmable and one can write routines or packages to extend the capabilities and to perform an automated analysis. For example L.M.Pismen and B.Y.Rubinstein present in [64] a collection of MATHEMATICA-based automated algorithms for the derivation of amplitude equations for dynamical systems in either symbolic or numerical form.

Which of the different methods is best suited for applications as discussed here depends on several factors. The most important of them certainly is to know which functions are available within the algebra system in use. Also the way how algebraic manipulations are carried out, the methods available to simplify expressions and other aspects have to be considered. Without hands-on experience with both, different analytical methods as well as algebra software packages, it is impossible to give preference to one of the methods discussed. As a consequence this also means that one shall not rule out a priori analytical methods that have attracted little attention in the past or have almost fallen in oblivion. It would not be the first "revival" of a method that was less practical in the past and that becomes useful now, due to new means for its application.

A substantial improvement of the quality of the analytical results can only be achieved by applying a higher-order approximation. However, as one can see from the methods presented so far, a first order approximation requires already a rather lengthy analysis. Of course, second order approximations are increasingly laborious and it is therefore no surprise that almost no efforts have been reported to apply a second order approximation to the problems in discussion. The only exception known to

2.2. Numerical methods

the author is found in the work [25] by S.Fatimah. For a system as given by Eqs. (2.58), (2.59) she takes into account second order effects. The effort was motivated by earlier results [18] for the example of a mechanical two-mass system with an extreme mass ratio where the first order approximation did give rather poor results. The qualitative behavior of the analytical results is substantially improved by increasing the order of the solution. The agreement with numerical results is of course also improved quantitatively, but could still be better.

As in many cases the limitations of approximate analytical solutions arise from two directions: order of the approximation and order of the system. For larger systems with more than two differential equations it becomes increasingly hard to find analytical solutions, even for a first order approximation. Three mass systems with some symmetry properties have been investigated so far by A. Tondl [90], [91], S. Fatimah [25] and Abadi [1]. Without the use of computer algebra this seems to be the best one can do with analytical methods.

2.2 Numerical methods

We will now discuss the numerical approach to the problem of finding stable and unstable solutions of self-excited systems in the presence of time-varying parameters.

2.2.1 Numerical simulation

A generic set of second order differential equations similar to the one stated by Eqs. (2.1)

$$u_i'' + \lambda_i u_i = \Phi_i(u_i, u_i', \tau), \quad (i = 1, 2, \dots, N), \quad (2.111)$$

can be easily transformed to a first order system of size $2N$,

$$\begin{aligned} u_i' &= v_i \\ v_i' &= \Phi_i(u_i, v_i, \tau) - \lambda_i u_i \end{aligned} \quad (i = 1, 2, \dots, N), \quad (2.112)$$

and finally formulated in the most general form as

$$y_j' = \Psi_j(y_j, \tau), \quad (j = 1, 2, \dots, 2N), \quad (2.113)$$

with $y_i = u_i$, $y_{i+N} = v_i$ and $\Psi_j(y_j, \tau)$ accordingly built. Note that there is no need to introduce a parameter ε in Eq. (2.111) because this

numerical method is not restricted to problems with a small parameter. Together with suitable initial conditions at time $\tau = 0$

$$y_j(\tau = 0) = y_{jc_j} \quad (2.114)$$

the classical *Initial Value Problem* (IVP) is established. To find the solution of Eqs. (2.113), (2.114), a number of numerical methods exist, subsumed under the category of integration algorithms.

As the reader is certainly aware, there are literally dozens of books available that cover all aspects of "the art" of numerical integration. So there is no need to continue repeating well known or easy to find facts (as in Eqs. (2.112) to (2.114)). Instead, we will discuss some practical aspects of applying numerical simulation in the context of studying parametrically excited systems.

The basic idea of a stability investigation by using numerical simulation is pretty simple. One integrates the set of differential equations, starting from some initial conditions and observes what happens. If the amplitudes vanish after some integration time, the trivial solution ($y_i = 0$) is called stable, if not the answer is "unstable". A result obtained that way is generally named "asymptotic stability in the sense of Lyapunov". A more precise formulation and mathematical definition can be found in practically every book on dynamical systems, see [59], [94], [96] and many others. In such a definition one will find $t \rightarrow \infty$ instead of the loose expression "after some time" and $y_i = 0$ instead of "vanish". This points already to the first difficulty that occurs with numerical simulation. Near the stability limit it may take very long to decide whether amplitudes decrease and will be cancelled or not. Therefore, termination criteria have to be established for a limit on the computational time as well as for numerical results that approach zero. These criteria have to be chosen such that computational time as well as accuracy of the results are kept within practical limits. However, in a strict sense the stability border cannot be found by this approach.

The major advantage of the simulation approach is that not only the stability interval can be found, but also amplitudes are calculated outside the stability interval. The proposed method of suppression of self-excited vibrations by parametric excitation also reduces the vibration level to a certain extent in the vicinity of a stability interval. This effect cannot be studied by a method which can only decide between stability and instability.

2.2. Numerical methods

An unstable linear system will exhibit unbounded amplitudes. Although it is not a problem in a numerical simulation to detect, when amplitudes increase beyond all limits, this is rarely a realistic situation. In most physical systems some nonlinearities will bound the amplitudes and an unstable system will reach some kind of limit cycle. In the case of quasi-periodic solutions oscillation amplitudes do not reach a constant value but are also time-varying. The frequency of this variation, sometimes called "beat frequency", approaches zero near a parametric resonance and can make it difficult to determine correct values for the minimum and maximum values of the amplitudes.

Other nonlinearities may arise from discontinuous parameter changes. In Section 1.4 various possibilities for the time-variation of a stiffness parameter are shown. Among them are design examples for continuous as well as discontinuous parametric excitation. With numerical simulation it is easy to model and simulate such systems with discrete model changes. For a parametric excitation the switching from one parameter value to another occurs at a preset time, represented by a time-event in the simulation environment. If a time-event is handled correctly by exactly hitting the event with the final integration step, by changing the parameter and by restarting the integration again, numerical simulation will not lead to numerical errors but give reliable results.

Parameter studies require the change of a characteristic parameter of the system in order to investigate the dependency of a result on this parameter. The most prominent parameter in the context of parametric vibration cancelling is certainly the frequency of the parametric excitation. In the old days of analog computers and equipment, changing a parameter continuously with respect to time was a very common practice. This so-called *sweep method* could also be implemented in numerical simulation, but has severe disadvantages compared to a step-by-step procedure. The crucial parameter for the sweep method is the sweep rate, which is the rate for changing the sweep parameter. The sweep rate must be sufficiently low to allow vibrations to fully build up or decay. Settings that work in a satisfactory way apart from resonances give erroneous results near the parametric resonance frequencies, see [17]. The reason for this deficiency was already mentioned, it is due to the dramatically increasing time needed to reach steady-state behavior. To correct this problem one would have to decrease the sweep rate, but down to such a low value that the time needed to compute a sweep across an interval would simply take too long.

The alternative to the sweep method is the step method, where the parameter variation is carried out in a discrete (step by step) manner. This method has been used extensively by the author in numerous studies and has been proven to be more reliable. Of course, all previous considerations on selecting appropriate termination criteria for a single simulation run and on picking the right amplitudes also apply to this method. Moreover, the above deliberations have to be solved in such a way that a parameter study can be carried out without user interaction.

The step method can be accelerated significantly by making a good choice for the initial conditions. In most cases this would be the solution of the previous integration run, provided that it was carried out with a parameter set slightly different from the actual set.

Numerical integration of differential equations is facilitated nowadays by widely used general purpose simulation languages or environments like ACSL [55], [8] and MATLAB/SIMULINK [56]. Since the computational time is an important factor in parameter studies, even for a small systems on a fast PC, compiling simulation languages can save a lot of time, compared to programs which work in an interpretative mode.

To recap, numerical simulation is certainly not the most elegant way to investigate the stability behavior and has the appeal of a "brute-force"-method. However, if applied correctly it can be used for all kinds of linear and non-linear systems and will provide useful and reliable results. All in all, simulation will always be the benchmark to verify any other result, obtained either analytically or numerically, unless physical experiments are available.

2.2.2 Floquet method

As suggested in the previous section, there is a more "elegant" way to investigate the stability of parametrically excited systems rather than the plain application of numerical simulation. This alternative method is based on Floquet's theorem. The price one has to pay for elegance is that this method only works for systems governed by *linear homogeneous* ordinary differential equations with periodic coefficients. Moreover, the method will only determine if the solution of the differential equation is exponentially increasing (unstable) or decreasing (stable) when started from non-zero initial conditions.

The FL-method is based on Floquet's theorem, postulated already

2.2. Numerical methods

in 1883. For a system of first order differential equations

$$\mathbf{y}' = \mathbf{A}(\tau)\mathbf{y}, \quad \mathbf{A}(\tau) = \mathbf{A}(\tau + T), \quad (2.115)$$

with a T -periodic matrix $\mathbf{A}(\tau)$ each fundamental matrix $\mathbf{M}(\tau)$ of the system can be represented as a product of two factors

$$\mathbf{M}(\tau) = \mathbf{P}(\tau)e^{\mathbf{C}\tau}, \quad (2.116)$$

where $\mathbf{P}(\tau)$ is a T -periodic matrix function and \mathbf{C} is a constant matrix. This is the content of the theorem. See F.Verhulst [96] for a discussion of various aspects of the theorem and the short proof.

We are interested in the determination of the stability of the system, and there are two different ways which lead to the result. One can determine the stability either from the eigenvalues of the *Floquet exponent matrix* \mathbf{C} or from the *monodromy matrix* $\mathbf{M}(T)$, which essentially is the state transition matrix evaluated after a period T . In principle the FL-method can be applied analytically as well as numerically. In fact, in Section 2.1.3 the Floquet theorem was used in Tondl's method to derive analytical conditions for the stability analysis of a two mass system. However, for large(r) systems the analytical calculation of eigenvalues becomes impossible.

Therefore, we now explain how the Floquet-method can be used to determine the stability of the system by a simple numerical procedure. As stated, the monodromy matrix $\mathbf{M}(T)$, evaluated after one period of the parametric excitation, contains the stability information in its eigenvalues. The monodromy matrix can be calculated numerically by repeated integration of the system equations over one period. We just have to start from independent sets of initial conditions and calculate the system response after one period T . Since it doesn't matter how the initial conditions look like, as long as they are independent, it is convenient to use the columns of the identity matrix \mathbf{I} as initial vectors to start from. We solve n initial value problems over one period T

$$\mathbf{y}' = \mathbf{A}(\tau)\mathbf{y}, \quad [\mathbf{y}(0)_1, \mathbf{y}(0)_1, \dots, \mathbf{y}(0)_n] = \mathbf{I}, \quad \tau = [0, T], \quad (2.117)$$

and arrange the results as follows

$$\mathbf{M}(T) = [\mathbf{y}(T)_1, \mathbf{y}(T)_2, \dots, \mathbf{y}(T)_n]. \quad (2.118)$$

The final step is to calculate the eigenvalues of the monodromy matrix

$$\Lambda = \text{eig}(\mathbf{M}(T)), \quad (2.119)$$

which, of course, is also carried out numerically. The eigenvalues of the monodromy matrix $\mathbf{M}(T)$ are named *characteristic multipliers*, some authors call them *Floquet multipliers*. The system is unstable if any of the eigenvalues are larger than one in magnitude

$$\max(|\Lambda_1|, |\Lambda_2|, \dots, |\Lambda_n|) \quad \begin{cases} < 1 & \text{stable} \\ > 1 & \text{unstable.} \end{cases} \quad (2.120)$$

By applying the FL-method, the computational effort to determine the stability of a mechanical system with n masses is reduced to $2n$ numerical integrations of the equivalent first order system over a period of T , plus the calculation of all eigenvalues of a $(2n \times 2n)$ -matrix. In general this will reduce the computational time significantly, compared to the straightforward numerical simulation. Note, however, that also the FL-method makes use of numerical simulation when the monodromy matrix is calculated.

Basically this method is easy to use and can be implemented with most numerical software packages. In the first part of the method, the numerical integration, one has to pay attention to terminate the integration exactly at the end of the period at time T . The monodromy matrix, and even more the eigenvalues, may be very sensitive to numerical errors in the solution vector $\mathbf{y}(T)$. The computation of the eigenvalues can be numerically challenging, see [44], but this mainly concerns rather large systems. Systems with a small number of equations, as investigated here, can be easily handled by standard numerical software as MATLAB and other similar packages.

2.2.3 Continuation method

The investigation of the stability behavior of a parametrically excited system can also be seen from a more general point of view, namely as a bifurcation analysis of a nonlinear system. Indeed, we can introduce time τ as an additional state and represent Eqs.(2.113) by a nonlinear $(2n + 1)$ -system of ODEs

$$\mathbf{y}' = \mathbf{f}(\mathbf{y}, \eta) \quad (2.121)$$

with a real parameter η . Using the terminology of bifurcation theory [94], [73], we are interested in the branching behavior of \mathbf{y} with respect to the branching parameter η (which is actually the PE-frequency). Boundaries between regions of stable equilibrium solutions and regions with

2.2. Numerical methods

periodic motions as stable solution are called *Hopf bifurcations*. Since the calculation of Hopf bifurcations is a rather elementary task for an up-to-date bifurcation software package, we can also use such codes as BIFPACK [73], AUTO97 [16] and CONTENT [43] to investigate our system. Properly applied, such software can also be used in the investigation of systems with periodic coefficients. This allows us to use features like continuation procedures to trace a solution branch and check for stability without additional programming effort. Some packages also have options for the two-parameter problem $\mathbf{y}' = \mathbf{f}(\mathbf{y}, \eta, \gamma)$ so that parameter studies can be carried out efficiently.

BIFPACK is a frequently used package consisting of a FORTRAN-based collection of subroutines, written and maintained by R. Seydel [74]. The calculation of the monodromy-matrix, path-following, branch-switching and classification of bifurcation points are among the capabilities of BIFPACK and make it a very versatile tool for the investigation of dynamical systems. AUTO97 by E.J.Doedel, [16], is another continuation and bifurcation software. The new version of its predecessors AUTO86 and AUTO94 incorporates algorithms for bifurcation analysis of homoclinic orbits and computation of Floquet multipliers.

CONTENT is a multi-platform integrated environment designed to investigate the properties of dynamical systems. It is capable of analyzing systems of ordinary differential equations as well as discrete-time dynamical systems defined by iterated maps. One can locate equilibria of ODE's by integration and perform a continuation of equilibrium bifurcations of codimension 1 and 2. A number of different bifurcation types can be identified like Fold, Cusp and Hopf bifurcations. Also continuation of periodic solutions is possible. MATCONT, see [15], is a bifurcation package which is a new implementation of CONTENT but based and embedded in the MATLAB-environment.

Application of bifurcation software, as mentioned above, as a tool for the investigation of parametric vibration suppression is still in its infancy. In [25] S. Fatimah reports about the application of CONTENT on a self-excited two-mass system with parametric stiffness excitation for vibration cancellation. Path-following of stability boundaries is demonstrated and Hopf bifurcations and Neimark-Sacker bifurcations are identified. In the future bifurcation software will further simplify and accelerate the study of parametrically excited systems.

Chapter 3

Investigation of 2-dof systems

This chapter is devoted to the demonstration and explanation of basic results of parametrically excited systems with two degrees of freedom. Since the effect of stabilizing a self-excited system by parametric excitation (parametric anti-resonance) can only occur in systems with at least two degrees of freedom, such systems are the most simple ones to exhibit this phenomenon.

3.1 Generic 2-dof system

We will introduce a rather general (generic) mechanical system with two masses, linear springs, viscous dampers and time-varying stiffnesses. By setting individual parameters of the system to zero, the system can be adapted (within limits) to represent different configurations of 2-dof systems. The differential equations that describe such a system can be derived from either a translational system or a torsional vibration system. In order to give a concrete example for the system which we will investigate now, such a system is sketched in Fig. 3.1.

The equations of motion of the mechanical systems shown in Fig 3.1 can be written in matrix form as

$$\mathbf{M}\ddot{\mathbf{x}} + \mathbf{C}\dot{\mathbf{x}} + \mathbf{K}\mathbf{x} + \cos(\omega t)\mathbf{P}^C\mathbf{x} + \sin(\omega t)\mathbf{P}^S\mathbf{x} = \mathbf{0} \quad (3.1)$$

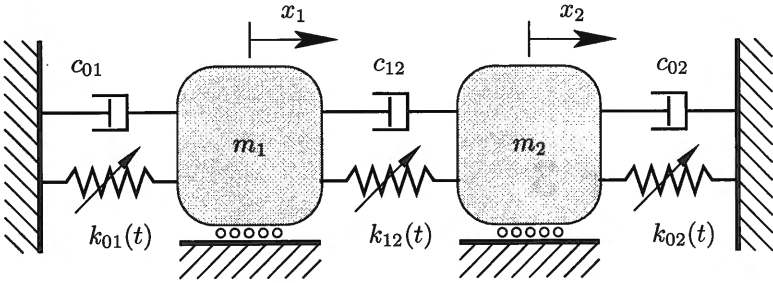


Figure 3.1: Generic 2-mass system

with the following time-independent matrices: mass matrix \mathbf{M} , damping matrix \mathbf{C} , stiffness matrix \mathbf{K} , and coefficient matrices $\mathbf{P}^{C,S}$ of the parametric stiffness variation. Last but not least the vector of deflections is denoted \mathbf{x} . Parametric stiffness excitation (PE) is introduced by $\cos(\omega t)$ and $\sin(\omega t)$ to allow for phase angles between PEs at different locations. Only single-frequency PE with frequency ω is considered for this system.

The system matrices of Eq. (3.1) for (2×2) -systems as shown in Fig. 3.1 are

$$\mathbf{M} = \begin{bmatrix} m_1 & 0 \\ 0 & m_2 \end{bmatrix}, \quad \mathbf{C} = \begin{bmatrix} c_{01} + c_{12} & -c_{12} \\ -c_{12} & c_{02} + c_{12} \end{bmatrix}, \quad (3.2)$$

$$\mathbf{x} = \begin{bmatrix} x_1 \\ x_2 \end{bmatrix}, \quad \mathbf{K} = \begin{bmatrix} k_{01} + k_{12} & -k_{12} \\ -k_{12} & k_{02} + k_{12} \end{bmatrix},$$

and

$$\mathbf{P}^C = \begin{bmatrix} p_{01}^c + p_{12}^c & -p_{12}^c \\ -p_{12}^c & p_{02}^c + p_{12}^c \end{bmatrix} \quad (3.3)$$

$$= \begin{bmatrix} e_{01}^c k_{01} + e_{12}^c k_{12} & -e_{12}^c k_{12} \\ -e_{12}^c k_{12} & e_{02}^c k_{02} + e_{12}^c k_{12} \end{bmatrix},$$

$$\mathbf{P}^S = \begin{bmatrix} p_{01}^s + p_{12}^s & -p_{12}^s \\ -p_{12}^s & p_{02}^s + p_{12}^s \end{bmatrix} \quad (3.4)$$

$$= \begin{bmatrix} e_{01}^s k_{01} + e_{12}^s k_{12} & -e_{12}^s k_{12} \\ -e_{12}^s k_{12} & e_{02}^s k_{02} + e_{12}^s k_{12} \end{bmatrix}.$$

3.1. Generic 2-dof system

The coefficients of the PE-matrices $\mathbf{P}^{C,S}$ are given in terms of the stiffness parameters of the time-independent stiffness matrix \mathbf{K} . In most practical applications the resulting stiffness

$$k_{ij}^{res}(t) = k_{ij}(1 + p_{ij}^c \cos(\omega t) + p_{ij}^s \sin(\omega t)) \geq 0 \quad (3.5)$$

cannot become negative at any time. Therefore a practical limitation for the coefficients $p_{ij}^{c,s}$ is

$$p_{ij}^{res} = \sqrt{(p_{ij}^c)^2 + (p_{ij}^s)^2} \leq 1. \quad (3.6)$$

In a mechatronic system, however, where the "stiffness" may be realized by the proportional gain of a controller, this restriction may be lifted to some extent.

3.1.1 Self-excitation mechanism

In this chapter we will consider negative damping as the mechanism for self-excitation. As discussed earlier in Section 1.1.1, negative damping can arise for various reasons and represents a general mechanism for self-excitation.

The damping matrix \mathbf{C} is assembled from the individual parameters c_{ij} of the various viscous damping elements in the system. To introduce self-excitation to the system, the location of the action of the self-excitation (SE) mechanism has to be determined. If self-exciting forces act on mass m_j a negative damping element $c_{0j}^{SE} < 0$ has to be introduced. If no structural damper c_{0j} is present, then $c_{0j} = c_{0j}^{SE} < 0$ already represents the SE-mechanism in Eq. (3.2). Otherwise the resulting equivalent damping parameter has to be calculated from

$$c_{0j}^{res} = c_{0j} + c_{0j}^{SE} \quad \text{with} \quad c_{0j}^{SE} < 0 \quad (3.7)$$

and accordingly inserted into \mathbf{C} . Frequently, self-exciting forces will be external forces, but of course internal self-excitation $c_{ij}^{SE} < 0$ is also possible and covered by the model.

From the definition of the damping matrix \mathbf{C} for the 2-dof system and from Eq. (3.7) it is clear that self-excitation expressed by $c_{0j}^{SE} < 0$ not necessarily changes a sign of the resulting coefficients of matrix \mathbf{C} . And even if the matrix element $C(1,1) < 0$ is negative, this may not cause an instability of the system, as we will investigate and see later.

3.1.2 Rescaling frequency and time

To prepare Eqs. (3.1) for numerical integration in the time domain, the first step is to make the equations explicit in the highest derivative

$$\begin{aligned}\dot{\mathbf{x}} &= \mathbf{w}, \\ \dot{\mathbf{w}} &= -\mathbf{M}^{-1} [\mathbf{C}\mathbf{w} + \mathbf{K}\mathbf{x} + \cos(\omega t)\mathbf{P}^C\mathbf{x} + \sin(\omega t)\mathbf{P}^S\mathbf{x}].\end{aligned}\quad (3.8)$$

This expanded set of equations is ready to be used with a simulation language like ACSL or one of the integration routines available in MATLAB (or any other package).

In a second step of reformulating the equations it is convenient to introduce a dimensionless PE-frequency η for an easier interpretation of the results. This can be achieved by relating the actual PE-frequency ω to a reference value $\hat{\Omega}$, a characteristic frequency of the system,

$$\eta = \frac{\omega}{\hat{\Omega}}. \quad (3.9)$$

The reference frequency $\hat{\Omega}$ may be selected from the global natural frequencies Ω_i as obtained from an eigenvalue analysis, see the following paragraphs. It is also possible, and sometimes advantageous, to use the natural frequency of a subsystem. If, for example, we assume that $k_{02} = 0$ for the system in Fig. 3.1, then mass m_2 and stiffness k_{12} would represent a mass-spring-subsystem and one might use frequency $\Omega_2^{sub} = \sqrt{k_{12}/m_2}$ as a reference value $\hat{\Omega}$.

Replacing ω by the dimensionless frequency η goes hand in hand with rescaling time t and introducing a dimensionless time τ

$$\tau = \hat{\Omega} t \quad (3.10)$$

since

$$\omega t = \eta \hat{\Omega} t = \eta \tau. \quad (3.11)$$

Subsequently the symbol "prime" (') will be used as a superscript to indicate differentiation with respect to the dimensionless time τ

$$\frac{dx}{dt} = \dot{x} = \hat{\Omega} \frac{dx}{d\tau} = \hat{\Omega} x'. \quad (3.12)$$

After carrying out the substitutions in Eq. (3.1)

$$\hat{\Omega}^2 \mathbf{M}\mathbf{x}'' + \hat{\Omega} \mathbf{C}\mathbf{x}' + \mathbf{K}\mathbf{x} + \cos(\eta\tau)\mathbf{P}^C\mathbf{x} + \sin(\eta\tau)\mathbf{P}^S\mathbf{x} = \mathbf{0} \quad (3.13)$$

3.1. Generic 2-dof system

and by introducing new symbols

$$\hat{\mathbf{M}} = \mathbf{M}, \quad \hat{\mathbf{C}} = \frac{1}{\hat{\Omega}} \mathbf{C}, \quad \hat{\mathbf{K}} = \frac{1}{\hat{\Omega}^2} \mathbf{K}, \quad \hat{\mathbf{P}}^{C,S} = \frac{1}{\hat{\Omega}^2} \mathbf{P}^{C,S}, \quad (3.14)$$

we obtain the rescaled version

$$\hat{\mathbf{M}}\mathbf{x}'' + \hat{\mathbf{C}}\mathbf{x}' + \hat{\mathbf{K}}\mathbf{x} + \cos(\eta\tau)\hat{\mathbf{P}}^C\mathbf{x} + \sin(\eta\tau)\hat{\mathbf{P}}^S\mathbf{x} = \mathbf{0} \quad (3.15)$$

and the equivalent first order system

$$\begin{aligned} \mathbf{x}' &= \mathbf{w}, \\ \mathbf{w}' &= -\hat{\mathbf{M}}^{-1} \left[\hat{\mathbf{C}}\mathbf{w} + \hat{\mathbf{K}}\mathbf{x} + \cos(\eta\tau)\hat{\mathbf{P}}^C\mathbf{x} + \sin(\eta\tau)\hat{\mathbf{P}}^S\mathbf{x} \right]. \end{aligned} \quad (3.16)$$

3.1.3 Normal form representation

Equations (3.8) and (3.16), respectively, are ready to apply numerical simulation, and we will use them in the next section, but one last step in the analysis is still needed. Knowing the natural frequencies of the system is necessary to determine the parametric combination resonance frequencies beforehand and helpful for a sound choice of a reference frequency. Furthermore, to apply the results of the analytical analysis, a normal form representation is required.

The straight-forward method to obtain the results needed is to carry out a modal analysis on the undamped linear time-invariant system (LTI-system)

$$\mathbf{M}\ddot{\mathbf{x}} + \mathbf{K}\mathbf{x} = \mathbf{0} \quad (3.17)$$

We follow the beaten path and assume regular system matrices, i.e. non-singularity of the mass matrix \mathbf{M} and a semi- or positive-definite stiffness matrix \mathbf{K} . Then the associated eigenvalue problem

$$[\mathbf{K} - \Omega^2\mathbf{M}] \mathbf{v} = \mathbf{0}, \quad (3.18)$$

can be solved by standard procedures. The results of the eigenvalue analysis are the natural frequencies Ω_i and the corresponding eigenvectors \mathbf{v}_i . We can arrange the frequencies in a diagonal matrix Ω^2 and the eigenvectors in the modal matrix Φ

$$\Omega^2 = \text{diag}(\Omega_1^2, \dots, \Omega_n^2), \quad \Phi = [\mathbf{v}_1, \dots, \mathbf{v}_n]. \quad (3.19)$$

with $(n = 1, 2)$ for the (2×2) -system of Eqs. (3.1). We can scale the eigenvectors \mathbf{v}_i so that

$$\Phi^T \mathbf{M} \Phi = \mathbf{I} \quad \text{and} \quad \Phi^T \mathbf{K} \Phi = \Omega^2 \quad (3.20)$$

holds. The essential output of the modal analysis is the transformation rule to convert the system from the original coordinates \mathbf{x} to modal coordinates \mathbf{y}

$$\mathbf{x} = \Phi \mathbf{y}. \quad (3.21)$$

By applying this transformation to system Eqs. (3.1) we obtain

$$\begin{aligned} \Phi^T \mathbf{M} \Phi \ddot{\mathbf{y}} + \Phi^T \mathbf{C} \Phi \dot{\mathbf{y}} + \Phi^T \mathbf{K} \Phi \mathbf{y} + \\ + \cos(\omega t) \Phi^T \mathbf{P}^C \Phi \mathbf{y} + \sin(\omega t) \Phi^T \mathbf{P}^S \Phi \mathbf{y} = \mathbf{0} \end{aligned} \quad (3.22)$$

and with Eqs. (3.20) and abbreviations

$$\Phi^T \mathbf{C} \Phi = \Theta \quad \text{and} \quad \Phi^T \mathbf{P}^{C,S} \Phi = \mathbf{Q}^{C,S} \quad (3.23)$$

the normalized system

$$\ddot{\mathbf{y}} + \Theta \dot{\mathbf{y}} + \Omega^2 \mathbf{y} + \cos(\omega t) \mathbf{Q}^C \mathbf{y} + \sin(\omega t) \mathbf{Q}^S \mathbf{y} = \mathbf{0}. \quad (3.24)$$

The purpose of the modal transformation was to obtain uncoupling for the undamped modal LTI-system

$$\ddot{\mathbf{y}} + \Omega^2 \mathbf{y} = \mathbf{0}. \quad (3.25)$$

The modal system can be rescaled with respect to time and PE-frequency in the same way as it was done with the original system. By applying the substitution Eq. (3.12) and denoting rescaled matrices in the same manner as in Eqs (3.14), we obtain the modal system for a dimensionless time

$$\mathbf{y}'' + \hat{\Theta} \mathbf{y}' + \hat{\Omega}^2 \mathbf{y} + \cos(\eta \tau) \hat{\mathbf{Q}}^C \mathbf{y} + \sin(\eta \tau) \hat{\mathbf{Q}}^S \mathbf{y} = \mathbf{0}. \quad (3.26)$$

Depending on the damping matrix \mathbf{C} of the original system, the damped modal system may be uncoupled or not. It is obvious from Eqs. (3.20) that any damping matrix that can be scaled by an arbitrary factor α , to equal the stiffness matrix

$$\mathbf{C} = \alpha \mathbf{K}, \quad (3.27)$$

3.2. Basic simulation results

will also become diagonal by the modal transformation. Therefore the modal system may or may not be uncoupled with respect to damping.

Of course the same holds for the coefficient matrices of the parametric excitation $\mathbf{P}^{C,S}$. However, since parametric stiffness excitation will most likely be installed only in one of the stiffness locations we have to expect that $\mathbf{Q}^{C,S}$ will not be diagonal after transformation Eqs. (3.23) and the single modes of the LTP-system will be fully coupled by the parametric excitation. This means that for an original system with parametric excitation in one single location, the PE will propagate in the modal system and appear in (almost) all possible locations. The same is true for the damping matrix when self-excitation is introduced as negative damping at a single location in the original damping matrix. The propagation of parameters in the modal matrices has some consequences for future parameter studies on modal systems, since modifying a single parameter of a modal system cannot be achieved (in general) by modifying an equivalent single parameter in the original system.

Finally, a few words on the different possibilities of deriving a normal form system, since the choice of the reference frequency $\hat{\Omega}$ is arbitrary. The general approach based on the modal matrix, as presented here, is best suited for numerical calculations and systems of any size. It does not prefer the selection of any particular $\hat{\Omega}$. However, to find handy analytical expressions, e.g. for the natural frequencies Ω_i , a smart choice of the reference frequency $\hat{\Omega}$ and introduction of convenient non-dimensional parameters is advised. Such "hand-selected" transformations for virtually all 2-dof mass-spring systems and also a number of 3-dof systems can be found in the books and monographs by A.Tondl, see [82], [83], [84], and [86].

3.2 Basic simulation results

A concrete mechanical system will be used now as a first example, to demonstrate the fundamental behavior of a 2-dof system under the combined effect of self-excitation and parametric excitation. The model investigated now is shown in Fig. 3.2. It differs from the generic model in Fig. 3.1 in two ways. Firstly, elements which have zero parameter values all the time are omitted in the drawing. Secondly, a nonlinear damping element ($\gamma_{02}^{vp} \dot{x}_2^2$) has been inserted between mass m_2 and the inertial reference frame. This element is needed in the simulation studies, when

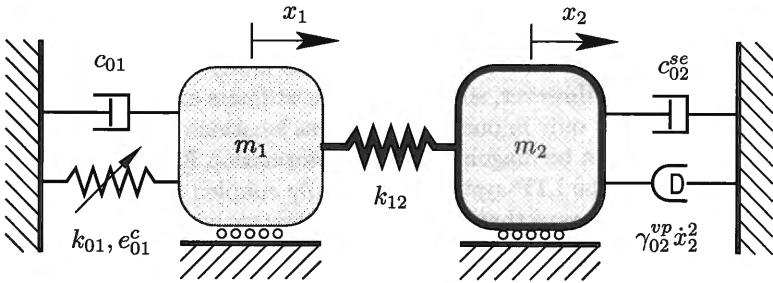


Figure 3.2: 2-mass system with cubic damping

limit cycles for vibration amplitudes shall be calculated. The differential equations for this system can be written in accordance with Eq. (3.1) and after rescaling with $\hat{\Omega} = 1$ as

$$\mathbf{M}\mathbf{x}'' + (\mathbf{C} + \mathbf{C}_{\text{cub}})\mathbf{x}' + \mathbf{K}\mathbf{x} + \cos(\eta\tau)\mathbf{P}^C\mathbf{x} = \mathbf{0}, \quad (3.28)$$

with the newly introduced matrix

$$\mathbf{C}_{\text{cub}}(\mathbf{x}'^2) = \begin{bmatrix} \gamma_{01}^{vp} x_1'^2 & 0 \\ 0 & \gamma_{02}^{vp} x_2'^2 \end{bmatrix}. \quad (3.29)$$

Matrix $\mathbf{C}_{\text{cub}}(\mathbf{x}'^2)$ generates forces proportional to the third power (cubed) of the respective velocity x_i' . Such a non-linear damping law is sometimes named after B. van der Pol. It has the effect of progressively increasing positive damping in the system and is therefore capable of compensating negative damping at a certain vibration level. At this level the limit cycle of the self-excited vibrations occurs.

As mentioned already, progressive damping is only needed for the calculation of time series in a situation when the system is unstable. Without such a damping component the amplitudes would increase to infinity, and the results do not make sense anymore, since the limitations of the model are then definitely exceeded. Moreover, in reality some kind of nonlinear behavior is present in a system or structure most of the time and will bound the vibration amplitudes. Therefore the assumption of a cubic damping element is less artificial as it might seem at the first moment. Last but not least, the effect of nonlinear damping also

3.2. Basic simulation results

Table 3.1: Default parameters for 2-dof system as shown in Fig. 3.2 and used in the following studies

Parameter	m_1	m_2	k_{01}	k_{12}	k_{02}	
	1.0	8.0	1.0	8.0	0.0	
Parameter	c_{01}^d	c_{12}^d	c_{02}^d	e_{01}	e_{12}	e_{02}
	0.15	0.0	0.0	0.2	0.0	0.0
Parameter	c_{01}^{se}	c_{12}^{se}	c_{02}^{se}	γ_{01}^{vp}	γ_{02}^{vp}	
	0.0	0.0	-0.16	0.0	(0.24)	
Frequency	Ω_1	$2\Omega_1$	$\Omega_1 + \Omega_2$	Ω_1^{sub}		
	0.3178	0.6356	3.4641	1.00		
Frequency	Ω_2	$2\Omega_2$	$\Omega_2 - \Omega_1$	Ω_1^{sub}		
	3.1463	6.2926	2.8284	1.00		

progressively decreases with decreasing velocity and vanishes completely for the trivial solution when the system is at rest.

The mechanical model shown in Fig. 3.2 is similar to the system investigated in [88]. Therefore one of the parameter sets employed therein is now used again. Table 3.1 lists the default values of all model parameters. No physical units are given in the table, nor in the diagrams that will follow. Since no specific application is considered it seems to be permissible to abstain from using units and consider all quantities as normalized with respect to some useful reference values. This also has the advantage that one may apply any coherent unit system to the data and results given here.

Knowing the natural frequencies of the system is necessary to calculate the combination resonance frequencies, where parametric resonances or anti-resonances (vibration suppression) may occur. The natural frequencies $\Omega_{1,2}$ of the 2-dof system are defined and can easily be calculated from

$$\begin{aligned} \Omega_1 &= \min(\text{eig}(\mathbf{M}^{-1}\mathbf{K})), & \Omega_1^{sub} &= \sqrt{k_{01}/m_1}, \\ \Omega_2 &= \max(\text{eig}(\mathbf{M}^{-1}\mathbf{K})), & \Omega_2^{sub} &= \sqrt{k_{12}/m_2}. \end{aligned} \quad (3.30)$$

The definition of frequencies of subsystems $\Omega_{1,2}^{sub}$ is also given. These frequencies are needed when they are used for scaling the original set of equations, see Eq. (3.9). Numerical values for the relevant frequencies

that may be encountered with the default set of parameters are listed at the bottom of Table 3.1.

Note from Table 3.1 that the default values for m_2 and k_{12} are much (8 times) larger than for m_1 and k_{01} . However, the frequencies of both subsystems are identical $\Omega_1^{sub} = \Omega_2^{sub} = 1$. To reflect the large differences of the chosen mass and stiffness values in Fig. 3.2, mass m_2 and stiffness k_{12} are plotted with bold lines.

In the following part we will use simulation as a tool to carry out numerical experiments with the model. To demonstrate the fundamental behavior of the system we will first have a look at time series of the deflections $x_{1,2}$ and see how the system behaves in the time domain. Since we will solve an Initial Value Problem for Eqs. (3.28), initial values for $x_{1,2}$ and $x'_{1,2}$ are needed and have to be chosen. For all subsequent simulation results the following set of initial conditions was used:

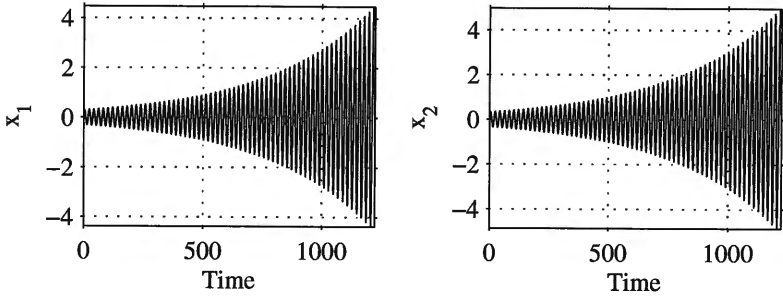
$$x_{1,2} = x'_{1,2} = 0.1. \quad (3.31)$$

The choice of initial values is not critical for this model since, in the case of stability, the trivial solution is attracted from any initial condition. Therefore the initial conditions mainly determine the size of the amplitudes at a given time and were selected to give easy-to-read diagrams.

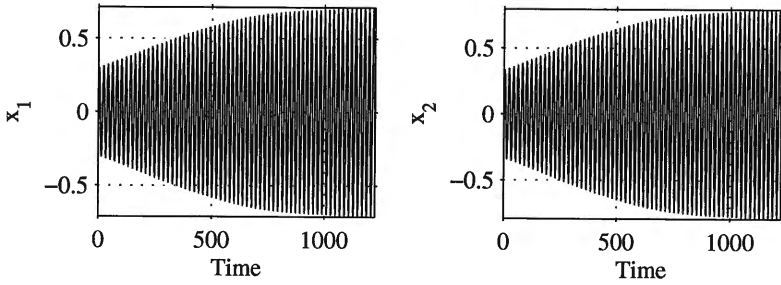
Another common feature in all Figs. 3.3 to 3.10 is that both deflections x_1 and x_2 are plotted. This is mentioned here because one will see later that the results are only marginally different. However, to prevent doubts and make sure that nothing interesting is missed both results are shown in this part.

The very first simulation result is shown in Figs. 3.3 and holds for parameters as listed in Table 3.1, except for the parametric excitation parameter $e_{01}^c = 0$, which is set to zero. Thus, only self-excitation is present and the system is unstable. To demonstrate the effect of the non-linear damping element, three different cases are shown. In Fig. 3.3(a) also non-linear damping is deactivated by setting $\gamma_{02}^{vp} = 0$. Starting from initial values the vibration amplitudes increase progressively and exceed the starting values by a factor of approximately 10 after 1000 time units. From the number of cycles within a period of time the vibration frequency can be calculated. It turns out that it hits almost exactly the lower natural frequency $\Omega_1 = 0.318$ of the system, which means that the system becomes unstable in the first vibrational mode. This is also confirmed by a close inspection of the time series of $x_{1,2}$ that shows

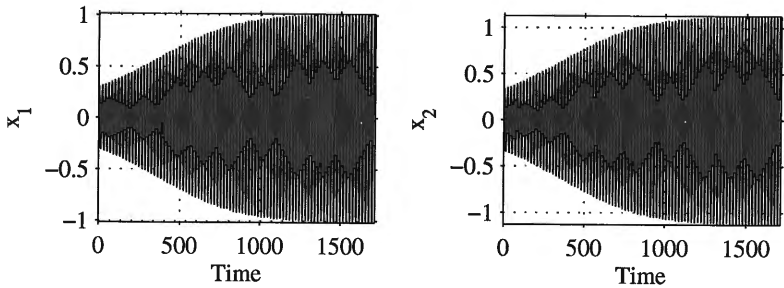
3.2. Basic simulation results



(a) Non-linear damping deactivated $\gamma_{02}^{vp} = 0$, unbounded amplitudes



(b) Limit cycle due to (nonlinear) cubic damping $\gamma_{02}^{vp} = 0.24$



(c) Larger limit cycle for weaker cubic damping $\gamma_{02}^{vp} = 0.12$

Figure 3.3: Unstable (self-excited) system due to negative damping. No parametric excitation present $e_{01}^c = 0$. Data as in Table 3.1.

that both signals are in phase. Since the components of the eigenvector of the first mode do not differ very much, the amplitudes of x_1 and x_2 are also about the same size.

In Figs. 3.3(b) and (c) non-linear damping is active and takes the default value of $\gamma_{02}^{vp} = 0.24$ in Fig. 3.3(b). One can see that a limit cycle is reached soon after 1000 time units. The amplitudes of the limit cycle are determined by the parameter γ_{02}^{vp} . To demonstrate this, Fig. 3.3(c) shows the result when parameter γ_{02}^{vp} is reduced by a factor of 2 and set to $\gamma_{02}^{vp} = 0.12$. Of course the amplitudes do not increase by the same factor since the system is non-linear.

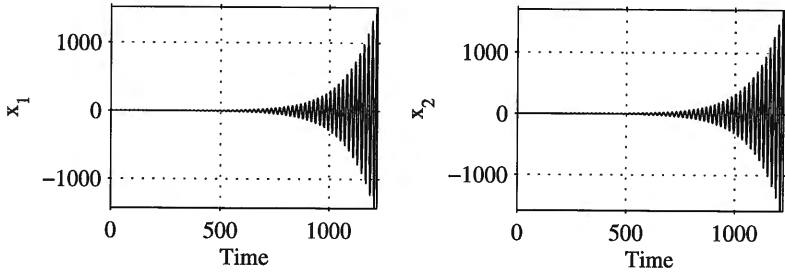
Figures 3.4 on the next page are obtained from the system with active parametric excitation but deactivated self-excitation $c_{02}^{se} = 0$. This result shall demonstrate the effect of pure parametric excitation at certain typical frequencies. Figure 3.4(a) shows the time series for vibration amplitudes when the parametric frequency η is equal to the first principal parametric resonance $2\Omega_1$. In order to allow a comparison with the previous result, non-linear damping is deactivated. At the end of the time scale both amplitudes x_1 and x_2 have reached values well above 1000. By comparing amplitudes with those of Fig. 3.3(a) one can see that the parametric resonance is much more violent than the self-excitation present in the previous result. This behavior has been also reported in the literature.

Cubic non-linear damping is capable of limiting the vibration amplitudes at the principal parametric resonance. This result is shown in Fig. 3.4(b). Due to the fast increase of the vibration amplitudes caused by the parametric resonance, the limit cycle is reached after about 500 time units. The maximum value obtained for a non-linear damping parameter of $\gamma_{02}^{vp} = 0.24$ is significantly larger than the limit cycle obtained with self-excitation, see Fig. 3.3(b). Obviously, for the chosen set of values, parametric excitation "pumps" more energy into the system than self-excitation does.

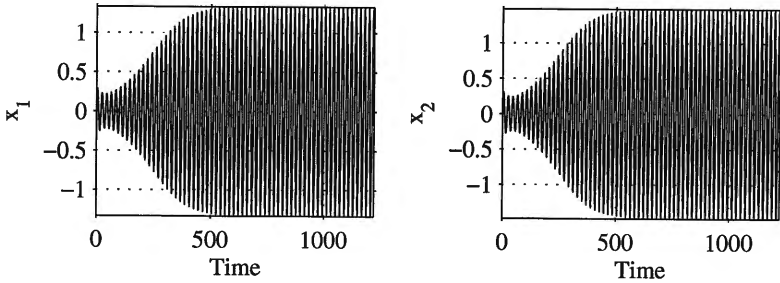
In the last result Fig. 3.4(c) the parametric excitation frequency was set to the parametric combination resonance $\Omega_2 - \Omega_1$. One can see clearly that this frequency is not resonant and therefore the initial vibrations decay quite fast. For a fair comparison the non-linear damping was again deactivated for this simulation result.

In Figures 3.5 on p. 74 both excitation types are activated. For subfigures (a), (b) and (c) the model parameters are the same as in the corresponding figures of the previous Fig. 3.4 (except for parameter c_{02}^{se}

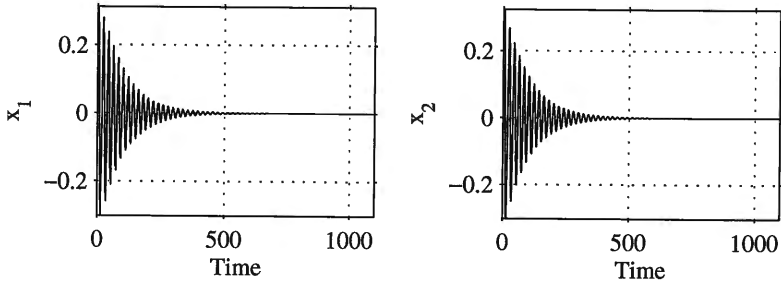
3.2. Basic simulation results



(a) Parametric excitation frequency $\eta = 2\Omega_1$, non-linear damping deactivated $\gamma_{02}^{vp} = 0$

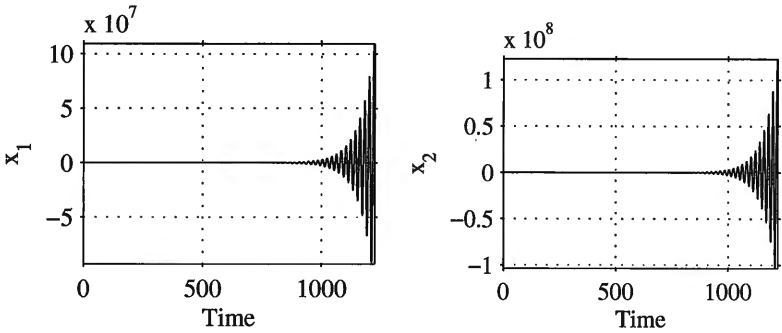


(b) Parametric excitation frequency $\eta = 2\Omega_1$, with (nonlinear) cubic damping $\gamma_{02}^{vp} = 0.24$

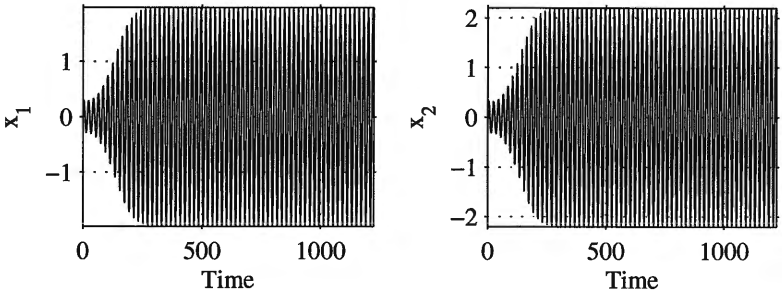


(c) Parametric excitation frequency $\eta = \Omega_2 - \Omega_1$, non-linear damping deactivated $\gamma_{02}^{vp} = 0$

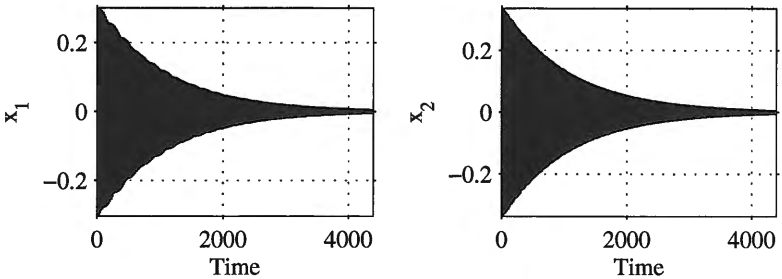
Figure 3.4: Parametric excitation active $e_{01}^c = 0.2$, but self-excitation deactivated $e_{02}^{se} = 0$. Data as in Table 3.1.



(a) Parametric excitation frequency $\eta = 2\Omega_1$, non-linear damping deactivated $\gamma_{02}^{vp} = 0$



(b) Parametric excitation frequency $\eta = 2\Omega_1$, with (nonlinear) cubic damping $\gamma_{02}^{vp} = 0.24$



(c) Parametric excitation frequency $\eta = \Omega_2 - \Omega_1$, non-linear damping deactivated $\gamma_{02}^{vp} = 0$

Figure 3.5: Parametric excitation and self-excitation active, see Table 3.1.

3.2. Basic simulation results

of course). From Fig. 3.5(a) one can see that the combined effect of self-excitation and parametric excitation leads to a dramatic increase of the vibration amplitudes. However, cubic damping still limits the vibration amplitudes on a somewhat higher level, see Fig. 3.5(b).

The most interesting result is shown in Fig. 3.5(c). Despite the presence of self-excitation and the absence of non-linear damping, the amplitudes decay due to the effect of the parametric excitation. Compared with Fig. 3.4(c), the rate of decay is not impressive but still the amplitudes will eventually vanish. This is an example for the case where full vibration suppression occurs at the parametric combination resonance $\Omega_2 - \Omega_1$.

Last but not least some results for other values of the parametric excitation frequency are presented in the following diagrams. Figure 3.6(a) shows a massive beat phenomenon at $\eta = 0.605$ close to $2\Omega_1$. This behavior makes it somewhat difficult and time consuming to find automatically by the simulation routine the stationary maximum values of the vibration signal. Either low-pass filtering of the vibration signals can be used to decide whether stationary conditions are reached or other methods for time series analysis have to be employed.

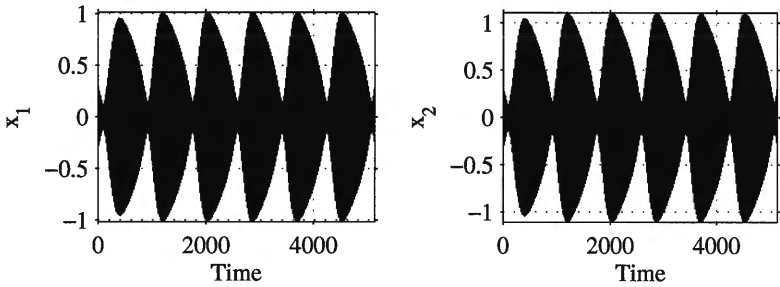
The next Fig. 3.6(b) shows a result in the vicinity of the parametric combination resonance $\Omega_2 - \Omega_1$. Obviously there is already some effect of the parametric excitation, but it is not sufficient to fully absorb the vibrations. However, the figure indicates that a certain reduction of amplitudes is achieved.

Finally, in Fig. 3.6(c) the PE-frequency is chosen almost exactly such that the level of suppression matches the initial conditions and therefore neither an increase nor a decrease of the vibration amplitudes is observed. From this figure and also from Fig. 3.5(c) it becomes clear that it is quite difficult and computationally very inefficient to find the exact frequency limits of the onset of full vibration cancelling from such time series.

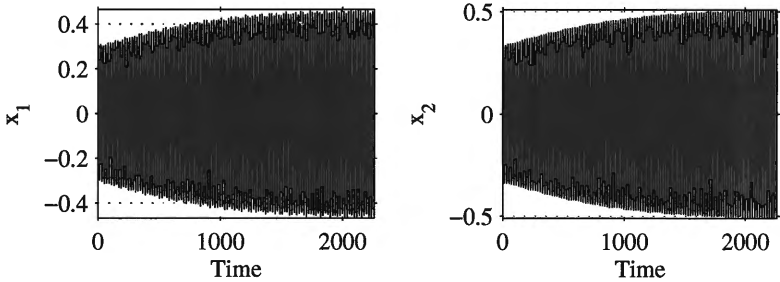
Variation of the parametric excitation frequency η

Having discussed some time series of the vibration amplitudes obtained at various frequencies of the parametric excitation we now can turn our attention to parameter studies. For a compact representation of the results only the maximum amplitudes, reached after stationary conditions prevail, are plotted in the following diagrams.

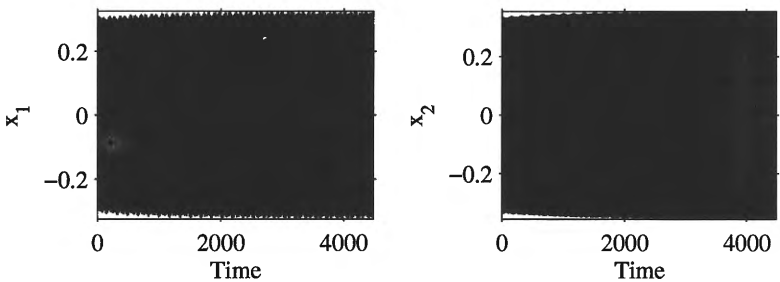
Figure 3.7 shows the maximum amplitudes of x_1, x_2 as a function of



(a) Parametric excitation frequency $\eta = 0.605$, with (nonlinear) cubic damping



(b) Parametric excitation frequency $\eta = 2.7$, with (nonlinear) cubic damping



(c) Parametric excitation frequency $\eta = 2.771$, with (nonlinear) cubic damping

Figure 3.6: Parametric excitation and self-excitation active, see Table 3.1.

3.2. Basic simulation results

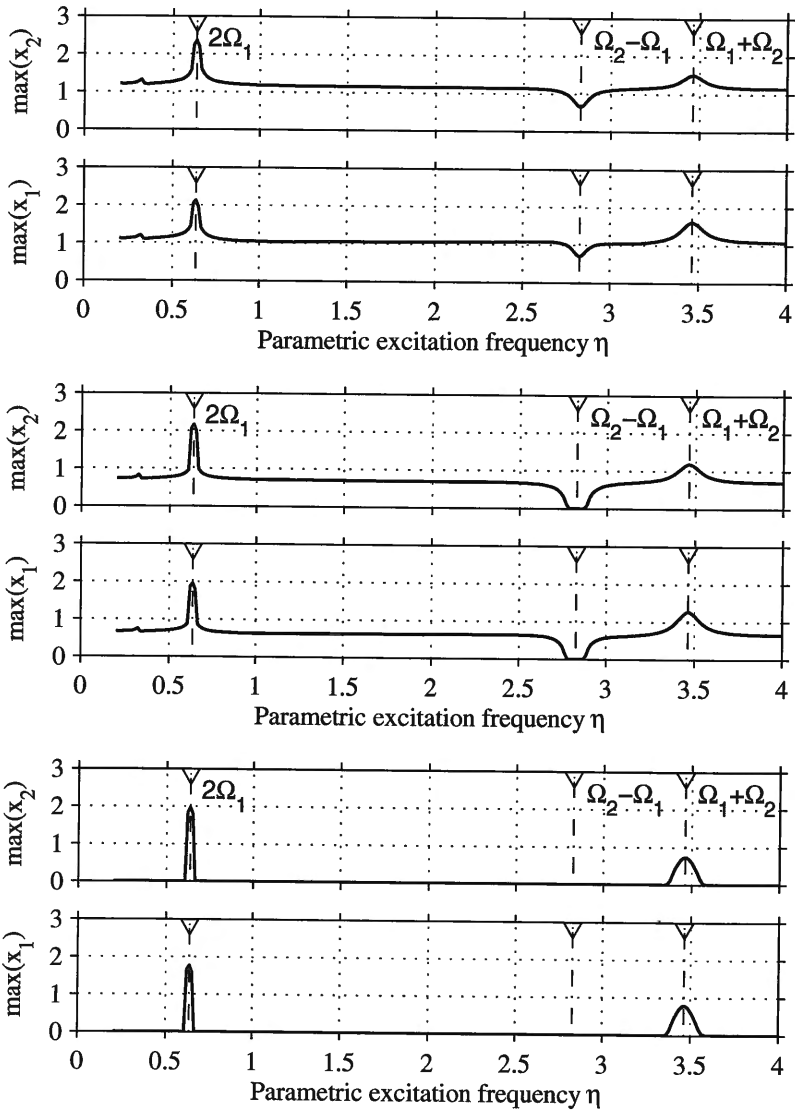


Figure 3.7: Simulation study for SE-parameter c_{02}^s : -0.2 (top), -0.15 (center), and -0.1 (bottom). See Table 3.1 for other data.

the PE-frequency η in the range of ($0.25 < \eta < 4$) for a system as defined by the data in Table 3.1. Three different cases are plotted in this figure. The diagram pairs from top to bottom hold for different values of the self-excitation parameter: $c_{02}^{se} = -0.2$ (top), $c_{02}^{se} = -0.15$ (center), and $c_{02}^{se} = -0.1$ (bottom).

The result in the center of Fig. 3.7 holds for the default parameter set of this example model, with the exception that c_{02}^{se} was reduced from -0.16 to -0.15 . The first primary parametric resonance at $\eta = 2\Omega_1 \approx 0.64$ points out and leads to the highest maximum amplitude values. On the other hand one can see the *frequency interval* in the vicinity of the combination resonance frequency $\eta = \Omega_2 - \Omega_1 \approx 2.83$, where the amplitudes completely vanish and full vibration suppression takes place. The second combination resonance frequency $\eta = \Omega_1 + \Omega_2 \approx 3.46$ appears as another peak in the amplitude diagrams, but this parametric resonance is not as pronounced as the first primary resonance. The second primary resonance frequency $\eta = 2\Omega_2 \approx 6.3$ does not fall within the frequency range shown. For PE-frequencies between those distinct values the maximum amplitudes reach a certain level that is practically independent of the PE-frequency and reflects the limit cycle that is reached.

The results shown at the bottom and on top of Fig. 3.7 demonstrate the effect of decrease and increase, respectively, of the SE-parameter. The diagram pair on top shows results for $c_{02}^{se} = -0.2$. This increase of negative damping reduces the stabilizing effect of the parametric excitation. The trivial solution for the system cannot be stabilized anymore at $\eta = \Omega_2 - \Omega_1$. Nevertheless, a certain reduction of the vibration level is still possible and visible in the plots. Finally, the diagrams at the bottom of Fig. 3.7 confirm that the system is stable for $c_{02}^{se} = -0.1$, regardless of the effect of parametric excitation. Of course, at the parametric resonance frequencies $2\Omega_1$ and $\Omega_1 + \Omega_2$ amplitudes still do occur.

To give a better impression how maximum vibration amplitudes depend on the PE-frequency η and the SE-parameter c_{02}^{se} , a close-up view of the vibration suppression range is shown in Figs. 3.8. Each point on the 3D-mesh corresponds to a specific combination of η and c_{02}^{se} and gives the maximum amplitudes for x_1 and x_2 , respectively. Every data point was obtained from a single simulation run starting from initial conditions as used in all previous runs, see Eqs. (3.31), and continued until stationary conditions were reached. In the case of a stable (or stabilized) system the trivial solution was approached eventually. The smoothness of the grid and the zero values obtained for stable conditions

3.2. Basic simulation results

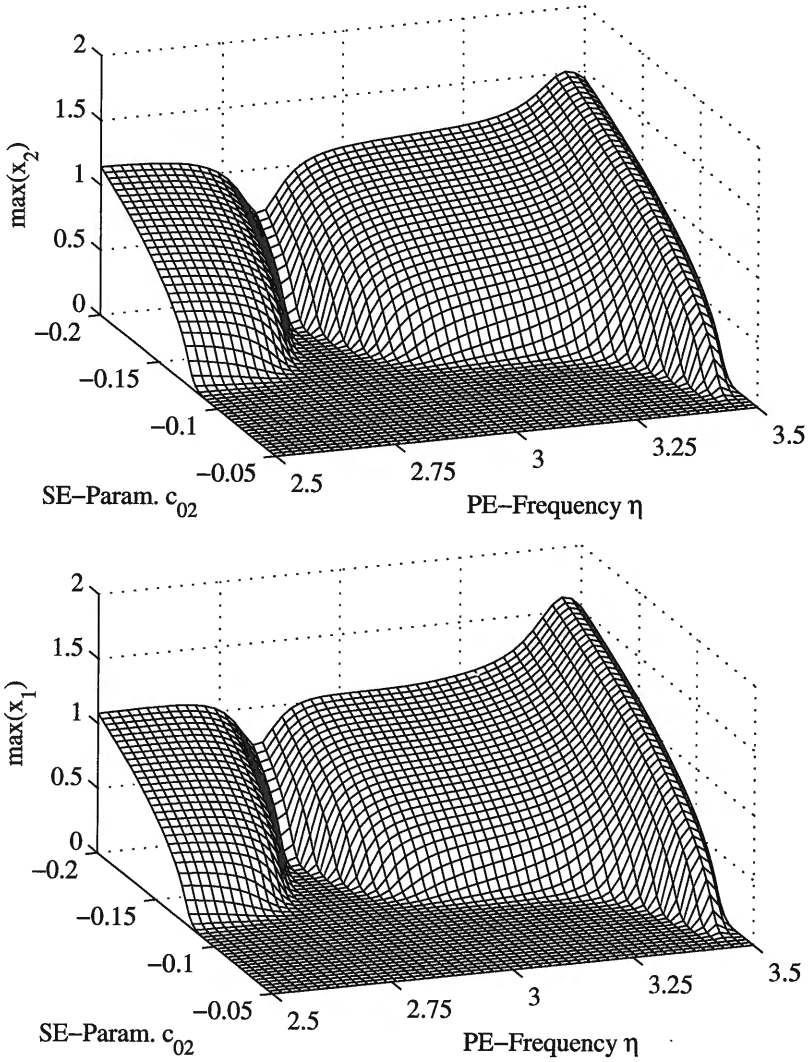


Figure 3.8: Simulation study for PE-frequency η and SE-parameter c_{02}^{se}

confirm that the simulation runs have not been terminated prematurely. Of course, the computation of such a diagram is quite time consuming and may take 10 minutes and more on an up-to-date PC, depending on the performance of hardware and software in use. Moreover, integration method, integration stepsize and termination criterion determine how long such calculations may take and have to be chosen carefully to keep computational time within reasonable limits.

In Figs. 3.9 again the maximum amplitudes of x_1, x_2 are shown for three different cases. As opposed to the previous Fig. 3.7, the diagram pairs from top to bottom hold for different values of the PE-excitation parameter: $e_{02}^c = 0.2$ (top), $e_{02}^c = 0.1$ (center), and $e_{02}^c = 0.0$ (bottom). The result on top of Fig. 3.7 holds for the default parameter set of this example model and may be compared with Fig. 3.7 (center) to see the small but visible difference in the maximum amplitudes caused by the different values of the SE-parameter (now $c_{02}^{se} = -0.16$ instead of -0.15 as in Fig. 3.7). The small increase in negative damping narrows the region of vibration suppression and raises the average vibration level a bit.

In Fig. 3.9 (center) the PE-excitation parameter is reduced by half ($e_{02}^c = 0.1$). This reduction lowers the amplitudes at parametric resonances considerably but also has an adverse effect on the vibration suppression. A small vibration reduction is still visible near $\eta = \Omega_2 - \Omega_1$, but that is all one can achieve for this parameter setting. To complete the variation of e_{02}^c , the figures at the bottom show the not unexpected result for $e_{02}^c = 0.0$.

A more favorable representation on how the PE-parameter affects the maximum amplitudes is shown by the 3D-mesh plots in Fig. 3.10. As one can see from this close-up diagram, $e_{02}^c = 0.2$ is almost the lower bound value to obtain full vibration suppression, since the mesh surface quite rapidly increases for values $e_{02}^c \leq 0.18$. The few "dings" in the otherwise immaculately smooth surface are caused by minor slips of the program routine which controls the detection of stationary conditions.

3.3 Numerical stability investigation

The previous section did show some results obtained from numerical simulation. To compute vibration amplitudes outside the domain of stability of the trivial solution, numerical simulation is the only means that works reliably and for all possible models. However, to just decide

3.3. Numerical stability investigation

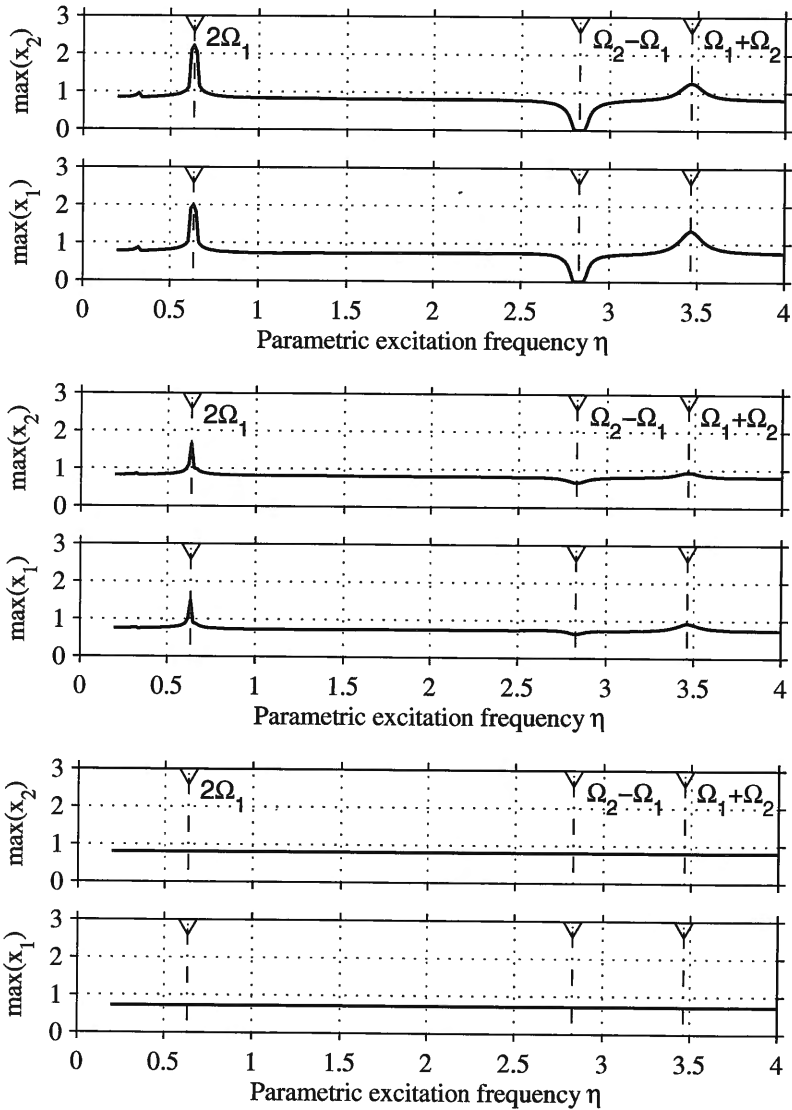


Figure 3.9: Simulation study for PE-parameter e_{02}^c : 0.2 (top), 0.1 (center), and 0.0 (bottom). See Table 3.1 for other data.

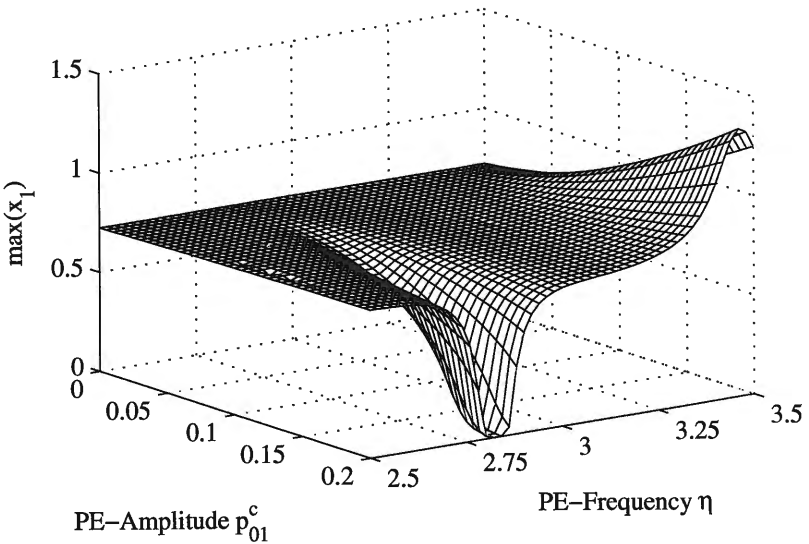
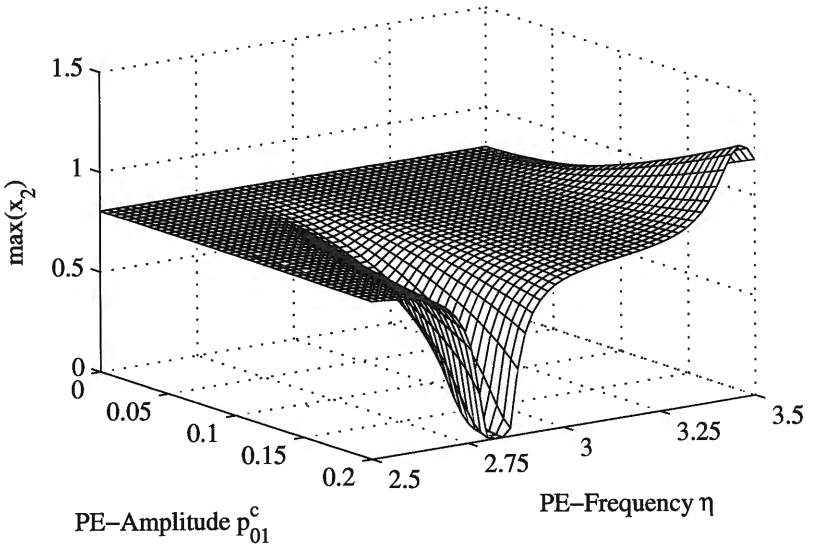


Figure 3.10: Simulation study for PE-frequency η and PE-parameter e_{02}^c

3.3. Numerical stability investigation

whether the trivial solution is stable or not a much faster approach is available. In Section 2.2.2 the Floquet-method was discussed and will now be applied to the previously investigated model by using numerical simulation.

We will continue to use the model as depicted in Fig. 3.2 with parameters as listed in Table 3.1. However, since the Floquet-method requires a linear model, the non-linear damping parameter γ_{02}^{vp} will be set to zero in all subsequent numerical studies.

To facilitate the comparison of the previous results with the new ones, we will continue to use the parametric excitation frequency η as the primary parameter for variation and select other parameters as a secondary variation parameter. The basic result from the numerical Floquet-method are the eigenvalues of the monodromy matrix $\mathbf{M}(T)$, see Eq. (2.119). The magnitude of the largest eigenvalue determines whether the trivial solution of the system is stable or not. If the value is smaller than 1, then the system is stable, if larger, the system is unstable, see conditions (2.120). Basically the outcome of the numerical Floquet-method is simply "yes" or "no". However, the absolute values of the eigenvalues, especially for the largest one, reveal also interesting information and give insight into the stability behavior of the system.

In Fig. 3.11(top) the magnitude of the maximum eigenvalue of the monodromy matrix is plotted over a range of the PE-frequency η and the SE-parameter c_{02}^{se} . A mostly flat surface is obtained with a very gentle downward inclination towards higher values of c_{02}^{se} . The most striking feature of this surface is a blade-like vertical structure that stands out well from the rest of the surface. The associated eigenvalues are all significantly above one, indicating an unstable region. Since these values occur at the primary parametric resonance frequency $\eta = 2\Omega_1$, this is how this particular instability is represented in the Floquet-analysis.

Two other features, although less obvious than the "blade"-structure, can be observed, one of them a groove in the surface, the other one a little ripple oriented parallel to the groove. By examining the frequencies where these structures occur it becomes clear that the "groove" represents the parametric anti-resonance at $\Omega_2 - \Omega_1$ and the "ripple" is caused by the parametric combination resonance $\Omega_1 + \Omega_2$. For stability of the system we have to look at those areas of the surface which stay below one, and vice versa for the unstable part. To help recognize these areas, all parts raising above a fictive plane at level one are colored dark and represent the unstable regions. In the areas below this plane the mesh

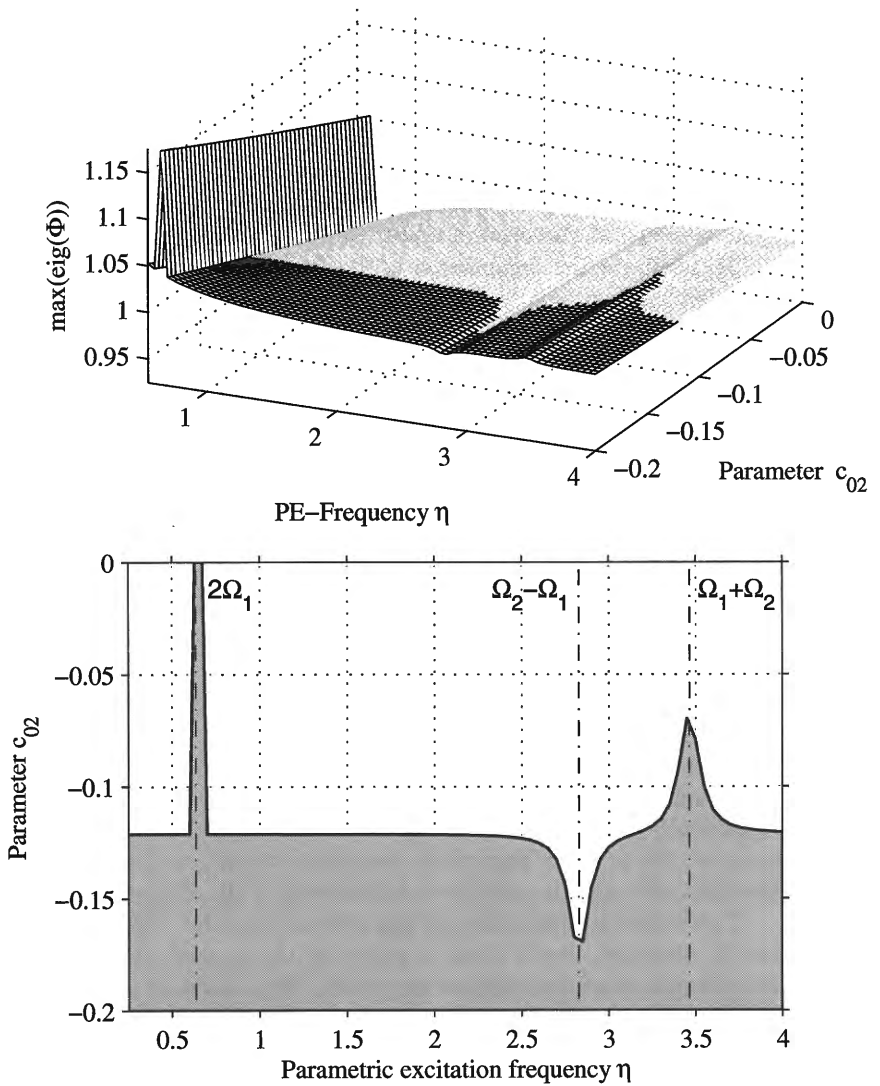


Figure 3.11: Surface plot of maximum eigenvalue magnitude (top). Stability chart (bottom). Dark areas indicate unstable system. Data as in Table 3.1 on p. 69

3.3. Numerical stability investigation

is colored bright and indicates stability of the system.

In combination with the inclination of the surface the stability region extends towards smaller values of the SE-parameter due to the "groove" at the parametric anti-resonance frequency. Because of the "ripple" the unstable area is extended to higher values of c_{02}^{se} at the combination resonance $\eta = \Omega_1 + \Omega_2$. Now that the underlying structure has become clear, the interpretation of simple 2D-plots, as e.g. the diagram at the bottom of Fig. 3.11, is made easier.

We continue to apply the numerical Floquet-method to the system to carry out some more parameter studies and to investigate the parameter range where vibration suppression is achievable. In Fig. 3.12 the diagram on top shows how the width of the stability interval near the combination anti-resonance $\eta = \Omega_2 - \Omega_1$ is affected by the PE-parameter e_{01}^e . As concluded already from the results of Fig. 3.10, a minimum value of $e_{01}^e > 0.175$ is necessary to bring about full vibration suppression at a frequency of $\eta = \Omega_2 - \Omega_1$. Increasing the amplitudes of the parametric excitation also increases the width of the interval. For values $e_{01}^e > 0.3$ a remarkably wide interval can be achieved, which might be of interest in a real application. A large interval means a robust method, since small parameter fluctuations will not endanger vibration suppression.

The bottom diagram of Fig. 3.12 shows a rather strange dependency of the stability region on the damping parameter c_{01} , the only (positive) damping element in the system. A rather narrow gap of varying width extends down to very small damping values. This result indicates that although nearly no viscous damping is present in the system, the negative damping of the SE-mechanism can still be compensated by parametric stiffness excitation. This is quite remarkable, since it points out that parametric excitation can be used as a substitute for conventional damping.

Figures 3.13 demonstrate the influence of the mass parameters m_1 and m_2 on the stability region. Starting from the default value of $m_2 = 8$ the frequency of the parametric anti-resonance does not change much in the investigated interval, since m_2 remains the dominant mass even for smaller values like $m_2 = 4$. However, the stability interval gets smaller for smaller values of the mass parameter. In contrast to the results for m_2 we observe that mass parameter m_1 has a significant influence on the parametric anti-resonance frequency. This is due to the fact that m_1 affects the second natural frequency Ω_2 of the system significantly, and as a consequence the combination anti-resonance $\Omega_2 - \Omega_1$. At a value of

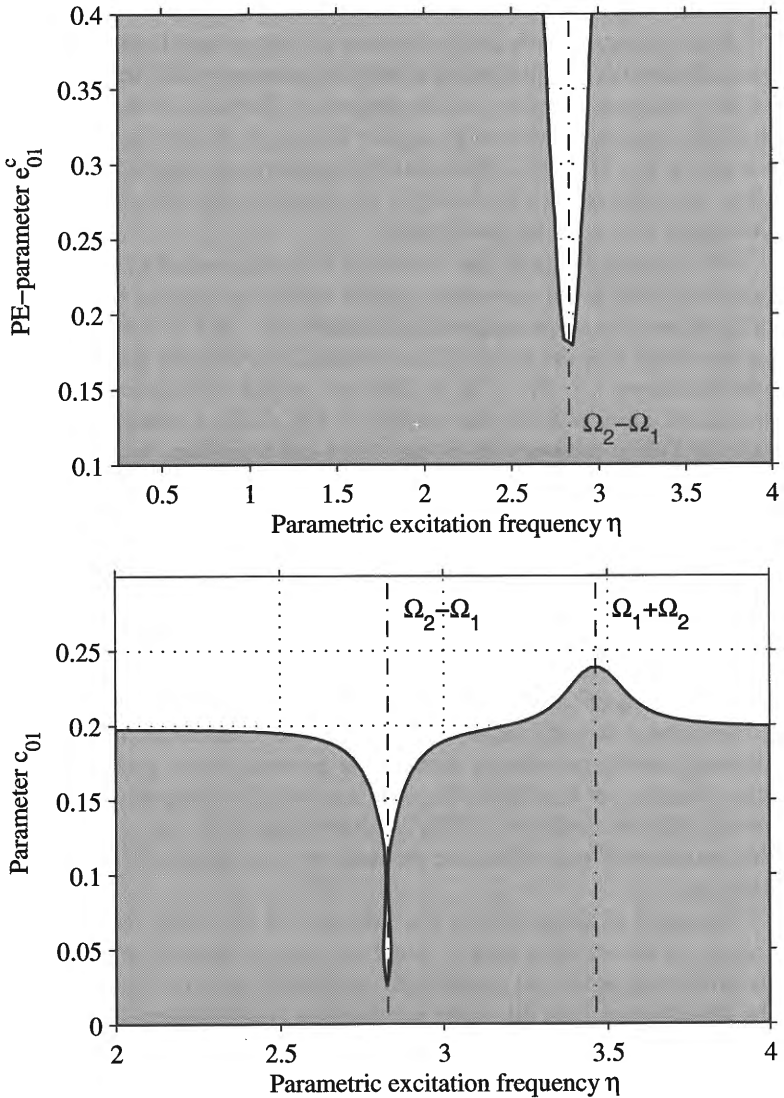


Figure 3.12: Stability charts for PE-parameter e_{01}^c (top) and damping parameter c_{01} (bottom). Dark areas indicate unstable system. Data as in Table 3.1 on p. 69

3.3. Numerical stability investigation

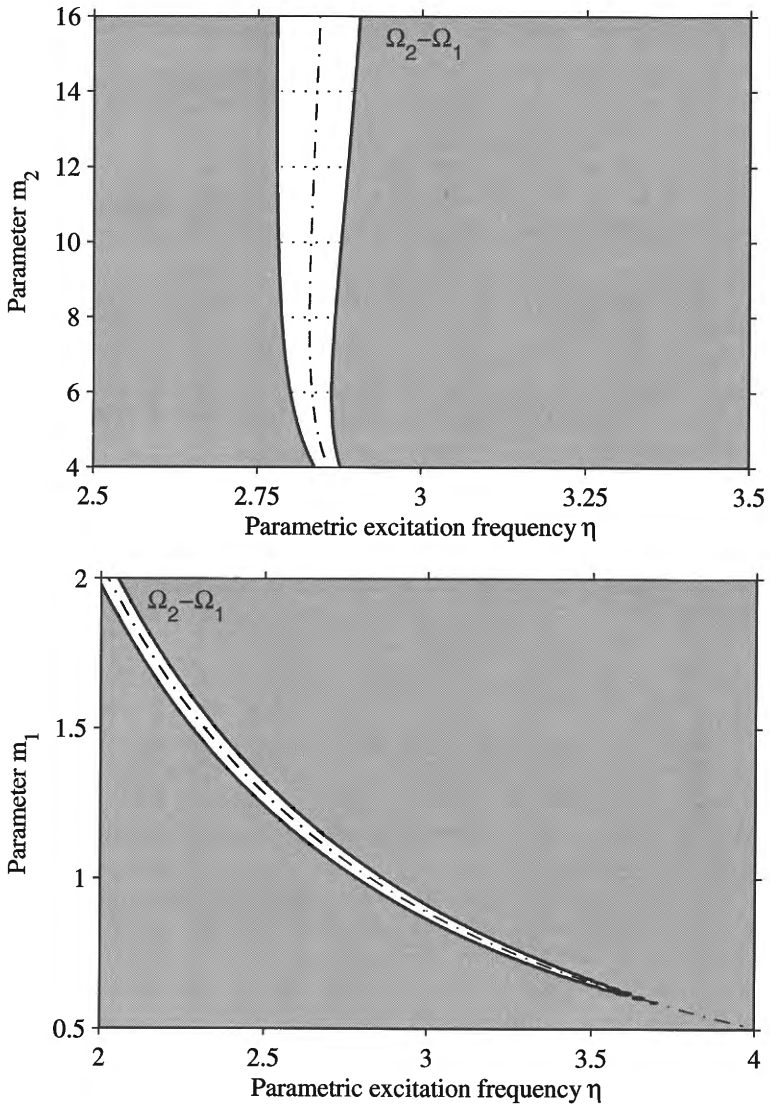


Figure 3.13: Stability charts for mass parameters m_2 (top) and m_1 (bottom). Dark areas indicate unstable system. Data as in Table 3.1 on p. 69

about $m_1 = 0.6$ the region of stability ends for the parameter set in use (Table 3.1).

To complete the survey on the influence of system parameters on the stability interval generated by parametric excitation, Fig. 3.14 shows the results of parameter studies on the stiffness parameters k_{12} and k_{01} . Both diagrams resemble the previous diagrams for the mass parameters but in reverse order. This is no surprise because the stiffness parameters have an inverse influence on natural frequencies compared to mass parameters. With respect to the variation of the base stiffness k_{01} it is worth noting that the amplitude of the parametric excitation $p_{01}^c = e_{01}^c k_{01}$ is also changed accordingly.

3.4 Comparison of analytical and numerical results

The results obtained from the numerical Floquet-method in the previous section have been computed with relatively little computational effort, compared to direct numerical integration. Each data point only needs the integration of the system equations over one period of the parametric excitation and the calculation of the eigenvalues of a (4×4)-matrix. If the numerical part of the job is handled diligently, the results obtained are of high accuracy. This remark has to be made, since it is quite obvious from Fig. 3.11 that minor errors in the eigenvalue computation of the monodromy matrix may result in large errors regarding the stability region. On the other hand the monodromy matrix itself can be very sensitive to errors in the numerical integration and must be calculated as precisely as possible.

Although traditionally analytical results serve as benchmarks for numerical methods, the opposite situation occurs here with respect to the comparison of analytical and numerical results. Since the numerical Floquet-method is highly accurate, under the premises mentioned above, we will use these results to test the validity of the analytical methods presented in Section 2.1. As concluded in Section 2.1.4, all approximation methods discussed basically lead to the same formula for the stability boundaries of a parametrically excited 2-dof system. Therefore we do not have to distinguish between different analytical methods in the following part and simply subsume them under the general name *first order approximation*.

3.4. Comparison of analytical and numerical results

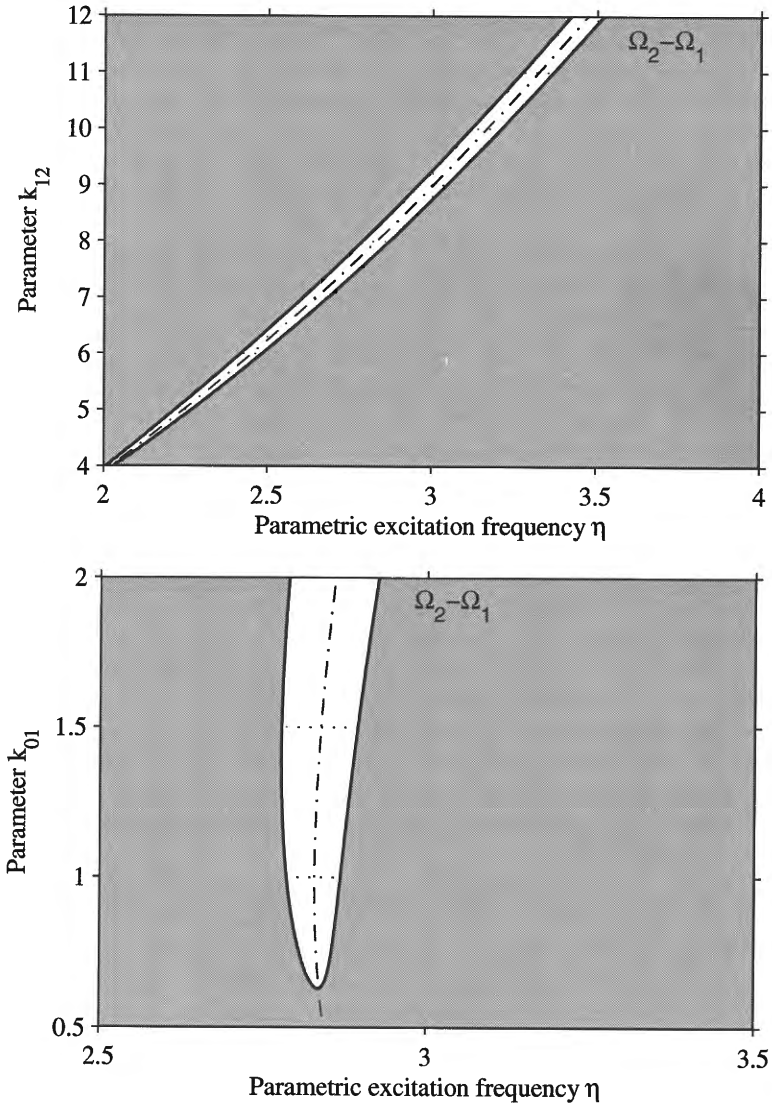


Figure 3.14: Stability charts for stiffness parameters k_{12} (top) and k_{01} (bottom). Dark areas indicate unstable system. Data as in Table 3.1 on p. 69

Analytical expressions for the stability limits can be derived for all kinds of parametric resonances. Here we will focus only on the parametric combination resonances $\Omega_1 + \Omega_2$ and $\Omega_2 - \Omega_1$. Primary parametric resonances like $2\Omega_1$ are not considered, although they did occur in the previous results. Analytical expressions for these resonances can be found in the literature, but since vibration suppression only occurs at combination resonances, the other parametric resonances are of little interest.

The comparison of results is carried out by superimposing numerical Floquet-results with results from the analytical first order approximation. Visual inspection of the outcome will be sufficient to get an overview how well or badly results match.

For the first comparison we take the basic result shown in Fig. 3.11 and zoom into the relevant PE-frequency range of $2 \leq \eta \leq 4$. Since the frequency range covers both the anti-resonance at $\Omega_2 - \Omega_1 \approx 2.83$ and the combination resonance at $\Omega_1 + \Omega_2 \approx 3.46$, two separate solutions have to be calculated from the first order approximation formulae for each of the resonance frequencies. Each formula is valid only for just one single parametric resonance and approximates the function in the vicinity of this frequency. Superimposing the results of the analytical analysis leads to Fig. 3.15(top). The analytical solution is plotted using dashed lines and consists of two separate results, approximating the anti-resonance at $\Omega_2 - \Omega_1$ as well as the resonance at $\Omega_1 + \Omega_2$.

The numerical and the analytical results agree extremely well, especially close to the resonance frequencies. In the range between the resonance frequencies the analytical solutions deviate from the numerical solution in opposite directions so that both analytical results cannot be patched together.

For the second comparison we investigate the strangely looking result at $\Omega_2 - \Omega_1 \approx 2.83$ shown in Fig. 3.12(bottom) and enlarge the PE-frequency range again to show more details. The combined numerical and analytical results are shown in Fig. 3.15(bottom). Again, both results agree very well despite the quite extreme shape of the stability region. However, the analytical solutions continue towards zero values of the damping parameter c_{01} indicating a further extension of the stable region, which is not confirmed by the numerical results. Obviously such spurious solutions may also be calculated in extreme cases like here and results have to be inspected carefully.

Further comparison studies are plotted in Figs. 3.16. The diagram

3.4. Comparison of analytical and numerical results

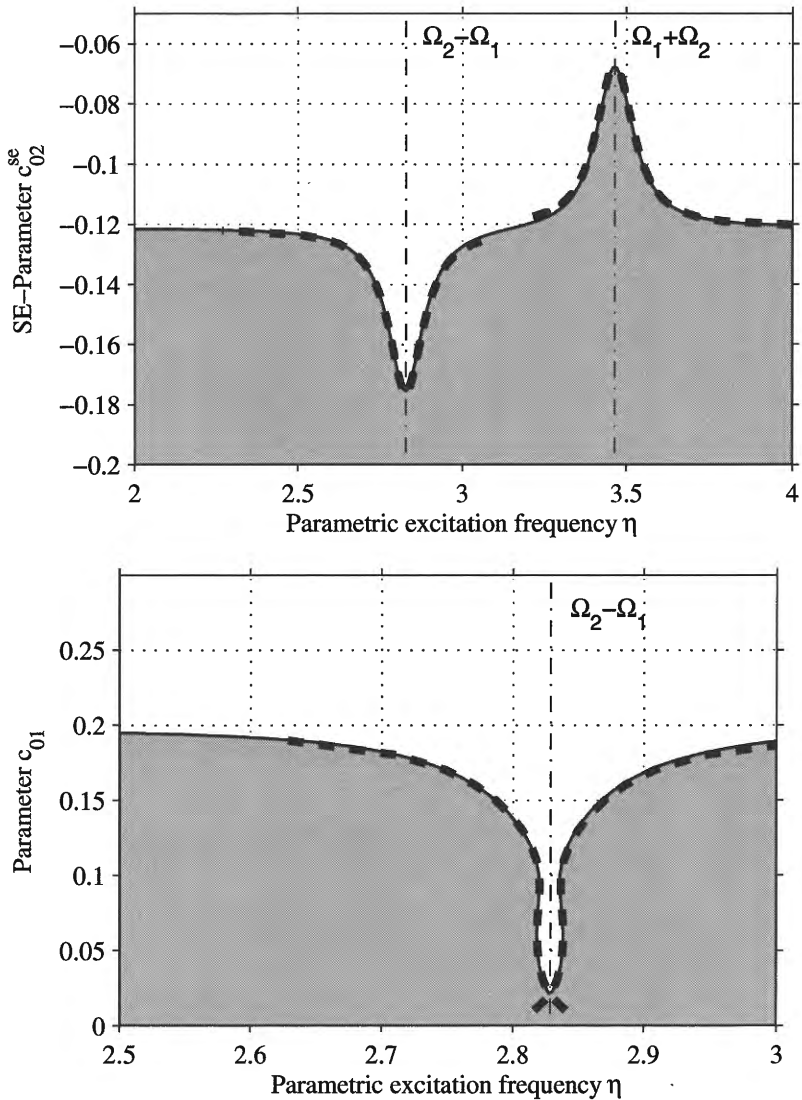


Figure 3.15: Comparison of numerical results (solid) and analytical results (dashed): (Top) SE-parameter c_{02} (cf. Fig. 3.11), (bottom) damping parameter c_{01} (cf. Fig. 3.12)

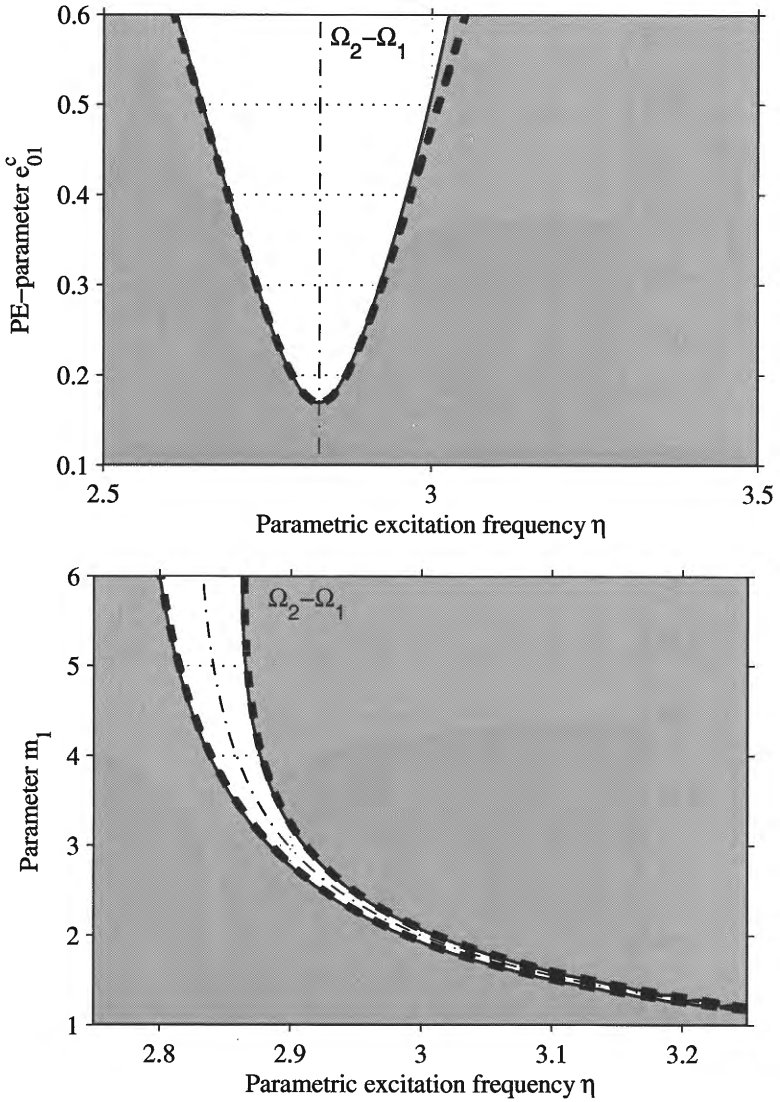


Figure 3.16: Comparison of numerical results (solid) and analytical results (dashed): (Top) SE-parameter e_{01}^c (cf. Fig. 3.11), (bottom) damping parameter x_1 (cf. Fig. 3.12)

3.5. Anti-resonance at $\Omega_2 - \Omega_1$

on top shows that even for a considerably high PE-excitation amplitude $e_{01}^c \approx 0.5$ the results agree surprisingly well. This good result could not be expected, because in the first order approximation the PE-amplitude is assumed to be a small parameter $e_{01}^c \ll 1$ which definitely does not hold in this example. As a last case, the parameter range of m_2 as in Fig. 3.12(top) is extended to smaller values. The stability region continues downwards and ends at $m_2 \approx 1$ in a narrow "vermiform appendix". The approximate solution by the analytical first order method has no problem with this shape and agrees perfectly well with the numerical result.

The outcome of the comparison between numerical results and the analytical first order approximation for this example is a very positive one. Therefore the analytical results will be used in the next section for further parameter studies. However, such a good agreement is not always guaranteed. In Section 5.2 a different 2-dof system is presented, where the first order approximation gives quantitatively and qualitatively wrong results for certain parameter sets.

3.5 Anti-resonance at $\Omega_2 - \Omega_1$

In the previous section we have confirmed that the analytical first order approximation works very well with the system as in Fig. 3.2 and parameters as given in Table 3.1. This allows us to use the approximate representation for further parameter studies of the parametric combination anti-resonance, which would be much more time consuming with the numerical methods discussed.

Now, the goal is to calculate the critical value of a certain parameter for the onset of stability or instability, i.e. the stability threshold as a function of two other parameters. Thereby we will introduce a third parameter to the diagram type as used in the previous Figs.3.11 to 3.15.

Because of the calculation method used for these diagrams, but also to make it easier to distinguish different diagrams shown in this section, the "waterfall-type" representation is used now. In all subsequent diagrams of this section the critical value for the SE-parameter c_{02} is plotted as a function of the PE-frequency η and a second parameter. The three-dimensional surface shown in the figures represents the stability threshold (the critical parameter value) which divides the parameter range in a stable and an unstable part. Values of the SE-parameter c_{02}

below the surface lead to an unstable system, and values above lead to stability. Since we use the analytical approximation consisting of two separate results, a gap will be observed between them. Other parametric resonances will not appear, since they were not included in the approximate solution.

Figure 3.17 (top) is an extension of Fig. 3.15 and shows the dependency of results on the PE-parameter e_{01}^{ξ} . The previous Fig. 3.16 is a cross-section in another direction of this comprehensive representation. Minimum and maximum values for the SE-parameter c_{02} are cut off for higher values of the PE-parameter for a favorable scaling. The continuation of values is easy to imagine from the shape of the threshold surface. One can see that higher values of the PE-amplitude not only widen the stability interval with respect to the PE-frequency η , but also allow the compensation of significantly larger (negative) values of the SE-parameter.

Figure 3.17 (bottom) is a study of the stiffness parameter k_{01} and is related to Fig. 3.14. It shows another possibility to extend the compensation potential of the parametric excitation. There is another way how to read this diagram. For example, for $k_{01} = 2$ the lowest value for the SE-parameter where the system is just stable without parametric excitation lies at $c_{02} = -0.1$. With parametric excitation at the appropriate frequency $\eta = \Omega_2 - \Omega_1$, the SE-parameter can be further reduced by more than -0.1 . The actual minimum value is cut off in the diagram. The effect of parametric excitation can be interpreted as the introduction of an equivalent damping to the system of a magnitude larger than 0.1.

Finally Fig. 3.18 shows parameter studies for the mass parameters m_2 and m_1 . The diagrams supplement the previous Figs. 3.13 and 3.16. Again, the main additional information contained in the new plots is the minimum value of the SE-parameter for which the system still can be stabilized by parametric excitation.

3.6 Anti-resonance at $\Omega_1 + \Omega_2$

So far the anti-resonance phenomenon always appeared at the combination resonance of difference-type $\Omega_2 - \Omega_1$. From the analytical analysis in Chapter 2.1 it is known that anti-resonance is also possible, in principle, for the combination resonance of summation-type $\Omega_1 + \Omega_2$. How-

3.6. Anti-resonance at $\Omega_1 + \Omega_2$

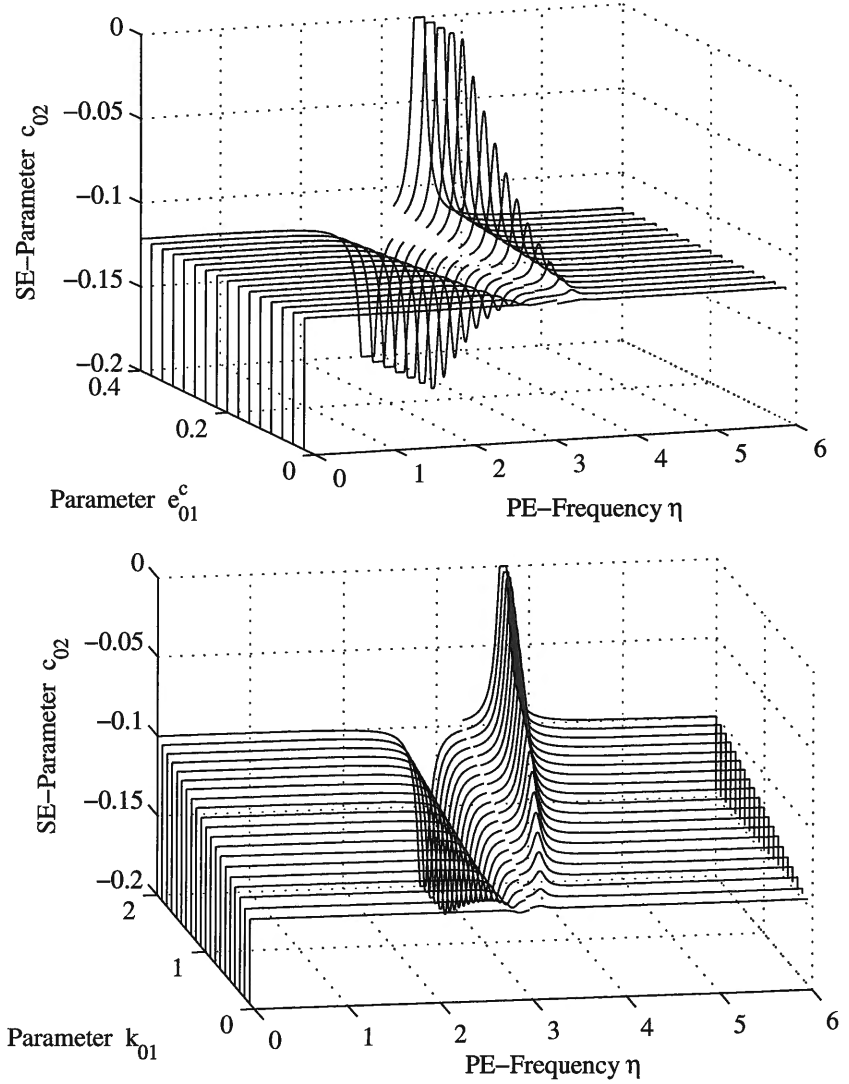


Figure 3.17: Critical SE-parameter obtained from analytical first order approximation. Data as given in Table 3.1 on p. 69

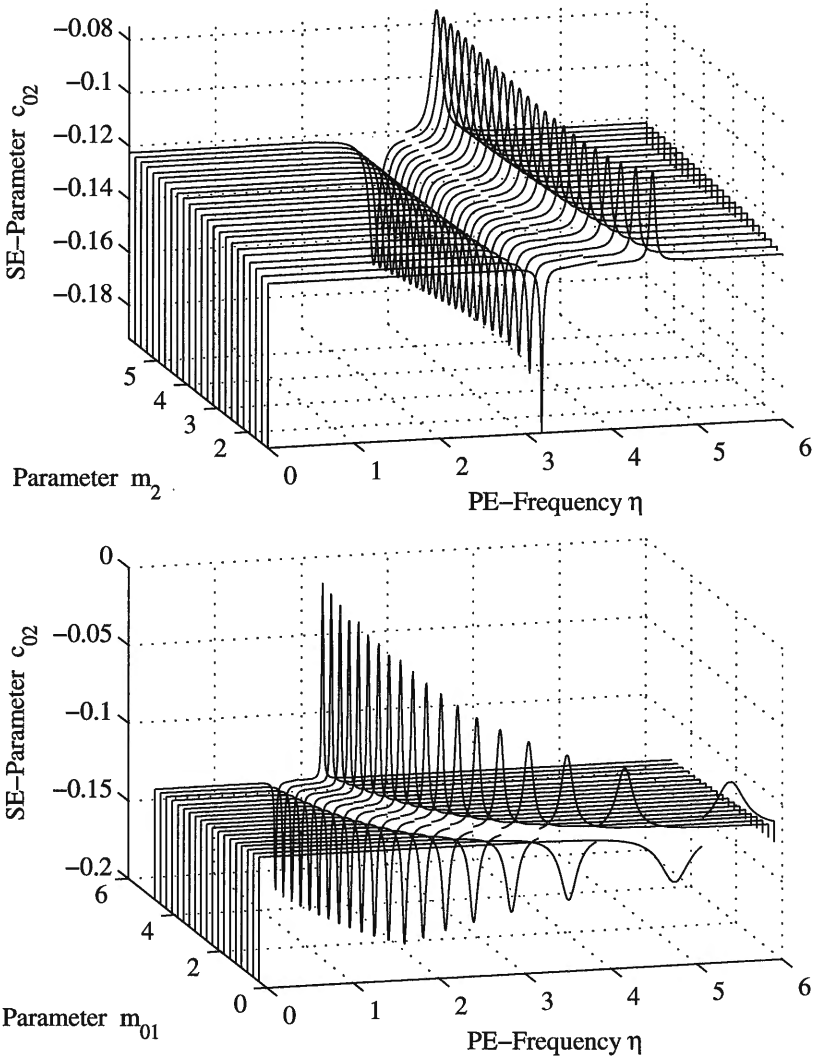


Figure 3.18: Critical SE-parameter obtained from analytical first order approximation. Data as given in Table 3.1 on p. 69

3.6. Anti-resonance at $\Omega_1 + \Omega_2$

Table 3.2: Default parameters for 2-dof system as defined by Eq. (3.32)

Parameter	m_1	m_2	k_{01}	k_{12}	k_{02}	
	1.0	8.0	1.0	8.0	0.0	
Parameter	c_{01}^d	c_{12}^d	c_{02}^d	e_{01}	e_{12}	e_{02}
	0.15	0.0	0.0	0.2	0.0	0.0
Parameter	c_{01}^{se}	c_{12}^{se}	c_{02}^{se}	k_{nc}	e_{nc}^c	
	0.0	0.0	-0.16	1.0	0.0	

ever, an analysis of the radical expression in either Eqs. (2.38),(2.39) or Eq. (2.80) reveals that it is not possible to obtain real values for the case of $\eta = \Omega_1 + \Omega_2$ for a conventional mechanical system as depicted in Fig. 3.1.

Despite this drawback, it is possible to show the desired effect if non-conservative forces are introduced to the system of Fig. 3.1. Starting from the generic linear 2-dof system as formulated in Eq. (3.1), F. Dohnal proposes in [14] to add a skew-symmetric matrix \mathbf{P}_{NC}^C to the (conservative) matrix of PE-parameters. By setting $\mathbf{P}^S = \mathbf{0}$ we obtain in accordance with Eq. (3.1)

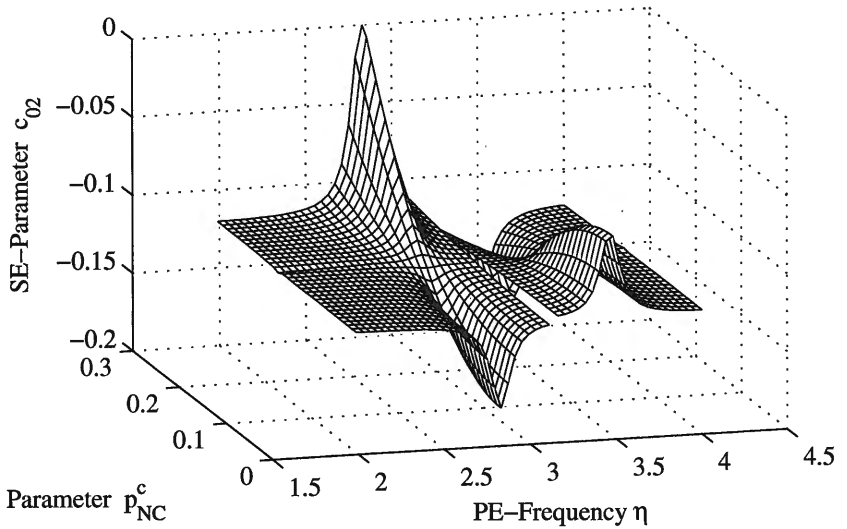
$$\mathbf{M}\ddot{\mathbf{x}} + \mathbf{C}\dot{\mathbf{x}} + \mathbf{K}\mathbf{x} + \cos(\omega t)(\mathbf{P}^C + \mathbf{P}_{NC}^C)\mathbf{x} = \mathbf{0}. \quad (3.32)$$

The newly introduced matrix is defined as

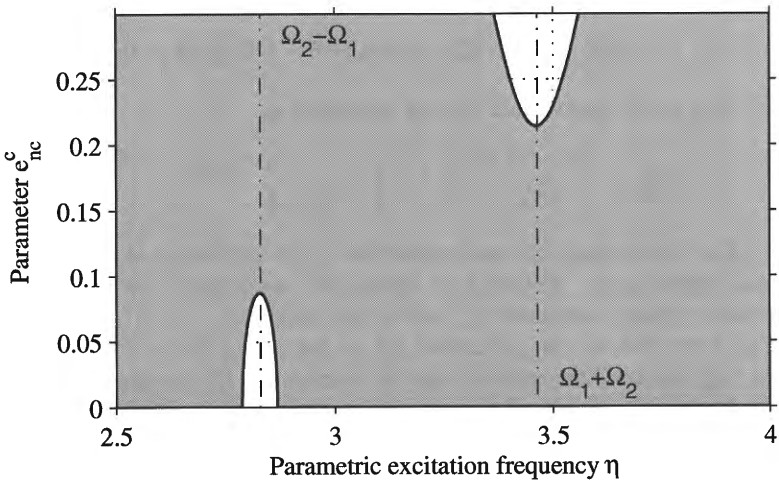
$$\mathbf{P}_{NC}^C = \begin{bmatrix} 0 & p_{nc}^c \\ -p_{nc}^c & 0 \end{bmatrix} = \begin{bmatrix} 0 & e_{nc}^c k_{nc} \\ -e_{nc}^c k_{nc} & 0 \end{bmatrix}. \quad (3.33)$$

For this system the analytical first order approximation can be applied right away. Figure 3.19 shows the result for a variation of the cross-coupling parameter e_{nc}^c within the range $[0.0, \dots, 0.3]$. Both plots in Fig. 3.19 hold for the parameter set as defined in Table 3.2. In Fig. (a) on top the critical value for the SE-parameter c_{02}^{se} is represented by a mesh plot with hidden lines removed for a better clarity. The result was obtained from analytical first order approximation, as one can tell from the gap between the two surfaces.

Starting with a value of $e_{nc}^c = 0$ we recognize the already familiar result of Fig. 3.11 (bottom). With increasing cross-coupling parameter the stabilizing effect of the anti-resonance at $\Omega_2 - \Omega_1$ is reduced as well as the resonance behavior of $\Omega_1 + \Omega_2$. At a value of $e_{nc}^c \approx 0.17$ both



(a) Critical SE-parameter obtained from analytical first order approx.



(b) Stability chart for $c_{02}^{s0} = -0.16$. White areas indicate stable system.

Figure 3.19: Stability investigation for a 2-dof system with non-conservative parametric excitation. Data as given in Table 3.2

3.6. Anti-resonance at $\Omega_1 + \Omega_2$

anti-resonance and resonance vanish and the system is unstable below $c_{02}^{se} = -0.12$ regardless of the PE-frequency. Beyond this limit value the situation reverses. A resonance which increases the amplitude develops at $\Omega_2 - \Omega_1$, whereas the anti-resonance evolves at $\Omega_1 + \Omega_2$.

Figure 3.19(b) shows a stability chart, obtained from numerical Floquet-analysis, for a distinct value of the SE-parameter $c_{02}^{se} = -0.16$. One can see that the regions of stability are indeed centered with respect to the corresponding combination resonance frequency. It is interesting to note that the stability interval for $\Omega_1 + \Omega_2$ widens significantly with increasing cross-coupling parameter e_{nc}^c .

The introduction of non-conservative forces by the cross-coupling matrix \mathbf{P}_{nc}^C might seem to be very artificial and not realistic in an actual system. However, non-conservative forces are well known in some mechanical systems as for example in rotating machinery. Usually they are not very welcome and mostly cause troubles, but at least they do exist in real systems. An option to generate such forces intentionally is a mechatronic device which processes measured signals and applies them to the system with some kind of actuator.

Chapter 4

Equivalent damping of parametric excitation

The bottom line of the last chapter is the conclusion that parametric stiffness excitation may not only "pump" energy into the system, but can also absorb vibration energy at a certain frequency. This frequency is termed *parametric anti-resonance frequency*, since it coincides with one of the parametric combination resonance frequencies, but has the opposite effect on the vibration amplitudes. The amount of energy withdrawn per time unit from the system determines whether just a vibration reduction or full vibration suppression is possible. Therefore it was already suggested that the effect of parametric stiffness excitation can also be seen as a kind of generalized damping.

We will focus on this idea now and continue to investigate a 2-dof system. Figure 4.1 shows the system under investigation in this chapter, which differs from the previous model (Fig. 3.2) with respect to the damping element c_{12} . This additional damper connects both masses and was added to make the model more realistic and account for some amount of relative damping that is always present, either unintentionally due to material damping or intentionally from a dedicated damping element. Only the linear(ized) system will be studied and cubic damping is not considered, since we will rely on the numerical Floquet-method almost exclusively.

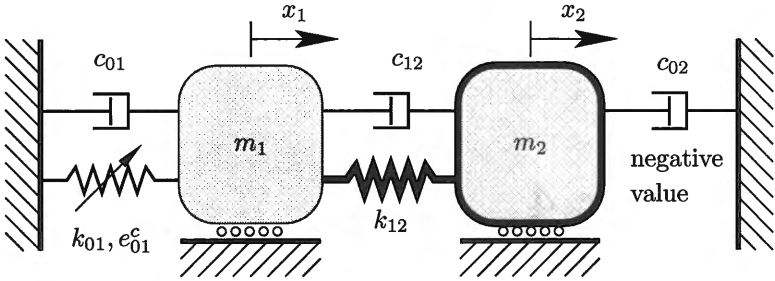


Figure 4.1: Mechanical 2-dof system with parametric stiffness excitation $k_{01}(1 + e_{01}^c) \cos(\eta\tau)$ and self-excitation due to negative damping $c_{02} < 0$. See Table 4.1 for default data.

4.1 System without coupling damper

The equations of motion for the system shown in Fig. 4.1 can be derived from the generic set Eqs. (3.1) by omitting zero elements and rescaling as

$$\mathbf{M}\mathbf{x}'' + \mathbf{C}\mathbf{x}' + \mathbf{K}\mathbf{x} + \cos(\eta\tau)\mathbf{P}^C\mathbf{x} = 0 \quad (4.1)$$

with matrices \mathbf{M} and \mathbf{K} structured as in Eqs. (3.2) and

$$\mathbf{P}^C = \begin{bmatrix} e_{01}^c k_{01} & 0 \\ 0 & 0 \end{bmatrix}. \quad (4.2)$$

Although the damping element c_{12} was introduced and matrix \mathbf{C} is defined as

$$\mathbf{C} = \begin{bmatrix} c_{01} + c_{12} & -c_{12} \\ -c_{12} & c_{02} + c_{12} \end{bmatrix}, \quad (4.3)$$

we will temporarily set $c_{12} = 0$ to obtain some needed results before we can break new ground with $c_{12} \neq 0$ in the following Section 4.2.

In the parameter studies so far, the PE-frequency η was a main parameter of variation. The following parameter studies will involve four parameters altogether, namely the damping parameters c_{01} , c_{12} , the SE-parameter c_{02}^{se} (which is considered as a damping parameter with negative value $c_{02}^{se} = c_{02} < 0$) and the amplitude factor of the parametric excitation e_{01}^c . Since we are already running out of dimensions for graphical representations, we will freeze the PE-frequency η at the parametric anti-resonance frequency $\Omega_2 - \Omega_1 = \eta$.

4.1. System without coupling damper

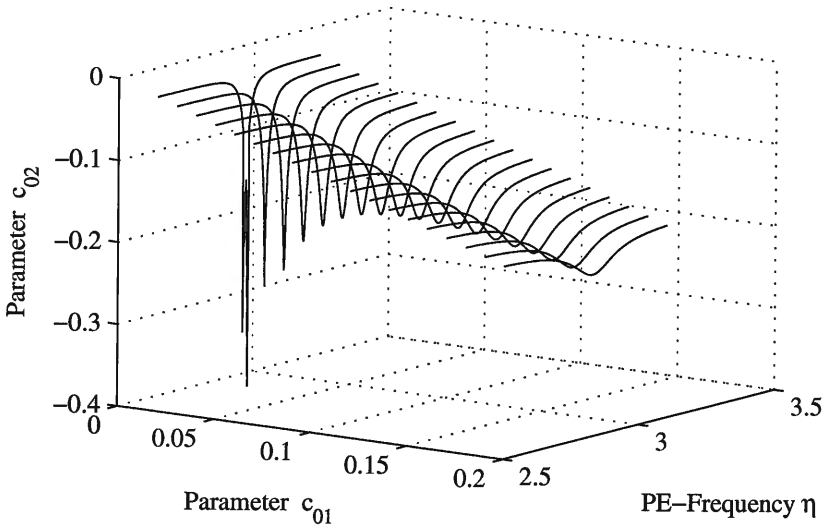


Figure 4.2: Stability threshold surface (obtained from analytical first order approximation) for 2-dof system. Stable above and unstable below surface. Data as given in Table 4.1.

It was shown in the previous chapter that this PE-frequency gave excellent results for the system under investigation, with respect to system stabilization and vibration amplitude reduction. As a last diagram of this kind Fig. 4.2 shows how the critical SE-parameter c_{02}^{se} depends on the damping parameter c_{01} and on the PE-frequency η . The following figures are composed of the intersection lines, which occur when the stability threshold surface as suggested by the array of lines in Fig. 4.2 is cut along $\eta = \Omega_2 - \Omega_1 = \text{const.}$

A few remarks on the result of Fig. 4.2 have to be made. First of all it is obvious that a low value of the damping parameter c_{01} favors the effect of parametric excitation by lowering the stability threshold to larger negative values of the SE-parameter. This seems to be somewhat counter-intuitive at first glance and we will investigate this result in more detail in the following. Secondly, the result was calculated using the analytical first order approximation. From the result at $c_{01} = 0.02$ (the line on the lower end of the parameter range) one can see that this

Table 4.1: Default parameters for 2-dof system as shown in Fig. 4.1 and used in the following studies

Parameter	m_1	m_2	k_{01}	k_{12}	k_{02}	
	1.0	8.0	1.0	8.0	0.0	
Parameter	c_{01}^d	c_{12}^d	c_{02}^d	e_{01}	e_{12}	e_{02}
	0.15	0.0	0.0	0.2	0.0	0.0
Parameter	c_{01}^{se}	c_{12}^{se}	c_{02}^{se}	$\eta = \Omega_2 - \Omega_1$		
	0.0	0.0	-0.16	2.8284		

calculation is not really reliable, since there is a spurious spike within the vibration suppression interval. For parameter values $0.02 > c_{01} \geq 0.0$ the results become increasingly faulty and cannot be used. Such extreme parameter values (extreme in the view of the analytical approximation) are beyond the validity range of the first order approximation. This is the reason for employing the much slower but also more accurate numerical Floquet-method for the following investigations.

To facilitate the interpretation of studies with active parametric excitation, a simple result for the plain system with no PE ($e_{01}^e = 0$) is quite useful. Figure 4.3 shows a stability chart for this case, which was obtained by examining the real part of the system eigenvalues. The areas of stability (white) and instability (gray) are plotted in terms of the damping parameter c_{01} and the SE-parameter $c_{02}^{SE} = c_{02}$. The stability boundary is composed of two practically straight bold lines forming a wedge. By continuing these lines, the unstable area is divided by dashed lines into three different areas, which are labelled "I", "II" and "B". Area "I" denotes the parameter range where the real part of the lower eigenvalues becomes positive, hence the first vibration mode becomes unstable. Consequently, area "II" represents instability of the second mode, and in the area "B" both modes are unstable.

The star-symbol (\star) in Fig. 4.3 is plotted at $c_{01} = 0.15$, $c_{02} = -0.16$ and shows where the 2-dof system with default parameters (see Table 4.1) is located with respect to the stability boundaries. One can see that the system is unstable in the first mode, which confirms our previous results.

From Fig. 4.3 it also becomes clear that negative damping (i. e. self-excitation) per se can be compensated if sufficient positive damping is present in the system. However, it depends on the location of the damping element whether it can compensate negative damping or not. This

4.1. System without coupling damper

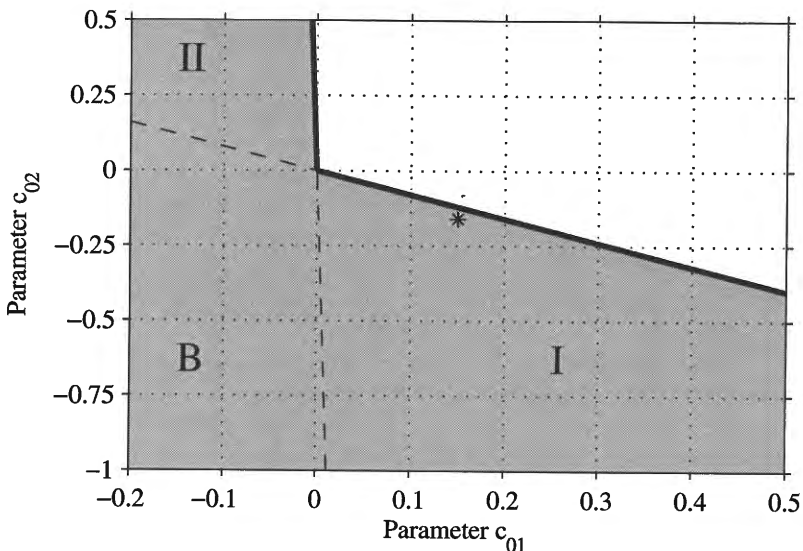


Figure 4.3: Stability chart for 2-dof system (Table 4.1) except for parametric excitation $e_{\delta_1}^0 = 0.0$ (without PE) and coupling damping element $c_{12} = 0.0$ (zero damping). White area indicates stability of trivial solution.

can be seen easily from the figure. Since both dampers c_{01} and c_{02} are located such that they are both effectively working when the system oscillates in the first mode, they can almost compensate each other. For $c_{01} = 0.5$ the corresponding value at the stability boundary is $c_{02} \approx -0.4$, which of course is not the same value, but not too far off.

For the second mode the situation is completely different. First of all, the second mode alone can only become unstable if $c_{01} < 0.0$ hold. Then c_{02} must be positive, and we have a situation in our 2-dof system, where the self-excitation and the positive damping element have changed places. Even a very small negative value of c_{01} needs a large positive c_{02} to stabilize the system, as one can see and extrapolate from the upper left corner of the diagram. Thinking in terms of vibration modes this outcome is pretty clear. Given the data of the default system, the second mode is characterized mainly by vibrations of mass m_1 , since it is much

smaller than mass m_2 . Therefore the (now positive) damper c_{02} is only marginally effective, which results in the poor performance of stabilizing the system. With respect to the second mode, the stability situation can be improved drastically by introducing a damper c_{12} . This damper is very effective for that mode, as we will see in the following section.

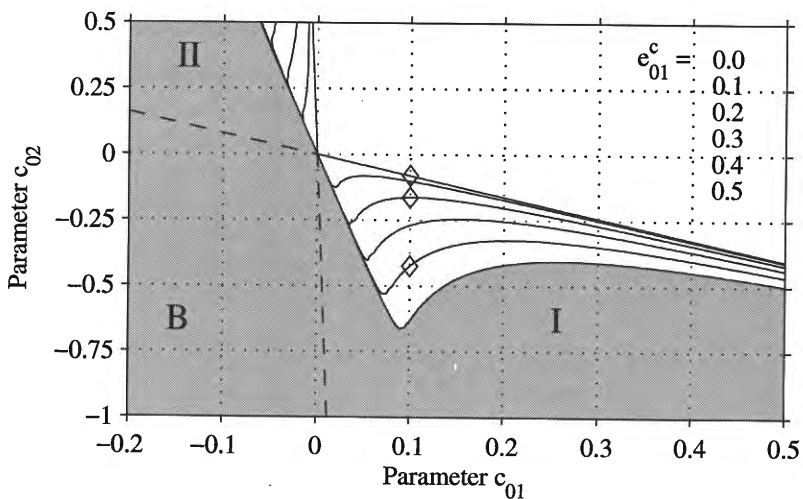
But before we turn to the case $c_{12} > 0$, we will activate parametric excitation and see how it affects the results. Figure 4.4(a) shows a stability map for different levels of the parametric excitation parameter e_{01}^c , ranging from zero excitation (as shown before) to $e_{01}^c = 0.5$. For the latter value the region of instability is shaded gray, for all other values just the stability boundaries are plotted.

Figure 4.4(a) is a very instructive diagram and contains important information. One recognizes that PE converts parts of unstable areas in area "I" and in area "II" into stable regions, but does not reach into area "B". For appropriate parameter sets either the first or the second mode can be stabilized. The $\sqrt{\quad}$ -like shape of the region that is stabilized in area "I" increases almost linearly with increasing PE-parameter, at least with respect to the maximum intrusion into the unstable region. The diamond symbol (\diamond) on three of the boundary lines will be needed later in combination with Figs. 4.7 to 4.9.

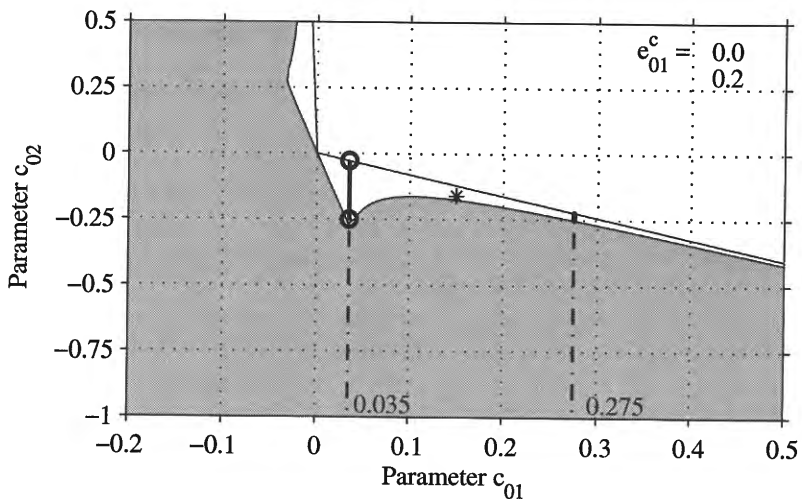
There are three asymptotes common for all threshold curves. Both stability boundaries of the system without PE serve as asymptotes for large values of the parameters c_{01} and c_{02} , respectively. A third asymptote can be identified that cuts through areas "I" and "II" and intersects the origin of the coordinate system. Parametric excitation of any level enlarges the stability region of the system, but its effectiveness depends significantly on the choice of parameters. This is visualized in Fig. 4.4(b).

Figure 4.4(b) shows the stability region for only two different values $e_{01}^c = 0$ and the default parameter value $e_{01}^c = 0.2$ to demonstrate the gain of damping obtained from PE. The star-symbol (\star) is used again to indicate default parameters and is now located in the stable region. Of course the benefit from PE must be related to the result of the plain system without parametric excitation. We keep all other parameters fixed, change only the damping parameter c_{01} and observe how the stability threshold is affected. For the parameter range $0 < c_{01} < 0.035$ there is an almost linear relationship between c_{01} and c_{02} . At $c_{01} \approx 0.035$ a local minimum for c_{02} is reached. This is the optimum value for c_{01} to maximize the benefit from PE for this parameter set. The difference between the two parameter values of c_{02} can be interpreted as the *equiv-*

4.1. System without coupling damper



(a) Variation of PE-parameter $e_{01}^c = 0.0 \dots 0.5$.



(b) Variation of PE-parameter: $e_{01}^c = 0.0$ and 0.2 .

Figure 4.4: Stability chart for 2-dof system (Table 4.1): without coupling damping element ($c_{12} = 0.0$). White areas indicate stability.

alent damping introduced by parametric excitation at the location of c_{02} .

Within $0.035 < c_{01} < \approx 0.1$ both values, the equivalent damping gain and the stability threshold, grow worse. The next interval $0.1 < c_{01} < 0.275$ is characterized by a further decrease of the damping gain, but the stability threshold continuously changes to higher values of the negative damping. At $c_{01} = 0.275$ the same level for the SE-parameter is reached as at the local minimum value $c_{01} \approx 0.035$. However, the benefit from PE is marginal if compared to the system without PE. Further increase of the damping parameter c_{01} lets the stability thresholds approach the asymptote.

Note also the consequence of the fact that the other asymptote runs through the origin of the stability chart and manifests an almost linear relationship between c_{01} and c_{02} near zero values. If a parameter combination is on the stability boundary for a certain level of the PE-parameter e_{01}^c and also lies on this asymptote, then a further increase of e_{01}^c does not have any positive effect on the performance of the system. In such a case the system is marginally stable no matter how high the PE-amplitude is increased. This is very important to realize, since it has to be taken into account when a real system is designed.

Finally let us show an interesting and instructive example that results from the complicated functional relationship of the stability boundary of the system parameters c_{01} and c_{02} . From Figs. 4.4 one can see that all stability boundaries in terms of c_{02} reach a maximum value for values of c_{01} after exceeding a local minimum at the optimal value for c_{01} . For a fixed value of the SE-parameter c_{02} and the PE-parameter e_{01}^c this may lead to surprising results if the damping parameter c_{01} is varied in combination with the PE-frequency η .

In Fig. 4.5 such a result is plotted for $c_{02} = -0.25$ and $e_{01}^c = 0.3$. Due to the "hump" of the stability threshold an isolated region of stability appears in the vicinity of $c_{01} = 0.075$ and explains the rather weird shape of the stability region in Fig. 3.12. This result also can serve as a warning concerning the application of path-following methods, since such isolated regions are very hard to find if good starting values are not available.

Another important detail that can be seen from the figure concerns the PE-frequency η . The parametric anti-resonance frequency $\Omega_2 - \Omega_1$ hits almost exactly the center of the isolated area and meets the other stability threshold line at the minimum value. This is reassuring since

4.2. System with non-zero coupling damper

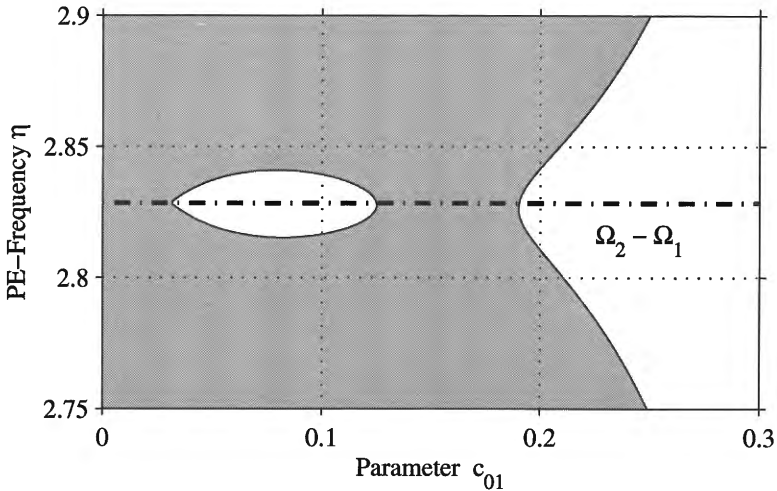
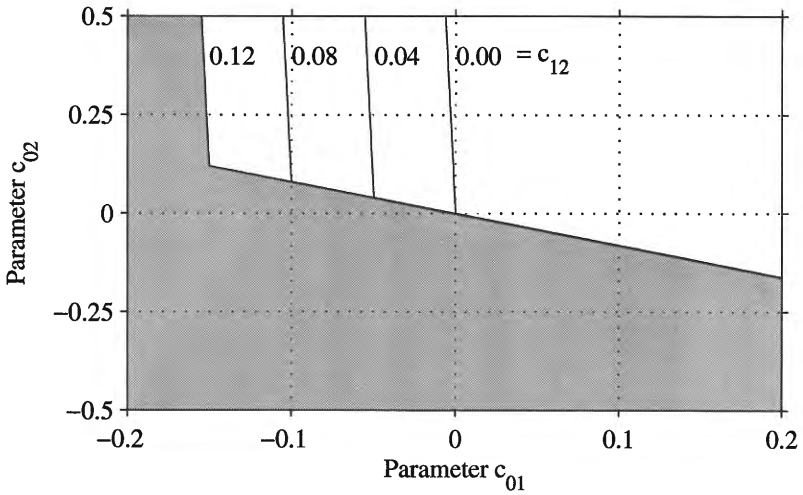


Figure 4.5: Stability chart for parameters $e_{01}^c = 0.3$, $c_{02} = -0.25$, $c_{12} = 0.0$. White areas indicate stability of the trivial solution.

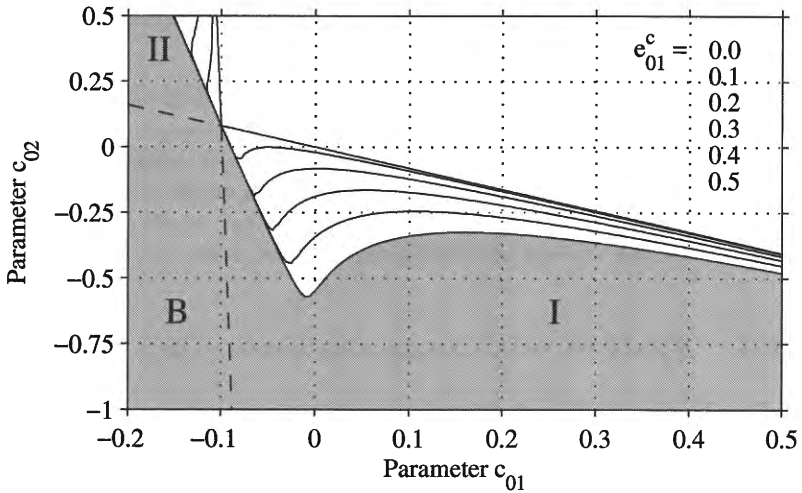
it confirms that restricting our study to just this frequency is justified for this system. We have to give emphasis to this conclusion, because it is not self-evident for all possible systems or even parameter sets. In Chapter 5 another 2-dof system will be presented which does not behave as benignly as the present system and which can serve as a counter-example for the method of investigation as used here.

4.2 System with non-zero coupling damper

After the extensive study of the case $c_{12} = 0$, now non-zero values are considered for the coupling damping element c_{12} . We start the same way as in the previous section and calculate a stability chart for the case when no parametric excitation is active. The corresponding diagram is shown in Fig. 4.6(a) and holds for different values of the damping parameter $c_{12} = [0.0, 0.04, 0.08, 0.12]$. The unstable region is shaded gray for the largest value given for c_{12} . The result as shown in the stability chart is not really surprising, since we have mentioned already that the coupling



(a) Parameter variation $c_{12} = 0.0 \dots 0.12$, without PE ($e_{01}^c = 0.0$).



(b) Variation of PE $e_{01}^c = 0.0 \dots 0.5$ for $c_{12} = 0.08$.

Figure 4.6: Stability chart for 2-dof system (Table 4.1): (a) without and (b) with parametric excitation. White areas indicate stability.

4.2. System with non-zero coupling damper

damping element is only effective when a relative motion between the masses m_1 and m_2 occurs. Therefore, the stability threshold of the first mode remains unchanged and only the stability border of the second vibration mode is affected almost exclusively. The stability region is extended to larger negative values of damper c_{01} , which does not seem to be of interest at the moment.

The next step is to activate parametric excitation and investigate the result. Figure 4.6(b) shows the stability regions for the single value $c_{12} = 0.08$ and different values of the PE-parameter $e_{01}^c = [0.0...0.5]$. By comparing this result with the previous one of Fig. 4.3(b) it is obvious that the new stability areas look very similar to the previous $\sqrt{\quad}$ -shape regions. In fact, a close inspection reveals that the stability borders are almost identical, only the origin is shifted along the stability threshold of the first mode as in Fig. 4.6(a).

Therefore the discussion of Fig. 4.6(b) can be reduced to conclusions that result from the shift of the stability region. Without doubt the most interesting aspect of the damping element c_{12} is the new possibility to move around the local minimum of the stability region. From Fig. 4.6(b), which holds for $c_{12} = 0.08$, it can be seen that the local minimum of the stability threshold, obtained for a PE-parameter of $e_{01}^c = 0.5$, occurs close to $c_{01} = 0.0$. Due to the coupling damper c_{12} , the minimum value of c_{02} has moved with respect to c_{01} from a value just below 0.1 (see Fig. 4.3) to barely below zero. The surprising result is the fact that for such a set of system-parameters the equivalent damping of the parametric excitation exceeds a value of 0.5 and occurs for zero damping at c_{01} .

To provide more insight into the quite complicated interdependence of the damping parameters and the PE-parameter, three parameter studies are presented in the following Figs. 4.7 to 4.9. These three figures are obtained for the default parameters as given in Table 4.1, except for the parameters of variation c_{01} , c_{12} and c_{02} and the PE-parameter e_{01}^c . Figure 4.7 holds for $e_{01}^c = 0$ (i. e. PE is not active), Fig. 4.8 is valid for the default value $e_{01}^c = 0.2$, and for Fig. 4.9 a value of $e_{01}^c = 0.4$ was used. One can get a good idea of the influence of each parameter on the results from these selected figures. An exhaustive parameter study would exceed the limits of this monograph.

All three figures are organized in the same manner. The figures on top show a 3D-plot of the stability threshold surface as a function of c_{01} , c_{12} and c_{02} for a selected value of the PE-parameter e_{01}^c . For parameter

combinations below the surface the system is unstable, above the surface stability prevails. These plots shall give a clear picture of the shape of the surface. Unfortunately, printing and reproduction of the mesh plots did not work very well in certain areas. The 3D-plots are too inconvenient to read or select individual data points. Therefore, contour plots of the surfaces shown above are additionally shown at the bottom and shall be used for this purpose. The previous Figs. 4.4 and 4.6 are cross sections of the respective stability threshold surface for constant values of c_{12} .

Figure 4.7 shows the case when the parametric excitation is not active ($e_{01}^c = 0$). The stability threshold appears as an inclined plane with an almost vertical and diagonal boundary for small values of c_{01} , c_{12} . This extremely steep boundary is already known from Figs. 4.3 and 4.6 as being the stability threshold for the second vibration mode. The mesh plot shows a flat triangular shaped area in the upper left corner that exceeds the data range on the vertical axis. This boundary is fictional and does not really exist. It indicates the starting level for the search routine of the stability threshold and was not removed in the final plot, since otherwise the mesh-plotting routine would have had even more troubles to plot the almost vertical boundary.

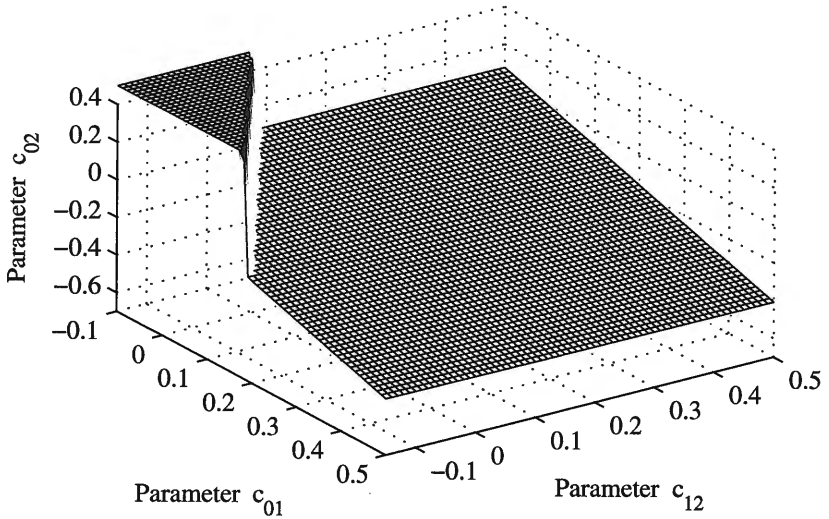
In the contour plot for the critical value of the SE-parameter $c_{02}^{se} = c_{02}$ a diamond symbol (\diamond) is plotted at $c_{12} = 0.0$, $c_{01} = 0.1$. The corresponding value of the stability threshold is $c_{02} = -0.08$. This point is marked for an easy comparison, also with the previous Fig. 4.4(a), where the same parameter combination is marked at the stability boundary for the system without PE ($e_{01}^c = 0$).

Figure 4.8 holds for the default value $e_{01}^c = 0.2$. In comparison with the previous figure we can see that the inclined plane bends downwards near the intersection with the steep boundary plane of the second mode. The intersection line becomes a narrow "groove" that basically is responsible for the most significant part of the vibration suppression effect. Other than in the previous figure the fictional part was removed, leaving a ragged and steep boundary surface to the left.

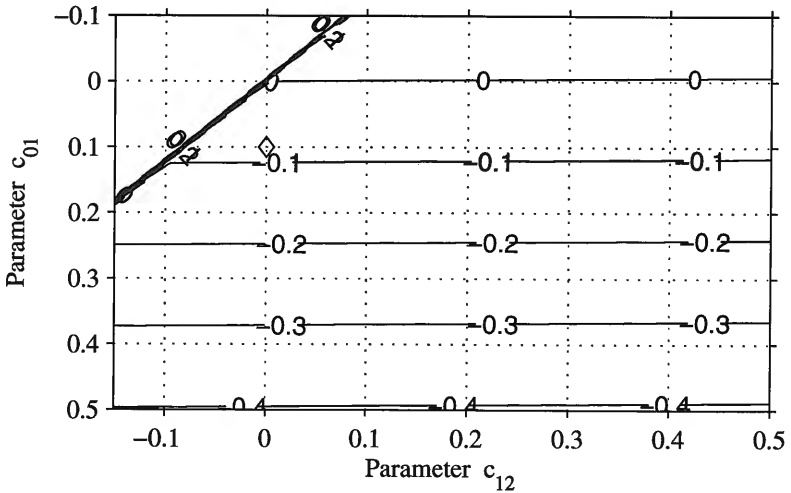
Again, the contour plot for the critical value of the SE-parameter $c_{02}^{se} = c_{02}$ contains a diamond symbol (\diamond) at $c_{12} = 0.0$, $c_{01} = 0.1$. The corresponding value of the stability threshold is $c_{02} \approx -0.16$ and can be found also in Fig. 4.4(a) at the stability boundary for $e_{01}^c = 0.2$.

The final Fig. 4.9 is valid for a PE-parameter of $e_{01}^c = 0.4$. Compared with the previous figures, the curvature of the inclined part of the surface has increased significantly. The groove has become deeper and

4.2. System with non-zero coupling damper

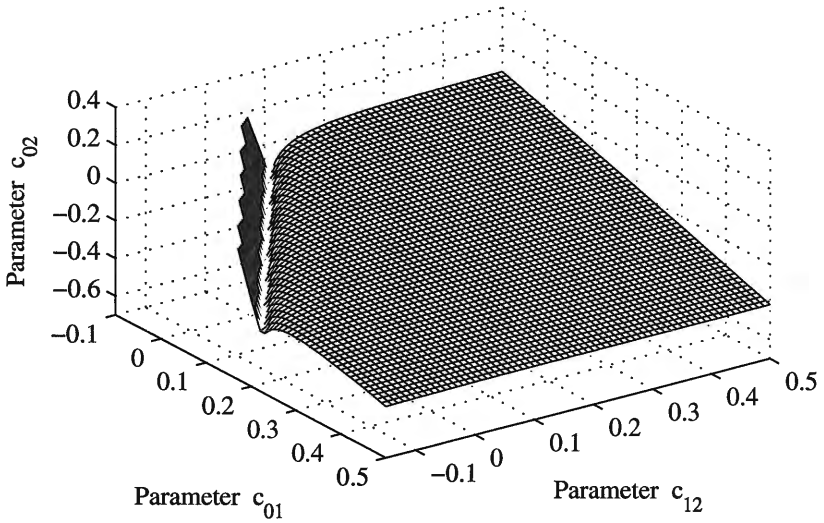


(a) Stability threshold surface (stable above surface).

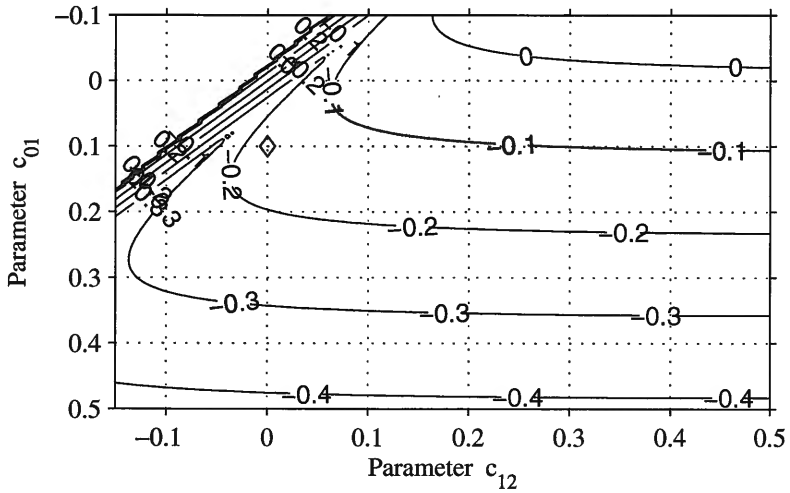


(b) Contour plot for critical value of parameter c_{02}

Figure 4.7: Stability chart for 2-dof system as shown in Fig. 4.1 with data as given in Table 4.1 except for $e_{01}^c = 0.0$ (without PE).



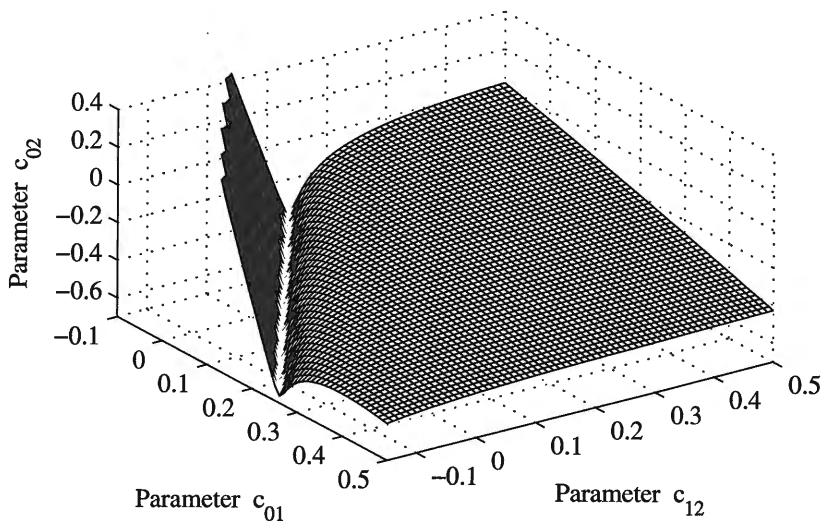
(a) Stability threshold surface (stable above surface).



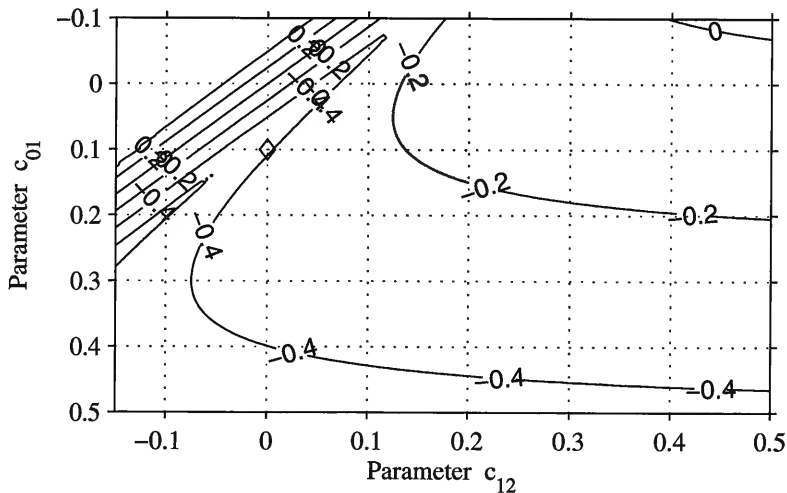
(b) Contour plot for critical value of parameter c_{02}

Figure 4.8: Stability chart for 2-dof system as shown in Fig. 4.1 with data as given in Table 4.1 (default value $e_{01}^c = 0.2$ for PE in use).

4.2. System with non-zero coupling damper



(a) Stability threshold surface (stable above surface).



(b) Contour plot for critical value of parameter c_{02}

Figure 4.9: Stability chart for 2-dof system as shown in Fig. 4.1 with data as given in Table 4.1 except for $e_{01}^c = 0.4$ (enhanced PE).

wider, and the inclination of the steep plane to the left has been further reduced. The value of the stability threshold at the diamond symbol (\diamond) is $c_{02} \approx -0.425$ and exhibits a progressive reduction of the permissible self-excitation parameter, compared with the previous results.

From all the results it is easy to recognize that increasing values of the damping parameter c_{12} have, in principle, a negative influence on the vibration suppression performance. However, this is not caused by the parametric excitation, but by the general behavior of the system without PE. Nevertheless, parameter c_{12} can be used to move the optimal parameter combination for maximum performance to a certain value of parameter c_{01} which is realistic or achievable in an actual application. The results and diagrams also include negative values for c_{12} since the performance improves for such values. Of course, a negative damping value is equivalent to self-excitation. Therefore, a really strange situation is considered where negative damping is desirable to improve the performance of the parametric excitation to suppress self-excited vibrations due to negative damping at another location, namely c_{02} . Although negative damping can be brought about quite easily in a mechatronic system by a closed-loop controller with appropriate derivative gain, a situation as just outlined does not seem to be of practical relevance.

4.3 Computational aspects

Finally a few comments will be made on the numerical procedure that was employed to generate Figs. 4.7 to 4.9, because it was different and more costly than for the previous results. Since the critical value of a third parameter at the stability threshold has to be calculated for a given pair of two parameters, say c_{01} , c_{12} , a search routine has to be used. The stability threshold appears as the critical parameter value where the maximum absolute value of the monodromy matrix reaches and crosses a value of one. Therefore, each point of the mesh is obtained from a root finding procedure which itself involves the repeated calculation of the monodromy matrix via numerical integration over one period of the parametric excitation. To keep computational time on a PC within reasonable limits for this costly task, a highly effective simulation environment [55], [8] was used and the user-provided routines were carefully optimized for computational speed.

Another problem arises from the shape of the stability surface to be

4.3. Computational aspects

calculated. The root-finding routine can be trapped by multiple zeros along the search direction. Therefore one has to make a smart choice for the third parameter that determines the search direction. For example, it is much more difficult to get the same result as shown in Fig. 4.9 when c_{12} and c_{02} are chosen as the basic parameters and c_{01} is the search variable for the instability boundary. Due to the fold of the stability threshold surface near the optimal parameter combinations one will have up to three penetrations, i.e. zeros for the root finding procedure in the parameter range as shown. Also, if c_{12} is chosen as the search direction, up to two intersections are encountered. Therefore c_{02} turns out to be the best choice for the search parameter, although there are still some difficulties for $c_{02} > 0$. In the very steep part of the stability threshold surface, near $c_{12} < 0$ and/or $c_{01} < 0$, the surface may have an overhanging part for $e_{01}^c > 0$ and may cause inaccurate results in this region. This overhang can be seen quite clearly in the upper left corner of Fig. 4.4. Since this affects only parts of the results we are not focused on in this section, no efforts were made to address this problem thoroughly and to improve the results.

Chapter 4. Equivalent damping of parametric excitation

Chapter 5

Parametric absorber for vibration suppression

The reduction of the *forced vibration* response of a mechanical system, especially at a certain part or location of the system, can be achieved by attaching a vibration absorber. Such an absorber basically is a tuned single-dof system which is attached to the original system and, when properly tuned, achieves a vibration reduction. This principle is well established, has been investigated thoroughly in the past, and is applied in practice many times. J.Q. Sun et al. present a rather complete and up-to-date survey on conventional absorbers in [80].

A conventional absorber modifies the frequency response function of the original system, especially in the vicinity of the tuning frequency, and lowers the vibration level of the system. A properly working absorber will reach maximum vibration amplitudes at the tuning frequency, while the location where the absorber is attached will experience a low vibration level at the same time. In principle, an energy transfer takes place from the location where the external excitation introduces energy into the system, to the vibration absorber, which counteracts the action of the external forces and (in general) dissipates energy.

In this chapter we will introduce the concept of a *parametric absorber*, which has little in common with the conventional absorber as outlined before. Only the basic idea of attaching an additional single-dof subsystem to a main system or structure is adopted and justifies the naming. We will call a substructure which incorporates a periodically

time-varying parameter a *parametric absorber (PA)*. The purpose of this novel kind of absorber will be the cancellation (or at least reduction) of *self-excited vibrations*. This is the major point which distinguishes the *PA* from a conventional absorber. In the previous chapters it has been shown that parametric excitation can stabilize the stationary (trivial) solution of a system. A properly designed parametric absorber will therefore stabilize the system and completely put it at rest.

The most simple application imaginable of this idea is an unstable single mass vibrational system which is stabilized by an additionally attached parametric absorber. Hence, we end up with a specialized version of the two-mass system as investigated in the previous chapter. In the next section we will introduce a generic single-mass main system with an attached parametric absorber, followed by two principle studies on the application of such a *PA*. The content of the first application has its roots in a conference contribution [18] by the author and A. Tondl and investigates vibration cancelling by parametric excitation of flow-induced vibrations of a main mass. The second study is based on a conference paper [21] by the author and will investigate dry friction as a source of self-excited vibrations.

5.1 Main system with parametric absorber

Figure 5.1 shows a generic linear 2-dof system which consists of a main system and parametric absorber attached to the main system. The latter consists of a main mass m_1 which is connected to the inertial reference frame by a constant main stiffness k_{01} . To emphasize also graphically the main system in Fig. 5.1, the main mass and stiffness are plotted with bold lines. In the application studies that will follow in the next sections the parameters of the main system will be chosen significantly larger than the corresponding parameters of the absorber system.

The main system is damped by the linear damping element c_{01}^d which is assumed to be at least not negative ($c_{01}^d \geq 0$). The usual graphical symbol for a viscous damper is used for this damper in Fig. 5.1.

Self-excitation forces which destabilize the single-dof system without absorber shall act on mass m_1 . We assume that the self-excitation present in the system can be represented by a negative damping element $c_{01}^{se} < 0$. A special symbol is used in Fig. 5.1, easily recognizable by the letter "S" which stands for "self-excitation". In the following appli-

5.1. Main system with parametric absorber

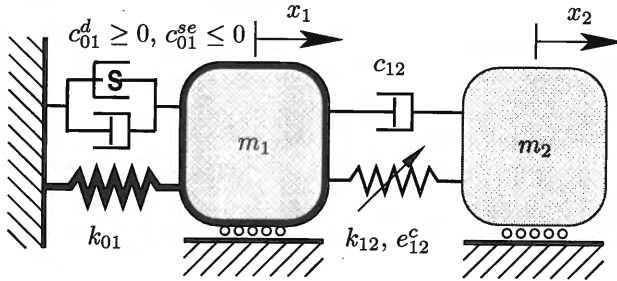


Figure 5.1: Mechanical model of a self-excited main system m_1 , c_{01}^d , k_{01} and c_{01}^{se} with parametric absorber m_2 , c_{12} , $k_{12}(1 + e_{12}^c \cos \eta\tau)$.

cation studies we will discuss how a self-excitation mechanism can be represented by such a negative linear damper. Of course, to obtain an unstable single-mass system $(c_{01}^{se} + c_{01}^d) < 0$ must hold.

The absorber system consists of the absorber mass m_2 which is assumed to be significantly smaller than the main mass m_1 . The absorber mass is attached to the main system by a stiffness element with harmonically time-varying stiffness

$$k_{12}^{res}(t) = k_{12} + p_{12}^c \cos \omega t = k_{12}(1 + e_{12}^c \cos \omega t) \quad (5.1)$$

with a constant mean stiffness k_{12} and a harmonically oscillating term with amplitude p_{12}^c and PE-frequency ω . In addition to the stiffness element a conventional positive damping element c_{12} is also inserted between the main mass and the absorber.

The equations of motion for the linear system shown in Fig. 5.1 can be derived from the generic set Eqs. (3.1). In matrix notation they read

$$\mathbf{M}\ddot{\mathbf{x}} + \mathbf{C}\dot{\mathbf{x}} + \mathbf{K}\mathbf{x} + \cos(\omega t)\mathbf{P}^C\mathbf{x} = \mathbf{0}, \quad (5.2)$$

if we keep only one (cosine) of the harmonic functions, since a phase angle cannot appear with just one parametric absorber as the single source for PE.

The matrices of Eq. (5.2) are defined for systems as shown in Fig. 5.1

as follows

$$\mathbf{M} = \begin{bmatrix} m_1 & 0 \\ 0 & m_2 \end{bmatrix}, \quad \mathbf{C} = \begin{bmatrix} (c_{01}^d + c_{01}^{se}) + c_{12} & -c_{12} \\ -c_{12} & c_{12} \end{bmatrix}, \quad (5.3)$$

$$\mathbf{x} = \begin{bmatrix} x_1 \\ x_2 \end{bmatrix} \quad \mathbf{K} = \begin{bmatrix} k_{01} + k_{12} & -k_{12} \\ -k_{12} & k_{02} + k_{12} \end{bmatrix},$$

and

$$\mathbf{P}^C = \begin{bmatrix} p_{12}^c & -p_{12}^c \\ -p_{12}^c & p_{12}^c \end{bmatrix} = \begin{bmatrix} e_{12}^c k_{12} & -e_{12}^c k_{12} \\ -e_{12}^c k_{12} & e_{12}^c k_{12} \end{bmatrix}. \quad (5.4)$$

Note that this system differs quite significantly from the system investigated in the previous Chapter 4, Figure 4.1. The location of the self-excitation has changed as well as the location of the parametric excitation. Damping for mass m_2 (now called absorber) is only provided by relative damping c_{12} . Also the mass ratio $M = m_1/m_2$ will change in the following examples to values > 1 , and we will see how this all affects the performance of vibration cancellation.

5.2 Cancelling flow-induced vibrations

We now consider a two-mass system in a vertical arrangement as shown in the scheme of Fig. 5.2(a). The main mass m_1 at the bottom shall be located in a moving medium with a constant flow velocity V_{flow} that may lead to self-excited vibrations. The mass m_2 on top, in combination with the time-varying stiffness $k_{12}(t)$ and the constant damping element c_{12} , represents the parametric absorber, which is attached to the main system in order to provide parametric vibration cancelling.

5.2.1 Effect of gravity forces

In the presence of gravity forces the equations of motion of this system are not homogeneous as in Eqs. (5.2). A constant vector $\mathbf{f}_{grav} = g[-m_1, -m_2]^T$ appears on the right hand side

$$\mathbf{M}\ddot{\mathbf{x}} + \mathbf{C}\dot{\mathbf{x}} + [\mathbf{K} + \cos(\omega t)\mathbf{P}^C]\mathbf{x} = \mathbf{f}_{grav}, \quad (5.5)$$

with g representing the acceleration of gravity. For a conventional mechanical system with time-independent stiffness elements the gravity

5.2. Cancelling flow-induced vibrations

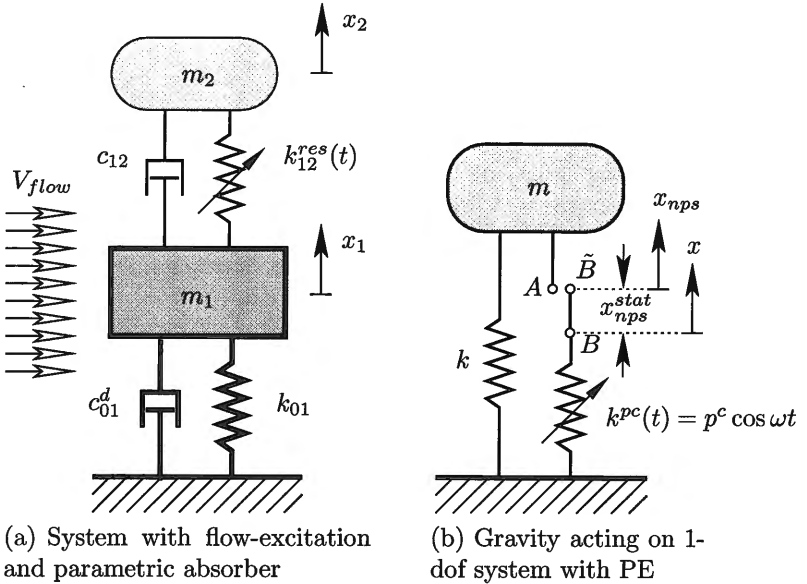


Figure 5.2: Mechanical models with parametric stiffness excitation to illustrate the effect of flow-excitation and gravity forces.

forces are just a preload to the system that results in static displacement x_1^{stat} , x_2^{stat} of both masses, which can be easily calculated from the equilibrium of forces. By referring the equations of motion to the static position of $m_{1,2}$, the constant preload \mathbf{f}_{grav} can be eliminated and a homogeneous system is obtained. With a time-dependent stiffness element $k_{12}(t)$, however, the situation is a different one. In general, the trivial solution $\ddot{x}_i = 0$, $\dot{x}_i = 0$, $x_i = x_i^{stat} = const.$ may not exist anymore.

In Fig. 5.2(b) this situation is addressed in an example showing a single-mass system in a gravity field. Stiffness k is constant, whereas $k^{pc}(t)$ is a time-varying stiffness defined as $k^{pc} = p^c \cos \omega t$. The coordinate x_{nps} describes the displacement of point A on mass m with respect to a position where the stiffness k is not prestressed, i.e. it generates no force for $x_{nps} = 0$. The corresponding point on the stiffness element $k^{pc}(t)$ is point \tilde{B} with coordinates $x_{nps} = 0$ for the undeflected spring.

We first consider the situation when point A is *not* connected to

\bar{B} . Under the effect of gravity the mass will move downwards and the equilibrium position is reached at

$$x_{nps}^{stat} = -\frac{m g}{k}. \quad (5.6)$$

The displacement of point A in the equilibrium position is x_{nps}^{stat} . The corresponding point on the stiffness element $k^{pc}(t)$ is point \bar{B} . The equilibrium position defines the origin of a new coordinate x .

Now we consider the situation when points A and \bar{B} are connected and we write down the sum of external forces acting on mass m . To simplify the analysis we take into account only forces from stiffness elements and the gravity force. We obtain

$$k x_{nps} + p^c \cos \omega t x_{nps} = -m g, \quad (5.7)$$

and with

$$x_{nps} = x + x_{nps}^{stat} \quad (5.8)$$

Eq. (5.7) becomes

$$k(x + x_{nps}^{stat}) + p^c \cos \omega t (x + x_{nps}^{stat}) = -m g. \quad (5.9)$$

After easy substitution and simplification we get

$$k x + p^c \cos \omega t \left(x - \frac{m g}{k}\right) = 0, \quad (5.10)$$

which is an expression which does not vanish for $x = 0$ and arbitrary time t . This result tells that a stationary equilibrium position cannot be obtained with this system.

If we connect points A and B of system Fig. 5.2(b) and carry out the same analysis as before, we obtain

$$k x + p^c \cos \omega t x = 0. \quad (5.11)$$

For this case the equilibrium position is not affected by the time-varying stiffness $k^{pc}(t)$. By analyzing what difference it makes if point A is connected to either point \bar{B} or B , one realizes that in the latter case the force to support the weight of mass m is not transmitted by the time-varying stiffness. In other words the time-varying stiffness elements must not experience the static shift. Obviously the parametric stiffness element has to be engaged at the static equilibrium position of the system. If this is observed, the system can be treated as if no constant external forces are acting on the system and the homogeneous generic model Eq. (5.2) is valid also for the system of Fig. 5.2(a).

5.2. Cancelling flow-induced vibrations

5.2.2 Modelling of flow-generated forces

As indicated in Fig. 5.2(a), the main mass m_1 shall be exposed to a moving medium with a constant flow velocity V_{flow} . Flow-induced lift and drag forces are generated by the medium flowing around the main mass, see Fig. 1.2(b) in Section 1.1.2. As outlined there, we can represent the total force acting on the main body by a resulting aerodynamic force $F_{x_1}^A$ in the direction of motion, which is perpendicular to the direction of flow. The second force component, aligned with the flow, acts perpendicularly to the motion of the mass and does not interest us here.

The resulting aerodynamic force $F_{x_1}^A$ is an external force, which can be calculated from

$$F_{x_1}^A = \frac{\rho}{2} A V_{flow}^2 C_x(V_{flow}, \dot{x}_1). \quad (5.12)$$

This expression defines $F_{x_1}^A$ as a nonlinear function of the flow velocity V_{flow} and the velocity \dot{x}_1 of the main mass, due to the aerodynamic force coefficient C_x which depends on the angle of attack $\alpha = -\arctan(\dot{x}/V_{flow})$ in a highly nonlinear manner, see Section 1.1.2. As also discussed there, the other symbols in Eq. (5.12) denote the constant medium density ρ and the characteristic area A of the cross-section. With the flow-generated force acting on the system, the equations of motion are, again, not homogeneous as in Eqs. (5.2). A vector $\mathbf{f}_{flow} = [F_{x_1}^A(\dot{x}_1), 0]^T$ appears on the right hand side of

$$\mathbf{M}\ddot{\mathbf{x}} + \mathbf{C}\dot{\mathbf{x}} + [\mathbf{K} + \cos(\omega t)\mathbf{P}^C]\mathbf{x} = \mathbf{f}_{flow} \quad (5.13)$$

and constitutes a nonlinear system of differential equations.

This system is already suitable for numerical integration, provided that an appropriate representation of the functional relationship of the aerodynamic coefficient $C_x(V_{flow}, \dot{x})$ is available. One may either use look-up tables generated from actual measurement data or analytical expressions with free parameters determined by a curve-fitting procedure of measurement data or CFD-results. In any case it will be important that non-linear terms are contained in the representations to provide amplitude bounding in the case of instability.

In reference [18], which investigates a similar mechanical model, an approximation frequently used to investigate wind-induced galloping instabilities is employed

$$F_{x_1}^A = [bV_{flow}^2(1 - \gamma\dot{x}_1^2)]\dot{x}_1, \quad (5.14)$$

with positive coefficients b and γ appropriately chosen. The part of the reference which contains numerical results presents maximum vibration amplitudes obtained from numerical simulation of a system as defined by Eqs. (5.13) and (5.14).

Here we will use an alternative approach and, as in the previous sections, will employ numerical Floquet-analysis to investigate the stability of the system. Only the linear and velocity-dependent part of the aerodynamic force $F_{x_1}^A$ will therefore be used. As already discussed in detail in Section 1.1.2, the general Eq. (5.12) for $F_{x_1}^A$ can be linearized in the vicinity of $\alpha = 0$ which is equivalent to $\dot{x}_1 = 0$ in terms of the variables used here. From Eqs. (1.15), (1.17) and (1.19) it is known that the aerodynamic force generated by the constant flow can be linearized and represented as a function of the velocity of mass m_1

$$F_{x_1}^{A-lin} \doteq -c^{ad} \dot{x}_1 = -\frac{\rho}{2} A V_{flow} \frac{\partial C_x}{\partial \alpha} \dot{x}_1 \quad (5.15)$$

with c^{ad} obtained for $\alpha = 0$, i.e. $\dot{x}_1 = 0$.

Since the constant parameters ρ , A and V_{flow} are all of positive value, only the slope of the vertical force coefficient $\frac{\partial C_x}{\partial \alpha}$ determines whether c^{ad} is also positive and adds damping to the system or $c^{ad} < 0$ and may destabilize the system. The aerodynamic force coefficients are mainly determined by the geometric shape of the section exposed to the flow and $\frac{\partial C_x}{\partial \alpha}$ may take on positive as well as negative values for different geometries. From numerous investigations, see e.g. [5] and [34] and references therein, it is known that simple rectangular sections lead to either positive or negative values, depending on the aspect ratio of the rectangle.

For example, a rectangle with a width to height ratio of 2:1 as plotted in Fig. 5.2(a) for m_1 has a negative coefficient of $\frac{\partial C_x}{\partial \alpha} \approx -3.0$. For a square (ratio of 1:1) $\frac{\partial C_x}{\partial \alpha} \approx -2.7$ holds, but a stretched rectangle of ratio 4:1 gives a positive value of $\frac{\partial C_x}{\partial \alpha} \approx 10$. All values mentioned hold for a certain range of the Reynolds-number.

The following numerical study does not address a specific application. Rather, we want to explore the characteristics of the parametric absorber. Consequently, all parameters of the flow model are combined in the single parameter c^{ad} and since we are mainly interested in the case of self-excitation, we use the symbol c^{se} instead of c^{ad} and define

$$c_{01}^{se} \sim c^{ad} = \frac{\rho}{2} A V_{flow} \frac{\partial C_x}{\partial \alpha}. \quad (5.16)$$

5.2. Cancelling flow-induced vibrations

We consider c_{01}^{se} to take on negative values and being proportional to c^{ad} to account for factors that adjust the physical units of c^{se} , if necessary.

Taking into account the assumptions on gravity forces and applying the linearized flow model to the mechanical system of Fig. 5.2(a), we are now at the point that this system can indeed be represented by the generic model as shown in Fig. 5.1. After changing to dimensionless parameters for the PE-frequency η and time τ we obtain

$$\mathbf{M}\mathbf{x}'' + \mathbf{C}\mathbf{x}' + \mathbf{K}\mathbf{x} + \cos(\eta\tau)\mathbf{P}^C\mathbf{x} = 0 \quad (5.17)$$

with matrices as defined in Eqs. (5.3) and (5.4).

5.2.3 Results of a numerical study

The (dimensionless) numerical values used in the following study are listed in Table 5.1 and have been chosen to be quite similar to those used in [18], although there is a minor difference in the model for the aerodynamic forces. What separates the following investigation from [18] in the first place is the application of a different numerical method. Note also, when comparing results, that the nomenclature is different. Secondly, we will now carry out parameter studies mainly for the stiffness parameter k_{12} of the absorber directly, rather than introducing relative quantities like $M = m_2/m_1$ and $Q^2 = \frac{m_1 k_{02}}{k_{12} m_2}$ as in [18]. This has the advantage that the influence of a single parameter, as the absorber stiffness, can be investigated, while other parameters are kept constant. This situation seems to be a more typical situation in a design process of an actual system.

A few words on the default values of the system parameters as given in Table 5.1 shall be added for easier interpretation of the following results. First of all it has to be pointed out that the mass ratio $m_1/m_2 = 10$ between the main mass and the absorber is large enough to consider the absorber a comparatively small mass. The additional mass of the absorber reduces the natural frequency of the system without absorber from $\Omega_1^{sub} = 1.0$ to $\Omega_1 \simeq 0.85$. The mean value of the absorber stiffness has been chosen such that the absorber system is close to an optimal value for a system without PE, to better work out the pros and cons of the parametric absorber. Damping parameters were chosen in a way that the sub-systems exhibit a reasonable damping ratio. For the default

Table 5.1: Default parameters for model of a self-excited main system with parametric absorber as shown in Fig. 5.1

Parameter	m_1	m_2	k_{01}	k_{12}
	10.0	1.0	10.0	1.0
Parameter	c_{01}^{se}	c_{01}^d	c_{12}^d	e_{12}^c
	-1.5	1.0	0.05	0.2
Frequency	Ω_1	$2\Omega_1$	$\Omega_1 + \Omega_2$	Ω_1^{sub}
	0.8543	1.7086	2.0248	1.00
Frequency	Ω_2	$2\Omega_2$	$\Omega_2 - \Omega_1$	Ω_2^{sub}
	1.1705	2.3410	0.3162	1.00

values these ratios are

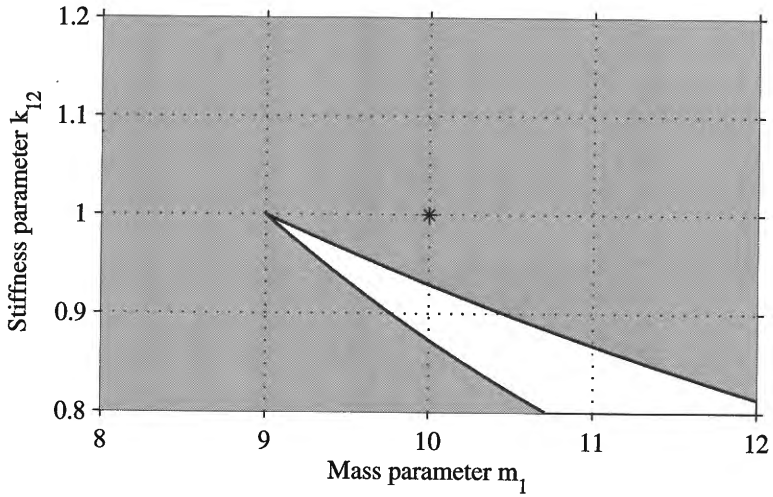
$$\zeta_1^{sub} = \frac{c_{01}^d}{2\sqrt{k_{01}m_1}} = 0.05, \quad \zeta_2^{sub} = \frac{c_{12}}{2\sqrt{k_{12}m_2}} = 0.025. \quad (5.18)$$

The equivalent damping parameter c_{01}^{se} of the self-exciting aerodynamical forces has to reduce the positive damping of the main system to a negative value ($c_{01}^d + c_{01}^{se}$) < 0 to justify an absorber, and should still destabilize the system even with additional damping obtained from the absorber without PE.

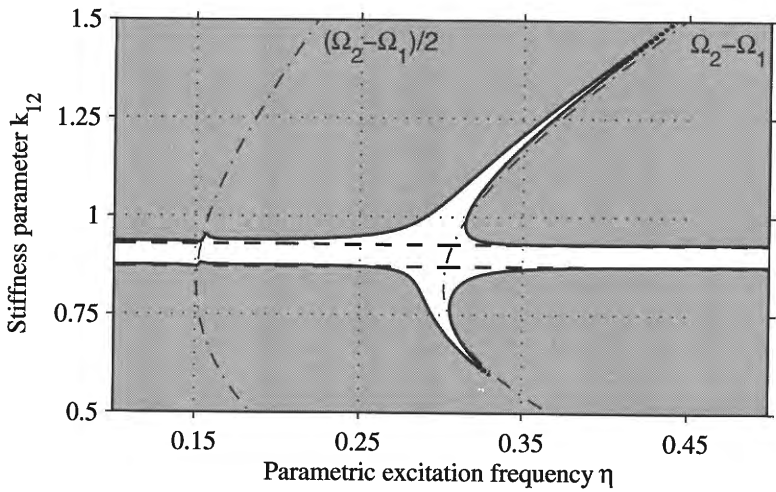
Figure 5.3(a) shows how close or distant the system is located from the stability border when the absorber is attached but parametric excitation is not active. The diagram represents a stability chart for the two parameters m_1 and k_{12} . The default values $m_1 = 10$ and $k_{12} = 1$ are indicated by a (★) star-symbol within the gray area that represents the parameter range for an unstable system. One can see that a reduction of the stiffness parameter from the default value down to $k_{12} = 0.9$ would bring the system into the wedge-shaped white area of stability. In fact, a region of stability extends from $k_{12} \approx 0.87$ to $k_{12} \approx 0.93$ for the default mass parameter $m_1 = 10$. We will again encounter this stability zone for the system with parametric excitation. On the other hand, by changing only the mass parameter m_1 of the main system, the stability region cannot be entered.

In Fig. 5.3(b) a stability chart is shown for the default mass parameter $m_1 = 10$. Instead of the mass parameter, the parametric excitation frequency η is varied and plotted on the horizontal axis. The variation parameter on the vertical axis is again the stiffness parameter k_{12} and

5.2. Cancelling flow-induced vibrations

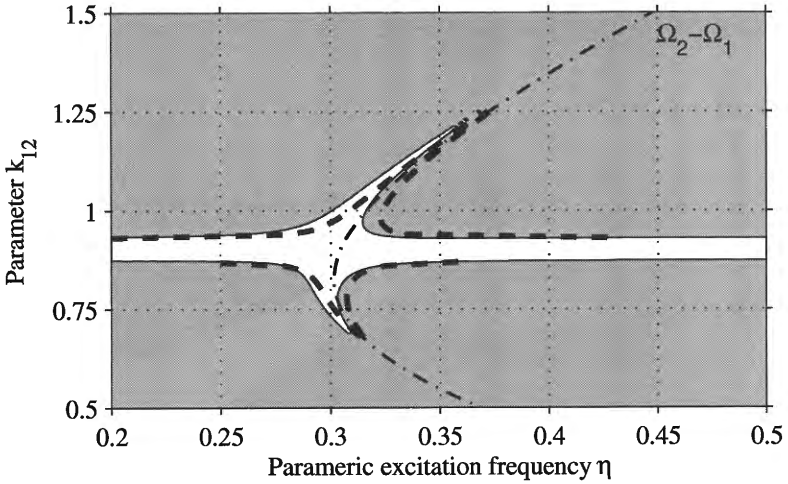


(a) Parametric excitation not active, $e_{12}^e = 0$. (\star) default values

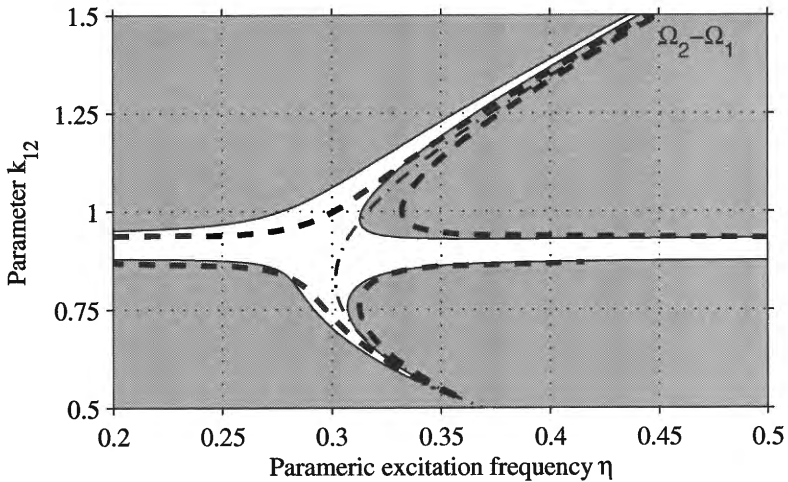


(b) Parametric excitation active, $e_{12}^e = 0.15$

Figure 5.3: Stability charts for a system with flow-induced self-excitation and parametric absorber. See Table 5.1 on p.128 for data.



(a) Comparison of analytical (- -) and numerical results, $e_{12}^e = 0.1$



(b) Comparison of analytical (- -) and numerical results, $e_{12}^e = 0.2$

Figure 5.4: Stability charts for a system with flow-induced self-excitation and parametric absorber. See Table 5.1 on p.128 for data.

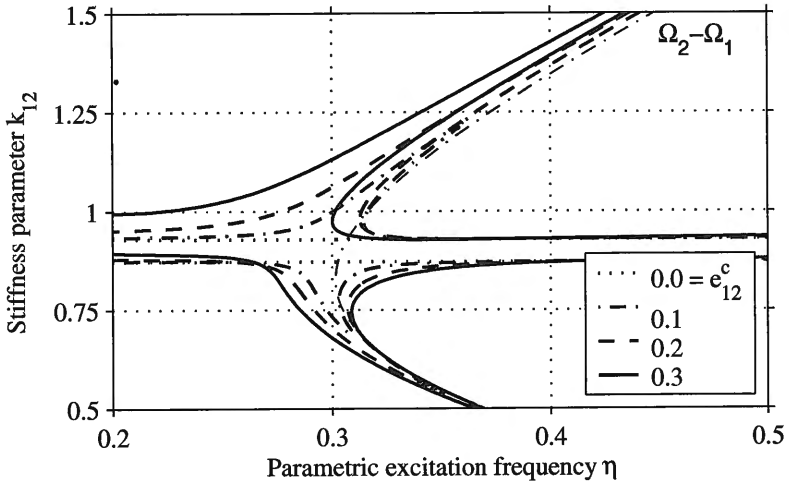
5.2. Cancelling flow-induced vibrations

the PE-amplitude is set to $e_{12} = 0.15$. Looking at the figure on top we recognize a stable region for the interval $k_{12} = [0.87\dots 0.93]$, which is independent of the PE-frequency η . Obviously, this stability region continues to exist and generates a stretched area, bounded by dashed lines, which is not significantly reduced or negatively affected by the parametric excitation. One can see this by comparing the solid lines with the dashed lines for the system with no PE. Quite the reverse happens with PE, and two "shark-fin"-like regions grow out of the stretched area. For easy reference, the combination resonance frequency $\Omega_2 - \Omega_1$ is plotted with a dash-dotted line, proving that the additional regions of stability are caused by a parametric anti-resonance near $\Omega_2 - \Omega_1$.

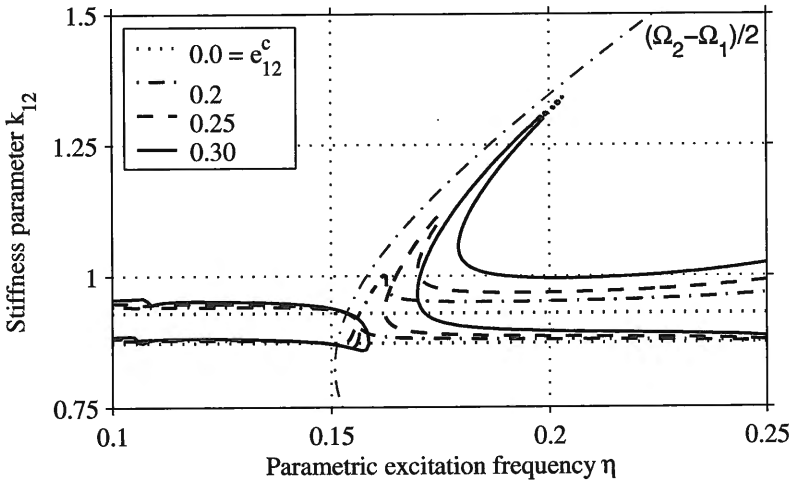
Even without a close-up of the relevant part of the figure, one recognizes that the line for $\Omega_2 - \Omega_1$ is definitely not the centerline of the extended stability regions. In fact, for most of the upper part the combination resonance frequency does not even fall into the stable region. This is a very important result, since it differs completely from the previous results in Chapter 3. As a negative consequence of this fact we have to give up the idea of using the combination resonance frequency $\Omega_2 - \Omega_1$ as our PE-frequency η . Instead, we will again have to vary η , at least near $\Omega_2 - \Omega_1$, to find the optimum frequency for parametric vibration cancelling.

Finally, in Fig. 5.3(b) we notice a very small spike of stability for $\eta \approx 0.151$. A comparison with the combination resonance frequency of the second order $(\Omega_2 - \Omega_1)/2$ reveals that for our system also this frequency shows up. In some of the following figures we will see that for other parameter sets the influence of the second order resonance will not stay as small and unimportant as it is here.

With the rather disappointing result concerning the mismatch of centerline and combination resonance frequency in mind, we have to compare again results from the analytical approximation with numerical results. In Fig. 5.4 two such comparisons are shown. Figure (a) on top holds for a PE-amplitude of $e_{12} = 0.1$ and Figure (b) for $e_{12} = 0.2$. The analytical results are plotted with bold dashed lines and superimposed by numerical results. The difference with respect to the centerlines occurs, of course, again. The shape of the stable area and the extension, though, is pretty well matched by the analytical results. Since the differences get even larger with increasing PE-amplitudes, we have to accept that analytical results are not as useful for this model as for the previous one in Chapter 3. We will therefore stick with the numerical Floquet-



(a) Stability near first order combination resonance ($\Omega_2 - \Omega_1$)



(b) Stability near second order combination resonance $(\Omega_2 - \Omega_1)/2$

Figure 5.5: Stability charts for a system with flow-induced self-excitation and parametric absorber. See Table 5.1 on p.128 for data.

5.2. Cancelling flow-induced vibrations

method for the following investigation of the parametric absorber and only compare results with respect to the combination resonance frequencies.

In Fig. 5.5(a) the numerical results from Figs. 5.4(a) and (b) are plotted again, and the results for $e_{12}^c = 0.0$ and $e_{12}^c = 0.3$ are added to complete this parameter study on the effect of the PE-amplitude. Due to the shift of the centerline of the stability region with increasing PE-amplitude, stable and unstable areas overlap for different values of e_{12}^c . Since shading the unstable areas gray, as in the previous figures, would make the plot even harder to read, this was not done here. Aside from the centerline shift we can see that an increasing PE-amplitude also widens the additional stability regions. Especially the extension to higher and lower values of k_{12} , respectively, is remarkable.

Increasing the PE-amplitude, however, has also some effect at the lower end of the frequency scale. Figure 5.4(b) shows the frequency range near the combination resonance frequency of the second order $(\Omega_2 - \Omega_1)/2$. We can see that the stretched stability region in the vicinity of $k_{12} = 0.9$ separates close to the second order resonance frequency for PE-amplitudes $e_{12}^c > 0.2$. What is a small spike for $e_{12}^c = 0.15$ in Fig. 5.3(b) becomes a narrow but quite long stability region for $e_{12}^c = 0.3$. It is interesting to note that, in contrary to the effect of the first order resonance frequency, no second spike occurs in the opposite direction.

A quite strange looking stability chart is shown in Figure 5.6. This diagram holds for the default values of Table 5.1, except for $e_{12}^c = 0.4$. For this parameter set a separation of the stability areas occurs near both combination resonance frequencies, and the former stretched stability region does not exist in-between anymore. Furthermore, for values of the PE-frequency $\eta < 0.15$, a third "rip" occurs and "rip #4" seems to evolve from a little spike. Higher order parametric resonance frequencies manifest themselves in these phenomena and make the results much harder to predict, but also more interestingly looking. The reader has certainly recognized that the figure on the title page of this monograph belongs to this series of results, and it holds for $e_{12}^c = 0.35$.

The next study will investigate what effect the "size" of the parametric absorber has on the capability of suppressing vibrations. Of course, for the dimensionless and still quite abstract model as used here, "size" cannot be defined in terms of geometric dimensions of the absorber. Instead, we relate "size" to the absorber mass m_2 and keep the dynamic parameters of the absorber constant when we change the "size". This

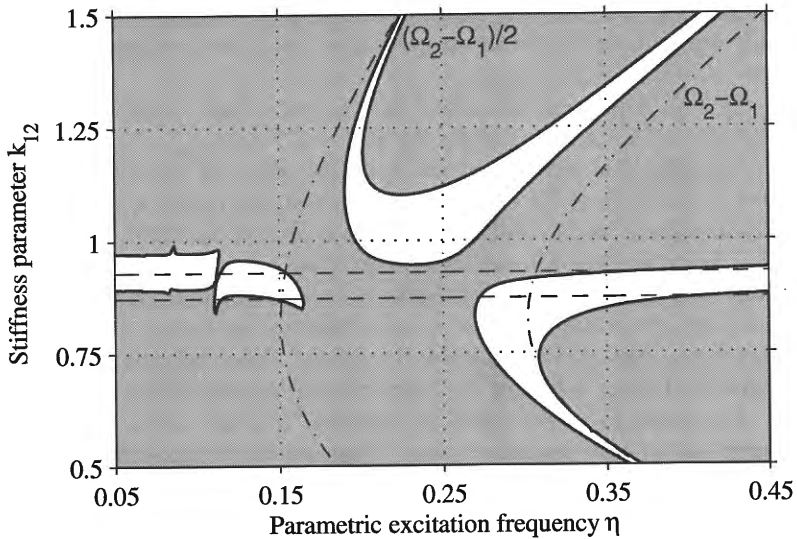


Figure 5.6: Stability chart for a system with flow-induced self-excitation and parametric absorber. $e_{12}^c = 0.4$, other data as in Table 5.1.

means that we will keep the natural frequency of the absorber at $\Omega_2 = 1.0$ and also the damping ratio at $\zeta_2^{sub} = 0.025$. To achieve this goal, we have to change the absorber stiffness k_{12} and the absorber damping element c_{12} simultaneously when mass m_2 is varied.

Figures 5.7(a),(b) and Fig. 5.8(a) refer to this parameter study. Starting from default values as listed in Table 5.1, the already known result is shown again in Fig. 5.7(a) as a reference. Reducing the "size" by 50% requires a lowering of the parameters $m_2 = 0.5$, $k_{12} = 0.5$ and c_{12} , accordingly. The PE-amplitude $e_{12}^c = 0.2$ remains unchanged, but the absolute value decreases because k_{12} is decreased. Fig. 5.7(b) shows the result for the smaller absorber. In principle, the anticipated effect of parametric vibration cancelling is still obtained from this absorber, although all stability areas become quite small and separation occurs.

Changing the "size" in the opposite direction leads to an absorber twice as heavy as the original one with parameters $m_2 = 2.0$, $k_{12} = 2.0$ and $c_{12} = 0.1$. The performance of this parametric absorber is shown in

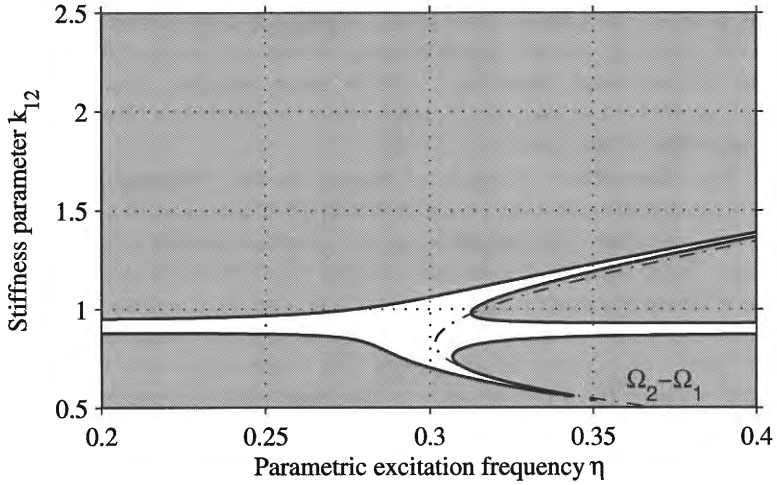
5.2. Cancelling flow-induced vibrations

the stability chart of Fig. 5.8(a). In comparison with the other results the stability area has become much larger, not only for the stability areas achieved by parametric excitation but also for the contribution from the "conventional" absorber. This is not a surprise, since the damping parameter c_{12} was also increased and therefore amplifies the energy dissipation in the system.

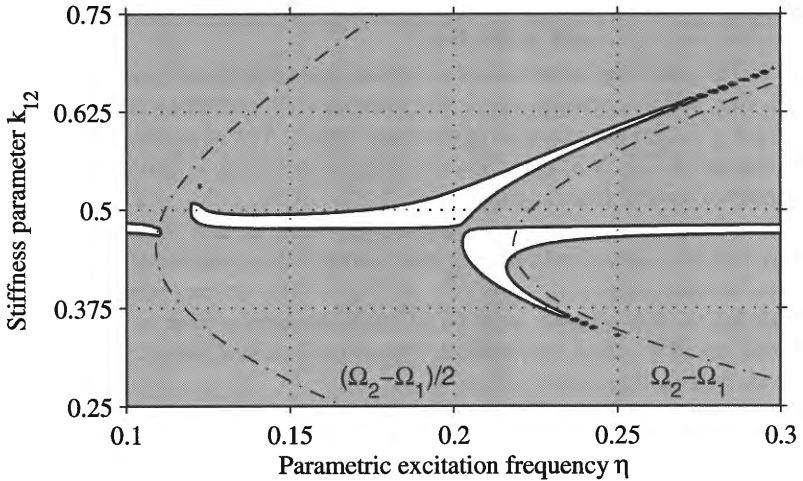
From these three "snapshots" we can see that vibration suppression by parametric excitation basically works for almost all sizes of the parametric absorber. To demonstrate and summarize this statement by a single diagram, we can calculate another result without the variation of the stiffness parameter k_{12} but where k_{12} is set to the same value as m_2 (since $\Omega_2 = 1 = \text{const.}$). This enables us to plot a stability chart for all "sizes" of parametric absorbers. For consistency with the previous plots we keep the PE-frequency as the main variation parameter on the horizontal axis. The stability chart obtained from this method of investigation is shown in Fig. 5.8(b). The stability area stretches from low frequencies for small absorbers to higher frequencies for heavier ones. This can be explained by the natural frequencies, which become increasingly separated for a 2-dof-system where the parameter values of both subsystems approach each other.

The stability interval for a certain parameter set m_2 , k_{12} and c_{12} in Fig. 5.8(b) corresponds to the interval that occurs at the same value for k_{12} in the corresponding previous figure. For example, the stability interval in Fig. 5.8(a) for $m_2 = 2$ at $k_{12} = 2$ is $\eta \simeq [0.41\dots 0.46]$. This interval can be found again in Fig. 5.8(b) at $m_2 = k_{12} = 2$. The strange "hook" at the lower end of the stability area in this diagram is caused by the increasing influence of the combination resonance frequency of the second order $(\Omega_2 - \Omega_1)/2$. In Fig. 5.7(b) one can already see that for $k_{12} = 0.5$ a small interval of stability occurs near $\eta \simeq 0.12$. For even smaller values this stability branch raises and leads to the result as observed in Fig. 5.8(b).

In this study we did stick to a subsystem frequency of $\Omega_2 = 1$, although it is obvious from Fig. 5.7(a),(b) and 5.8(a) that a slightly lower value for k_{12} (and hence Ω_2) would make the system perfectly stable without parametric excitation. So one might ask the question whether PE is only good for correcting a faultily tuned absorber and is unnecessary for a correctly designed system? To answer this question, results from another study are shown in Figs. 5.9. This time we keep all parameters fixed except for the the PE-frequency and mass m_1 . The moti-



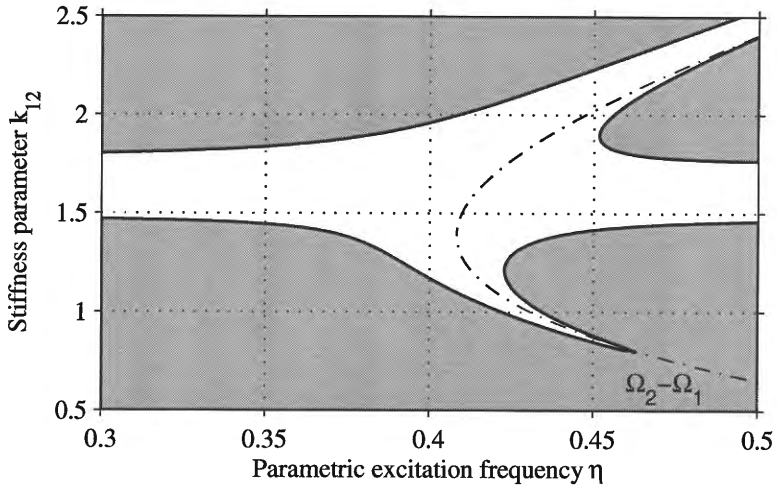
(a) Default data: $m_2 = 1.0$, $k_{12} = 1.0$ and $c_{12} = 0.05$



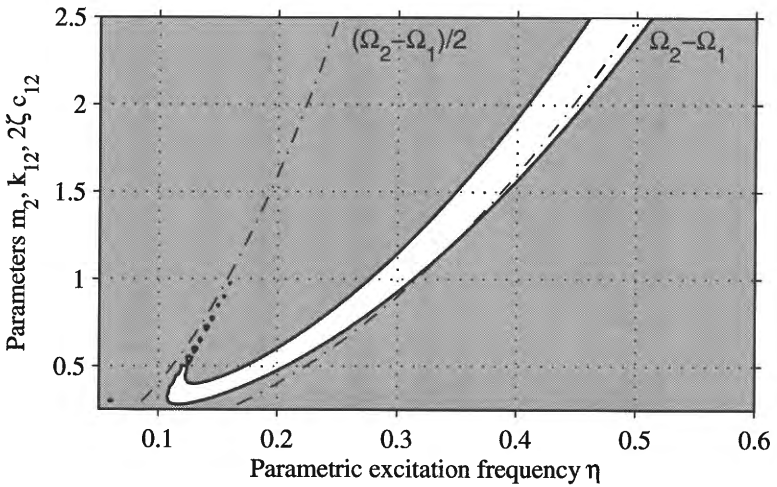
(b) Modified data: $m_2 = 0.5$, $k_{12} = 0.5$ and $c_{12} = 0.025$

Figure 5.7: Stability charts for a system with flow-induced self-excitation and parametric absorber. See Table 5.1 on p.128 for data.

5.2. Cancelling flow-induced vibrations

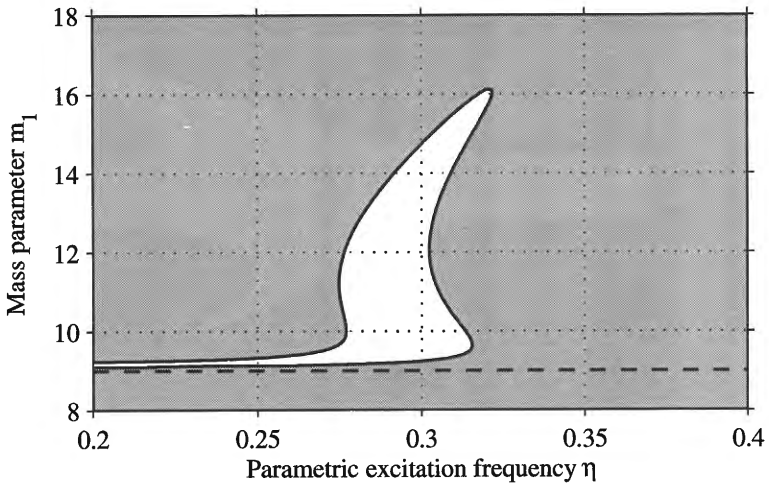


(a) Modified data: $m_2 = 2$, $k_{12} = 2$ and $c_{12} = 0.1$

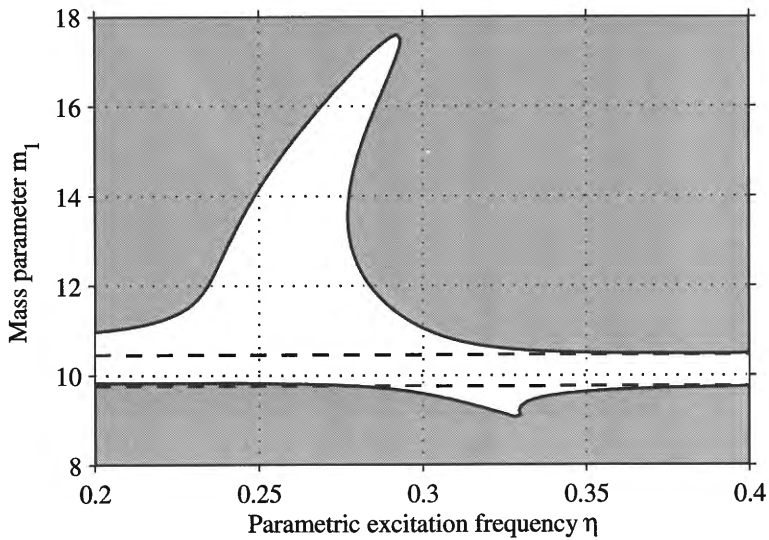


(b) Parameter study for constant dynamical parameters $\Omega_2^{sub} = 1.0$ and $\zeta_2^{sub} = 0.025$ of the absorber subsystem.

Figure 5.8: Stability charts for a system with flow-induced self-excitation and parametric absorber. See Table 5.1 on p.128 for data.



(a) Default data: $m_2 = 1.0$, $k_{12} = 1.0$ and $c_{12} = 0.05$



(b) Modified data: $k_{12} = 0.9$

Figure 5.9: Stability charts for a system with flow-induced self-excitation and parametric absorber. See Table 5.1 on p.128 for data.

5.2. Cancelling flow-induced vibrations

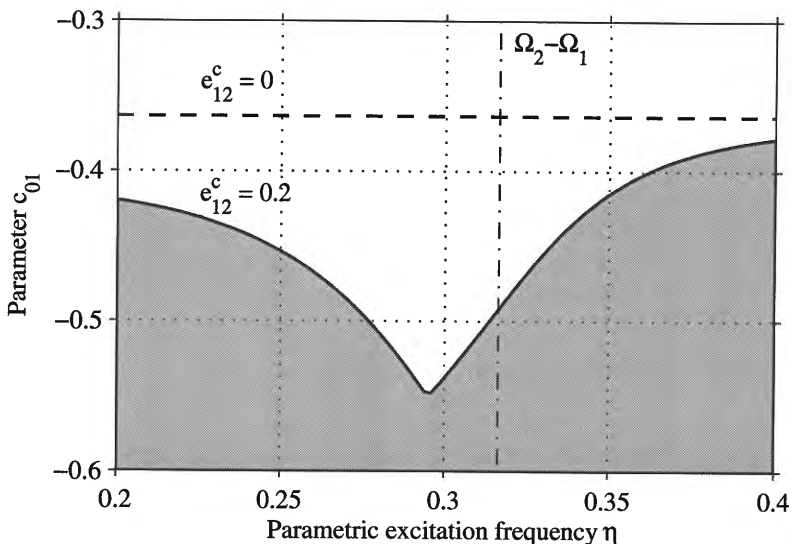


Figure 5.10: Stability chart for a system with flow-induced self-excitation and parametric absorber. See Table 5.1 on p.128 for data.

variation to study a variation of the main mass comes from the possibility that m_1 might be a very slowly but significantly varying parameter in a certain real system. In Fig. 5.9(a) the default values are used. The horizontal, dashed line at $m_1 = 9$ corresponds to the singular point ($m_1 = 9, k_{12} = 1$) of Fig. 5.3(a) and indicates the only value where the system is marginally stable. The white area demonstrates the effect of the parametric absorber. For a PE-frequency of $\eta \simeq 0.3$ the system is stabilized for a surprisingly large range of the mass parameter m_1 . Of course, this behavior cannot be achieved with a conventional absorber tuned for a single frequency of the main system.

The stability chart of Fig. 5.9(b) was obtained for parameters as before, but with the absorber stiffness set to $k_{12} = 0.9$, which stabilizes the initial system without PE. Again a variation for m_1 is calculated, showing the stretched stability region of the conventional system between two dashed lines. A variation of m_1 is only possible within very small limits. By activating the parametric absorber, the stable range is again

significantly extended to higher values of m_1 .

As a last study for this system with default parameters, Fig. 5.10 presents the maximum value permitted for the combined parameter $c_{01} = c_{01}^d + c_{01}^e$ to keep the system stable. The conventional system is represented by the dashed line for $e_{12}^c = 0$ at $c_{01} = -0.364$. For a PE-amplitude of $e_{12}^c = 0.2$ a significant gain in damping can be achieved by the parametric absorber. Also, one can clearly see that the optimal PE-frequency does not coincide with the combination resonance frequency $\Omega_2 - \Omega_1$. This complicates the optimization of a parametric absorber, but is not a fundamental problem.

5.2.4 Remarks and conclusion

The previous results show that the suppression of flow-induced vibrations by a so-called *parametric absorber* is possible. Although the numerical investigation was carried out for a system with non-dimensional parameters, the mass and stiffness ratio for the absorber sub-system with respect to the main system was chosen such that it might reflect a practical application. It turned out that the effect of parametric vibration suppression can be achieved within a wide range of the mass and stiffness ratio.

Note that two significant observations were made in the course of the parameter studies. First of all, the prediction of the optimal PE-frequency is not a trivial task as it was for the previous system discussed in Section 4. Especially for very small absorbers (i.e. small value of the mass ratio m_{abs}/m_{main}) the difference between the parametric combination resonance frequency and the optimal parametric excitation frequency can be considerable and has to be taken into account. Furthermore, the performance of such an absorber, when attached to a self-excited system, is to a certain extent related to the size of the absorber. Of course, this had to be anticipated, since one cannot expect a "micro-absorber" to be as effective as a larger unit.

For really small absorbers both effects come hand in hand and make it difficult for analytical methods to predict the behavior of the system. In [18] this problem was discussed for the first time. In [25] S. Fatimah did rise to the challenge to find a better analytical solution rather than the first order approximation, which is obviously not adequate to the complex behavior of such a system. She was ambitious enough to carry out a second order approximation of the system for the case of the combination

5.3. Suppression of friction-induced vibrations

resonance $\Omega_2 - \Omega_1$. Results are presented for the maximum amplitudes as a function of the PE-frequency and the ratio of the sub-system frequencies. Although they look quite promising, a direct comparison with numerical results is not shown and it seems that the last word has not been spoken yet on this matter. In the view of the previously presented result it becomes quite obvious that also the second order combination resonance $(\Omega_2 - \Omega_1)/2$ has some influence, at least for small absorbers. Unfortunately, this observation really opens the can of worms and adds another dimension of complexity to the problem. All in all we can say that the analytical treatment of small sized absorbers continues to be an interesting challenge. On the other hand, numerical methods work fine for such systems and are not at all intimidated by a more or less extreme choice of parameters for the absorber system.

Another candidate for the queue of open questions is the decay time needed to put the self-excited system to rest by the parametric absorber after an initial disturbance. So far we were satisfied by the result that the system can be stabilized at all by a properly tuned parametric absorber. For a practical application time is certainly also a factor to be considered, and we may be interested in an absorber that suppresses the self-excited vibrations *fast*. In fact, this could also be a motivation to apply a parametric absorber although the conventional absorber is capable of stabilizing the system, but is not (always) fast enough. Of course, with numerical simulation we have a tool at hand to compute time-series of the vibration amplitudes and derive decay rates. The equivalent damping of the parametric excitation also gives a good idea in which direction design parameters should be modified to improve the time response. A more systematic approach could be to formulate an optimization problem that minimizes the largest eigenvalue of the monodromy matrix with respect to certain design parameters, like PE-frequency, PE-amplitude, mass, stiffness and damping of the absorber system, etc. Such investigations will be very useful in the future, when the application of parametric absorbers will reach a more concrete stage.

5.3 Suppression of friction-induced vibrations

Dry friction may provoke self-induced vibrations, chatter and squeal and causes more or less serious problems in all kinds of machines which ex-

hibit contacting parts undergoing relative motion. Friction-induced vibrations are therefore of growing interest and concern to designers as well as operators of machines. Excessive wear of components, surface damage, fatigue failure and noise can all be attributed to friction-induced vibrations and require the attention of specialists from different scientific disciplines as e.g. tribology as well as applied dynamics. This multidisciplinaryity is also reflected by the vast literature on this topic and we name just a few references [40], [27] and [4] which contain numerous contributions and cover many aspects of friction related research.

Based on some recent research by the author [21] we will apply the concept of a parametric absorber to an almost identical mechanical system as investigated in the previous section. It will also consist of a main mass and a parametric absorber attached to the main system to counteract the self-excitation mechanism, which is now dry friction.

5.3.1 Analytical representation of dry friction

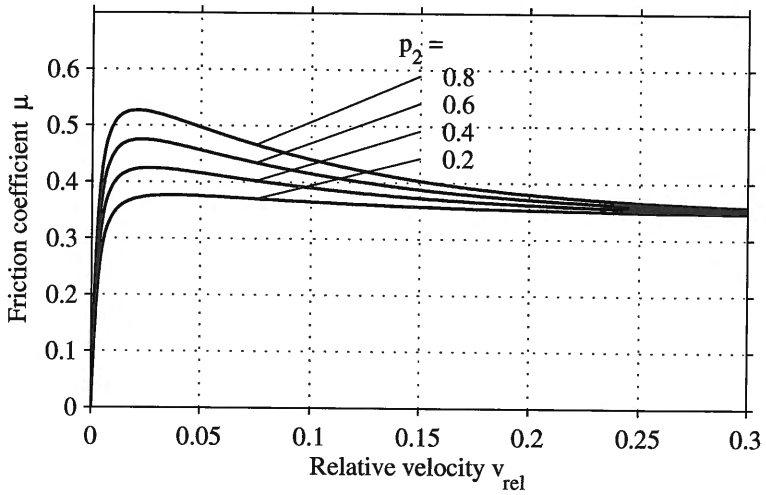
In Chapter 1.1.3 friction was already discussed and its role was pointed out as being a very common mechanism in mechanical systems to induce self-sustained vibrations. One of the most important parameters on which friction forces depend is the relative velocity between the two sliding surfaces. The dependency of friction on the sliding speed has been subject of numerous investigations, see e.g. [27]. A very simple mathematical representation for classical vibration problems is a linear function with friction forces alternating between negative and positive values, depending on the sign of the relative velocity. More complicated velocity-friction functions have been measured (see e.g. P. Stelter [78]) and different models have been proposed to study friction induced vibrations. It is typical and also essential for the dynamic system that in many cases the friction decreases with increasing velocity. Such a speed-range with a negative slope of the friction function usually occurs at low velocities and may start at or in the vicinity of zero velocity.

For the subsequent numerical analysis of the 2-dof system, a continuous representation of the friction-velocity function is convenient. As proposed and successfully applied by Popp et al. [65], a parameterized model can be defined by the function

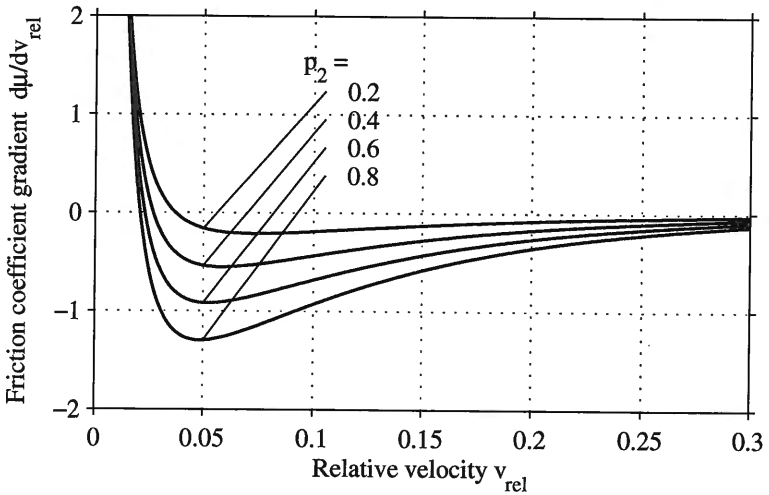
$$\mu(v_{rel}) = p_1(1 + p_2 \exp(-p_3|v_{rel}|))\operatorname{atan}(p_4 v_{rel}) \quad (5.19)$$

for the friction coefficient $\mu(v_{rel})$. Constant parameters $p_1 \dots p_4$ determine

5.3. Suppression of friction-induced vibrations



(a) Friction coefficient μ for different values of polynomial coeff. p_2



(b) Friction coefficient gradient $\hat{\mu}$ for different values of p_2

Figure 5.11: Friction coefficient μ and gradient $\hat{\mu}$ as a function of sliding speed v_{rel} . Approx. by Eqs. (5.19), (5.21): $p_1 = 0.22$, $p_3 = 10$, $p_4 = 400$

the shape of the function and are used for curve-fitting as needed. Figure 5.11(a) shows $\mu(v_{rel})$ for some typical values of the parameters p_i . The friction force f_{fric} is assumed to be proportional to the normal force f_{norm} and is therefore obtained from

$$f_{fric} = \mu(v_{rel})f_{norm}. \quad (5.20)$$

This continuous representation avoids discrete transitions between *sticking* and *slipping*. In fact, full sticking is not possible with this friction model. However, it was shown in [65] that this model gives practically the same results as discontinuous friction models. On the other hand, a continuous function has several advantages concerning the analytical and numerical analysis.

As mentioned earlier, dynamic stability of a mechanical system is significantly affected by negative damping which is equivalent to a negative slope of the friction-velocity function. From the analytical expression Eq. (5.19) we obtain for the derivative of $\mu(v_{rel})$

$$\hat{\mu} = \frac{d\mu}{dv_{rel}} = -p_1 p_2 p_3 \text{sign}(v_{rel}) \exp(-p_3 |v_{rel}|) \arctan(p_4 v_{rel}) + p_1 (1 + p_2 \exp(-p_3 |v_{rel}|)) p_4 / (1 + p_4^2 v_{rel}^2). \quad (5.21)$$

Figure 5.11(b) shows friction coefficient gradients $\hat{\mu}$ corresponding to the friction coefficient functions of diagram Fig. 5.11(a).

5.3.2 Single-mass model with friction

To obtain a reference solution for the system without parametric absorber, we will first investigate only the main system under the action of friction forces. This will illustrate the problem which will be solved later by a parametric absorber. Figure 5.12 shows the main mass m_1 on a moving belt running at constant speed v_{belt} . The main mass is connected to the inertial reference frame via a linear, constant spring k_{01} and a viscous damper c_{01} . The nonlinear equation of motion for this system was already mentioned in Section 1.1.3 and is repeated for easy reference

$$m_1 \ddot{x}_1 + c_{01} \dot{x}_1 + k_{01} x_1 = m_1 g (v_{belt} - \dot{x}_1). \quad (5.22)$$

Note that symbol g is commonly used for the acceleration of gravity, but may also be seen here in a more general way as a load factor.

5.3. Suppression of friction-induced vibrations

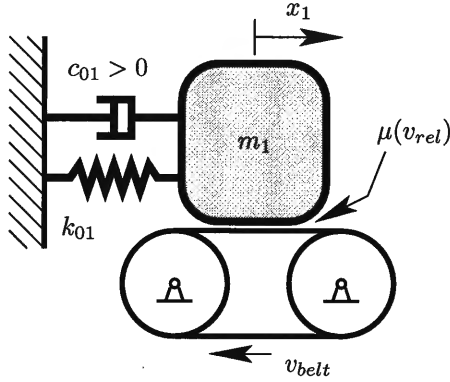


Figure 5.12: Single-dof system with friction-induced self-excitation forces acting on mass m_1

Table 5.2: Default parameters for single-dof model (main mass system) as shown in Fig. 5.12

Parameter	m_1	k_{01}	c_{01}	Ω_1^{sub}	ζ_1^{sub}
	1.0	$(10 \cdot 2\pi)^2$	π	$10 \cdot 2\pi$	$2.5 \cdot 10^{-2}$
Common params.: $p_1 = 0.22$, $p_2 = \text{var.}$, $p_3 = 10$, $p_4 = 400$, $g = 9.81$					

We are now interested in the stability threshold with respect to the damping parameter c_{01} . This means that we are looking for the minimum damping to guarantee stability of the trivial solution $\dot{x}(t) = 0, x(t) = x_{stat}(v_{belt}) = \text{const.}$ Since the friction coefficient μ depends on the relative velocity $v_{rel} = (v_{belt} - \dot{x})$, the critical damping can be expressed in terms of the belt velocity. For easier interpretation of the results we will use the dimensionless damping ratio

$$\zeta_1^{sub} = \frac{c_{01}}{2\sqrt{k_{01}m_1}} \quad (5.23)$$

instead of the physical damping parameter c_{01} . We will name this parameter the critical damping ratio ζ_{1-crit} if it holds for the system at the stability limit.

To calculate some typical results we have to make a choice for system

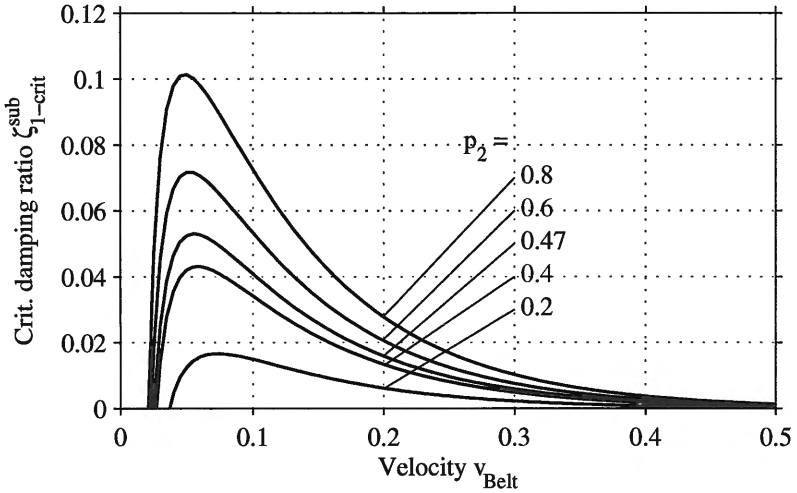


Figure 5.13: Critical damping ratio ζ_{1-crit}^{sub} of 1-dof system for friction-velocity functions as in Figs. 5.11

parameters. The friction function Eq. (5.19) will be used in all subsequent examples, with parameters p_i as given in the figure caption of Fig. 5.11. Data for the single-mass system are listed in Table 5.2 and may be seen as either dimensionless quantities, obtained from making the equations non-dimensional, or as quantities represented in a coherent unit system.

Figure 5.13 shows some typical results for this single-dof system. Each curve holds for a certain parameter p_2 of the friction coefficient function $\mu(v_{rel})$ and gives the critical damping ratio ζ_{1-crit}^{sub} at the stability boundary for a given speed v_{belt} . For a damping ratio $\zeta_1^{sub} < \zeta_{1-crit}^{sub}$, the stationary deflection

$$x_{1-stat} = \frac{m_1}{k_{01}} g \mu(v_{belt}) \quad (5.24)$$

of mass m_1 is unstable. Any disturbance of the system will initiate self-excited vibrations which will end in a limit cycle. Note that there exists a maximum critical damping $\zeta_{1-crit-MAX}^{sub}$ at a certain speed $v_{belt-\zeta-MAX}$. Of course this is the speed for $\hat{\mu}_{neg-MAX} = \min(\hat{\mu})$, i.e. the slope reaches

5.3. Suppression of friction-induced vibrations

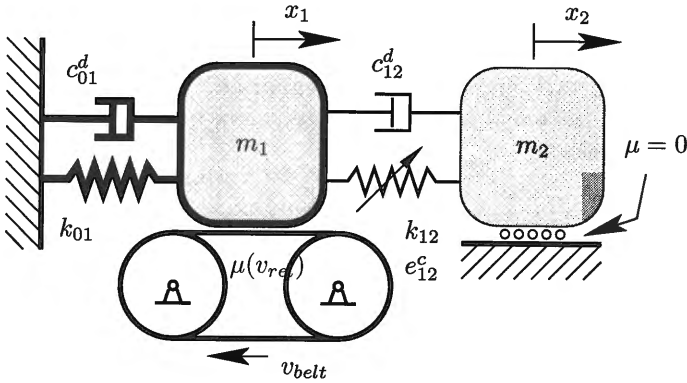


Figure 5.14: System consisting of a friction-excited main mass m_1 and a parametric absorber m_2 with time-dependent connecting stiffness $k_{12}^{res}(t)$.

the maximum negative value. Any damping ratio $\zeta_1^{sub} < \zeta_{1-crit-MAX}^{sub}$ of the main system below the maximum critical damping will result in a loss of stability for a certain speed range of belt operation. If the damping ζ_1^{sub} cannot be increased sufficiently and friction conditions cannot be changed, an operation within the critical speed range will result in self-excited vibrations.

5.3.3 System with Parametric Absorber

Let us now attach the parametric absorber to the main system and consider a 2-dof system as shown in Fig. 5.14. Note that dry friction forces only act on the main mass. Friction between the absorber mass and the guidance is not considered here. As in the previous section, the absorber consists of a mass m_2 connected to the main mass by a time-varying stiffness element $k_{12}^{res}(t)$ and a viscous damper c_{12} . The stiffness variation is assumed to be a harmonic function $k_{12}^{res}(t) = k_{12}(1 + e_{12}^c \cos \omega t)$, with PE-frequency ω and PE-amplitude $k_{12}e_{12}^c$.

Due to the friction forces acting on the main mass we obtain a non-homogeneous set of differential equations as the equations of motion for the system

$$\mathbf{M}\ddot{\mathbf{x}} + \mathbf{C}\dot{\mathbf{x}} + [\mathbf{K} + \cos(\omega t)\mathbf{P}^C]\mathbf{x} = \mathbf{f}_{fric}. \quad (5.25)$$

This system is almost identical to the previous example in Section 5.2 and only differs with respect to the force vector on the right-hand side. Therefore we do not need to repeat matrices \mathbf{M} , \mathbf{C} , \mathbf{K} , \mathbf{P}^C but simply refer to Eqs. (5.3) and (5.4). What remains to be discussed is the vector \mathbf{f}_{fric} which has only one non-zero entry, since friction forces act only on the main mass

$$\mathbf{f}_{fric}(v_{belt}, \dot{x}_1) = \begin{bmatrix} m_1 g \mu(v_{belt} - \dot{x}_1) \\ 0 \end{bmatrix}. \quad (5.26)$$

The non-linear friction function $\mu(v_{belt}, \dot{x}_1)$ is given by Eq. (5.19). Note that gravity forces do not play a role in this system, except for generating the normal (contact) force $m_1 g$ between mass m_1 and the moving belt. We have therefore reached the same point as earlier in the analysis of the flow-excited system. Equations (5.25) are ready for numerical simulation, but need to be linearized for a stability investigation using the numerical Floquet-method. Linearization with respect to a given constant velocity of the belt can be carried out by using the analytical expression Eq. (5.21) and leads to

$$\mathbf{f}_{fric}(v_{belt}, \dot{x}_1) \doteq \begin{bmatrix} -m_1 g \hat{\mu}(v_{belt}) \dot{x}_1 \\ 0 \end{bmatrix}. \quad (5.27)$$

By defining $c_{01}^{se}(v_{belt}) \sim c_{fric}(v_{belt}) = m_1 g \hat{\mu}(v_{belt})$ we have converted the system with linearized friction-induced self-excitation forces into the generic 2-dof system as defined in Section 5.1. Note that the self-excitation parameter c_{01}^{se} depends on the velocity of the belt and will be negative when $\hat{\mu} < 0$. Figure 5.11(b) now becomes useful and shows the value of the gradient for different velocities $v_{rel} = v_{belt}$. As we can see there is a narrow area for very small velocities where the gradient is positive and hence $c_{fric} > 0$. This area is typical for the analytical approximation which exhibits a large but finite, positive gradient for $v_{rel} = 0$. When the gradient reaches zero and enters the negative range, a characteristic value of the belt velocity is reached, since this marks the begin of destabilizing forces generated by friction. However, with sufficient (positive) damping available from the damping elements c_{01}^d and c_{12}^d , a stable operation might still be possible. The necessary amount of damping in the system for stable operation without parametric excitation will be investigated in the next section.

5.3. Suppression of friction-induced vibrations

Table 5.3: Parameters for model of a self-excited main system with conventional absorber as used for results Fig. 5.15 and 5.16. Bracketed {values} vary in Figs. as mentioned and hold only for dotted lines.

Parameter	m_1	k_{01}	p_2	c_{01}^d	ζ_1^{sub}
Set (i)	1.0	$(10 \cdot 2\pi)^2$	0.47	π	0.025
Set (ii)	1.0	$(10 \cdot 2\pi)^2$	0.525	π	0.025
Parameter	m_2	k_{12}	e_{12}^c	c_{12}^d	ζ_2^{sub}
Set (i)	0.1	$\{10 \cdot (2\pi)^2\}$	0.0	$\{\pi/10\}$	0.025
Set (ii)	0.5	$\{50 \cdot (2\pi)^2\}$	0.0	$\{\pi/2\}$	0.025
Frequency	Ω_1	$\Omega_1 + \Omega_2$		$2\Omega_1$	Ω_1^{sub}
Set (i)	$\{53.68\}$	$\{147.09\}$		$\{107.36\}$	$10 \cdot 2\pi$
Set (ii)	$\{44.43\}$	$\{133.29\}$		$\{88.86\}$	$10 \cdot 2\pi$
Frequency	Ω_2	$\Omega_2 - \Omega_1$		$2\Omega_2$	Ω_2^{sub}
Set (i)	$\{73.55\}$	$\{19.87\}$		$\{147.09\}$	$\{10 \cdot 2\pi\}$
Set (ii)	$\{88.86\}$	$\{44.43\}$		$\{177.72\}$	$\{10 \cdot 2\pi\}$
Common parameters: $p_1 = 0.22$, $p_3 = 10$, $p_4 = 400$, $g = 9.81$					

5.3.4 Results for system with conventional absorber

To obtain results for the system with a conventional absorber, we turn off parametric excitation by setting $\mathbf{P}^C = \mathbf{0}$ ($e_{12}^c = 0$). As with the single-dof system we can again calculate a critical value for the damping ratio ζ_1^{sub} , where the 2-dof system is at the local stability limit. This can be carried out numerically by calculating the complex eigenvalues of the linearized system Eqs. (5.25) and (5.27). A root-finding routine iterates the value of ζ_1^{sub} until an eigenvalue crosses the imaginary axis and the critical parameter is found.

Numerical values for the system parameters are needed for this procedure and are listed in Table 5.3. Given values are dimensionless quantities, but coherent physical units may be added. Note, for instance, that a dimensionless frequency $\Omega = 62.83 = 10 \cdot 2\pi$ can easily be interpreted as frequency of 10Hz. Data for the main system are chosen the same as for the previous single-dof model, see Table 5.2. Two different parameter sets were used for the 2-dof model (see Table 5.3) to point out the influence of the mass ratio m_2/m_1 and also of the friction coefficient parameter p_2 on the results. The dependency of the stability limit on

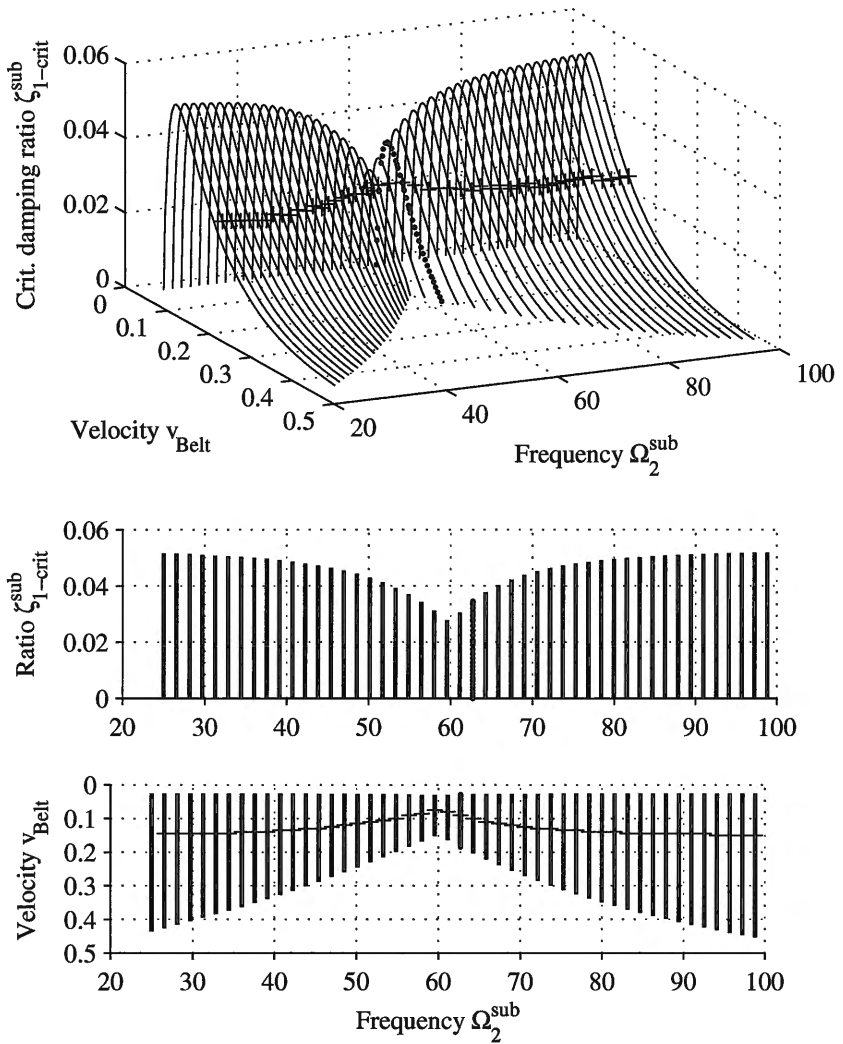


Figure 5.15: Critical damping ratio ζ_{1-crit} for 2-mass system with conventional absorber. Parameter set (i) as in Table 5.3. Contour line at $\zeta_{1-crit} = 0.025$.

5.3. Suppression of friction-induced vibrations

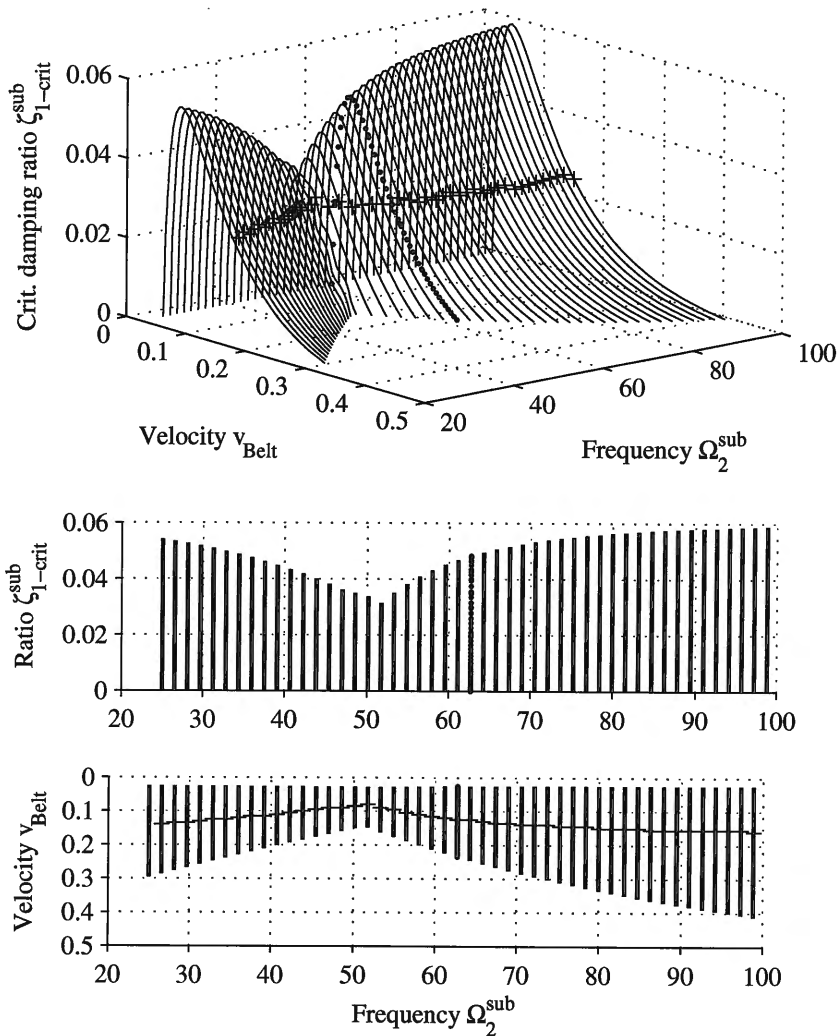


Figure 5.16: Critical damping ratio ζ_{1-crit} for 2-mass system with conventional absorber. Parameter set (ii) as in Table 5.3. Contour line at $\zeta_{1-crit} = 0.025$.

the belt velocity is of primary interest and consequently v_{belt} will be used as one parameter of variation in all the following studies. Since proper tuning is essential for a conventional absorber, the natural frequency of the absorber subsystem Ω_2^{sub} was chosen as a second parameter for variation. Note that the absorber mass was kept constant, but the absorber stiffness k_{12} was changed to obtain the frequency variation. Of course, the absolute values of e_{12} and also c_{12}^d were changed accordingly.

Figures 5.15 and 5.16 show results for parameter sets (i) and (ii), respectively. For both diagrams holds that actual damping ratios ζ_1^{sub} below the plotted threshold lines will lead to an unstable system because damping will not be sufficient to suppress self-excited vibrations. From the subplots one can easily determine the appropriate tuning frequency for this (conventional) absorber system. The minimum value of the necessary damping ratio indicates the optimal tuning frequency.

From Figs. 5.15 for a system with parameter set (i) one can see that a completely detuned absorber $\Omega_2^{sub} = 100$ needs a minimum damping ratio of $\zeta^{sub} > 0.05$ for stability. This value can be lowered significantly to $\zeta^{sub} \approx 0.03$ for the optimally tuned absorber at $\Omega_2^{sub} \approx 60$. The benefit of the absorber can be directly seen by comparing this result with the respective result for $p_2 = 0.47$ in Fig. 5.13.

The system parameters of set (ii) for the results in Figs. 5.16 differ with respect to the much larger absorber mass ($m_2 = 0.5$) and the more demanding friction function ($p_2 = 0.525$). As one can see, the optimal tuning frequency drops due to the larger mass m_2 . Because of the steeper friction function the bigger absorber cannot reduce the minimum damping ratio for the optimally tuned system. In fact, it is slightly higher, and for the mistuned absorber a value close to $\zeta^{sub} \approx 0.06$ is reached.

Just two numerical examples were shown, and a thorough parameter study would be needed to demonstrate the limitations of a conventional absorber. Nevertheless, one can see where stability limits exist for the present system which cannot be lowered with an optimal, but still conventional, absorber system. In the following we will use these results as a baseline and will compare how parametric excitation can help to further increase the stability limit of the system.

5.3. Suppression of friction-induced vibrations

Table 5.4: Parameters for model of a self-excited main system with parametric absorber as used for results Fig. 5.3 and 5.18. Bracketed {values} changed in subfigures

Parameter	m_1	k_{01}	p_2	c_{01}^d	ζ_1^{sub}
Set (iii)	1.0	$(10 \cdot 2\pi)^2$	{ 0.45 }	π	0.025
Set (iv)	1.0	$(10 \cdot 2\pi)^2$	0.525	2.12	0.025
Parameter	m_2	k_{12}	e_{12}^c	c_{12}^d	ζ_2^{sub}
Set (iii)	0.1	$10 \cdot (2\pi)^2$	0.2	$\pi/10$	0.025
Set (iv)	0.5	$3.6 \cdot 10^3$	{0.1}	$\pi/2$	0.025
Frequency	Ω_1	$\Omega_1 + \Omega_2$		$2\Omega_1$	Ω_1^{sub}
Set (iii)	53.68	147.09		107.36	$10 \cdot 2\pi$
Set (iv)	47.74	159.37		95.49	$10 \cdot 2\pi$
Frequency	Ω_2	$\Omega_2 - \Omega_1$		$2\Omega_2$	Ω_2^{sub}
Set (iii)	73.55	19.87		147.09	$10 \cdot 2\pi$
Set (iv)	111.63	63.88		223.26	$13.5 \cdot 2\pi$
Common parameters: $p_1 = 0.22$, $p_3 = 10$, $p_4 = 400$, $g = 9.81$					

5.3.5 Results for system with parametric absorber

The diagrams in the following figures show the results of 2-dimensional parameter studies for the system with parametric excitation activated at the absorber. For all studies the belt velocity v_{belt} and the parametric excitation frequency η were used as the main parameters for variation. The numerical studies were carried out by application of numerical Floquet analysis. For a given set of system parameters a grid with sufficient resolution was established for the range of the variation parameters and stability was determined numerically. Stability (or instability) of the trivial solution for chosen parameter combinations were marked within the grid and finally the stability boundary between stable and unstable regions was calculated and plotted.

Figure 5.17 shows a stability chart for parameter set (iii) of the 2-mass system (see Table 5.4). Parameter p_2 of the friction coefficient function Eq. (5.19) was chosen as the third parameter of variation. Contour lines are plotted for different values of p_2 to indicate the stability or instability areas within the range of η and v_{belt} . For $p_2 = 0.45$ the unstable region is shaded gray and white areas indicate stability for the system. A gap

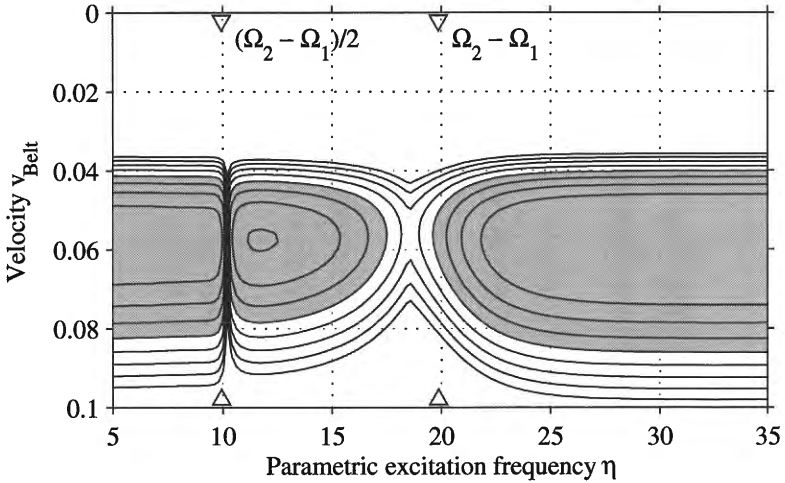
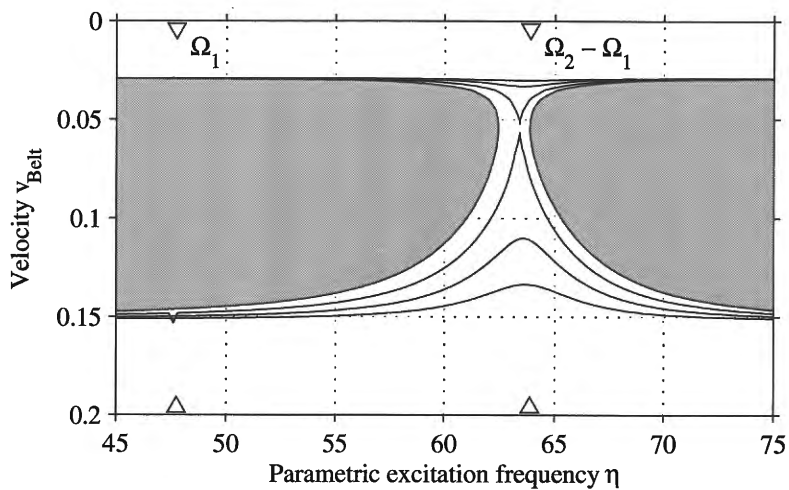


Figure 5.17: Stability chart for 2-mass system. Parameter set (iii) of Table 5.4. Shaded areas indicate unstable system. Variation of $p_2 = 0.42 \dots 0.45$ (shaded) $\dots 0.49$

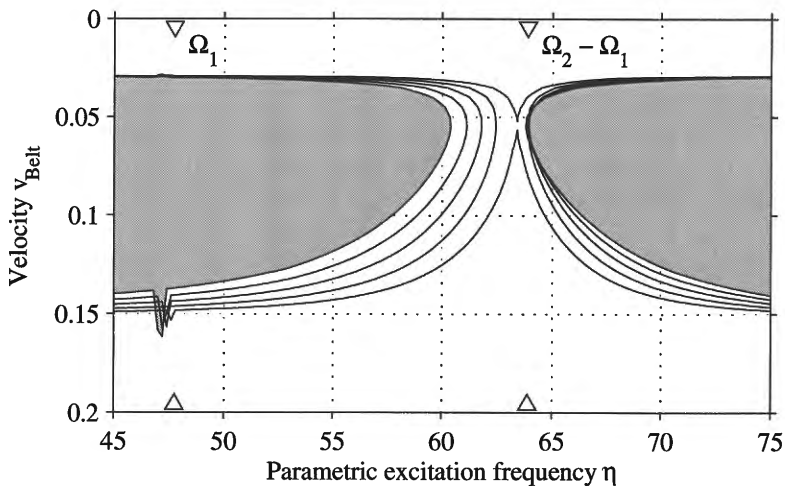
occurs in the instability area (gray band) that is centered around $v_{belt} \approx 0.06$ near a PE-frequency of $\eta \approx 18$. The optimal PE-frequency is close to but not exactly the parametric combination resonance frequency $\Omega_2 - \Omega_1$. At the optimum PE-frequency the system is stable at all speeds of the belt. Higher values of p_2 close the "gap" and for $p_2 = 0.47$ stability is lost near $v_{belt} \approx 0.055$. For PE-frequencies far off the optimum frequency the range of instability for v_{belt} becomes almost identical with the values for the conventional system and can be compared with the previous results (see the contour line at $\zeta_1^{crit} = 0.025$ in Figs. 5.15). Another interesting feature of Fig. 5.17 is the extremely narrow "gap" near $\eta = 10$, which corresponds to the combination resonance frequency of second order $(\Omega_2 - \Omega_1)/2$. As already seen in Section 5.2, this higher order resonance frequency also generates a (very small) region of stability.

In the following Figs. 5.18 the PE-amplitude parameter e_{12}^c is used for a parameter study. Parameter set (iv) in Table 5.4 holds for this result and it can be compared with previous results obtained from set (ii) in Table 5.3 for the conventional absorber system, see Figs. 5.16.

5.3. Suppression of friction-induced vibrations



(a) Variation of $e_{12}^c = 0.10 \dots 0.25$ (shaded)



(b) Variation of $e_{12}^c = 0.20 \dots 0.40$ (shaded)

Figure 5.18: Stability chart for 2-mass system. Parameter set (iv) of Table 5.4. Shaded areas indicate unstable system. Variation of e_{12}^c

Table 5.5: Parameters for model of a self-excited main system with parametric absorber as used for results Fig. 5.19 and 5.20. Bracketed {values} changed in subfigures

Parameter	m_1	k_{01}	p_2	c_{01}^d	ζ_1^{sub}
Set (v)	1.0	$(10 \cdot 2\pi)^2$	0.525	π	0.025
Set (vi)	1.0	$(10 \cdot 2\pi)^2$	0.600	π	0.025
Parameter	m_2	k_{12}	e_{12}^c	c_{12}^d	ζ_2^{sub}
Set (v)	0.5	$\{50 \cdot (2\pi)^2\}$	0.2	$\{\pi/2\}$	0.025
Set (vi)	0.5	$\{200 \cdot (2\pi)^2\}$	0.5	$\{\pi\}$	0.025
Frequency	Ω_1	$\Omega_1 + \Omega_2$		$2\Omega_1$	Ω_1^{sub}
Set (v)	$\{44.43\}$	$\{133.29\}$		$\{88.86\}$	$10 \cdot 2\pi$
Set (vi)	$\{49.87\}$	$\{208.39\}$		$\{99.56\}$	$10 \cdot 2\pi$
Frequency	Ω_2	$\Omega_2 - \Omega_1$		$2\Omega_2$	Ω_2^{sub}
Set (v)	$\{88.86\}$	$\{44.43\}$		$\{177.72\}$	$\{10 \cdot 2\pi\}$
Set (vi)	$\{158.61\}$	$\{108.83\}$		$\{317.22\}$	$\{20 \cdot 2\pi\}$
Common parameters: $p_1 = 0.22$, $p_3 = 10$, $p_4 = 400$, $g = 9.81$					

Note that in this previous diagram there is no stable operation of the system possible at a damping ratio of $\zeta_1 = 0.025$ for all speeds v_{belt} .

From Fig. 5.18(a) the minimum PE-amplitude parameter $e_{12}^c > 0.2$ can be determined. The best PE-frequency is found slightly below the combination resonance frequency $\Omega_2 - \Omega_1$ and further decreases for increasing e_{12}^c . For values $e_{12}^c \geq 0.3$ the result become more favorable since the minimum stability interval increases for the PE-frequency and makes the system more robust with respect to small variations of the PE-frequency or of system parameters. A small "spike" of increased instability at the lower end of the PE-frequency range appears. As indicated in the figure, this spike appears near Ω_1 , which is interesting since the natural frequencies of the system usually are not resonance frequencies for a parametric excitation. In fact, small resonance originates from the primary combination resonance of the second order $\eta_{1/2}^{pr} = 2\Omega_1/2$.

Figures 5.19 and 5.20 show results for a variation of the tuning frequency Ω_2^{sub} of the parametric absorber. Since the absorber mass m_2 was kept constant in this study, a variation of Ω_2^{sub} is equivalent to a variation of the stiffness k_{12} of the absorber. Of course, changing this parameter also affects the natural frequencies of the system, and the

5.3. Suppression of friction-induced vibrations

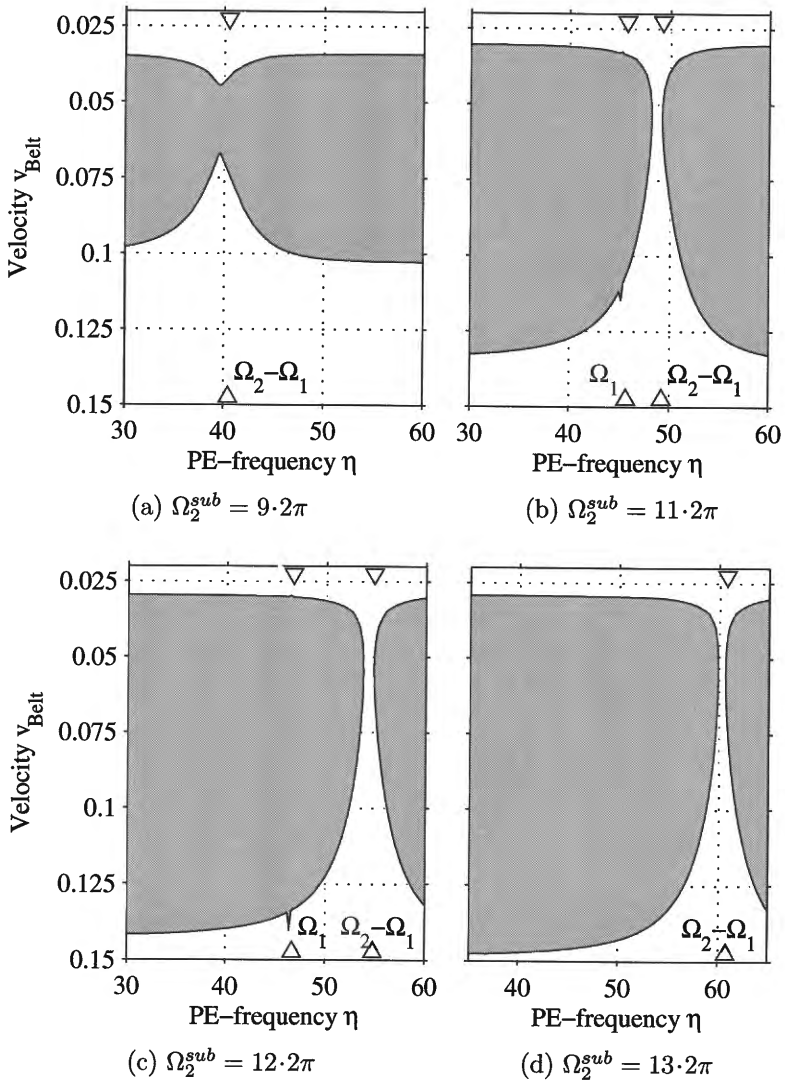


Figure 5.19: Stability chart for 2-mass system. Parameter set (v) of Table 5.5. Variation of absorber stiffness $\sqrt{k_{12}} \sim \Omega_2^{sub}$

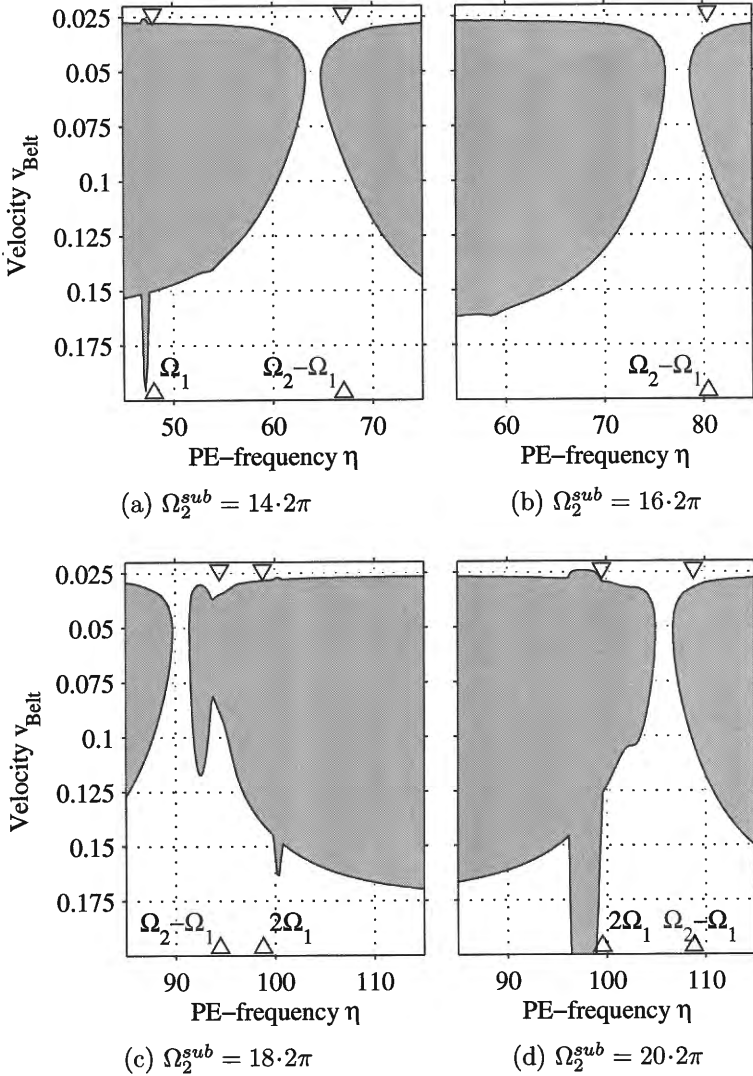


Figure 5.20: Stability chart for 2-mass system. Parameter set (vi) of Table 5.5. Variation of absorber stiffness $\sqrt{k_{12}} \sim \Omega_2^{sub}$

5.4. Concluding remarks

combination resonance frequency $\Omega_2 - \Omega_1$ moves to higher values with increasing tuning frequency Ω_2^{sub} . To obtain easy-to-read diagrams, only one result was plotted in each sub-figure. Changing the tuning frequency alters the behavior of the conventional system, especially in the vicinity of the optimal tuning frequency, see Figs. 5.15, 5.16. Therefore the results of Figs. 5.19 and 5.20 combine various effects and interpretation is a bit challenging. Note also that parameter sets (v) and (vi) use slightly different values for parameter p_2 .

Figure 5.18 is a kind of a starting point for the series of results in Fig. 5.19, since it holds for $\Omega_2^{sub} = 13.5 \cdot 2\pi$ which is a bit above $\Omega_2^{sub} = 13 \cdot 2\pi$ as used in Fig. 5.19(d). The results in Figs. (a) to (d) show that with increasing parameter Ω_2^{sub} the speed range of instability increases simultaneously. For $\Omega_2^{sub} > \approx 9.6 \cdot 2\pi$ a stable operation for all speeds of the belt is possible. Further increase of Ω_2^{sub} maintains the stable area, but it gets smaller with respect to the PE frequency and vanishes again as shown in Fig. 5.18 for $\Omega_2^{sub} = 13.5 \cdot 2\pi$ and $e_{12}^c = 0.2$.

The study in Figs. 5.19 is continued in Figs. 5.20 with respect to the variation of Ω_2^{sub} , but with increased friction coefficient parameter $p_2 = 0.6$ and a higher PE-parameter $e_{12}^c = 0.5$ to compensate for the increased level of self-excitation (see parameter set (vi) in Table 5.5). Compared to the previous results, some parametric resonances now appear in the frequency range shown. Especially for $\Omega_2^{sub} = 20 \cdot 2\pi$ a massive parametric resonance shows up near $\eta \approx 2\Omega_1$. As long as the PE frequency is selected properly, however, a nearby resonance has no influence on the vibration cancelling effect. Of course, having in mind a robust system and taking into account uncertainties of the system, one would try to avoid a resonance close to the PE-frequency.

5.4 Concluding remarks

In this chapter the concept of a *parametric absorber* for the suppression of self-excited vibrations was introduced. A parametric absorber is defined here as a secondary mass system connected to the primary (main) system by a time-varying stiffness and a time-independent linear damping element. In contrast to a (tuned) dynamic absorber as used in systems with forced excitation and which suppresses vibrations only at a single frequency when damping is very small, the parametric absorber offers a frequency range of vibration cancellation. Like the damped con-

ventional absorber the parametric absorber extracts vibration energy from the system. In addition to that the parametric excitation adds "equivalent damping" to the system and thereby stabilizes the unstable system. In case of an already stable system the parametric absorber increases the decay rate for the system to reach the stationary (trivial) solution.

The two studies in Sections 5.2 and 5.3 did show that the application of a parametric absorber does not depend on the type of self-excitation. If the SE-mechanism can be represented by an equivalent negative damping parameter, a parametric absorber can be applied. The size of the absorber, expressed in terms of mass ratio and stiffness ratio with respect to the main system, may vary within a large range. However, performance is increased for larger absorber systems for various reasons, and secondary effects from the parametric excitation can be kept low. Parametric excitation will also introduce parametric resonances which lead to very violent vibrations that may even exceed the vibration level of self-excited vibrations. Such frequencies have to be avoided of course, but they are predictable by a numerical analysis and, in general, do not cause a problem.

The investigations presented here show that the proposed concept of a parametric absorber functions in principle. Further work will have to investigate a broader range of system parameters to find parameters of optimal performance of a parametric absorber. Nevertheless, the results obtained so far hold for linear systems and for linearized systems in the vicinity of the linearization point, respectively. Global stability will also have to be considered in the future. Domains of attraction for a system with parametric absorber will be needed to ensure robustness with respect to periodic and transient disturbances.

Chapter 6

Vibration cancelling in a rotor system

The phenomenon of self-excitation is well established in rotor dynamics. As in other systems or structures, self-excited vibrations may lead to large vibration amplitudes which may ultimately damage or even destroy rotating machinery. Therefore, there has always been a vital interest in understanding the underlying mechanisms and in avoiding such vibrations, see the comprehensive discussions e.g. in the books [82], [13], [101] and [26], authored by some of the leading researchers in this field.

A rotor experiencing self-excited vibrations is basically an unstable system whose vibration amplitudes are bounded by some kind of nonlinearities in the case of permanent non-destructive operation. Due to the motion of the rotor shaft observed in such cases, the expressions *whip* and *whirl* are frequently associated with instabilities of rotor systems. What makes rotor dynamics so challenging (and interesting) are the different causes that may trigger self-excitation: hysteretic whirl due to internal damping, forward whirl due to gyroscopic moments, fluid bearing whip, and labyrinth seal instability to mention some of the most common phenomena. However, in many cases the self-excitation mechanism can be attributed to the presence of either non-conservative forces or negative damping in the rotor system.

Of course, there are numerous methods, ideas and strategies to avoid or to counteract such destabilizing mechanisms. There is no room here to even briefly discuss them and the interested reader has to be re-

ferred to the relevant literature. In the context of parametric vibration suppression, as discussed in this monograph, it is worth noting that new developments evolve from the application of *advanced design components* in rotating machinery. "Advanced components" is used as a general expression for what is also known as "active elements", "smart structures" and "mechatronic devices". Active magnetic bearings are widely known as such an "advanced component" in rotating machinery, but other designs (e.g. active fluid bearings) and further ideas do exist. Taking advantage of the new possibilities offered by such advanced elements is a current trend in rotor dynamic research. For example, to counteract non-conservative forces, a new control algorithm for a rotor supported by active magnetic bearings was presented recently by M. Hirschmanner in [35] and [36].

In the following we will investigate parametric stiffness excitation as a means to suppress self-excited vibrations in a rotor system. Since this application is closer to a real system as the previous examples in this monograph we also have to think about the actual realization of parametric excitation. Therefore it is important to realize that nowadays a number of possibilities exist to actively control parameters of a mechanical system. Starting from simple ideas as outlined already in the introductory Chapter 1 all kinds of "smart materials", "smart fluids" and "structronic devices" [28], [95] are available to bring about the necessary periodic change of a system parameter. At the end of the line, or as the most general view of a parametric excitation, we can see some kind of actively controlled actuator that generates and applies forces to the system, equivalent to the change of one or more system parameters. However, the winning idea of vibration suppression by parametric excitation is the fact that it is a *passive control method* and therefore an extensive control system can be avoided.

We will now continue to develop the concept of parametric vibration suppression and apply it to a more complex system. The content of this chapter is based on previous works by A. Tondl and the author. An initial study [89] was followed by a more elaborate investigation [19] where simulation results for a rotor system are presented. T. Pumhössel investigated symmetric 4-dof and 6-dof rotor systems with isotropic bearings and he also made a study on an 8-dof model. These results were published in [66] and [20]. Recently also the influence of rotor unbalance was considered for the first time by A. Tondl and the author in [93].

6.1. Rotor model with parametric stiffness excitation

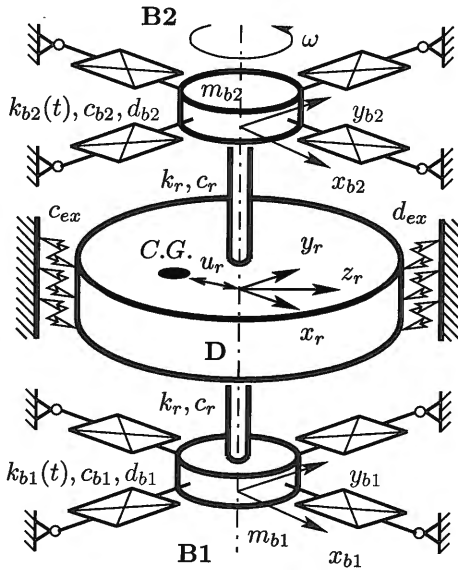


Figure 6.1: Sketch of the Laval/Jeffcott rotor.

6.1 Rotor model with parametric stiffness excitation

The mechanical model of the rotor as used in the following study is based on the classical Laval/Jeffcott-rotor model. We consider a massless, flexible shaft in vertical position with isotropic properties. Torsional vibrations are beyond the scope of this study and are excluded by assuming a torsionally rigid shaft. Also the rotational speed ω of the rotor shall be constant ($\dot{\omega} = 0$). A lumped mass m_r , representing a rigid disk, is attached at the midspan position D of the rotor to the shaft. The displacement of the disk is described by two translational degrees of freedom x_r , y_r , see Fig. 6.1. Rotational degrees of freedom are not introduced since the moment of inertia of the disk, for axes perpendicular to the axis of rotation, is assumed to be negligible. An investigation which includes both translational and rotational degrees of freedom for

Table 6.1: Definition of coordinate systems and complex notation.

	Inertial ref. frame O	Rotating ref. frame R
Disk	$z_r = x_r + iy_r$	$\zeta_r = \xi_r + i\eta_r$
Bearing B1	$z_{b1} = x_{b1} + iy_{b1}$	$\zeta_{b1} = \xi_{b1} + i\eta_{b1}$
Bearing B2	$z_{b2} = x_{b2} + iy_{b2}$	$\zeta_{b2} = \xi_{b2} + i\eta_{b2}$

the rotor disk is found in [66]. Mass unbalance of the disk is taken into account and may cause unbalance excitation of the system. Symbol u_r is used as the unbalance parameter for the disk. Stiffness and damping properties k_r and c_r hold for each segment of the shaft.

At both ends of the rotor shaft two bearing stations $B1$ and $B2$ are located, respectively. Lumped masses m_{b1} , m_{b2} are assumed to represent mass concentrations of the rotating counterparts of the bearings. Each station is assigned two translational degrees of freedom, x_{b1} , y_{b1} and x_{b2} , y_{b2} , respectively. Radial bearing stiffness and damping is denoted $k_{b_j}^{res}(t)$ and c_{b_j} . The bearing stiffness $k_{b_j}^{res}(t)$ is changed periodically, according to

$$k_{b_j}^{res}(t) = k_{(b1,b2)(x,y)}^{res}(t) = k_{b_j}(1 + e_{b_j}^c \cos(\varpi t)) \quad (6.1)$$

with the constant stiffness parameter k_{b_j} , with $p_{b_j}^c = k_{b_j} e_{b_j}^c$ as the amplitude of the harmonic stiffness variation and with ϖ as the frequency of the parametric excitation. Note that the radial stiffness is open-loop controlled in the same manner at both bearings and for both directions with zero phase lag. For $k_{b1}^{res}(t) = k_{b2}^{res}(t) = k_b^{res}(t)$ parametric stiffness excitation is identical in both directions and at both bearing stations.

As commonly used in the analysis of rotor systems a rotating reference frame R is introduced which rotates with respect to the inertial reference frame O at the constant angular speed ω of the rotor. Also, complex notation is employed for brevity. See Table 6.1 for the definition of various symbols used in the further analysis.

Forces acting on the rotor disk are generated by various sources. The linear elastic shaft generates a restoring force proportional to the relative deflection of the shaft. The elastic component of the shaft force is given by

$$F_{el,r}^O = -k_r(2z_r - z_{b1} - z_{b2}). \quad (6.2)$$

6.1. Rotor model with parametric stiffness excitation

This force is always of conservative type and acts as a restoring force on the disk.

The unbalance force $F_{ub,r}$ acts in the opposite direction and causes a constant radial deflection at the disk and at the bearing stations with respect to the rotating reference frame. It depends on the rotational speed ω of the rotor and on the unbalance eccentricity u_r and can be represented in the inertial reference frame by

$$F_{ub,r}^O = m_r u_r \omega^2 \exp(i\omega t). \quad (6.3)$$

We will consider unbalance forces only at the disk station of the rotor.

6.1.1 Self-excitation mechanisms

Forces resulting from internal damping of the shaft are generated by a relative motion of the disk with respect to the bearing stations. They are described as

$$F_{di,r}^R = -c_r(\dot{\zeta}_r - \dot{\zeta}_{b1}) - c_r(\dot{\zeta}_r - \dot{\zeta}_{b2}) \quad (6.4)$$

in the rotating reference frame R . A transformation into the inertial reference frame O leads to

$$F_{di,r}^O = -c_r[(2\dot{z}_r - \dot{z}_{b1} - \dot{z}_{b2}) - i\omega(2z_r - z_{b1} - z_{b2})], \quad (6.5)$$

with ω as the constant angular speed of the disk. This representation clearly shows the destabilizing nature of the internal damping above a critical speed ω_{crit} due to the non-conservative forces. They result from the positive term $c_r i\omega(2z_r - z_{b1} - z_{b2})$ which linearly increases with the speed of the rotor.

Another typical source of destabilizing forces in a rotor system are e.g. labyrinth seals. Due to the axial pressure gradient within the gap, non-conservative forces are generated which increase with increasing rotor speed and can ultimately destabilize a rotor system. These external forces can be described in the rotating reference frame R by

$$F_{ex,r}^R = -c_{ex}\dot{\zeta}_r, \quad (6.6)$$

and after transformation into the inertial reference frame O they read

$$F_{ex,r}^O = -c_{ex}[\dot{z}_r - i\omega z_r]. \quad (6.7)$$

In a real rotor system there is almost always some amount of progressive damping present, although it might not be sufficient to keep the self-excited vibrations at an acceptable level. To reproduce this behavior, and also to avoid numerical overflow when calculating numerical results, nonlinear damping forces were added to the external forces acting on the disk and at the bearing stations. A frequently employed functional relationship is used where the effective damping coefficient increases quadratically with the deflection

$$F_{d,r}^O = -d_r z_r \bar{z}_r \dot{z}_r, \quad (6.8)$$

$$F_{d,bj}^O = -d_{bj} z_{bj} \bar{z}_{bj} \dot{z}_{bj}, \quad j = 1, 2. \quad (6.9)$$

Symbol \bar{z} is used to denote the conjugate complex of z . Of course we have to keep in mind that any amplitudes obtained from numerical calculations which do not vanish, depend on this non-linear damping model and the ruling coefficients d_r and d_{bj} .

6.1.2 Equations of motion

The equations of motion for the rotor system described above can be derived from Newton's law and the following system of three second order differential equations is obtained:

$$\begin{aligned} & m_r \ddot{z}_r + k_r (2z_r - z_{b1} - z_{b2}) \\ & + c_r [(2\dot{z}_r - \dot{z}_{b1} - \dot{z}_{b2}) - i\omega(2z_r - z_{b1} - z_{b2})] \\ & + c_{ex} [\dot{z}_r - i\omega z_r] + d_r z_r \bar{z}_r \dot{z}_r = m_r u_r \omega^2 e^{i\omega t}, \end{aligned} \quad (6.10)$$

$$\begin{aligned} & m_{bj} \ddot{z}_{bj} + k_{bj} (1 + e_{bj}^c \cos(\varpi t)) z_{bj} - k_r (z_r - z_{bj}) \\ & - c_r [(\dot{z}_r - \dot{z}_{bj}) - i\omega(z_r - z_{bj})] \\ & + c_{bj} \dot{z}_{bj} + d_{bj} z_{bj} \bar{z}_{bj} \dot{z}_{bj} = 0. \end{aligned} \quad (6.11)$$

Note that subscript bj in $(z_{bj}, \dot{z}_{bj}, \dots)$ has to be substituted by $(j = 1, 2)$ in Eq.(6.11) and subsequent formulas to account for both bearing stations. A non-dimensional time τ is introduced

$$\tau = \omega_r t, \quad (6.12)$$

based on the characteristic frequency ω_r of the disk-shaft subsystem

$$\omega_r = \sqrt{2k_r/m_r}. \quad (6.13)$$

6.1. Rotor model with parametric stiffness excitation

By rescaling time and after rearranging the equations we obtain for the mass at the disk station

$$\begin{aligned} z_r'' + \frac{1}{2}(2z_r - z_{b1} - z_{b2}) \\ + \frac{c_r}{m_r \omega_r} [(2z_r' - z_{b1}' - z_{b2}') - i \frac{\omega}{\omega_r} (2z_r - z_{b1} - z_{b2})] \\ + \frac{c_{ex}}{m_r \omega_r} [z_r' - i \frac{\omega}{\omega_r} z_r] + \frac{d_r}{m_r \omega_r} z_r \bar{z}_r z_r' = u_r \frac{\omega^2}{\omega_r^2} e^{(i \frac{\omega}{\omega_r} \tau)}, \end{aligned} \quad (6.14)$$

and at the bearing stations

$$\begin{aligned} z_{bj}'' + \frac{k_{bj}}{m_{bj} \omega_r^2} (1 + e_{bj}^c \cos(\frac{\varpi}{\omega_r} \tau)) z_{bj} - \frac{1}{2} \frac{m_r}{m_{bj}} (z_r - z_{bj}) \\ - \frac{c_r}{m_{bj} \omega_r} [(z_r' - z_{bj}') - i \frac{\omega}{\omega_r} (z_r - z_{bj})] \\ + \frac{c_{bj}}{m_{bj} \omega_r} z_{bj}' + \frac{d_{bj}}{m_{bj} \omega_r} z_{bj} \bar{z}_{bj} z_{bj}' = 0. \end{aligned} \quad (6.15)$$

Introducing the following non-dimensional coefficients for convenience

$$\begin{aligned} M_j &= \frac{m_r}{m_{bj}}, & \nu &= \frac{\omega}{\omega_r}, & q_j &= \frac{\omega_{bj}}{\omega_r}, & \eta &= \frac{\varpi}{\omega_r}, \\ \omega_{bj} &= \sqrt{k_{bj}/m_{bj}}, & \kappa_r &= \frac{c_r}{m_r \omega_r}, & \kappa_{ex} &= \frac{c_{ex}}{m_r \omega_r}, \\ \kappa_{bj} &= \frac{c_{bj}}{m_{bj} \omega_r}, & \delta_r &= \frac{d_r}{m_r \omega_r}, & \delta_{bj} &= \frac{d_{bj}}{m_{bj} \omega_r}, \end{aligned} \quad (6.16)$$

yields the complex representation

$$\begin{aligned} z_r'' + \kappa_r [(2z_r' - z_{b1}' - z_{b2}') - i\nu(2z_r - z_{b1} - z_{b2})] + \\ \frac{1}{2}(2z_r - z_{b1} - z_{b2}) + \kappa_{ex} [z_r' - i\nu z_r] + \delta_r z_r \bar{z}_r z_r' = u_r \nu^2 \exp(i\nu\tau), \end{aligned} \quad (6.17)$$

$$\begin{aligned} z_{bj}'' - \kappa_r M_j [(z_r' - z_{bj}') - i\nu(z_r - z_{bj})] + \kappa_{bj} z_{bj}' \\ + q_j^2 (1 + e_{bj}^c \cos(\eta\tau)) z_{bj} - \frac{1}{2} M_j (z_r - z_{bj}) + \delta_{bj} z_{bj} \bar{z}_{bj} z_{bj}' = 0. \end{aligned} \quad (6.18)$$

For numerical simulation the real matrix form of Eqs.(6.17) and (6.18) is needed. For the disk station we obtain

$$\begin{aligned}
 & \begin{Bmatrix} x_r'' \\ y_r'' \end{Bmatrix} + \begin{bmatrix} 2\kappa_r + \kappa_{ex} & 0 \\ 0 & 2\kappa_r + \kappa_{ex} \end{bmatrix} \begin{Bmatrix} x_r' \\ y_r' \end{Bmatrix} \\
 & + \begin{bmatrix} \delta_r(x_r^2 + y_r^2) & 0 \\ 0 & \delta_r(x_r^2 + y_r^2) \end{bmatrix} \begin{Bmatrix} x_r' \\ y_r' \end{Bmatrix} \\
 & + \begin{bmatrix} 1 & \nu(2\kappa_r + \kappa_{ex}) \\ -\nu(2\kappa_r + \kappa_{ex}) & 1 \end{bmatrix} \begin{Bmatrix} x_r \\ y_r \end{Bmatrix} \\
 & + \begin{bmatrix} -\kappa_r & 0 \\ 0 & -\kappa_r \end{bmatrix} \begin{Bmatrix} x_{b1}' \\ y_{b1}' \end{Bmatrix} + \begin{bmatrix} -\frac{1}{2} & -\nu\kappa_r \\ \nu\kappa_r & -\frac{1}{2} \end{bmatrix} \begin{Bmatrix} x_{b1} \\ y_{b1} \end{Bmatrix} \\
 & + \begin{bmatrix} -\kappa_r & 0 \\ 0 & -\kappa_r \end{bmatrix} \begin{Bmatrix} x_{b2}' \\ y_{b2}' \end{Bmatrix} + \begin{bmatrix} -\frac{1}{2} & -\nu\kappa_r \\ \nu\kappa_r & -\frac{1}{2} \end{bmatrix} \begin{Bmatrix} x_{b2} \\ y_{b2} \end{Bmatrix} = \begin{Bmatrix} f_{rx-u} \\ f_{ry-u} \end{Bmatrix}
 \end{aligned} \tag{6.19}$$

with the vector of unbalance forces

$$\begin{Bmatrix} f_{rx-u} \\ f_{ry-u} \end{Bmatrix} = \begin{Bmatrix} u_r \nu^2 \cos \nu\tau \\ u_r \nu^2 \sin \nu\tau \end{Bmatrix}. \tag{6.20}$$

For the bearing stations the equations of motion Eqs. (6.18) read in real matrix form

$$\begin{aligned}
 & \begin{Bmatrix} x_{bj}'' \\ y_{bj}'' \end{Bmatrix} + \begin{bmatrix} \kappa_r M_j + \kappa_{bj} & 0 \\ 0 & \kappa_r M_j + \kappa_{bj} \end{bmatrix} \begin{Bmatrix} x_{bj}' \\ y_{bj}' \end{Bmatrix} \\
 & + \begin{bmatrix} \delta_{bj}(x_{bj}^2 + y_{bj}^2) & 0 \\ 0 & \delta_{bj}(x_{bj}^2 + y_{bj}^2) \end{bmatrix} \begin{Bmatrix} x_{bj}' \\ y_{bj}' \end{Bmatrix} \\
 & + \begin{bmatrix} \frac{1}{2} M_j & \nu\kappa_r M_j \\ -\nu\kappa_r M_j & \frac{1}{2} M_j \end{bmatrix} \begin{Bmatrix} x_{bj} \\ y_{bj} \end{Bmatrix} \\
 & + \begin{bmatrix} q_j^2(1 + e_{bj}^c \cos(\eta\tau)) & 0 \\ 0 & q_j^2(1 + e_{bj}^c \cos(\eta\tau)) \end{bmatrix} \begin{Bmatrix} x_{bj} \\ y_{bj} \end{Bmatrix} \\
 & + \begin{bmatrix} -\kappa_r M_j & 0 \\ 0 & -\kappa_r M_j \end{bmatrix} \begin{Bmatrix} x_r' \\ y_r' \end{Bmatrix} \\
 & + \begin{bmatrix} -\frac{1}{2} M_j & -\nu\kappa_r M_j \\ \nu\kappa_r M_j & -\frac{1}{2} M_j \end{bmatrix} \begin{Bmatrix} x_r \\ y_r \end{Bmatrix} = \begin{Bmatrix} 0 \\ 0 \end{Bmatrix}.
 \end{aligned} \tag{6.21}$$

Note that Eqs. (6.17), (6.18) as well as Eqs. (6.19),(6.21) are non-linear due to the progressive damping introduced at the disk and the

6.1. Rotor model with parametric stiffness excitation

bearing station of the rotor. The system equations derived hold for a quite general rotor system. Although the disk position is assumed to be symmetric with respect to the bearing stations, there is asymmetry possible with respect to the bearing parameters. However, first studies become more clear if we reduce the number of different parameters and consider two identical bearing stations.

The symbols used for a rotor with both bearings having identical properties are derived from the original parameters by omitting the subscript j :

$$\begin{aligned}
 m_b &= m_{bj}, & q &= q_j = \frac{\omega_b}{\omega_r}, \\
 k_b &= k_{bj}, & \omega_b &= \omega_{bj} = \sqrt{k_b/m_b}, \\
 c_b &= c_{bj}, & \kappa_b &= \kappa_{bj} = \frac{c_b}{m_b \omega_r}, \\
 e_b^c &= e_{bj}^c, & M &= M_j = \frac{m_r}{m_b}, \\
 d_b &= d_{bj}, & & j = 1, 2.
 \end{aligned} \tag{6.22}$$

Consequently, Eq. (6.21) has to be adapted to the new symbols and now reads

$$\begin{aligned}
 & \left\{ \begin{array}{c} x''_{bj} \\ y''_{bj} \end{array} \right\} + \left[\begin{array}{cc} \kappa_r M + \kappa_b & 0 \\ 0 & \kappa_r M + \kappa_b \end{array} \right] \left\{ \begin{array}{c} x'_{bj} \\ y'_{bj} \end{array} \right\} \\
 & + \left[\begin{array}{cc} \delta_b(x_{bj}^2 + y_{bj}^2) & 0 \\ 0 & \delta_b(x_{bj}^2 + y_{bj}^2) \end{array} \right] \left\{ \begin{array}{c} x'_{bj} \\ y'_{bj} \end{array} \right\} \\
 & + \left[\begin{array}{cc} \frac{1}{2}M & \nu \kappa_r M \\ -\nu \kappa_r M & \frac{1}{2}M \end{array} \right] \left\{ \begin{array}{c} x_{bj} \\ y_{bj} \end{array} \right\} \\
 & + \left[\begin{array}{cc} q^2(1 + e_b^c \cos(\eta\tau)) & 0 \\ 0 & q^2(1 + e_b^c \cos(\eta\tau)) \end{array} \right] \left\{ \begin{array}{c} x_{bj} \\ y_{bj} \end{array} \right\} \\
 & + \left[\begin{array}{cc} -\kappa_r M & 0 \\ 0 & -\kappa_r M \end{array} \right] \left\{ \begin{array}{c} x'_r \\ y'_r \end{array} \right\} \\
 & + \left[\begin{array}{cc} -\frac{1}{2}M & -\nu \kappa_r M \\ \nu \kappa_r M & -\frac{1}{2}M \end{array} \right] \left\{ \begin{array}{c} x_r \\ y_r \end{array} \right\} = \left\{ \begin{array}{c} 0 \\ 0 \end{array} \right\}.
 \end{aligned} \tag{6.23}$$

6.1.3 Eigenvalue analysis

From the introduction to parametric resonances in Section 1.2.2 we recall that a system with parametric excitation may exhibit *Principal Parametric Resonances* at frequencies $\eta_{j/n}^{pr}$ and *Parametric Combination Reso-*

nances at frequencies $\eta_{j\pm k/n}^{cr}$ for the PE-frequency η , see Eq. (1.36) and Eq. (1.37):

$$\eta_{j/n}^{pr} = \frac{2\Omega_j}{n}, \quad (n = 1, 2, 3, \dots), \quad (6.24)$$

$$\eta_{j\pm k/n}^{cr} = \frac{|\Omega_j \pm \Omega_k|}{n}, \quad (j, k = 1 \dots m). \quad (6.25)$$

Symbols Ω_j and Ω_k denote the j -th (k -th) natural frequency of the system. The denominator n represents the order of the parametric resonance.

In order to predict the appropriate PE-frequency for vibration suppression in the rotor system, and also to explain the results obtained, it is necessary to know the natural frequencies of the system. Therefore, all undamped natural frequencies $\Omega_{(1..6)}$ have to be calculated from the homogenous, linearized system of Eqs.(6.17), (6.18). However, since the rotor system is isotropic with respect to the directions x , y of reference frame O , only three different natural frequencies do exist. It would not be a problem to use actual values for the system parameters, formulate an eigenvalue problem and solve it numerically. Nevertheless, to allow for an analytical solution of the natural frequencies we will assume symmetry of the rotor also with respect to the bearing stations, i.e. that all parameters of both stations are identical.

To derive a set of appropriate equations for the eigenvalue analysis, we start from Eq.(6.17) and Eq. (6.18), but substitute Eqs. (6.22) for identical bearing parameters. In a next step we omit all damping terms and remove unbalance and parametric excitation. This leads to the following set of equations

$$\underbrace{\begin{bmatrix} M & 0 & 0 \\ 0 & 1 & 0 \\ 0 & 0 & 1 \end{bmatrix}}_{\mathbf{M}} \underbrace{\begin{Bmatrix} z_r'' \\ z_{b1}'' \\ z_{b2}'' \end{Bmatrix}}_{\mathbf{z}''} \quad (6.26)$$

$$+ \underbrace{\begin{bmatrix} M & -\frac{1}{2}M & -\frac{1}{2}M \\ -\frac{1}{2}M & \frac{1}{2}M + q^2 & 0 \\ -\frac{1}{2}M & 0 & \frac{1}{2}M + q^2 \end{bmatrix}}_{\mathbf{K}} \underbrace{\begin{Bmatrix} z_r \\ z_{b1} \\ z_{b2} \end{Bmatrix}}_{\mathbf{z}} = \underbrace{\begin{Bmatrix} 0 \\ 0 \\ 0 \end{Bmatrix}}_{\mathbf{0}},$$

and in brief matrix notation we obtain

$$\mathbf{Mz}'' + \mathbf{Kz} = \mathbf{0}. \quad (6.27)$$

6.2. Method of investigation

From Eqs.(6.26) the natural frequencies $\Omega_1 < \Omega_2 < \Omega_3$ can be obtained in analytical form as

$$\Omega_{1,3} = \sqrt{\frac{1}{2}(1 + \frac{1}{2}M + q^2) \mp \sqrt{\frac{1}{4}(1 + \frac{1}{2}M + q^2)^2 - q^2}}, \quad (6.28)$$

$$\Omega_2 = \sqrt{\frac{1}{2}M + q^2}. \quad (6.29)$$

The analysis can be continued and analytical expressions can also be found for the eigenvectors of the system. We refrain from presenting them here because they are quite lengthy and we do not need them in the further investigation. It is important though to realize which vibration mode corresponds to the frequencies Ω_j . For this system Ω_1 is the frequency of the first bending mode of the rotor, sometimes also called the "U-mode" because of the shape of the shaft deformation. For this mode an in-phase vibration of the disk and the bearing masses occurs. The second mode, corresponding to Ω_2 , is named the "S-mode". Since we have neglected the rotational inertia of the disk and because the rotor is symmetric with respect to the disk station, the "S-mode" exhibits only counter-phase deflections at the bearing stations. The disk will not participate in the vibration since it is located at the neutral point of this mode. As a consequence this mode cannot be excited by forces acting on the disk. The third mode is the "W-mode" which shows a synchronized motion of both bearing masses, in counter-phase to the disk motion at a frequency of Ω_3 .

From this discussion it becomes quite clear that we will have to deal almost exclusively with vibrations of the first and possibly the third mode, since the parametric excitation is assumed to act in phase at the bearing stations. Unbalance forces and destabilizing gap forces are applied only to the rotor disk and cannot excite the second mode. Internal damping forces act on all three masses but are also synchronized with respect to the bearing stations.

6.2 Method of investigation

The eigenvalue analysis of the fully symmetric model did reveal that the first and the third vibration mode are sufficient to describe this model. As a consequence a minimal model consisting of just these two modes

can be established. In fact, this model was used by A. Tondl in a very first study [89] of the application of parametric excitation on a rotor system with self-excitation due to internal damping of the shaft. In that paper the analytical Tondl-Floquet method of Section 2.1.3 is applied and conditions for the parameters of the rotor system are presented to achieve full vibration quenching. In a follow-up work [19] by the author and A. Tondl, numerical simulation was employed to investigate a similar basic rotor system. T. Pumphössel also used numerical simulation quite intensively to investigate 4-dof, 6-dof and 8-dof rotor systems, see [66] and [20]. Although such systems have to be considered as low-dof systems from the viewpoint of multibody dynamics, they are already beyond the capabilities of analytical methods if no symmetries are present to split up the model or to reduce its order.

Therefore, in general only numerical methods can be used for the investigation of rotating systems. With the clear advantage of faster computational speed, the numerical Floquet-method is certainly superior to direct numerical simulation. However, in the presence of unbalance excitation the situation reverses, since the Floquet-method cannot be applied in general when two different excitation frequencies are present.

The following first numerical study will consider a rotor system without unbalance excitation and two different sources of self-excitation. The second study will investigate an almost identical system with unbalance excitation. Of course it would be possible to use numerical Floquet-analysis for study #1 and then switch to numerical simulation for study #2. However, this seems to be quite inconsistent and is not really helpful in relating the results to each other. Therefore numerical simulation was used exclusively for the two final numerical studies.

For the following results numerical integration of the system equations (6.19) and (6.23) in the time domain was carried out by using ACSL [55]. Starting from (basically) arbitrary initial conditions integration was continued over a predefined period of time. After reaching that terminal point it was checked whether steady-state conditions were reached or not. Normally this was the case, and for vibration cancelling the vibrations at the disk and the bearing stations had (almost) vanished. If not, the simulation was continued for more periods and finally terminated when a time criterion became effective. Occasionally, though, low frequency beats were observed in the regime of self-excitation and caused minor errors in the results, see also the comments in Section 2.2.

6.3 Study of a balanced rotor

All diagrams shown below are two-dimensional parameter studies of the maximum vibration amplitudes $x_{R,max}$ at the rotor disk station. The parameter chosen for the abscissa is the excitation frequency ratio $\eta = \varpi/\omega_r$. Actual amplitudes of $x_{R,max}$ can be estimated by using the 3D-diagrams on top of the figures. Symbols and parameters as used in the study are listed in Table 6.2. The most interesting regions in the plots represent zero amplitudes, i.e. vibration cancellation. They are colored in white for easy recognition. Vibration cancelling occurs (if at all) always when η coincides with the combination frequency $\eta = \Omega_3 - \Omega_1$. Since self-excitation is not possible unless the critical speed is exceeded, areas of $x_{r,max} = 0$ can be found in the plotted results which are not caused by parametric excitation. Typically, these regions are independent of η and stretch from the lower to the upper limit of the frequency parameter.

As the bearing characteristics are assumed to be isotropic, the maximum amplitudes in both directions x and y are identical. Therefore, only results for the x -direction are presented here. Since the major focus of this investigation lies on vibration suppression which will occur simultaneously at the disk and at the bearing stations, the vibration amplitudes at the latter are not shown, because they do not reveal new information.

6.3.1 Self-excitation due to internal damping

We will now consider internal damping as the only source of self-excitation for the rotor. The default values of the system parameters are listed in Table 6.3. Parameter κ_r represents internal damping and is set to $\kappa_r = 0.05$. Self-excitation by external gap forces is not considered here ($\kappa_{ex} = 0.0$).

Rotational speed of the rotor

The first result in Fig. 6.2 shows how the critical speed of the rotor depends on the frequency η of the parametric excitation. For a PE-frequency $\eta < 1$ or $\eta > 4$ the stability threshold is close to a rotational speed of the rotor of $\nu \approx 1$. This is also the critical speed for the corresponding system without parametric excitation for which the internal

Table 6.2: List of symbols as used for dimensionless model parameters in the following investigations of a rotor system. See also Eqs. (6.16)

Parameter	Description	Definition
M	Mass ratio	$\frac{m_r}{m_b}$
q	Frequency ratio	$\frac{\omega_b}{\omega_r}$
κ_r	Internal damping of the shaft *)	$\frac{c_r}{m_r \omega_r}$
κ_{ex}	External damping due to gap forces **)	$\frac{c_{ex}}{m_r \omega_r}$
κ_b	Damping at bearing stations	$\frac{c_b}{m_{bj} \omega_r}$
e_b^c	Amplitude of parametric excitation	see Eq.(6.1)
u_r	Amplitude of unbalance excitation **)	see Eq.(6.3)
δ	Parameter of nonlinear damping	$\frac{d_b}{m_b \omega_r}$
η	Frequency of parametric excitation	$\frac{\varpi}{\omega_r}$
ν	Rotational speed of the rotor	$\frac{\omega}{\omega_r}$
ω_r	Frequency of disk-shaft subsystem	$\sqrt{2k_r/m_r}$
ω_b	Frequency of bearing subsystem	$\sqrt{k_b/m_b}$
Ω_1	First natural frequency of the system	see Eq.(6.28)
Ω_2	Second natural frequency of the system	see Eq.(6.29)
Ω_3	Third natural frequency of the system	see Eq.(6.28)
$\Omega_3 - \Omega_1$	Param. combination resonance frequ.	see Ω_1, Ω_3
$\Omega_1 + \Omega_3$	Param. combination resonance frequ.	see Ω_1, Ω_3

*) Source of self-excitation

***) Source of external (forced) excitation

6.3. Study of a balanced rotor

Table 6.3: Default parameters for model of the rotor system with self-excitation due to internal damping. For results see Figs. 6.2 to 6.7 with symbol \diamond indicating default parameters.

Parameter	M	q	κ_r	κ_b	e_b^c	δ	ν
	4.0	2.0	0.05	0.1	0.2	0.05	1.2
Frequency	Ω_1	Ω_2	Ω_3	$\Omega_3 - \Omega_1$	$\Omega_1 + \Omega_3$		
	0.792	2.450	2.524	1.732	3.316		

damping parameter κ_r and the rotor speed ν solely determine the stability threshold. Near the parametric combination resonance frequency $\Omega_3 - \Omega_1 = 1.73$ a significant increase of the critical speed is observed and the phenomenon of parametric vibration suppression occurs. For an optimally chosen PE-frequency, which is practically identical with $\Omega_3 - \Omega_1$, the improvement for the critical speed is about 40% at a PE-amplitude of $e_b^c = 0.2$.

From the 3D-plot on top in Fig. 6.2 one can also see that the increased stability range does not end abruptly but changes gently to small vibration amplitudes. Even beyond this additional area of stability a certain amount of vibration reduction is still possible at the PE-frequency of $\eta = \Omega_3 - \Omega_1$ which may be of value in a practical application.

Next to the additional area of stability a region of increased amplitudes is observed for $\eta = 1.58$. At this frequency the primary parametric resonance of the first order $\eta_{1/1}^{pr} = 2\Omega_1$ occurs and causes a higher vibration level for a quite narrow range of the PE-frequency. Also a parametric combination resonance shows up in the diagram for $\eta = 3.32$, where $\eta_{1+3/1}^{cr} = \Omega_1 + \Omega_3$ is found. Although the increase of the vibration level by this combination resonance is not very pronounced in the instability region, it lowers the critical speed by 25% to $\nu_{crit} = 0.75$. The adverse effect of the true parametric resonances is indisputable but can be avoided easily by choosing the appropriate PE-frequency. Of course, for a robust system that can also tolerate minor uncertainties of parameters a close encounter of the anti-resonance frequency with a true resonance frequency should be avoided.

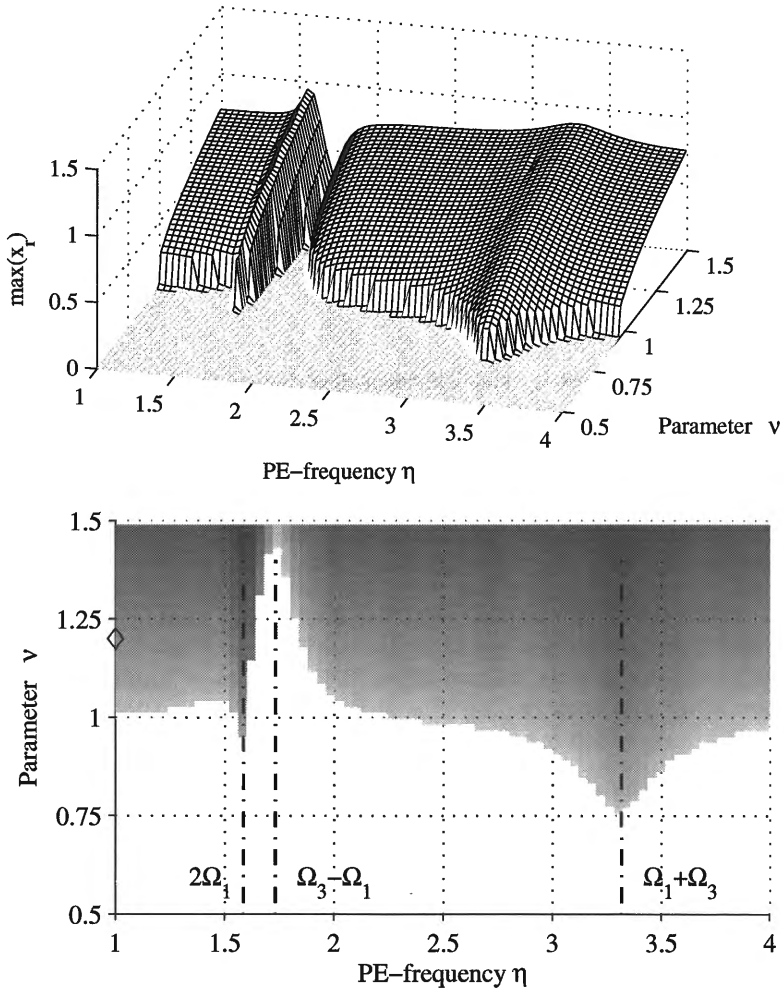


Figure 6.2: Parameter study for rotor with internal damping as source of self-excitation. Maximum amplitudes $\max(x_R)$ at rotor disk. White areas indicate regions of vibration cancellation.

6.3. Study of a balanced rotor

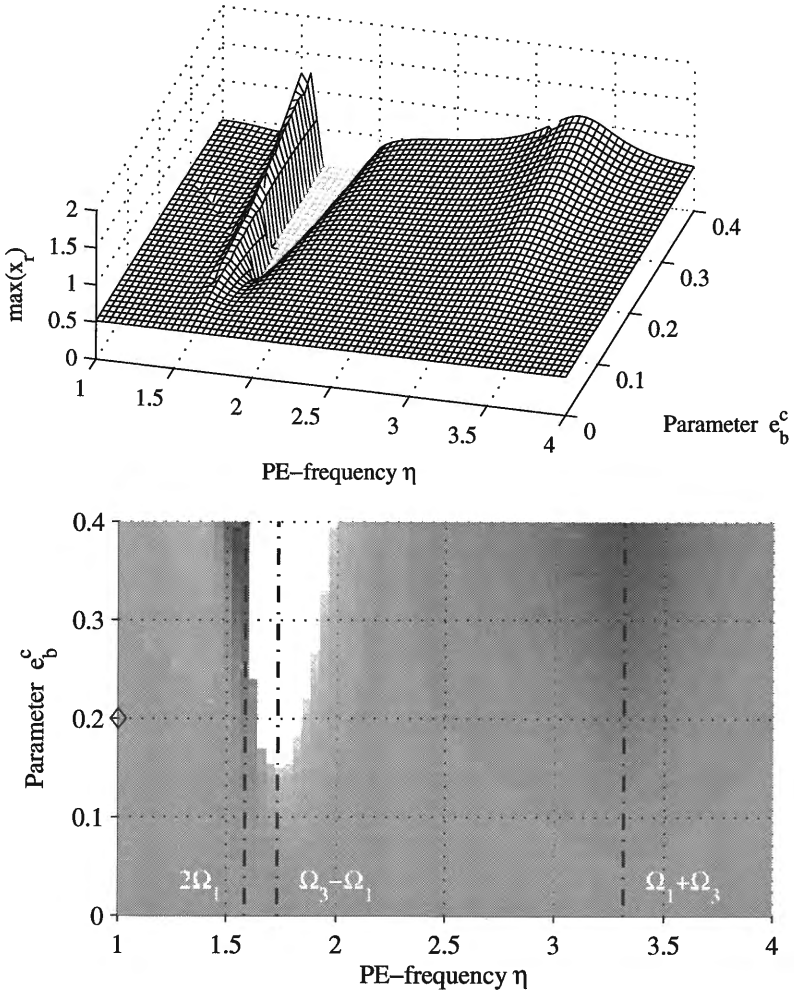


Figure 6.3: Parameter study for rotor with internal damping as the source of self-excitation. Maximum amplitudes $\max(x_R)$ at rotor disk. White areas indicate regions of vibration cancellation.

Parametric excitation amplitude

The second parameter available with parametric excitation that can be chosen for maximum performance is the amplitude e_b^c of the parametric excitation. The diagrams in Fig. 6.3 hold for a rotor speed of $\nu = 1.2$ and show the effect of the PE-amplitude on the vibration level in the system. At the optimal PE-frequency $\eta = \Omega_3 - \Omega_1$ a minimum value of about $e_b^c \approx 0.16$ is necessary to bring about the vibration suppression effect. Any amplitude values $e_b^c > 0.15$ lead to a stable system for PE-frequencies at or near the anti-resonance frequency. For increasing values of the PE-amplitude the stability interval with respect to the PE-frequency gets considerably larger and reaches almost $\Delta\eta_{stab} \approx 0.4$ at $e_b^c = 0.4$.

Both parametric resonances show up at $2\Omega_1$ and $\Omega_1 + \Omega_3$, respectively, and increase with increasing PE-amplitude. Especially from the 3D-plot it is easy to see that the primary resonance $\eta_{1/1}^{pr} = 2\Omega_1$ is much more pronounced but also more restricted than the combination resonance $\eta_{1+3/1}^{cr}$.

The basic observation from this parameter study is the existence of a threshold value for the PE-amplitude. Any PE-amplitude exceeding the minimum value cannot improve the stability of the system itself when the optimal PE-frequency is used. However, the added equivalent damping of the parametric excitation still can get larger and transients will decay faster for larger amplitudes.

Parameter of internal damping

The second parameter which is directly related to the self-excitation mechanism is the internal damping κ_r of the shaft. In Fig. 6.4 a variation of this parameter is carried out in the range of $\kappa_r = [0...0.1]$ for a rotational speed of $\nu = 1.2$. It is not a surprise that the shape of the stability threshold in this diagram is very similar to that of Fig. 6.2. This becomes quite clear when we look at Eq. (6.19) and remember that the product of ν and κ_r appears in the cross-coupling matrices of the non-conservative forces.

From this figure one can determine the maximum internal damping permissible, either for a system without parametric excitation or at the optimum PE-frequency. We can see that parametric excitation stabilizes the system even if the internal damping is twice as much as at the stability threshold for a conventional system.

6.3. Study of a balanced rotor

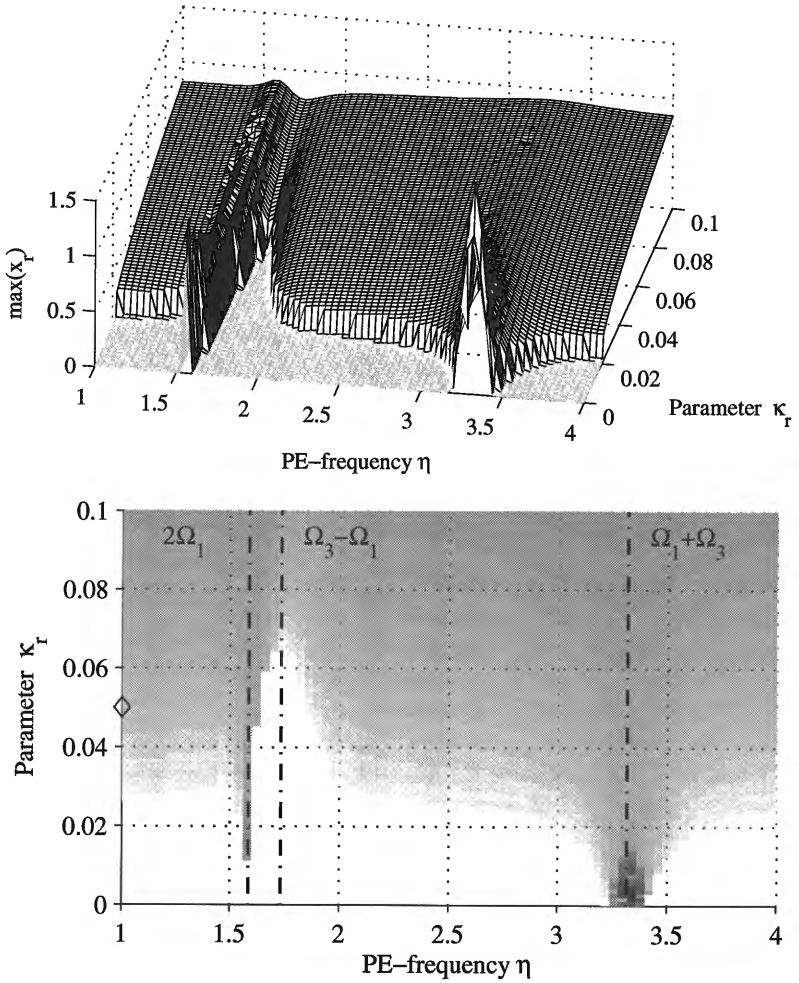


Figure 6.4: Parameter study for rotor with internal damping as source of self-excitation. Maximum amplitudes $\max(x_R)$ at rotor disk. White areas indicate regions of vibration cancellation.

With no internal damping at all ($\kappa_r = 0$) the rotor system behaves like a basically stable system with parametric excitation and exhibits strong, narrow-banded parametric resonances for $\eta_{1/1}^{pr}$ and $\eta_{1+3/1}^{cr}$.

Damping at the bearing stations

The second source of damping in the system is located at the bearing stations. The damping provided by the bearings always contributes to the dissipation of energy in the system. From Fig. 6.5 one can see that the conventional system needs at least a value of $\kappa_b \approx 0.25$ to become stable for default parameters. Parametric excitation almost seems to cause a miracle since it reduces the the necessary damping at the bearing stations to nil. This is certainly a remarkable result and shows the potential which this method of vibration suppression holds.

By recalling the principal idea of Chapter 4 we can express the effect of parametric excitation in terms of an equivalent damping at the bearing station.

Variation of the mass ratio

So far we only looked at damping parameters and excitation parameters. Now we will change the tuning of the rotor system and investigate the mass ratio $M = m_r/m_b$ of the disk mass in relation to the bearing mass. A large value of M therefore means a massive disk and a comparatively small mass concentration at the bearing stations. The default value for the mass ratio was $M = 4$ in the previous studies, see also Table 6.3.

Figure 6.6 shows how the stability of the system is related to the mass ratio and the PE-frequency. The main features of the figures are the "canyon" of vibration suppression that cuts through the region of instability and the parametric resonances that rise above the general level of vibration. The assignment of these features to the according parametric resonance frequencies can be seen from the annotation of the bottom figure. In all previous figures the parametric resonance frequencies were independent of the variation of the respective parameter. This has changed now, since the mass ratio M has a direct influence on the natural frequencies of the system and, hence, changes also the parametric resonance frequencies.

It is interesting to see that an increasing mass ratio increases the interval of stability. Starting from the default value of $M = 4$, the interval

6.3. Study of a balanced rotor

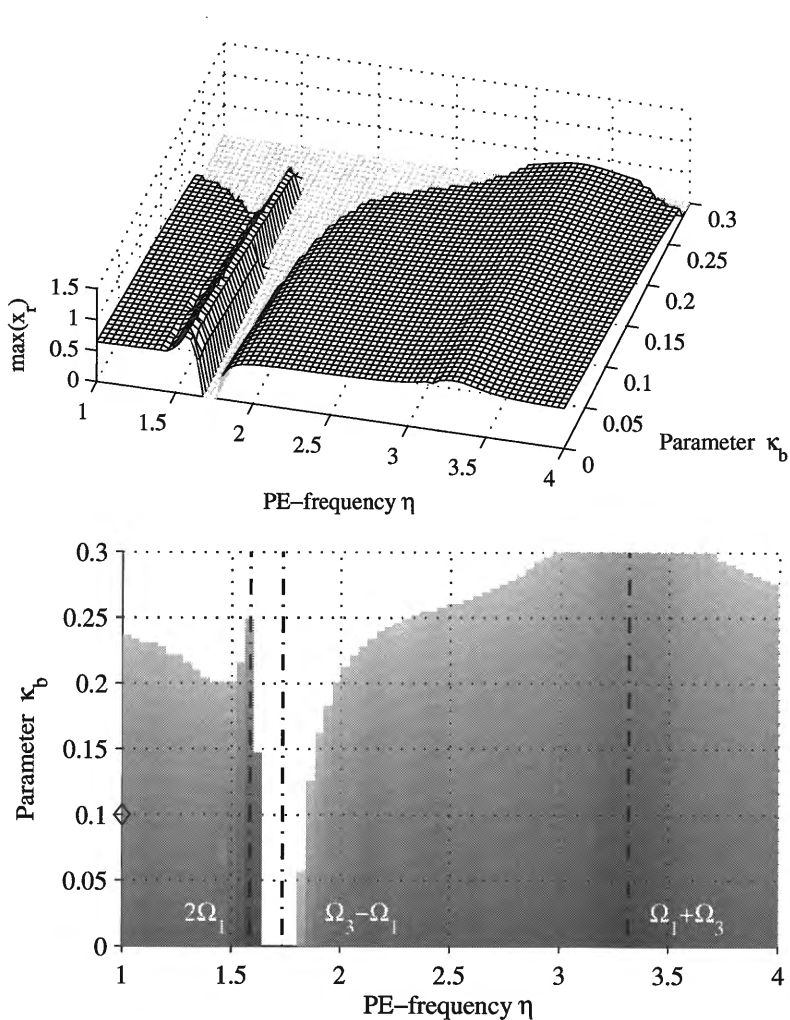


Figure 6.5: Parameter study for rotor with internal damping as source of self-excitation. Maximum amplitudes $\max(x_R)$ at rotor disk. White areas indicate regions of vibration cancellation.

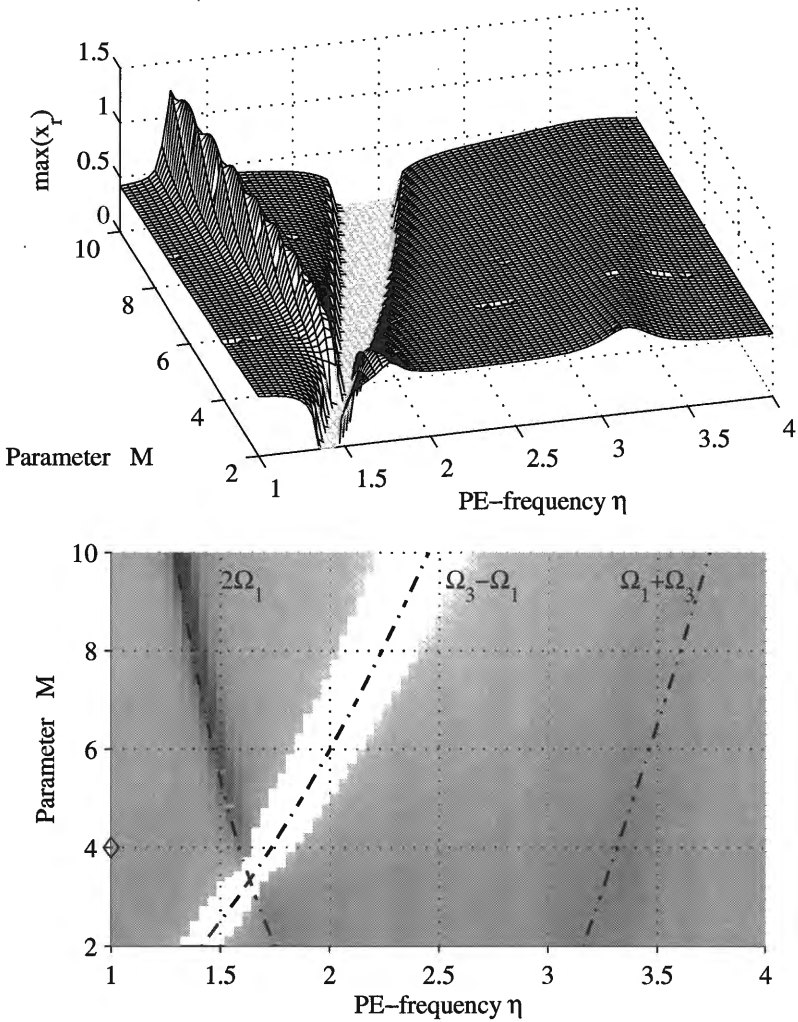


Figure 6.6: Parameter study for rotor with internal damping as source of self-excitation. Maximum amplitudes $\max(x_R)$ at rotor disk. White areas indicate regions of vibration cancellation.

6.3. Study of a balanced rotor

almost doubles at $M = 10$. This result is in agreement with previous results in Chapter 3 where an increase of the main mass also enlarged the stability interval. However, note the difference between this study and the previous one. Here we do not only change a single parameter when $M = m_r/m_b$ is varied since it is defined as a ratio. Moreover, even if we think of changing just the nominator (or the denominator) we have to keep in mind that other parameters like q and κ are related to the mass parameters. Therefore we have to be careful when using these dimensionless quantities.

A very interesting detail has to be pointed out in Fig. 6.6. For $M \approx 3.3$ a strange situation occurs since the parametric anti-resonance $\Omega_3 - \Omega_1$ and the principal parametric resonance $2\Omega_1$ take on identical values. In fact, at this parameter value for M the two frequency lines intersect and parametric resonance and anti-resonance compete directly. As one can see, the winner is the anti-resonance since it suppresses the resonance and the self-excitation at the same time.

Variation of the frequency ratio

The last study in this series is a variation of the frequency ratio $q = \omega_b/\omega_r$ which is a kind of tuning parameter. This parameter is related to the natural frequencies of the system and consequently the resonance frequencies are changed significantly when a variation is carried out. Figure 6.7 shows the result of this study. For values $q < 1.5$ the system is stable and self-excitation does not exceed the critical value. At the default value $q = 2.0$ the meanwhile well known stability interval near $\eta = 1.73$ appears. A further increase of the parameter shifts the optimal PE-frequency to higher values and the stability interval gets smaller at the same time. For $q > 3.5$ full vibration suppression is not possible anymore, but still a reduction of the vibration level is observed.

6.3.2 Self-excitation due to destabilizing gap forces

The second part of this study on the balanced rotor investigates how self-excitation of the rotor system generated by non-conservative gap forces can be cancelled by parametric excitation. The corresponding system parameter κ_{ex} is set to a default value of $\kappa_{ex} = 0.1$ to provide the same level of damping and of non-conservative forces to the rotor disk as in the previous example by internal damping. Internal damping of the shaft is

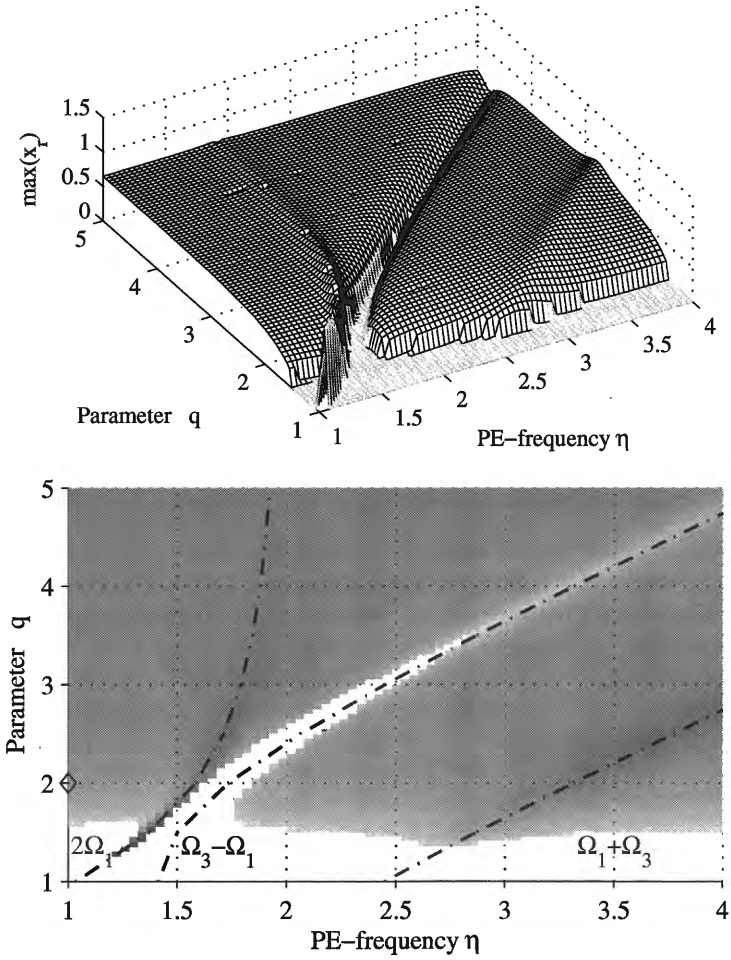


Figure 6.7: Parameter study for rotor with internal damping as source of self-excitation. Maximum amplitudes $\max(x_R)$ at rotor disk. White areas indicate regions of vibration cancellation.

6.3. Study of a balanced rotor

Table 6.4: Default parameters for model of the rotor system with self-excitation due to internal damping. For results see Figs. 6.8 to 6.9 with symbol \diamond indicating default parameters.

Parameter	M	q	κ_{ext}	κ_b	e_b^c	δ	ν
	4.0	2.0	0.1	0.1	0.2	0.05	1.2
Frequency	Ω_1	Ω_2	Ω_3	$\Omega_3 - \Omega_1$	$\Omega_1 + \Omega_3$		
	0.792	2.450	2.524	1.732	3.316		

not considered here ($\kappa_R = 0.0$). Default values of other parameters (see Table 6.4) are the same as in the previous example to make possible a direct comparison of results.

As we will see in the following, the results are largely similar to the previous results for the rotor with internal damping. Therefore the discussion can be shorter now and will mainly concentrate on the differences between the two studies which are nevertheless quite significant.

Rotational speed of the rotor

Figure 6.8 shows how the critical speed of the rotor depends on the frequency η of the parametric excitation. The stability threshold for the system without parametric excitation is lower now and close to a rotational speed of $\nu \approx 0.88$. At the parametric combination resonance frequency $\Omega_3 - \Omega_1 = 1.73$ parametric vibration suppression occurs and the critical speed is again significantly increased. At this PE-frequency the improvement of the critical speed is about 40%, which is virtually the same as in the previous example for internal damping.

From the 3D-plot in Fig. 6.2 one can see that the primary parametric resonance of the first order $\eta_{1/1}^{pr} = 2\Omega_1 = 1.58$ has almost disappeared and is much less significant than before. On the other hand, the parametric combination resonance $\eta_{1+3/1}^{cr} = \Omega_1 + \Omega_3$, showing up at $\eta = 3.32$, is much more pronounced for this case. This leads to a reduction of the critical speed of almost 45% at $\eta = \eta_{1+3/1}^{cr}$. Obviously, the two parametric resonances frequencies $\eta_{1/1}^{pr}$ and $\eta_{1+3/1}^{cr}$ have switched roles in this example and the latter will now appear as the resonance provoking a narrow frequency band of significantly increased amplitudes.

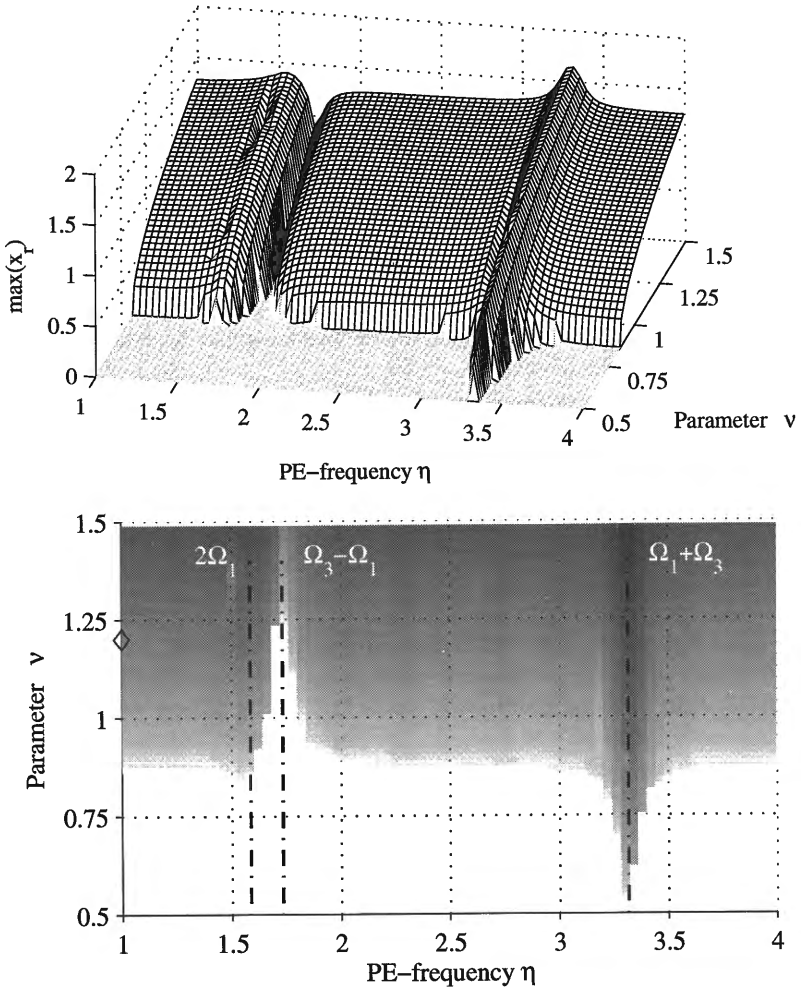


Figure 6.8: Parameter study for rotor with external gap damping as the source of self-excitation. Maximum amplitudes $\max(x_R)$ at rotor disk. White area indicates regions of vibration cancellation.

6.3. Study of a balanced rotor

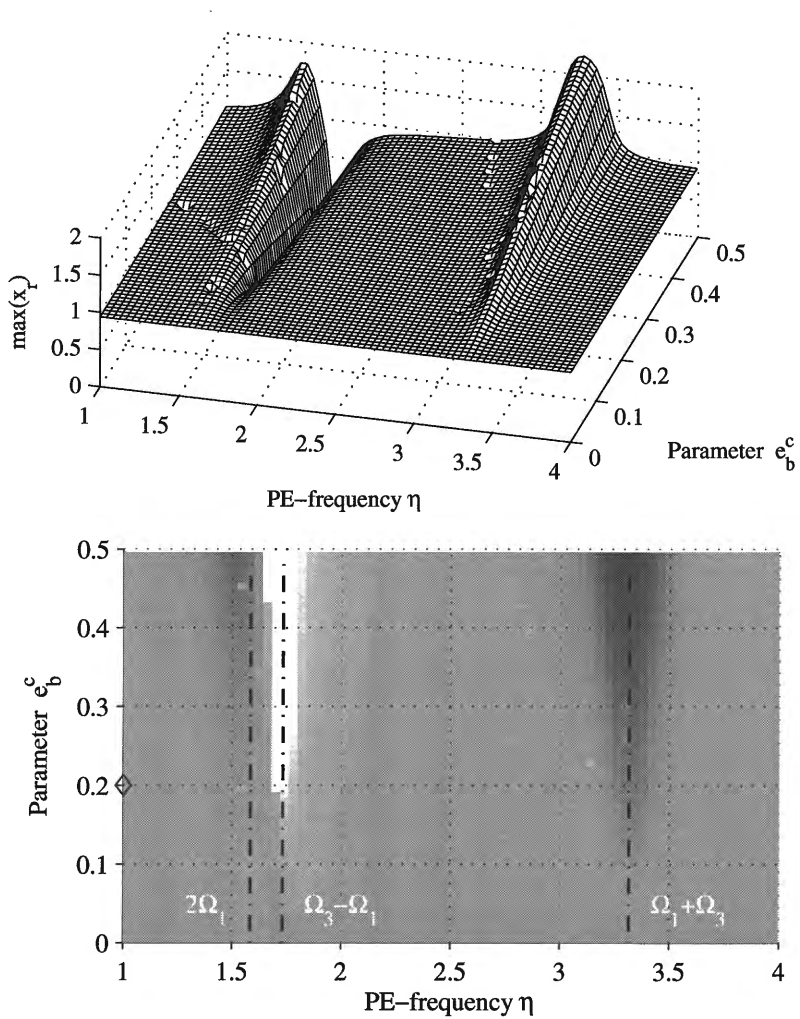


Figure 6.9: Parameter study for rotor with external gap damping as the source of self-excitation. Maximum amplitudes $\max(x_R)$ at rotor disk. White area indicates regions of vibration cancellation.

Parametric excitation amplitude

The amplitudes at the rotor disk station as a function of the two parametric excitation parameters η and e_b^c are shown in Fig. 6.9. A major difference in the results for external gap damping $\kappa_{ex} \neq 0$ compared to internal damping $\kappa_r \neq 0$ can be seen even for a parametric excitation amplitude $e_b^c = 0$. The vibration level of the dimensionless displacement at the disk station reaches values of $\max(x_r) \approx 1$. With the previous result, shown in Fig. 6.3 we obtained $\max(x_r) \approx 0.5$, almost half the value as now with external gap damping. This means that the self-excitation effect due to this kind of damping is significantly stronger and therefore makes it much harder for the parametric excitation to achieve vibration suppression.

As a consequence the minimum parametric excitation amplitude e_b^c to achieve full vibration cancellation is now barely below the default value of $e_b^c = 0.2$. An increase of the PE-amplitude at a PE-frequency of $\eta = \Omega_3 - \Omega_1$ moves the system away from the stability border to a more safe choice of parameters. Nevertheless, the stability interval does not increase for increasing PE-amplitudes as much as it did in the previous case, which is another consequence of the stronger effect of the self-excitation mechanism.

Parameter of external gap damping

In Fig. 6.10 a variation of the external gap damping parameter κ_{ex} is carried out. This parameter introduces damping to the system but at the same time determines the level of self-excitation in combination with the rotor speed ν . Therefore this figure resembles Fig. 6.8.

The default value of $\kappa_{ex} = 0.1$ is indicated in the 2D-plot at the bottom and one can see that the system is far away from the stability threshold of $\kappa_{ex} \approx 0.02$ for no (or completely detuned) parametric excitation. At a PE-frequency of $\eta = \Omega_3 - \Omega_1$ we have almost reached the maximum level for κ_{ex} at the given rotor speed of $\nu = 1.2$ to obtain vibration cancelling.

Damping at the bearing stations

The result shown in Fig. 6.11 differs significantly from the previous Fig. 6.5. Note that the scaling of the axis for κ_b starts at a minimum value of 0.3, which is above the default value of $\kappa_b = 0.1$! With external

6.3. Study of a balanced rotor

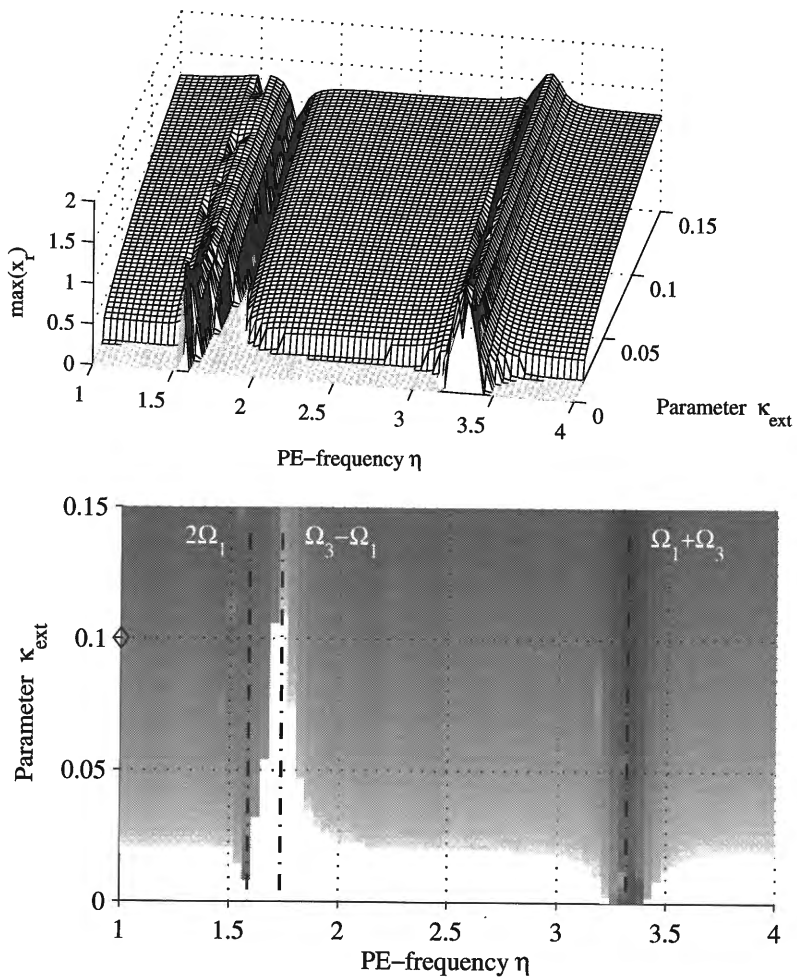


Figure 6.10: Parameter study for rotor with external gap damping as the source of self-excitation. Maximum amplitudes $\max(x_R)$ at rotor disk. White area indicates regions of vibration cancellation.

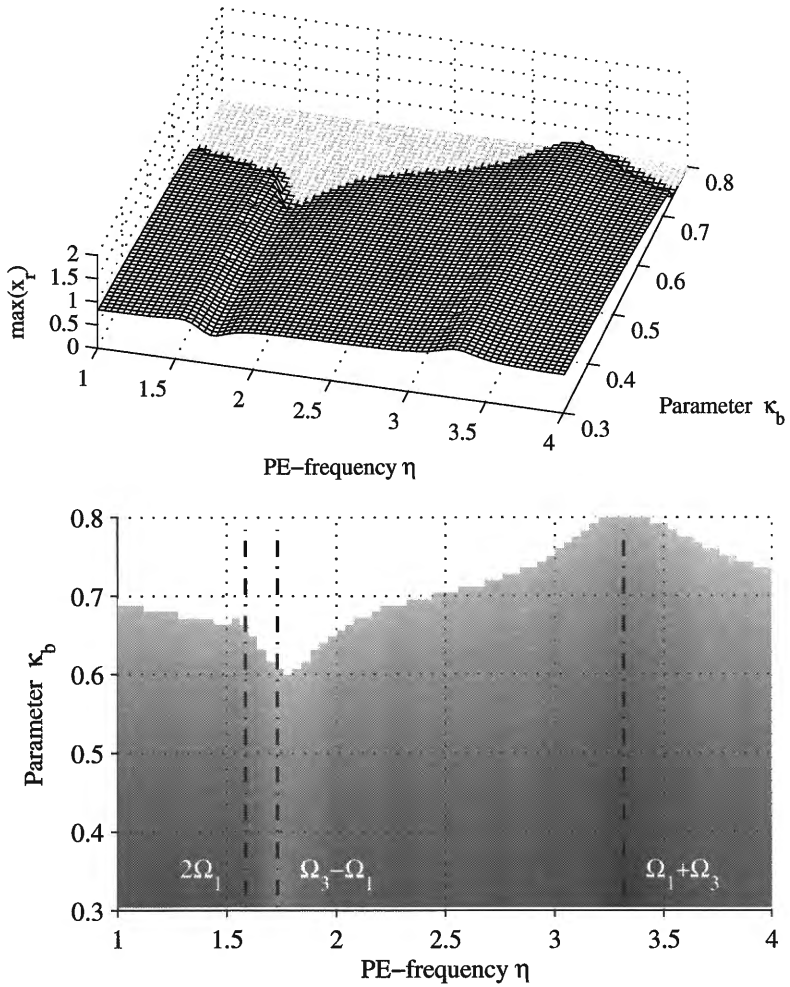


Figure 6.11: Parameter study for rotor with external gap damping as the source of self-excitation. Maximum amplitudes $\max(x_R)$ at rotor disk. White area indicates regions of vibration cancellation.

6.3. Study of a balanced rotor

gap damping as the source of self-excitation it is no longer possible to operate the rotor system under stable conditions without damping at the bearing stations. A comparably high level of $\kappa_b \approx 0.7$ has to be reached to obtain stability without parametric excitation.

Parametric vibration suppression is still effective near the combination resonance frequency $\eta \approx \Omega_3 - \Omega_1$, but the gain of equivalent damping is not really impressive. The necessary level of damping at the bearing station drops by as little as 10% to $\kappa_b = 0.6$. This result has to be seen in comparison with Fig. 6.5, where the rotor system could be stabilized even without any damping at the bearing stations.

From this parameter study we can see again that not only the level of self-excitation but also both locations of the self-excitation mechanism and of the parametric excitation have a great influence on the performance of parametric excitation.

Variation of the mass ratio

The last two parameter studies concern the tuning parameters of the rotor system. We first discuss the influence of the mass ratio $M = m_r/m_b$ of the mass of the disk in relation to the bearing mass. Figure 6.12 looks almost like the previous Fig. 6.6, but is quite different with respect to an important detail. The interval of stability now gets smaller with increasing mass ratio M . In fact, full vibration quenching is only possible for values up to $M \approx 5.5$ at the appropriate PE-frequency. Beyond this value the amplitudes can be reduced to some extent, but not fully cancelled.

We recall the result from Fig. 6.6 and note that the influence of the mass ratio has now reversed. With external gap damping as the source of self-excitation smaller values of the mass ratio are more favorable for parametric vibration suppression.

Variation of the frequency ratio

Finally the frequency ratio $q = \omega_b/\omega_r$ is used as the parameter of variation and Fig. 6.13 shows the result of this study. It is not much of a surprise that the principal dependency of the stability interval on the frequency ratio is reversed when compared with Fig. 6.7. Vibration cancelling now starts near the default value of $q = 2.0$ and is possible for q even beyond a value of 5. Due to the high level of self-excitation the

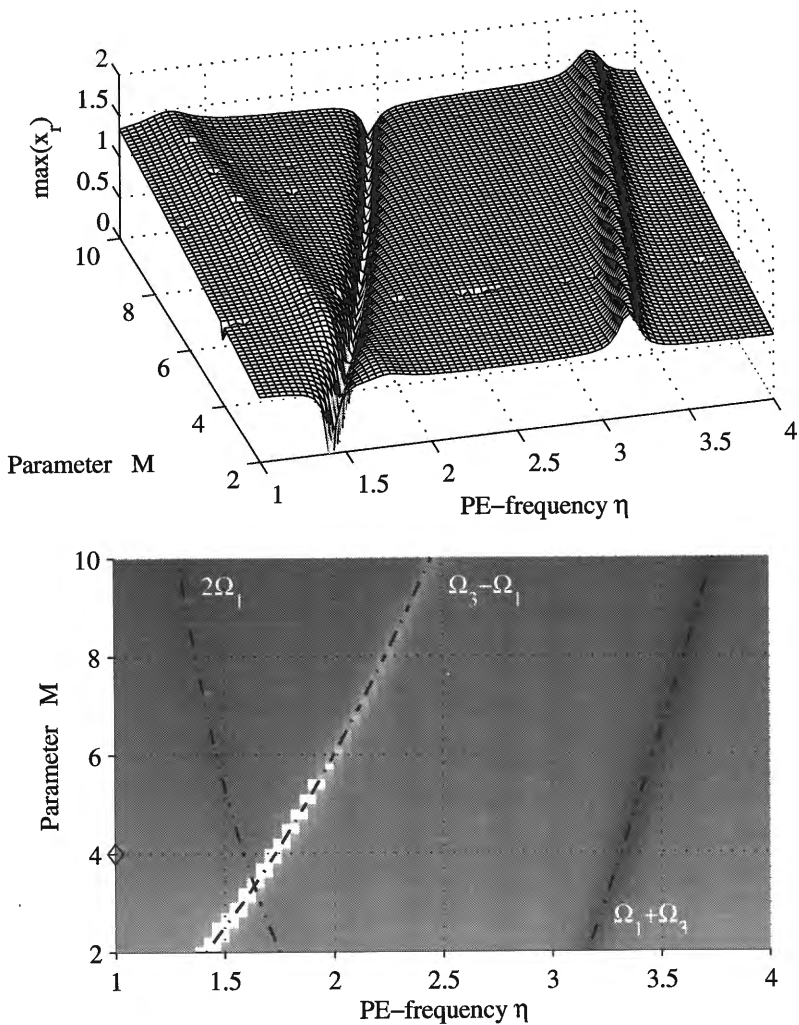


Figure 6.12: Parameter study for rotor with external gap damping as the source of self-excitation. Maximum amplitudes $\max(x_R)$ at rotor disk. White area indicates regions of vibration cancellation.

6.3. Study of a balanced rotor

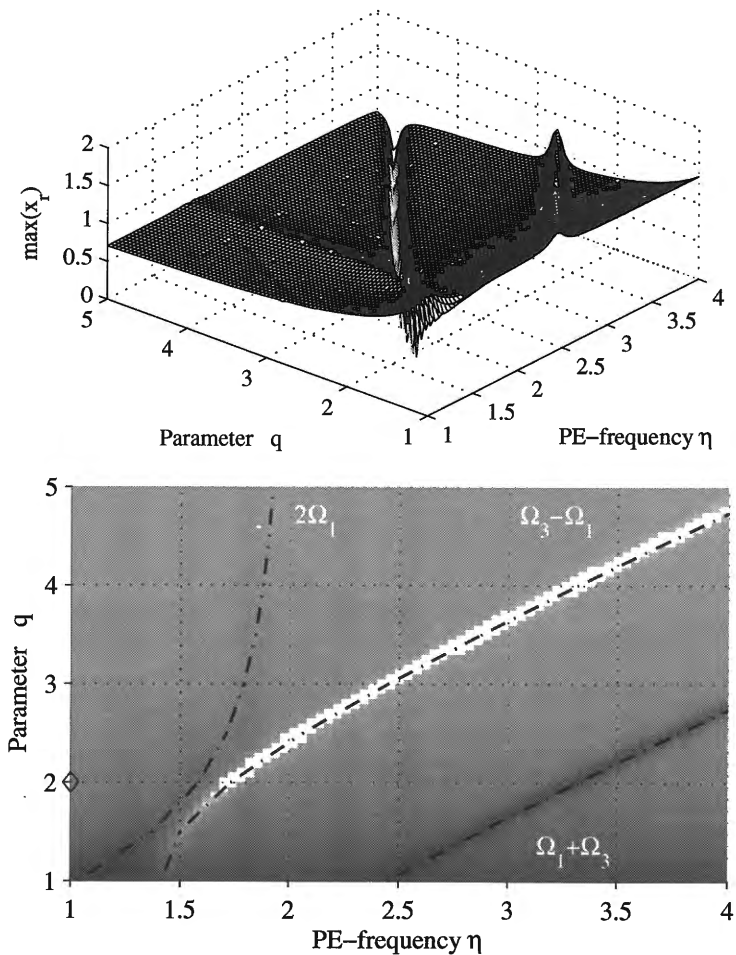


Figure 6.13: Parameter study for rotor with external gap damping as the source of self-excitation. Maximum amplitudes $\max(x_R)$ at rotor disk. White area indicates regions of vibration cancellation.

stability interval is quite narrow and widens only a little bit, but it is present and would allow at least small deviations of the PE-frequency.

Concluding remarks

In summing up the results of this second study we conclude that the parameter set chosen for this study did not favor the application of parametric excitation as a mean to suppress self-excited vibrations generated by external non-conservative gap forces. A smaller mass ratio M or/and a higher frequency ratio q gives much better results, see [66] and [20]. However, the study did show that it is a matter of a properly designed system to effectively use parametric excitation for vibration suppression. The effect itself can be achieved for a self-excitation mechanism acting at any location of the rotor system.

6.4 Study of a rotor with mass unbalance

In a real rotor system it is not possible to avoid a certain amount of mass unbalance. Such an unbalance can be represented by external periodic forces, acting on the rotor, see e.g. [101] and [26]. With respect to parametric stiffness excitation of the rotor system the important question arises how these external forces may influence the effectiveness of suppressing self-induced vibrations.

This interesting topic was investigated for the first time by A. Tondl and the author in [93]. In this reference a brief analytical study is carried out for a generic system with parametric excitation as defined by Eq. (2.82). The system referred to is enlarged by a periodic excitation on the right-hand side, as frequently used for rotor systems to represent unbalance excitation, see Eq. (6.20). Under the assumption of a sufficiently small external excitation it is possible to apply the Tondl-Floquet method (see Chapter 2.1.3) and prove that the external excitation does not affect the ability of the parametric excitation to stabilize the system.

In the following section we will continue with the numerical investigation of the rotor system. The equations of motion have already been derived in Section 6.1.2 and led to the set of equations (6.19), (6.20) and (6.23). In the previous section this set was used, but the unbalance parameter u_r was set to zero. In principle we only have to activate this parameter and rerun the simulation program. To verify the analytical

6.4. Study of a rotor with mass unbalance

Table 6.5: Default parameters for model of a self-excited rotor system with mass unbalance as used for results in Figs. 6.14 to 6.19

Parameter	M	q	κ_b	ν	δ
All sets	4.0	2.0	0.1	1.2	0.05
Parameter	u_e	e_b^c	κ_r	η	
Set (i)	0	0	0.05	n.a.	
Set (ii)	0	0.2	0.05	1.732	
Set (iii)	0	0.2	0	1.732	
Set (iv)	0.1	0	0.05	n.a.	
Set (v)	0.1	0	0	n.a.	
Set (vi)	0.1	0.2	0.05	1.732	
Frequency	Ω_1	Ω_2	Ω_3	$\Omega_3 - \Omega_1$	$\Omega_1 + \Omega_3$
All sets	0.792	2.450	2.524	1.732	3.316

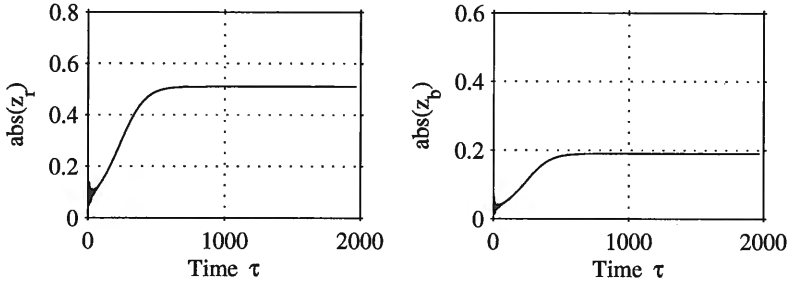
results in a first study, internal damping of the shaft is chosen to be the only self-excitation mechanism acting on the rotor system.

6.4.1 Self-excitation due to internal damping

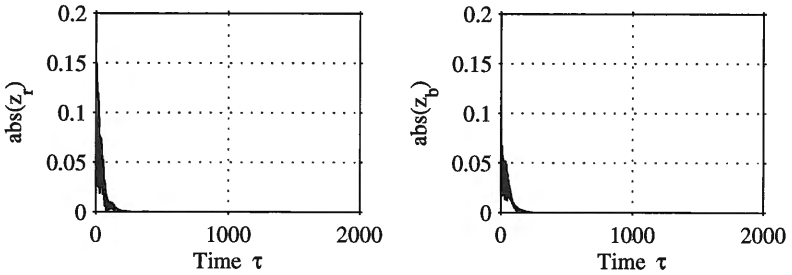
Numerical simulations were made for system parameters as listed in Table 6.5. Note that this is basically the same symmetric system as used in the previous studies. The system has undamped natural frequencies $\Omega_1 = 0.792$, $\Omega_2 = 2.524$ and the quenching frequency is the combination resonance frequency $\eta_{3-1/1}^{cr} = \Omega_3 - \Omega_1 = 1.732$. Six time histories show the result of the numerical simulation.

Time histories of the deflection $|z_r|$ at the disk station and $|z_b|$ at the bearing stations are presented in Figs. 6.14 and Figs. 6.15. Subplots on the left-hand side hold for the disk station and plots on the right-hand side for the bearing station. Note that the principal result is, of course, the same at all stations, but the amplitude levels are different. First we study each source of excitation individually, then we combine them to see how they interact.

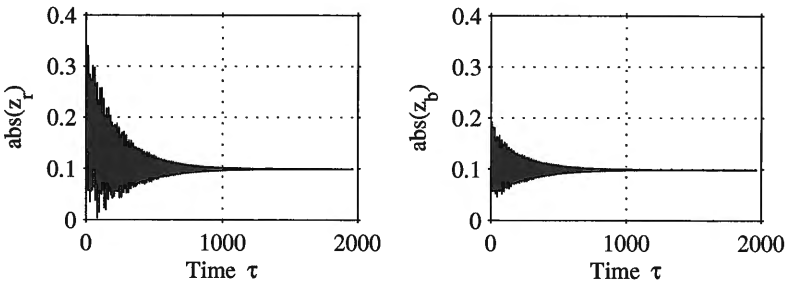
The first Fig. 6.14(a) shows the deflections for the unstable rotor due to internal damping exceeding the critical value. Starting from an initial disturbance the vibration amplitudes reach a limit value due to progressive damping δ after about 600 time units.



(a) Only self-excitation due to internal damping $\kappa_r = 0.05$, set (i)



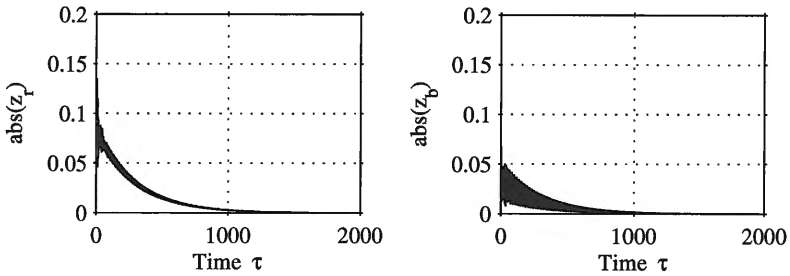
(b) Only parametric excitation $e_p^e = 0.2$, $\eta = 1.73$, set (ii)



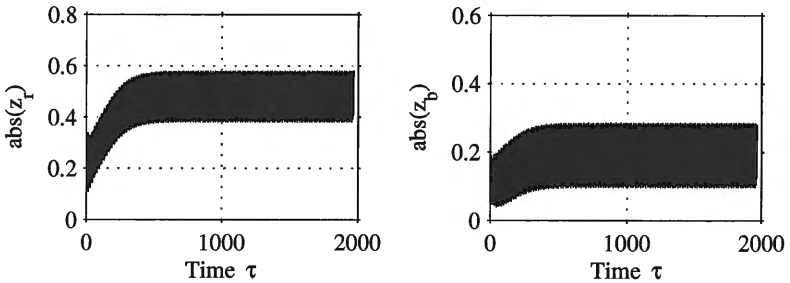
(c) Only unbalance excitation $u_e = 0.1$, set (iii)

Figure 6.14: Time histories of deflection $|z_r|$ at disk station (left) and $|z_b|$ at bearing station (right) for different excitation sources (see annotation of figures). Default system values see Table 6.5.

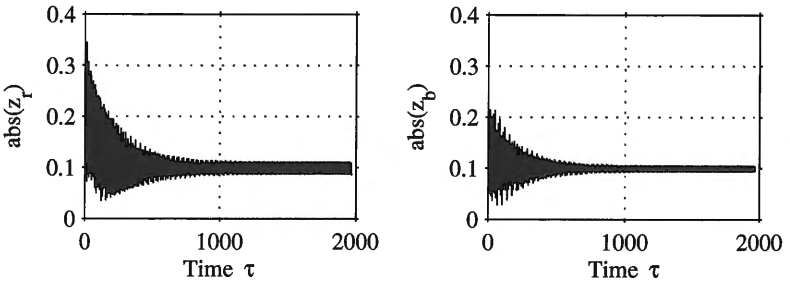
6.4. Study of a rotor with mass unbalance



(a) Self-excitation by internal damping $\kappa_r = 0.05$ and parametric excitation $e_b^c = 0.2$, $\eta = 1.73$, set (iv)



(b) Self-excitation by internal damping $\kappa_r = 0.05$ and unbalance excitation $u_e = 0.1$, set (v)



(c) Unbalance excitation $u_e = 0.1$, self-excitation by internal damping $\kappa_r = 0.05$ and parametric excitation $e_b^c = 0.2$, $\eta = 1.73$, set (vi)

Figure 6.15: Time histories of deflection $|z_r|$ at disk station (left) and $|z_b|$ at bearing station (right) for various combinations of different excitation sources (see annotation of figures). Default system values see Table 6.5.

Figure 6.14(b) shows a result for the rotor system when only parametric excitation is acting on the system. For a parametric excitation frequency which coincides with the anti-resonance frequency $\Omega_3 - \Omega_1$ the initial disturbance vanishes quickly and the system exhibits stable behavior. Of course, selecting $\eta = 3.316$ would result in an unstable system due to the parametric combination resonance $\eta_{1+3/1}^{cr}$.

Finally, Fig. 6.14(c) shows the well known behavior of a rotor system with unbalance excitation. Transient vibrations decay after about 1000 time units and the periodic unbalance response remains to be the only vibration of the system. In the rotating coordinate system of the rotor this synchronous vibration is represented by constant deflections for $|z_r|$ and $|z_b|$.

Figure 6.15(a) on the next page was calculated for the rotor system with self-excitation and vibration cancelling parametric excitation. It confirms the numerical results of the previous section and shows that for an ideally balanced rotor and for the frequency of the parametric excitation corresponding to parametric anti-resonance the self-excited vibration is fully suppressed.

In Fig. 6.15(b) self-excitation is combined with unbalance excitation, but parametric excitation is not active. Although the investigated system is nonlinear due to progressive damping, the result basically is a superposition of the self-excited vibrations in the first mode of the system and the synchronous unbalance response.

Finally all three excitation components are allowed to act simultaneously on the rotor. In this multi-excitation case the self-excited vibration component is suppressed, but not the component due to the unbalance, see and compare Figs. 6.15(c) and 6.14(c). This result is in perfect agreement with the analysis carried out in [93].

Having shown the transient time response of the system for various combinations of excitation types we will now present a few results from parameter studies where stationary maximum values are plotted. Parameter studies are presented in Figs. 6.16 to 6.19, showing maximum values $\max(|z_r|)$ of the rotor deflection as a function of η , see Fig. 6.16, and of the rotor speed ν for different values of the PE-amplitude e_b^c , the internal damping parameter κ_r and the unbalance parameter u_r .

Figure 6.16 investigates the rotor system when self-excitation and parametric excitation act on the system, but unbalance excitation is not present. The diagrams shows the deflection at the rotor station as a function of the PE-frequency η and the PE-amplitude e_b^c . Actually,

6.4. Study of a rotor with mass unbalance

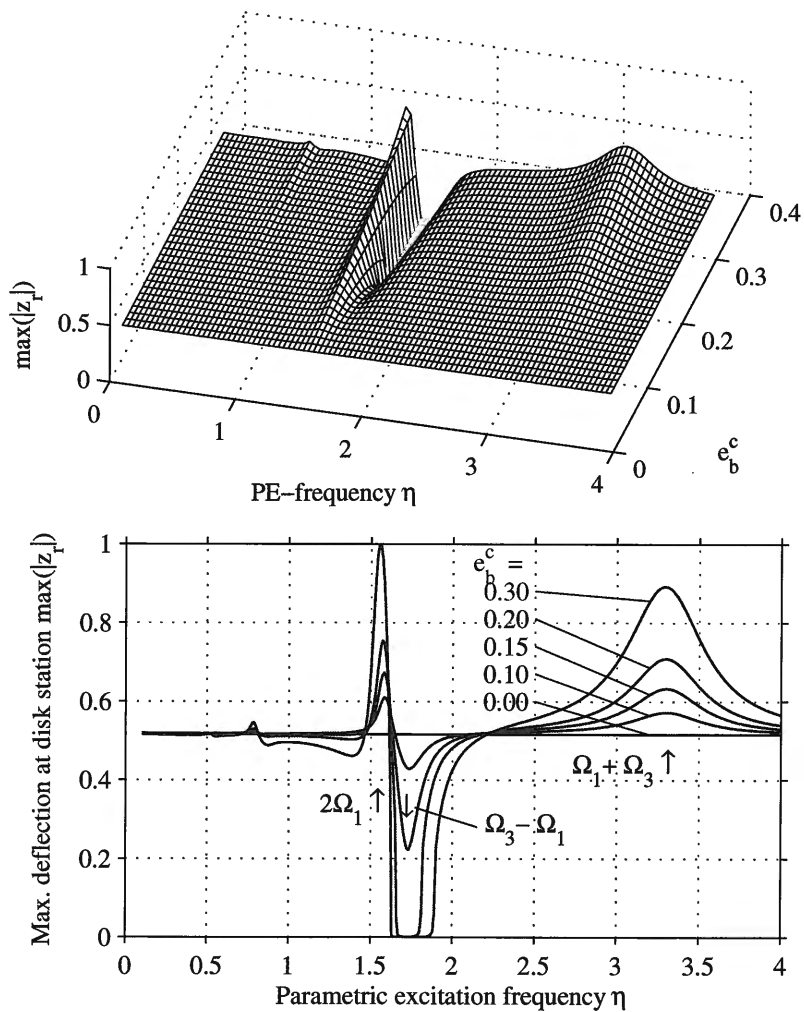


Figure 6.16: Rotor with parametric excitation $e_b^c \neq 0$, $\eta \neq 0$ and self-excitation by internal damping $\kappa_r = 0.05$ at rotational speed $\nu = 1.2$. No unbalance excitation. Default system values see Table 6.5.

this result is not new and a similar plot was already shown in Fig. 6.3 with a somewhat different scaling and parameter range. The figure was included here again just for consistency in the documentation and to make it easier to compare this result with results from the following studies.

Figure 6.17 shows again a study for the parametrically and self-excited rotor system without unbalance. This time the maximum rotor deflections are plotted as a function of the rotor speed ν and the PE-amplitude e_b^c for a fixed PE-frequency $\eta = \Omega_3 - \Omega_1$. One can see that with increasing parametric excitation amplitude e_b^c the onset of self-excited vibrations is shifted from a critical speed of $\nu_{crit} \approx 1$ to higher values of ν , even exceeding $\nu_{crit} \approx 2$ for $e_b^c = 0.3$. In the 2D-figure at the bottom the sharp increase of the maximum rotor deflections at the stability threshold is conspicuous. A closer inspection reveals a fold in the steep part of the surface that leads a jump phenomenon.

The last but one figure in this series of results is Fig 6.18. A parameter study for the rotor with self-excitation from internal damping and unbalance excitation is shown. Parametric excitation is not active in this example. The time history of Fig. 6.15(b) corresponds to this result. One can see that the rotor system behaves as a regular, externally excited system up to rotational speeds of $\nu \approx 1$. At $\nu = \Omega_1$ the first critical speed is passed and a resonance occurs due to the unbalance excitation. Above this speed, amplitudes decrease and in the case of no internal damping ($\kappa_r = 0$) they continue to become smaller until the second critical speed at $\nu = \Omega_3$ occurs. However, for a system with internal damping $\kappa_r > 0$ the rotor will become unstable before reaching the second critical speed. Depending on the level of internal damping the stability threshold moves down to a rotational speed of $\nu \approx 1$ for $\kappa_r = 0.05$. For rotational speeds exceeding the stability threshold the rotor system behaves very much like the self-excited system without unbalance excitation as shown in Fig. 6.17. Nevertheless, the third mode Ω_3 still influences the maximum amplitudes and creates interesting results, as e.g. a local anti-resonance phenomenon for small values of $\kappa_r \approx 0.01$.

Finally, in Fig. 6.19 a result with all three kinds of excitation mechanisms acting simultaneously is presented. The parameter variation is carried for the rotational speed ν of the rotor and the unbalance parameter u_r . The dominating feature of both diagrams is the resonance at Ω_1 which grows with increasing unbalance parameter u_r . This behavior had to be expected, because the rotor system operates at $\nu = \Omega_1$

6.4. Study of a rotor with mass unbalance

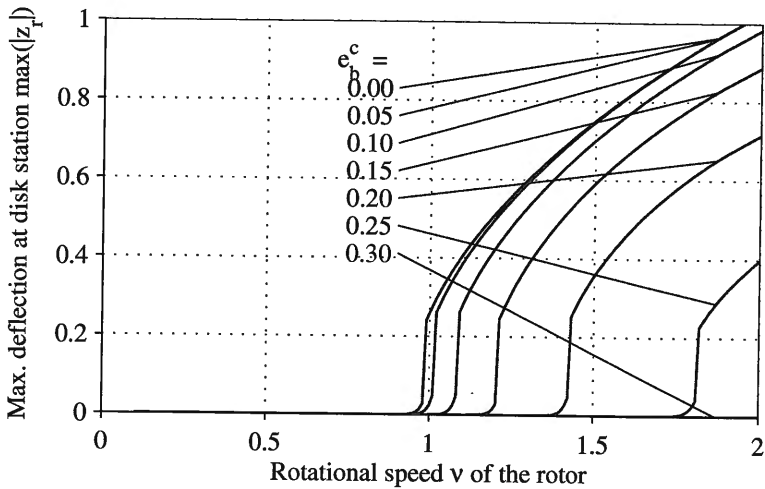
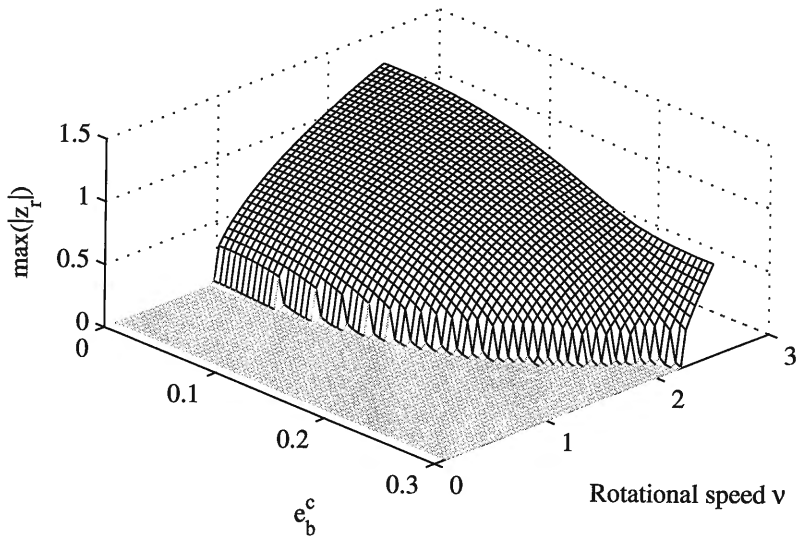


Figure 6.17: Rotor with parametric excitation $e_b^c \neq 0$, $\eta = 1.73$ and self-excitation by internal damping $\kappa_r = 0.05$. No unbalance excitation. Default system values see Table 6.5.

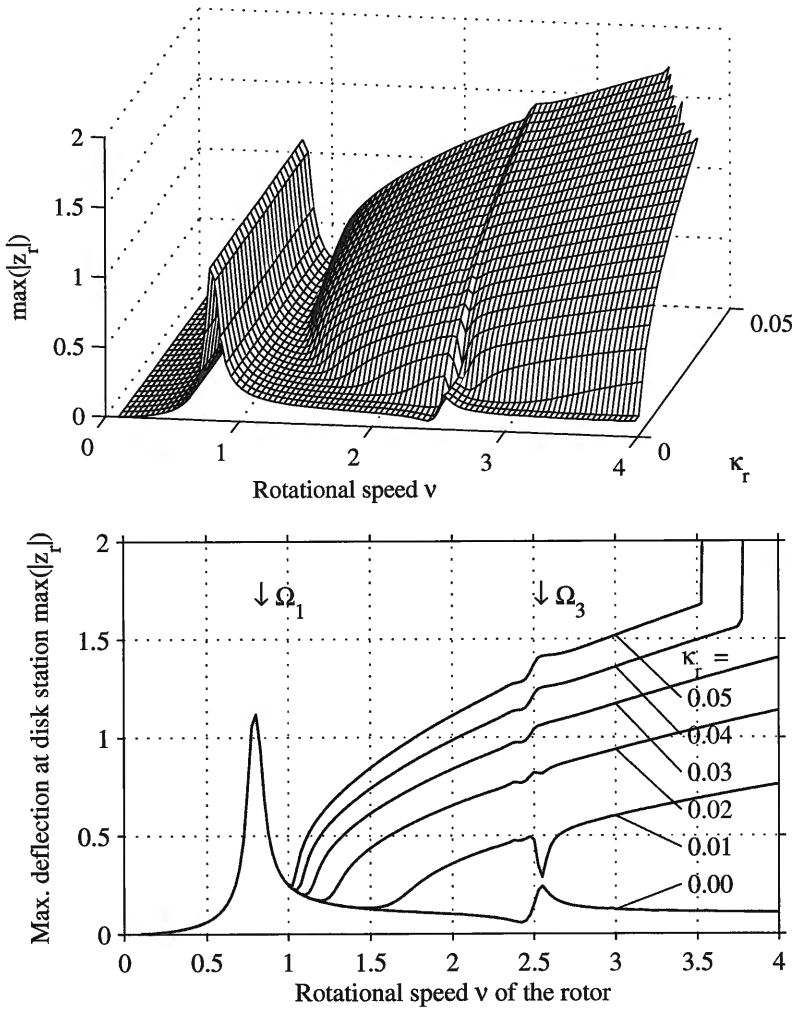


Figure 6.18: Rotor with unbalance $u_r = 0.1$ and self-excitation by internal damping $\kappa_r \neq 0$. No parametric excitation. Default system values see Table 6.5.

6.4. Study of a rotor with mass unbalance

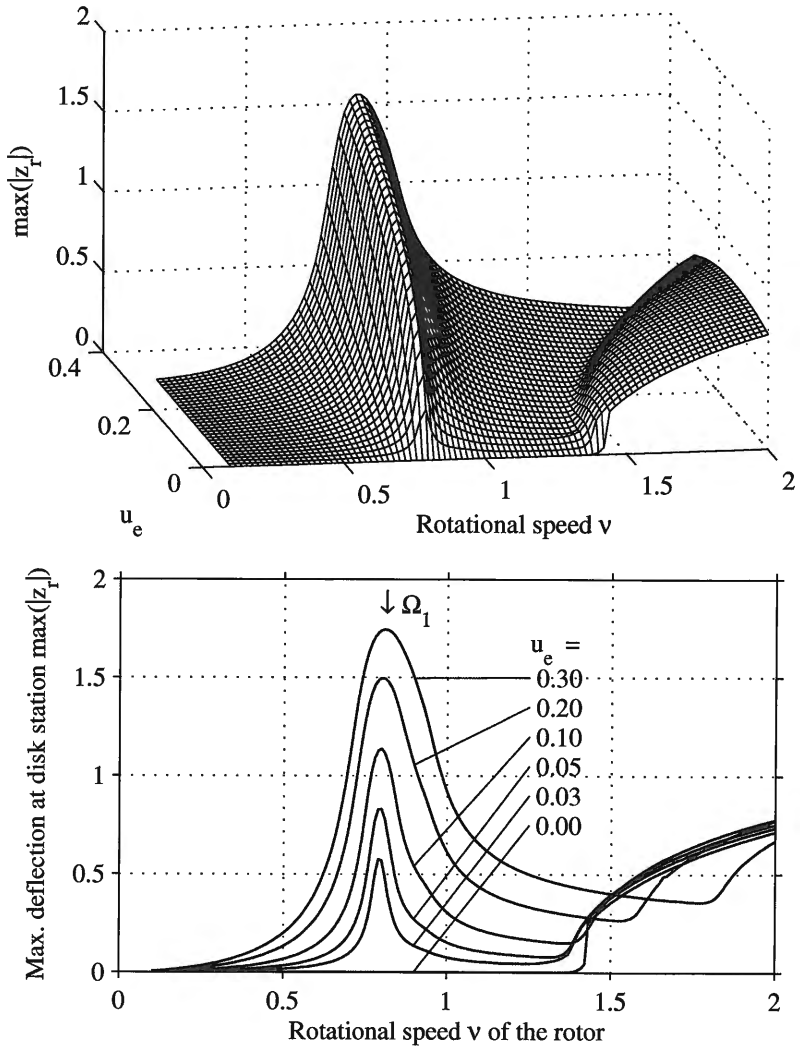


Figure 6.19: Rotor with unbalance $u_r \neq 0$, parametric excitation $e_b^c = 0.2$, $\eta = 1.73$ and self-excitation by internal damping $\kappa_r = 0.05$. Default system values see Table 6.5.

below the stability threshold. Parametric excitation does not have an influence on the synchronous vibrations, neither positive nor negative, in this frequency range.

The most interesting feature is the shift of the stability threshold from $\nu_{crit} \approx 1$ without parametric excitation to $\nu_{crit} > 1.4$ for PE-parameters $e_b^c = 0.2$ and $\eta = 1.73$ as used here. This shift clearly shows that parametric excitation is highly effective and increases the stability threshold by at least 40% despite the presence of unbalance excitation. Moreover, the stabilization phenomenon is even positively affected by an increasing unbalance parameter. One recognizes that the stability threshold moves upwards to higher values of ν and reaches a value of $\nu_{crit} \approx 1.8$ at the maximum level of the unbalance parameter $u_r = 0.3$. This interesting consequence of the interaction between unbalance and self-excitation in the presence of a parametric excitation is a newly discovered phenomenon and is worth to be investigated more thoroughly in future studies.

6.5 Concluding remarks

A novel concept to cancel self-excited vibrations in rotor systems was presented in this chapter. Via open-loop control of the bearing stiffness a parametric excitation is introduced to the system. The idea is investigated by a numerical study of a symmetric Laval/Jeffcott-rotor.

The mechanical model employed in this chapter has six degrees of freedom and is therefore a significantly more complex model as previous ones. The investigation carried out for this model shows that the phenomenon of vibration cancelling by parametric excitation is not limited to 2-dof systems as used in the previous chapters. The order of this rotor model can be reduced by taking advantage of symmetry properties, but in the numerical study the full 6-dof system was used. Moreover, T. Pumphössel has carried out first studies [66] on an 8-dof rotor system and obtained similar results for the symmetric case. In the case of an asymmetric rotor with symmetric parametric excitation the effect of vibration cancelling was still obtained up to a certain limit of the asymmetry parameter. Further studies for an asymmetric rotor with a more general scheme of the parametric excitation are needed and will explore the potential for vibration suppression available by this method.

Another difference between the investigation presented in this chap-

6.5. Concluding remarks

ter and in the previous chapters concerns the self-excitation mechanism. In the examples of Chapters 3 to 5 different manifestations of negative damping as the fundamental source of self-excitation were investigated. The self-excitation mechanisms acting on the rotor system are internal damping of the shaft and external gap excitation/damping. Both these types of damping generate non-conservative forces which increase with increasing rotor speed and ultimately destabilize the system. This mechanism and the kind of forces generated thereby are of different nature compared with self-excitation due to negative damping. Therefore this chapter shows that parametric vibration suppression is applicable to various mechanisms of self-excitation.

Finally, in the last section an external (forced) excitation of the rotor system is also considered. As predicted by an analytical study, the stabilizing effect is not negatively affected by the external excitation. This result is also very remarkable, because some kind of external excitation will be present in almost any real-world system, structure or machine. Research will have to be continued on the interaction of all three kinds of excitation and further extended to the excitation of the bearing support, which is another common source of external excitation of a rotor system.

Chapter 7

Synopsis and outlook

Self-excited vibrations represent an unwanted, sometimes even dangerous phenomenon for many machines, structures and devices. Great efforts have therefore been made to investigate such vibrations and to study methods of suppression. Depending on the situation, different strategies and methods of vibration reduction are in use. This monograph is focused on the cancellation, or at least the reduction, of self-induced vibrations in mechanical systems by means of parametric stiffness excitation.

The first chapter provides an introduction to self-excitation in mechanical systems, explains different mechanisms which lead to self-sustained vibrations and gives some examples. A section follows which reviews the research on parametric excitation. Basic effects of parametric excitation are discussed, as e.g. the different types of parametric resonances and the stabilizing effect which can be achieved by parametric excitation. Parametric vibration cancelling is introduced as a method to fight self-excited vibrations. Finally some basic design examples are presented to show how parametric stiffness excitation can be realized in an actual mechanical system.

Chapter 2 is focused on the analysis of parametrically excited systems which are described by differential equations with periodic coefficients. The chapter consists of two parts. Part one gives an overview on analytical methods for the investigation of such systems. The Method of Successive Approximation, the Method of Averaging and the Tondl-Floquet-method are discussed in detail, compared and applied to a generic set of

two differential equations. These equations describe a two-mass system with parametric excitation as investigated extensively in the following chapters. The second part of Chapter 2 deals with numerical methods and outlines the methods used for numerical studies.

The third chapter is devoted to the demonstration and explanation of some basic results obtained from a system with simultaneous self-excitation and parametric excitation. Since the effect of stabilization of a self-excited system by parametric excitation can only occur in systems with at least two degrees of freedom, a generic 2-dof system is introduced. First numerical studies are carried out by numerical simulation and it is shown that parametric excitation can stabilize the stationary (trivial) solution of a system. Then the numerical Floquet-method is applied to investigate the stability of the system and the results are compared with results obtained from analytical methods.

In the following Chapter 4 the effect of parametric excitation with respect to the stabilization of an unstable system is compared with the amount of positive damping necessary to bring about the same result. Based on this consideration, the effect of parametric excitation is expressed in terms of *equivalent damping*. A parameter study is carried out for a two-mass system with parametric excitation and the gain of stability is shown as a function of the parameters of the conventional damping elements in the system.

In Chapter 5 the concept of a *parametric absorber* is introduced which incorporates a periodically time-varying stiffness parameter. This new kind of absorber has little in common with a tuned-mass absorber as used to suppress forced vibrations. Only the basic idea of attaching an additional single-dof subsystem to a main system or structure is adopted and justifies the naming. Two different kinds of self-excitation mechanisms are considered. In the first part self-sustained vibrations of the main mass are caused by a constant flow of a medium which generates motion-induced vibrations. In the second part the dependence of the dry friction coefficient upon velocity is the reason for self-induced vibrations. In both cases the self-excitation mechanism can be interpreted as a negative damping component present in the system. Numerous parameter studies for both systems show in which parameter range the absorber achieves good or less favorable results. Frequency and amplitude of the parametric excitation are key parameters for the performance of the absorber. However, the mass ratio of main mass to absorber mass, and equally the stiffness ratio, put limits to the size of the absorber if a

certain performance level has to be reached.

In the last Chapter a more complex mechanical model of a 6-dof rotor system is investigated. The investigations carried out for this model show that the phenomenon of vibration cancelling by parametric excitation is not limited to simple 2-dof systems as used in the previous chapters. There is also a different self-excitation mechanism acting on the rotor system compared to those employed in the previous chapters. In the examples of Chapters 3 to 5 different manifestations of negative damping are the source of self-excitation. The rotor system experiences self-excitation from internal damping of the shaft and from destabilizing gap forces. Both types generate non-conservative forces which increase with increasing rotor speed and ultimately destabilize the system. The results of this chapter clearly demonstrate that parametric vibration suppression is applicable to various mechanisms of self-excitation. In a final study also unbalance excitation of the rotor is taken into account. As the numerical simulation results show, the stabilizing effect is not affected by an external periodic excitation.

In the investigation of vibration suppression by parametric excitation a point has now been reached where the fundamental concept and the basic idea are well understood and analytical methods and numerical tools suitable for the problem are available. These first studies prove that the effect of parametric vibration suppression is of a magnitude which promises to be of relevance for practical applications.

Further research on parametric vibration cancelling is still needed to reach a level of knowledge so that actual applications can be seriously considered. Multi-degree of freedom systems have to be investigated, because real-world systems may need more than two or three vibrational modes to be taken into account. Some steps in this direction have been made already in [91] and [92], where a three-mass system was investigated. Also [25] and [1] are references dealing with systems of similar order. Investigations for systems with a higher level of complexity will have to show if and how parametric excitation may initiate additional parametric resonances that might interfere with the parametric anti-resonance.

Of course, realization of a time-varying stiffness is the key to any practical application of the method. In the first chapter a few simple design examples are given with two of them exhibiting a discontinuous variation of the time-dependent stiffness parameter. Such an open-loop "bang-bang" control might be even easier to realize than a smooth har-

monic variation of the stiffness parameter. Two studies have been carried out already that investigate the effect of a discontinuous parametric excitation, see [47] and [48]. It turns out that the shape of the periodic function is almost irrelevant for the anti-resonance effect. Only frequency and amplitude of the first harmonic of the periodic stiffness function determine the level of vibration suppression to be achieved. This is a quite remarkable result, since it opens the door to a lot more possibilities for an actual design. Also, in [48] a study is included which applies a general type of a mechanical dissipative actuator to realize the periodic parameter change and which excels the vibration suppression performance of a simple harmonic stiffness variation.

In this monograph analytical and numerical methods have been applied to investigate the effect of parametric vibration cancelling, but no experimental work has been reported. The final proof for this method and the validation of the simulation results will require to demonstrate the effect in an experiment with some kind of (electro-)mechanical realization of the models investigated.

Thanks to funding received from the Austrian Science Foundation (FWF)¹, this next step is planned for the near future and will certainly provide interesting results. However, A. Tondl's first results were obtained from an analog computer which, in fact, was already a first physical experiment with an electrical system.

¹FWF - Fonds zur Förderung der Wissenschaften, Project P-16248, started on April 1, 2003

Bibliography

- [1] Abadi: *Nonlinear Dynamics of Self-excitation in Autoparametric Systems*. Ph.D. Dissertation, Utrecht University, 2003.
- [2] Awrejcewicz J.: *Analysis of Self-Excited Vibration Due to Dry Friction in a System with Two Degrees of Freedom*. Sci. Bull. Lodz Technical University, 635, 82, 1993.
- [3] Benjamin T.B., Ursell F.: *The stability of the plane free surface of a liquid in vertical periodic motion*. Proc. R. Soc. London, Ser. A 225, pp. 505-515, 1954.
- [4] Blazejczyk-Okolewska B., Czolczynski K., Kapitaniak T., Wojewoda J.: *Chaotic Mechanics in Systems with Impacts and Friction* World Scientific Series on Nonlinear Science, Series A, Vol. 36, Singapore, 1999.
- [5] Blevins R.D.: *Flow-induced vibration*. New York: Van Nostrand Reinhold 1977.
- [6] Bolotin V.V.: *Kinetische Stabilität elastischer Systeme*. Berlin, 1961.
- [7] Bolotin V.V.: *The Dynamic Stability of Elastic Systems*. Berlin, 1964.
- [8] Breiteneker F., Ecker H., Bausch-Gall I.: *Simulation mit ACSL*. Fortschritte in der Simulationstechnik Band 2, Braunschweig, Vieweg 1993.
- [9] Butcher E.A., Sinha S.C.: *Symbolic bifurcation boundaries and time-dependent resonance sets of time-periodic nonlinear systems*.

- In: Proc. of 1999 ASME Design Eng. Tech. Conf., DETC99/VIB-8315, Sept. 12-15, 1999, Las Vegas, Nevada.
- [10] Cartmell M.: *Introduction to Linear, Parametric and Nonlinear Vibrations*. London, Chapman and Hall 1990.
- [11] Case W.: *The pumping of a swing from the seated position*. Am. J. Phys. 58, pp. 463-467, 1990.
- [12] Case W.: *The pumping of a swing from the standing position*. Am. J. Phys. 64, pp. 215-220, 1996.
- [13] Childs D.: *Turbomachinery Rotordynamics* Wiley Interscience, New York, 1993.
- [14] Dohnal F.: *Application of the Averaging Method on parametrically excited 2dof-systems*. Project Report PES-#1, Inst. for Machine Dynamics and Measurement, Vienna Univ. of Technology, 2003.
- [15] Dhooge A., Govaerts W., Kuznetsov Y.A., Mestrom W., Riet A.M.: *CL_MATCONT: A continuation toolbox in MATLAB*, Utrecht University, 2003.
- [16] Doedel E. J., Champneys A. R., Fairgrieve T. F., Kuznetsov Y. A., Sandstede B., Wang, X.-J.: *AUTO97: Continuation and bifurcation software for ordinary differential equations*. Dep. of Computer Science, Concordia University, Montreal, Canada, 1997.
- [17] Ecker H., Tondl A.: *Investigation of Parameter- and Self-excited Systems - Some computational aspects*. In: Proc. of Colloquium Dynamics of Machines 2000, (Dobias, E., ed.), Prague, Czech Republic, Feb. 8-9, 2000.
- [18] Ecker H., Tondl A.: *Suppression of flow-induced vibrations by a dynamic absorber with parametric excitation*. In: Proc. of 7th Int. Conf. on Flow-Induced Vibrations - FIV2000, (Brauchli, ed.), Lucerne, Switzerland, June 19-21, 2000.
- [19] Ecker H., Tondl A.: *Ein Beitrag zur Unterdrückung selbsterregter Schwingungen in einem Rotorsystem*. Tagungsbeitrag zur fünften internationalen Tagung Schwingungen in rotierenden Maschinen (SIRM), 26.-28. Februar 2001, Wien, Österreich.

Bibliography

- [20] Ecker H., Pumphössel T., Tondl A.: *A Study on Parametric Excitation for Suppressing Self-excited Rotor Vibrations*. Proc. of 6th Int. Conf. on Rotor Dynamics (IFToMM), Sept.30–Oct.3, 2002, Sydney, Australia.
- [21] Ecker H.: *A parametric absorber for friction-induced vibrations*. In: Proc. ASME Design Eng. Techn. Conf. DETC2003, (Shabana A.A., ed.), Paper VIB-48474, Chicago, IL, Sept. 2-6, 2003.
- [22] Ecker H., Tondl A.: *Stabilization of a rigid rotor by a time-varying stiffness of the bearing mount*. The Eighth Int. Conf. on Vibrations in Rotating Machinery, held by IMechE, 7. - 9.Sept. 2004, Swansea, UK (paper submitted).
- [23] Eicher N.: *Einführung in die Berechnung parametererregter Schwingungen*. TUB-Dokumentation Weiterbildung, Heft 1, Berlin, 1981.
- [24] Elmer F.J.: *The Pendulum Lab*. Web-page, 2003, <http://monet.physik.unibas.ch/~elmer/pendulum/parres.htm>.
- [25] Fatimah S.: *Bifurcations in dynamical systems with parametric excitation*. Dissertation, Utrecht University, 2002.
- [26] Gasch R., Nordmann R., Pfützner H.: *Rotordynamik*. 2nd ed., Springer Verlag, Berlin, 2002.
- [27] Guran A., Pfeiffer F., Popp K. (eds.): *Dynamics with Friction - Modeling, Analysis and Experiments*. Series on Stability, Vibration and control of Systems, Series B, Vol.7, World Scientific, Singapore, 1996.
- [28] Guran A., Tzou H.S., Anderson G., Natori M. (eds.): *Structronic Systems: Smart Structures, devices and systems. Part I: Materials and Structures*. Series B, Vol.4, World Scientific, Singapore, 1998.
- [29] Guttalu R.S., Flashner H.: *Stability analysis of periodic systems by truncated point mappings*. J. Sound and Vibration 189(1), pp.33-54, 1996.
- [30] Hagedorn P.: *Kombinationsresonanz und Instabilitätsbereiche zweiter Art bei parametererregten Systemen mit nichtlinearer Dämpfung*. Ingenieur-Archiv, Vol. 38, pp. 80-96, 1969.

- [31] Hagedorn P.: *Non-Linear Oscillations*. 2nd ed., Oxford University Press, Clarendon Press, Oxford 1988.
- [32] Hagedorn P., Kraus M.: *Aeolian Vibrations: Wind Energy Input Evaluated from Measurements on an Energized Transmission Line*. In: Proc. of IEEE Summer Power Meeting, IEEE Paper 90 SM 346-7 PWRD, Minneapolis, July 1990.
- [33] Harris C.M.: *Shock and Vibration Handbook*. 4th ed., New York: McGraw-Hill 1996.
- [34] Hémon P., Santi F.: *On the aeroelastic behaviour of rectangular cylinders in cross-flow*. J. Fluids and Structure 16(7), pp.855-889, 2002.
- [35] Hirschmanner M., Steinschaden N., Springer H.: *Adaptive Control of a Rotor Excited by Destabilizing Cross-Coupling Forces*. Proc. of 6th Int. Conf. on Rotor Dynamics (IFToMM), Sept.30–Oct.3, 2002, Sydney, Australia.
- [36] Hirschmanner M.: *Control of Unbalance and Self-Exciting Forces by Active Magnetic Bearings*. Ph.D-Thesis, Vienna University of Technology, Sept. 2003.
- [37] Hsu C.S.: *On the parametric excitation of a dynamic system having multiple degrees of freedom*. J. Appl. Mechanics, Vol.30, Trans. ASME, Vol.85, 1963, pp.367-372.
- [38] Hsu C.S.: *Further results on parametric excitation of a dynamic system*. J. Appl. Mechanics, Vol.32, Trans. ASME, Vol.87, pp.373-377, 1965.
- [39] Hsu C.S., Cheng W.-H.: *Steady-state response of a dynamical system under combined parametric and forcing excitations*. J. Appl. Mechanics, Vol.41, Trans. ASME, Vol.96, pp.371-378, 1974.
- [40] Ibrahim R.A.(ed.): *Friction-induced vibration, chatter, squeal, and chaos*. Proc. of Winter Annual Meeting of ASME, DE-Vol.49, New York:ASME. Anaheim/CA, Nov.8-13, 1992.
- [41] Kauderer H.: *Nichtlineare Mechanik*. Springer, Berlin, 1958.

Bibliography

- [42] Kidachi H., Onogi H.: *Note on the stability of the nonlinear Mathieu equation*. Prog. Theor. Phys. Vol. 98, No. 4, 1997.
- [43] Kuznetsov Y., Levintin V.: *CONTENT: Integrated environment for the analysis of dynamical systems*. Centrum voor Wiskunde en Informatica, Amsterdam, The Netherlands, 1997.
ftp://ftp.cwi.nl/pub/CONTENT.
- [44] Lust K.: *Improved Numerical Floquet Multipliers*. International Journal of Bifurcation and Chaos, 11(9):2389-2410, 2001.
- [45] Magnus W., Winkler S.: *Hill's Equation*. J. Wiley, New York, 1966.
- [46] Magnus K., Popp K.: *Schwingungen*. G.B.Teubner, Stuttgart, 1997.
- [47] Makihara, K., Ecker, H.: *Comparison Of Open-Loop Stiffness Control Methods To Suppress Self-Excitation*. In: Proc. 1st Int. Industrial Simulation Conf. (Guerri, J.C, Pajares, A., Palau, C., eds.), pp.180-187, Valencia, Spain, June 9-11, 2003.
- [48] Makihara, K., Ecker, H., Dohnal, F.: *Stability Analysis of Open-loop Stiffness Control to Suppress Self-excited Vibrations*. J. of Vibration and Control, accepted 2003.
- [49] Matthias, A.: *Tilgung selbsterregter Schwingungen durch Parametererregungen*. Diplomarbeit, TU-Wien, April 2000.
- [50] McDonald R., Sri Namachchivaya N.: *Parametric Stabilization of a Gyroscopic System*. J. Sound and Vibration 255(4), pp. 635-662, 2002.
- [51] Mettler E.: *Eine Theorie der Stabilität der elastischen Bewegung*. Ing.-Arch. 16, pp. 135-146, 1947.
- [52] Mettler E.: *Allgemeine Theorie der Stabilität erzwungener Schwingungen elastischer Körper*. Ing.-Arch. 17, pp. 418-449, 1949.
- [53] Meyer F.: *Stability analysis of large parametrically excited linear vibration systems*. Dissertation, ETH Zurich, Switzerland, 1984.
- [54] Montagnier P., Spiteri R.J. and Angeles J.: *Numerical Integration of Linear, Time-Periodic Systems via Chebyshev Polynomials*. Report TR-CIM-98-02, Centre for Intell. Machines, McGill Univ., Montreal, Quebec, Canada, 1998.

- [55] N.N.: *ACSL-Advanced Continuous Simulation Language - Reference Manual, Ed. 11.8*. Copyright © 1999 by AEgis Technologies Group, Huntsville, AL, USA.
- [56] N.N.: *MATLAB 6.0*. Copyright © The MathWorks, Natick, USA, 2001.
- [57] N.N.: *MAPLE 7.00*. Copyright © Waterloo Maple Inc., 2001
- [58] Nayfeh A.H.: *Perturbation Methods*. J.Wiley, New York, 1973.
- [59] Nayfeh A.H., Mook D.T.: *Nonlinear Oscillations*. J.Wiley, New York, 1979.
- [60] Nguyen P.H.: *An exploration of parametric excitation as a tool for vibration control*. PhD-Thesis, Georgia Institute of Technology, June 2000.
- [61] Okubo H.; Takano K.; Matsushita O.; Watanabe K.; Hirase Y.: *Vibration and Control of Axially Moving Belt System: Analysis and Experiment by Parametric Excitation*. J. of Vibration and Control, vol. 6, no. 4, pp. 589-605, 2000.
- [62] Olvera A., Prado E., Czitrom S.P.R.: *Performance improvement of OWC systems by parametric resonance*. In: Proc. of "Wave Energy for the New Millennium", Fourth European Wave Energy Conference, Aalborg, 2000.
- [63] Pandiyan, R., Sinha, S.C.: *Analysis of Time-Periodic Nonlinear Dynamical undergoing Bifurcations*. Nonlinear Dynamics 8, pp. 21-43, 1995.
- [64] Pismen L.M., Rubinstein B.Y.: *Computer Tools for Bifurcation Analysis: General Approach with Applications to Dynamical and Distributed Systems*. Int. J. Bif. Chaos, 9, 983, 1999.
- [65] Popp, K., Hinrichs, N., and Oestreich, M.: *Analysis of a self excited friction oscillator with external excitation*. In: Dynamics with Friction - Modeling, Analysis and Experiment, (Guran, A., Pfeiffer, F., and Popp, K., eds.), Series B, Vol. 7 of *Series on Stability, Vibration and Control of Systems*, World Scientific, Singapore 1996.

Bibliography

- [66] Pumphössel T.: *Untersuchung der Wirkung von Selbst- und Parametererregungen an einem Laval-Rotor*. Diplomarbeit, TU-Wien, Februar 2002.
- [67] Rand, R.H.: *Lecture Notes on Nonlinear Vibrations*. Cornell Univ., 2000. <http://www.tam.cornell.edu/randdocs/>
- [68] Rand, R.H.: *2:2:1 Resonance in the Quasiperiodic Mathieu Equation*. In: Proc. ASME Design Eng. Techn. Conf. DETC2003, (Shabana A.A., ed.), Paper VIB-48563, Chicago, IL, Sept. 2-6, 2003.
- [69] Richards J.A.: *Analysis of Periodically Time-Varying Systems*. Berlin, Springer 1983.
- [70] Sanders J.A, Verhulst F.: *Averaging methods in nonlinear dynamical systems*. Appl. Math. Sciences 59, 1985.
- [71] Schmidt G.: *Parametererregte Schwingungen*. VEB Dt. Verlag der Wissenschaften, Berlin, 1975.
- [72] Schmidt G., Tondl A.: *Non-Linear Vibrations*. Cambridge University Press, Cambridge, 1986.
- [73] Seydel R.: *Practical Bifurcation and Stability Analysis. From Equilibrium to Chaos*. Second Edition. Springer Interdisciplinary Applied Mathematics, Volume 5. Springer, New York, 1994.
- [74] Seydel R.: BIFPACK - *a program package for continuation, bifurcation and stability analysis*. Ulm, 1996.
(Available at <http://www.bifurcation.de/software.html>).
- [75] Seyranian A.P., Solem F., Pedersen P.: *Stability analysis for multi-parameter linear periodic systems*. Arch Applied Mechanics, Vol. 69, No. 3, pp. 160-180, 1999.
- [76] Sinha S.C., Pandiyan R.: *Analysis of Quasilinear Dynamical Systems with Periodic Coefficients via Liapunov- Floquet Transformation*. Int. J. Non-Linear Mechanics Vol. 29, pp. 687-702, 1994,
- [77] Sinha S.C., Pandiyan R., Bibb J.S.: *Liapunov-Floquet Transformation: Computation and Application to Periodic Systems*. J. Vibration and Acoustics, Vol. 118, pp. 209-219, 1996.

- [78] Stelter P.: *Nichtlineare Schwingungen reibungserregter Strukturen*. Dissertation, Fortschrittsberichte Reihe 11, Nr. 137, VDI-Verlag Düsseldorf, 1990.
- [79] Stoker J.J.: *Nonlinear Vibrations in Mechanical and Electrical Systems*. Wiley, New York, 1950.
- [80] Sun J.Q., Jolly M.R., Norris M.A.: *Passive, adaptive and active tuned vibration absorbers-A survey*. Trans. ASME, Vol. 117, pp.234-242, 1995.
- [81] Tondl A.: *Method for determination of quasiharmonic vibrations*(in Czech language). Aplikace Matematiky, 4, pp. 278-289, 1959.
- [82] Tondl A.: *Some Problems Of Rotor Dynamics*. Chapman and Hall, London, 1965.
- [83] Tondl A.: *On the interaction between self-excited and forced vibrations*. Monographs and Memoranda, No. 20, National Research Institute for Machine Design, Prague, 1976.
- [84] Tondl A.: *On the interaction between self-excited and parametric vibrations*. Monographs and Memoranda, No. 25, National Research Institute for Machine Design, Prague, 1978.
- [85] Tondl A., Fiala V.: *A contribution to the analysis of parametric combination resonances of a nonlinear system* (in Czech language). Strojnícky časopis, 39(3), pp. 283-293, 1988.
- [86] Tondl A.: *Quenching of Self-Excited Vibrations*. Academia, Prague and Elsevier Science Publ., Amsterdam, 1991.
- [87] Tondl A.: *To the problem of quenching self-excited vibrations*. Acta Technica CSAV 43, pp. 109-116, 1998.
- [88] Tondl A., Ecker H.: *Cancelling Of Self-Excited Vibrations By Means Of Parametric Excitation*. Proceeding of the 1999 ASME Design Engineering Technical Conferences (DETC), Sept. 12-15, 1999, Las Vegas, Nevada, USA.
- [89] Tondl A.: *Self-Excited Vibration Quenching In A Rotor System By Means Of Parametric Excitation*. Acta Techn. CSAV 45, pp. 199-211, Institute of Electrical Engineering, Acad. Sci. Czech Republic, 2000.

Bibliography

- [90] Tondl A.: *Two parametrically excited chain systems*. Acta Techn. CSAV 47, pp. 67-74, Institute of Electrical Engineering, Acad. Sci. Czech Republic, 2002.
- [91] Tondl A.: *Three-mass self-excited system with parametric excitation*. Acta Techn. CSAV 47, pp. 165-176, Institute of Electrical Engineering, Acad. Sci. Czech Republic, 2002.
- [92] Tondl A., Ecker H.: *On the problem of self-excited vibration quenching by means of parametric excitation*. Archive of Applied Mechanics 72, pp. 923-932, 2003.
- [93] Tondl A., Ecker H.: *Self-excited vibration quenching using parametric excitation: The effect of an additional external excitation*. In: Proc. of 6th Int. Conf. on Vibration Problems, ICOVP-2003, Liberec, Czech Republic, Sept. 2003.
- [94] Troger H., Steindl A.: *Nonlinear Stability and Bifurcation Theory*. Springer-Verlag, 1991.
- [95] Tzou H.S., Guran A., Gabbert U., Tani J., Breitbach E. (eds.): *Structronic Systems: Smart Structures, devices and systems. Part II: Systems and Control*. Series B, Vol.4, World Scientific, Singapore, 1998.
- [96] Verhulst, F.: *Nonlinear Differential Equations and Dynamical Systems*. Springer-Verlag, 2000.
- [97] Wolfram, S.: *The Mathematica book*, 3rd ed., Wolfram Media, Cambridge Univ. Press, 1996.
- [98] Xu J., Gasch R.: *Modale Behandlung linearer periodisch zeitvarianter Bewegungsgleichungen*. Arch. Appl. Mechanics 65, pp. 178-193, 1995.
- [99] Yakubovich V.A., Starzhinskii V.M.: *Linear Differential Equations with Periodic Coefficients*. J. Wiley & Sons, New York, 1975.
- [100] Yamamoto T., Saito A.: *On the vibrations of "summed and differential types" under parametric excitation*. Memoirs of the Faculty of Engineering, Nagoya Univ., Japan, Vol. 22, No. 1, pp. 54-123, 1970.

- [101] Yamamoto T., Ishida Y.: *Linear and nonlinear rotordynamics*. New York: John Wiley 2001.
- [102] Zhou J., Hagiwara T.: *Stability Analysis of Continuous-Time Periodic Systems via the Harmonic Analysis*. 2001 American Control Conference, Arlington, Virginia, pp. 535–540, 2001.
- [103] Zwillinger D.: *Handbook of Differential Equations*. Academic Press Inc., Boston, MA, 1998.

Authors Index

- Abadi, 21, 53
Anderson, G., 162
Angeles, J., 30
- Bausch-Gall, I., 56, 116
Benjamin, T.B., 14
Bibb, J.S., 29, 30
Blazejczyk-Okolewska, B., 142
Blevins, R.D., 5, 8, 126
Bolotin, V.V., 15
Breitbach, E., 162
Breitenecker, F., 56, 116
Butcher, E.A., 30
- Cartmell, M., 15, 18, 29, 51
Case, W., 14
Champneys, A.R., 59
Cheng, W.-H., 30
Childs, D., 13, 161
Czitrom, S.P.R., 18
Czolczynsk, K., 142
- Dhooge, A., 59
Doedel, E.J., 59
Dohnal, F., v, 41, 43, 51, 97
- Ecker, H., 21, 45, 50, 53, 55,
56, 69, 116, 120, 125,
127, 140, 142, 162,
172, 194, 198
Eicher, N., 33, 34, 37
- Elmer, F.J., 19
- Fairgrieve, T.F., 59
Fatimah, S., 21, 52, 53, 59,
140
Fiala, V., 22
Flashner, H., 30
- Gabbert, U., 162
Gasch, R., 13, 29, 161, 194
Govaerts, W., 59
Guran, A., 8, 142, 162
Guttalu, R.S., 30
- Hémon, P., 126
Hagedorn, P., 5, 8, 18
Hagiwara, T., 30
Harris, C.M., 11
Hinrichs, N., 142, 144
Hirase, Y., 20, 21
Hirschmanner, M., 162
Hsu, C.S., 30
- Ibrahim, R.A., 8, 142
Ishida, Y., 11, 13, 50, 161,
194
- Jolly, M.R., 2, 119
- Kapitaniak, T., 142
Kauderer, H., 15

- Kidachi, H., 15
 Kraus, M., 5
 Kuznetsov, Y.A., 59
- Levintin, V., 59
 Lust, K., 58
- Magnus, K., 13
 Magnus, W., 15
 Matsushita, O., 20, 21
 McDonald, R., 20, 21
 Mestrom, W., 59
 Mettler, E., 15
 Meyer, F., 29
 Montagnier, P., 30
 Mook, D.T., 15, 29, 51, 54
- Natori, M., 162
 Nayfeh, A.H., 15, 29, 39, 51,
 54
 Nguyen, P.H., 19, 21
 Nordmann, R., 13, 161, 194
 Norris, M.A., 2, 119
- Oestreich, M., 142, 144
 Okubo, H., 20, 21
 Olvera, A., 18
 Onogi, H., 15
- Pandiyar, R., 29, 30
 Pedersen, P., 30
 Pfützner, H., 13, 161, 194
 Pfeiffer, F., 8, 142
 Pismen, L.M., 52
 Popp, K., 8, 13, 142, 144
 Prado, E., 18
 Pumhössel, T., 45, 50, 162,
 164, 172, 194, 204
- Rand, R.H., 15, 29
- Richards, J.A., 15, 29
 Riet, A.M., 59
 Rubinstein, B.Y., 52
- Saito, A., 18
 Sanders, J.A., 39, 40
 Sandstede, B., 59
 Santi, F., 126
 Schmidt, G., 15, 18, 19, 29,
 32-34, 51
 Seydel, R., 58, 59
 Seyranian, A.P., 30
 Sinha, S.C., 29, 30
 Solem, F., 30
 Spiteri, R.J., 30
 Springer, H., 162
 Sri Namachchivaya, N., 20, 21
 Starzhinskii, V.M., 29
 Steindl, A., 54, 58
 Steinschaden, N., 162
 Stelter, P., 142
 Stoker, J.J., 15
 Sun, J.Q., 2, 119
- Takano, K., 20, 21
 Tani, J., 162
 Tondl, A., 13, 18, 19, 21-23,
 32, 35, 45, 50, 53, 55,
 67, 69, 120, 125, 127,
 140, 161, 162, 172,
 194, 198
 Troger, H., 54, 58
 Tzou, H.S., 162
- Ursell, F., 14
- Verhulst, F., 29, 39-41, 51,
 54, 57
- Wang, X.-J., 59

Authors Index

Watanabe, K., 20, 21

Winkler, S., 15

Wojewoda, J., 142

Wolfram, S., 52

Xu, J., 29

Yakubovich, V.A., 29

Yamamoto, T., 11, 13, 18, 50,
161, 194

Zhou, J., 30

Zwillinger, D., 29

Index

Absorber

- conventional, 119, 120, 135, 139, 141, 149, 152, 159
- parametric, 119, 120, 122, 126–128, 133, 135, 139, 140, 142, 147, 153, 159
- tuned, 2, 119, 135, 139, 141, 152

Analytical method

- Averaging, 29, 39, 51
- Harmonic Balance, 51
- Hill's determinante, 29
- Multiple Scales, 51
- Perturbation technique, 29, 30
- Poincaré-Linsted, 51
- Successive Approximation, 31, 37, 45, 51
- Tondl-Floquet, 45, 51, 171

Approximation

- first order, 7, 21, 35, 45, 49, 51–53, 90, 93, 97
- second order, 52, 140

Asymptote, 106

Bearing

- fluid-film, 10, 161, 162
- magnetic, 162

Bifurcation

- Hopf, 21, 59
- Neimark-Sacker, 21, 59

Controller

- closed-loop, 116
- open-loop, 20, 164, 204, 209

Criterion

- Routh-Hurwitz, 44, 50
- termination, 54, 56, 80

Damping

- equivalent, 63, 94, 101, 108, 128, 180
- negative, 3, 63, 121
- non-linear, 68, 70, 72, 166
- progressive, 68, 169, 195

Eigenvalue, 4, 12, 57, 58, 65, 83, 149, 169

Eigenvector, 65, 72

Excitation

- forced, 1, 14, 20
- gap, 165, 183
- parametric, 13–15, 19, 38, 67, 101, 153
- self-excitation, 2, 5, 8, 10, 63, 161
- unbalance, 164, 172, 194

- Initial conditions, 54, 56, 57
- Monodromy matrix, 57–59, 83, 116, 141
- Normal form, 34, 65, 67
- Numerical method, 53, 172
 - Simulation, 53
- Parametric resonance, 15
 - combination, 170
 - first order, 17, 38, 185
 - primary, 83
 - principal, 18, 170
 - second order, 131, 133, 141, 154, 156
- Pendulum, 14, 19, 20, 26
- Pumping, 17
- Root-finding, 4, 50, 116, 117, 149
- Rotor system, 10, 45, 161
- Software
 - Acsl, 56, 116
 - Auto97, 59
 - BifPack, 59
 - Content, 59
 - Maple, 43, 52
 - Mathematica, 43, 52
 - Matlab, 56, 58, 59
- Stability, 12, 54, 56
 - chart, 16
 - condition, 23, 44
- Swing, 13, 15, 17
- Time
 - computational, 54, 56, 58, 80, 116
 - non-dimensional, 166

Über den Autor ...



Horst Ecker received his diploma degree in 1980 and his doctoral degree in 1990 in Mechanical Engineering from Vienna University of Technology (TU Vienna). At that time he was working mainly in Vehicle Dynamics, Tire Mechanics and also on torsional vibration problems. In 1995 he was awarded a Max Kade research stipend and spent a year as a research scholar at Duke University, Durham, North Carolina. His research was focused on the nonlinear dynamics of rotors supported by magnetic bearings. In the late 90's he became interested in vibrations of parametrically excited systems and started a research project on this topic.

In March 2004 he received the habilitation degree (*venia docendi*) and became a docent for Technical Dynamics at TU Vienna. Since October 2004 he is an Associate Professor (a.o.Univ.Prof.) at the Institute of Mechanics and Mechatronics at TU Vienna.

Über diesen Band ...

Self-excited vibrations in mechanical systems can be very dangerous for machines and structures. Therefore, means and methods to avoid or suppress such vibrations are of great importance. In this monograph the rather novel idea of employing parametric excitation for Vibration suppression is investigated thoroughly. By introducing a time-periodic stiffness parameter it is possible to enhance positive damping in the system and thereby cancel self-excited vibrations.

Analytical methods are presented for an approximate stability investigation of low-dimensional systems with periodic coefficients. For the most part a numerical method, based on simulation, is used, to compute domains of stability for self-excited systems and decide on the effectiveness of the proposed method. Many results are presented for simple 2-degrees-of-freedom systems, but in the last chapter also a more complex rotor system is investigated.

Über diese Reihe ...

Die Bände dieser neuen ASIM - Reihe Fortschrittsberichte Simulation konzentrieren sich auf neueste Lösungsansätze, Methoden und Anwendungen der Simulationstechnik (Ingenieurwissenschaften, Naturwissenschaften, Medizin, Ökonomie, Ökologie, Soziologie, etc.).

ASIM, die deutschsprachige Simulationsvereinigung (Fachausschuss 4.5 der GI - Gesellschaft für Informatik) hat diese Reihe ins Leben gerufen, um ein rasches und kostengünstiges Publikationsmedium für derartige neue Entwicklungen in der Simulationstechnik anbieten zu können.

Die Fortschrittsberichte Simulation veröffentlichen daher: * Monographien mit speziellem Charakter, wie z. B. Dissertationen und Habilitationen * Berichte zu Workshops (mit referierten Beiträgen) * Berichte von Forschungsprojekten * Handbücher zu Simulationswerkzeugen (User Guides, Vergleiche, Benchmarks), und Ähnliches.

Die Kooperation mit den ARGESIM Reports der ARGESIM vermittelt dabei zum europäischen Umfeld und zur internationalen Publikation.